IMPROVING CLINICAL OUTCOMES IN RENAL HIFU THERAPY

ROBERT W. RITCHIE

DPHIL IN SURGERY

MT 2008 - TT 2012

Supervisors:

Mr Thomas Leslie (Nuffield Department of Surgical Sciences, University of Oxford)

Professor Constantin Coussios (Institute of Biomedical Engineering, University of Oxford)

Nuffield Department of Surgery

University of Oxford

Oriel College

University of Oxford

Abstract

The rising incidence of small, asymptomatic renal tumours discovered using abdominal imaging during the investigation of unrelated symptoms has fuelled the desire for new therapies which avoid surgical excision. Extracorporeal High Intensity Focused Ultrasound (HIFU) was proposed as one of these modalities but so far clinical research has been inconclusive. The present work was designed to improve these clinical outcomes through the conduct of further clinical trials, laboratory based research and the translation of new technology into existing HIFU devices.

A Phase II clinical trial of patients (n=13) with newly diagnosed <4cm renal tumours (clinical stage T1a) was designed, peer reviewed and received ethical approval (Ox REC 09/H0606/04). Ten of 13 patients underwent renal HIFU using a clinical HIFU device (Model JC/JC200, HAIFU, China). One patient could not be treated due to poor tumour visualisation after anaesthesia and two patients could not be treated as they became unwell before or during anaesthesia. Histological evidence of HIFU ablation in either tumour or normal renal parenchyma was seen in all ten patients. Evidence of sub-total tumour ablation was seen in 8/10 of patients. Grade 1 (<50%), 2 (50-90%) & 3 (90-99%) ablation was achieved in 4/10, 3/10 & 3/10 patients respectively but complete (100%) tumour ablation was not possible. HIFU treatment caused minimal morbidity – no Grade III-V (Clavien-Dindo) complications related to HIFU treatment occurred. Grade I skin pain and induration was seen in 9/10 patients; Grade II skin pain occurred in a single patient.

Patient demographics, imaging and tumour characteristics were used to design parameters to improve patient selection for renal HIFU. The tumour location, thickness of peri-nephric fat and renal nephrometry score were useful predictors of successful screening for treatment.

Diligent use of these factors could limit unnecessary treatments and improve ablation outcomes.

It is well known that ultrasound imaging of small renal masses can be challenging. Ultrasound imaging often deteriorates further during HIFU as the abdominal wall and fat tissues swell and cause increased attenuation. This loss of imaging quality was clearly demonstrated in this clinical trial and resulted in the early termination of treatment, before endpoints were reached, in a number of cases.

The current clinical method for monitoring the success of HIFU ablation using hyperecho analysis of B-mode ultrasound images is also questionable. Laboratory based studies using ex-vivo bovine liver subjected to HIFU confirmed that hyperecho monitoring had low sensitivity, predictive values and overall accuracy.

A novel method of HIFU monitoring – passive mapping of the emissions received from acoustic cavitation activity and other sources of non-linearity during HIFU treatment – is believed to represent a significant opportunity to improve feedback. This technique uses the passively received signature of cavity activity which, when time-reversed, gives high-resolution images of the precise location of the activity. Laboratory-based ex-vivo work, using a commercially available ultrasound system (z.one, Zonare, USA), demonstrates its superiority over hyperecho monitoring. Indeed, thresholds could be applied to successfully predict HIFU ablation with high sensitivity and specificity.

This technique was successfully translated into the clinical setting through the design of a Passive Acoustic Mapping (PAM) device. Custom-built receiving elements were applied without limiting the function of the existing HIFU devices. Both pre-clinical and ethically-

approved clinical studies demonstrated its safe integration without significant impact on the device energy output or treatment accuracy.

Using similar passive beamforming algorithms, acoustic cavitation activity was successfully mapped and corresponded with the location of thermal ablation in both ex-vivo tissue phantoms and during clinical HIFU therapy.

It is believed that the development of new patient selection parameters will eliminate target those patients who are most suitable for renal HIFU – small tumours, minimal peri-nephric fat & low nephrometry score.. The use of PAM will lead to a significant improvement in the efficacy of treatment. It can be successfully applied to existing devices and predicts the location and extent of HIFU ablation with greater accuracy that existing techniques.

Table of Contents

Table of Figures

List of Tables

List of Abbreviations

ADL	Activities of daily living
AE	Adverse event
AP	Antero-posterior
BPH	Benign prostatic hyperplasia
BUBBL	Biomedical Ultrasonics, Biotherapy & Biopharmaceuticals Laboratory
CC	Cranio-caudal
CE-MRI	Contrast-enhanced magnetic resonance imaging
CK7	Cytokeratin 7
CRF	Case report form
CRP	C-reactive protein
CRY	Cryotherapy
CSA	Cross-sectional area
CT	Computed tomography
CTCAE	Common toxicity criteria for adverse events
dB	Decibel
FFT	Fast fourier transform
FN	False negative
FP	False positive
H&E	Haemotoxylin & eosin
HIFU	High-intensity focused ultrasound
LR	Likelihood ratio
MDT	Multi-disciplinary team
MHz	Megahertz
MPa	Megapascal
MRI	Magnetic resonance imaging
N/A	Not applicable
Np	Neper
NPV	Negative predictive value
NS	Nephrometry score
NSS	Nephron-sparing surgery
PAM	Passive acoustic mapping
PC	Prostate cancer
PCD	Passive cavitation detector
PN	Partial nephrectomy
PPV	Positive predictive value
PRF	Proton resonant frequency
PRFP	Peak rarefactional pressure

PZT	Piezoceramic zirconate titanate
RCT	Randomised controlled trial
RFA	Radio-frequency ablation
RFB	Radiation force balance
RN	Radical nephrectomy
ROC	Receiver operator curve
ROI	Region of interest
R_x	Treatment
SEM	Standard error of mean
SNR	Signal-to-noise ratio
SOC	System order class
TN	True negative
TP	True positive
Trans	Transverse
VHL	Von Hippel-Lindau
μm	Micrometre

Acknowledgements

It is always the case in the conduct of trials and research that the support of numerous people is required and gratefully received. It is not possible for me to acknowledge each and every individual so I would like to thank anybody who I am not able to mention directly.

Foremost I would like to thank my supervisors who have provided guidance and support throughout my research. It has been a privilege to be Mr Tom Leslie's first DPhil student and I am sure there will be many more. He has been hugely supportive, always willing to lend a hand and a huge source of entertainment. He is a remarkable pragmatic and has an enviable ability to succeed even when progress seems unlikely. My co-supervisor, Professor Constantin Coussios has been the inspiration and drive behind my project and indeed many others. His many attributes include the combination of raw intelligence, practicality, ambition and determination. His ability to translate basic science to clinical practice is something which all academics will admire.

Although not a direct supervisor, Mr David Cranston has been an instrumental feature of both my academic and clinical training since I arrived in Oxford in 2006. He has been a father-figure to many urological trainees during his career and has an unshakeable belief that hard work and persistence leads to success. Additionally I am grateful to him and to Mr Mark Sullivan for their efforts in assisting the clinical trial. Anyone with experience of trial conduct will know that its success, or lack of, is primarily dependent on the ability to recruit patients.

With the trial in mind I would also like to thank each and every patient who agreed to join the study. The trial was entirely voluntary and required an additional anaesthetic. Very few patients declined to participate and it is only a result of such altruistic gestures that clinical research can continue to produce exciting results. My belief in the inherent good of people has been re-affirmed by their willingness to risk their time and well-being purely for the future benefit of others.

In the conduct of the trial I have had exceptional clinical support. My thanks go to Dr Mark Stoneham, Dr Andris Klucniks and Dr Oliver Dyar whose anaesthetic skills are such that I would willingly receive them should the need ever arise. In addition, three anaesthetic nurses – John Cox, Suni Surendran and Lani Fabiosa – provided vital support without which the study would not have been possible. I would also like to thank Sister Karen Doig who came to my aid on innumerable occassions as we moved from our old unit in the new Radiology department. I was ably assisted with analysis of the clinical data by our lead radiologist – Dr Rachel Phillips – and by several pathologists, namely Dr Gareth Turner, Professor Ian Roberts, Dr Ran Pereira, Dr Lisa Browning and Dr Clare Verrill.

Much of my work was undertaken in collaboration with the BUBBL lab at the University of Oxford, led by Professor Coussios. I was hugely fortunate to benefit from the assistance of several post-doctoral fellows and DPhil students, in particular, Dr Jamie Collin, Dr Carl Jensen, Miklós Gyöngy and Stuart Faragher (the later two are both now Drs!). I am in no doubt that they are the most gifted group of people I have ever worked with and they have each gone beyond the call of duty to assist me during my research. Without their help the vast majority of my work would not have been possible.

Finally, I would like to acknowledge the funding support that I have received during my research. The Oxford Biomedical Research Centre generously funded my work, the entire clinical trial and the transfer to the new HIFU unit. In addition, the charity Urology Cancer Research and Eduction (UCARE) generously paid my university fees during the course of my studies.

1 Introduction

HIFU is the only truly non-invasive ablative therapy for cancer. Clinical outcomes have been variable to date. This chapter summarises work undertaken to improve these outcomes in the course of this thesis.

1.1 High Intensity Focused Ultrasound

The desire for minimally-invasive surgical techniques has been a key driver of medical device development over the last three decades. The benefits of shorter hospital stays, quicker recovery times, earlier return to work, less pain and fewer complications are obvious for the patient, hospital trusts and society as a whole. The first kidney was removed using keyhole (laparoscopic) techniques in 1990 by Dr Ralph Clayman. Since then, a number of minimally-invasive energy ablative therapies have been developed and tested in renal cancer. High Intensity Focused Ultrasound (HIFU) represented the least invasive option – truly scarless surgery. When used appropriately, HIFU can treat various malignant and benign solid tumours, often with minimal or no side-effects beyond mild pain. Proof of concept in renal cancer was established initially in animal studies and then in clinical studies, including trials conducted in Oxford. These trials produced varying degrees of success – difficulties were found with patient selection, tumour imaging, treatment monitoring and outcome assessment. This thesis was designed to address these challenges with the ultimate goal of improving clinical outcomes in renal HIFU.

1.2 Thesis Outline

This thesis begins in Chapter 2 with a review of the background literature and evidence for HIFU ablation of tumours, with particular emphasis on renal cancer. The design, implementation, conduct and results of a new, ethically-approved clinical trial of renal HIFU is then reported in Chapter 3. Throughout this trial, the results were used to develop parameters which predict successful HIFU outcomes and also to create hypotheses with regard to the role of peri-nephric fat and renal nephrometry in clinical outcomes. Laboratory based experiments were conducted to test these hypotheses and are discussed in Chapters 4 & 5. A novel technique for monitoring HIFU ablation using passive acoustic mapping (PAM) is described in Chapter 6. This new technology was developed by fellow researchers at the University of Oxford and was tested in ex-vivo animal tissue. Custom-built equipment was designed to implement this technique on clinical HIFU devices and the proof of concept, reported in Chapter 7, was demonstrated in ex-vivo animal tissue. This monitoring device was fully translated into the clinical setting through its use in patients with newly diagnosed renal cancer. Chapter 8 amalgamates these chapters to discuss the implications for patient care and demonstrates the essential translational component of contemporary medical research. Finally, in Chapter 9, the main achievements are summarised together with suggestions for future research in renal HIFU.

2 Literature Review

This chapter reviews the basic principles of ultrasound mechanism of action of HIFU and the monitoring of clinical HIFU therapy. The clinical uses of HIFU, with particular reference to renal cancer are reviewed in detail.

2.1 Ultrasound

Ultrasound refers to mechanical vibrations at frequencies above the threshold for human hearing, typically 20KHz. Ultrasound is produced by piezoelectric materials via the reverse piezoelectric effect – application of an alternating electric potential of a certain frequency to produce material vibrations at that same frequency. The amplitude of the vibrations is maximised by supplying the incoming electric potential at the resonant frequency of the piezoelectric material. Modern ultrasonic transducers use lead zirconate titanate (PZT). At low intensities ultrasound can propagate through tissue without causing damage. Indeed, ultrasound in the 1-20MHz range is widely used in diagnostic imaging, including pre-natal surveillance.

2.2 Ultrasound interaction with tissue

2.2.1 Ultrasound propagation

As the mechanical ultrasound wave passes through tissue, the alternating cycles of compression and rarefaction cause molecular oscillations which may propagate either

perpendicular (shear wave) or parallel (pressure wave) to the transducer axis. Ultrasonic shear waves are highly absorbed and play little role in the medical application of ultrasound. At relatively low pressures, ultrasound propagates in a linear fashion, unchanged in morphology although decreased in amplitude due to absorption and reflection. However, at biomedically relevant intensities, nonlinear propagation occurs and must be considered [1-4]. Non-linear propagation occurs as the positive pressure phase of the acoustic wave travels faster through the medium than the negative pressure phase, converting an initially sinusoidal wave into a saw tooth-shaped wave. Consequently, the initial propagating monochromatic wave generates multiple harmonic frequencies of the fundamental, as shown in Figure 1.

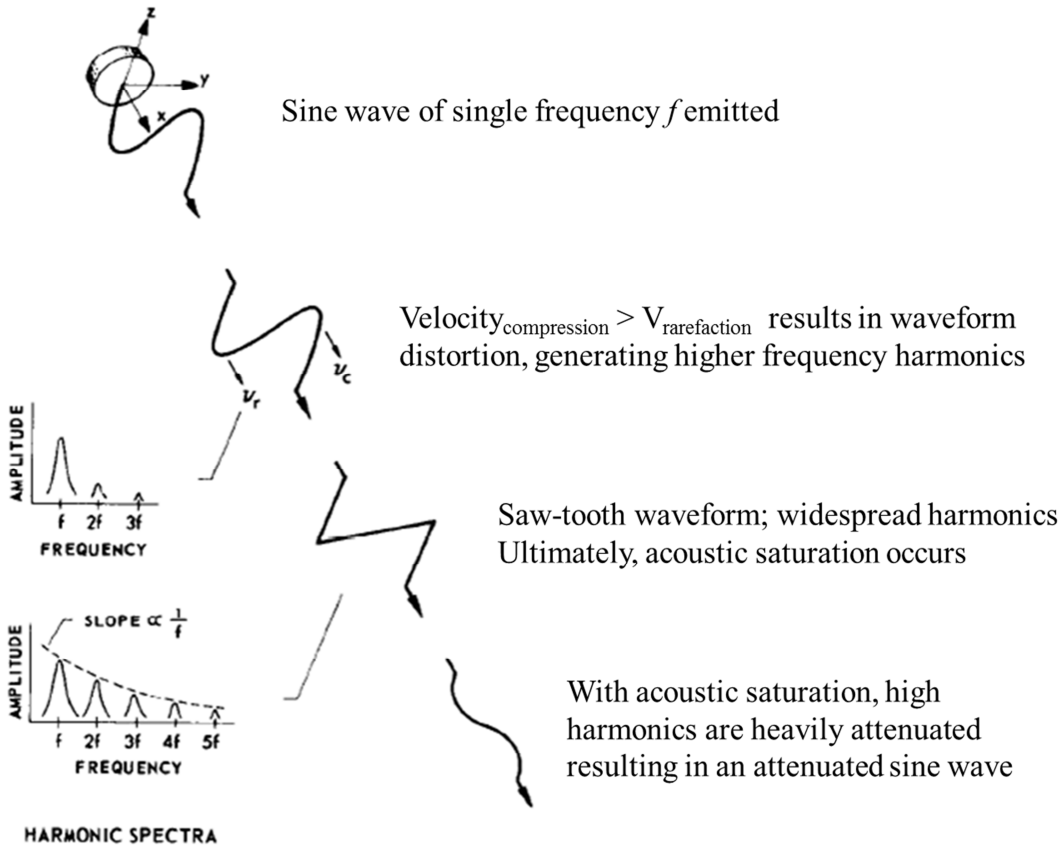

Figure 1 – Schematic of non-linear propagation of an acoustic wave leading to shock-wave formation and generation of multiple harmonics (adapted from [5])

Because attenuation in tissue is a strong monotonically increasing function of frequency [6] these higher harmonics are more readily absorbed, resulting in enhanced local heat deposition.

2.2.2 Speed of sound & non-linearity

The speed of sound propagation through any medium is determined by the medium's compressibility and its density. In general terms, the speed of sound *c* is given by the formula

$$c = \sqrt{\frac{k}{\rho}}$$

where k is the coefficient of stiffness (bulk modulus) and ρ is the density. The speed of sound therefore increases with stiffness and decreases with density. The speed of sound in pure water at 20°C & 37°C is 1482.3m/s & 1523.6m/s respectively [7].

As discussed, ultrasound propagation cannot be assumed to be linear. The degree of non-linear behaviour within a medium is described by the non-linear parameter – *B/A*. The values *B* & *A* are derived from an equation relating pressure variations to density variation in the medium. Typical values for *B/A* in various media are shown in Table 1. It is the pressure changes within the medium that result in the transfer of energy from the fundamental frequency signal into higher order harmonics. The degree of non-linear propagation increases with increasing incident amplitude, frequency and distance of propagation.

Table 1 – Typical values for the coefficient of non-linearity *B/A* for various media [8]

Medium	*B/A*
Blood	6.1
Brain	6.6
Fat	10
Liver	6.8
Muscle	7.4
Water	5.2

It is noteworthy in the context of this thesis, that the *B/A* parameter for fatty tissue is high – significantly higher than other human tissues. Consequently, propagation of ultrasound through fat tissue is likely to result in non-linear behaviour with the generation and resultant attenuation of multiple harmonic frequencies. It is also significant that this non-linear behaviour is more likely to occur in fat tissue located further away from the driving transducer – in clinical HIFU this is analogous to tissue lying deep with the abdominal cavity.

2.2.3 Attenuation in tissue

Attenuation is the gradual loss of intensity of any flux through a medium. Specifically in biomedical acoustics, attenuation represents two distinct processes – absorption and scattering. The variation in acoustic pressure as the propagating wave passes through tissue leads to shear motion of particles within it; this absorption of energy results in heating. In addition, areas of inhomogeneity in tissue result in scattering of the incident waveform – in a truly homogenous medium this does not occur. The gradual loss of amplitude is quantifiable – the amplitude attenuation coefficient of a medium (α) is the sum of the absorption coefficient (α_a) and the scattering coefficient (α_s). The attenuation coefficient exhibits a power-law dependence on frequency, whilst overall attenuation clearly depends on the propagation path length through a particular material. The attenuation coefficient is therefore

normally expressed in either Np/m/MHz$^{\gamma}$ or dB/m/MHz$^{\gamma}$, where γ is a material-specific constant.

An acoustic wave can be characterized not only by its pressure amplitude, but also by its acoustic intensity, which represents the energy delivered per unit area of tissue per unit time and is typically expressed in W/cm^2. For a travelling harmonic plane wave, the acoustic intensity is related to pressure amplitude by

$$I = \frac{P^2}{2\rho c}$$

where P represents the pressure amplitude, ρ the density and c the speed of sound in the medium.

As an ultrasound beam passes through a finite thickness of tissue, the intensity I can be calculated as follows:

$$I = I_0 e^{-\mu x}$$

where I_0 is the inital intensity (x=0), x is the tissue thickness and μ is the intensity attenuation coefficient which can be calculated as

$$\mu = 2\alpha$$

It is noteworthy that whilst non-linear propagation serves to transfer energy to higher harmonics, the frequency dependence of absorption leads to energy dissipation. Consequently with increasing propagation distance, the non-linear waveform reverts to a near sinusoidal, albeit significantly damped, pattern, as shown in Figure 1.

2.2.4 Thermal ablation

An ultrasonic wave will pass unchanged through a perfectly homogenous, non-absorbing medium. However, inhomogeneous tissue acts as both a scatterer and an absorber, thus incident acoustic energy results in heating as the wave propagates. The level of heating is increased if nonlinear propagation dominates, as harmonic frequencies are more readily absorbed [9].

The biological response to hyperthermia is variable and dependent upon both the degree and duration of temperature elevation [10]. Elevations of up to 4ºC occur during physiological stress such as strenuous exercise. Indeed localised hyperthermia increases oxygen tension in wounds [11] and may promote both soft tissue and fracture healing [12, 13]. In vivo temperatures of up to 43ºC seem tolerable without permanent damage unless endured for long periods of time [14]. Above 43ºC, cellular reproduction ceases if the temperature is maintained for at least one hour and survival is unlikely above 45ºC. The importance of 60 minutes' exposure at 43ºC led to the concept of Cumulative Equivalent Minutes (CEM_{43}) – a measurement of thermal dose which provides an estimate of the physiological outcome of exposure to different temperatures for varying durations [15]. Above 50ºC cells death occurs rapidly and a one second exposure at 56ºC is sufficient for irreversible cell death [16].

The mechanism of thermal ablation is not fully understood but the predominant mechanism is protein aggregation [17]. Proteins are the functional components of cells and consist of strings of amino acids which form an alpha helix or beta strand around one another, held by hydrogen bonds. This secondary structure forms a three-dimensional globule through further tertiary interactions in the form of hydrogen or disulphide bonds. These bonds, which are responsible for the macromolecular structure, are relatively weak and susceptible to

disruption in response to insults such as heat. Exposure of these hydrophobic bonds leads to irreversible protein aggregation and loss of function. Macroscopic analysis of thermal ablation in tissue demonstrates a characteristic opaque lesion quite distinct from the surrounding normal tissue; histology reveals coagulative necrosis [18, 19].

2.3 HIFU induced thermal ablation

At medical diagnostic intensities, ultrasound imaging is considered safe. Importantly, this has been confirmed in ultrasound imaging of the foetus which is felt to be most vulnerable due to the preponderance of heat-susceptible rapidly dividing cells [20, 21]. HIFU intensities are several orders of magnitude greater than that used in diagnostic ultrasound and are administered in a continuous rather than pulsed waveform. By tightly focusing the ultrasound beam high *in situ* pressures can be achieved in a small, clearly defined region. The incident mechanical energy is converted into heat and subsequently dissipates into the surrounding tissue, exacerbated *in vivo* by regional blood flow. However, if this rate of heating is rapid and exceeds the rate of heat dissipation, a local temperature rise will occur (see Figure 2). Temperatures can reach 80ºC or more and result in sharply demarcated regions of coagulative necrosis with sparing of surrounding tissue outside the focus [22]. Such a level of heat rise, even for short periods of time, will lead to cell death [10]. The exact dimensions of the focal region is transducer dependent; for clinical HIFU transducers used in the context of this thesis this is typically 12mm in length, 3mm in width and cigar-shaped.

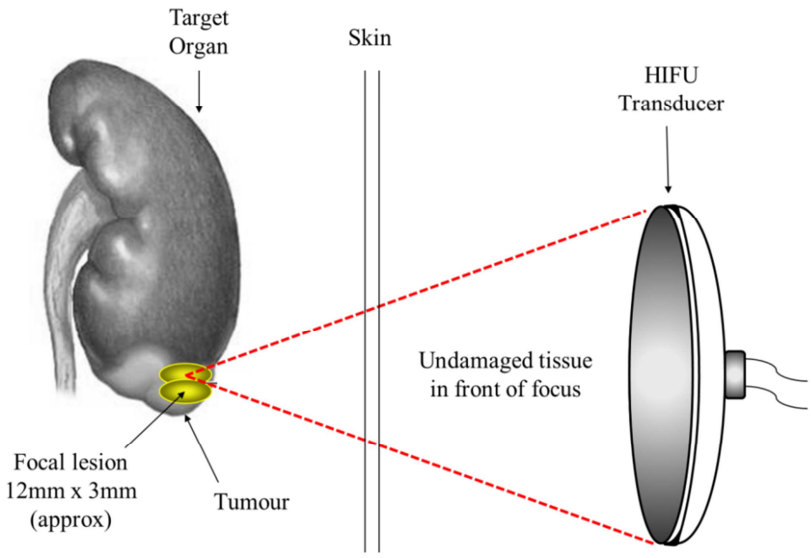

Figure 2 – Schematic of HIFU lesion formation in a renal tumour

Given the spatial and temporal profile of a HIFU pulse, the intensity across a specific area will vary depending on its position and the timing within a pulse. It is therefore possible to describe the intensity in terms of the average or peak spatial and temporal intensity – I_{SATA}, I_{SPTA}, I_{SATP} or I_{SPTP}. The beam profile can be mapped using a hydrophone and the power determined with a radiation force balance (RFB), described in Chapter 10.5. These measurements are conventionally performed in degassed water and are thus free-field estimates; low transducer power outputs are also used to minimise any non-linear propagation effects – the measurements can then be extrapolated to higher power outputs. The focal size is described by measuring either the distance between the half maximum intensity, as shown in Figure 3, or the distance between the half maximum pressure. This represents respectively the -3dB (intensity) or -6dB (pressure) full-width-half-maximum. This method provides a repeated and communicable measurement of a transducer profile.

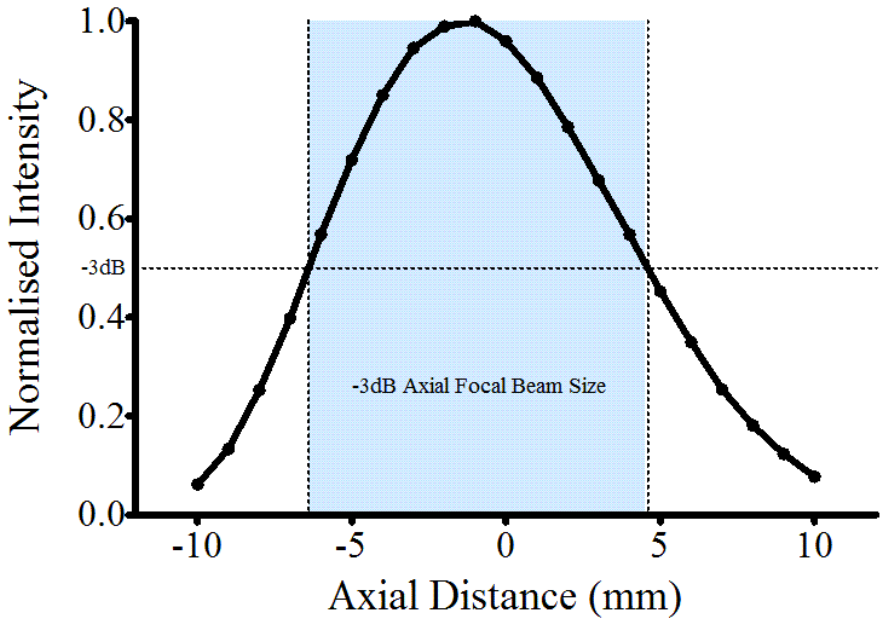

Figure 3 – Example axial beam profile of a HIFU transducer showing the normalised axial intensity and the -3dB focal beam size corresponding to a 50% drop in intensity.

The rate of heat deposition in tissue due to absorption can be approximated using a simple equation:

$$\frac{dQ}{dt} = 2\alpha I$$

where α is absorption coefficient adjusted for the insonating frequency and *I* is the acoustic intensity. In general, because absorption dominates over scattering in tissue propagation and therefore, a reasonable approximation is achieved if the absorption coefficient is replaced with the attenuation coefficient α.

The use of HIFU to induce tissue damage was first described in 1927 [23]. The first clinical application was not described until the 1950s when Fry *et al.* used high energy ultrasound to create lesions in the central nervous system [24, 25]. The concept of using HIFU to treat malignant tumours was first suggested by Burov ([26]) and led to studies of the acoustic properties and damage threshold of mammalian tissues [27-31]. In principle at least, HIFU

tumour ablation fulfils many of the criteria for an ideal treatment – non-invasive, safe and acceptable to both patients and medical staff. However, new techniques are judged fundamentally by their oncological efficacy in comparison with current gold standard therapies. Given this, the use of ultrasound as a therapeutic modality developed little until the 1990s due to the lack of good quality imaging to effectively target and monitor treatment.

Over the last 20 years, diagnostic imaging technologies have developed rapidly – ultrasound and cross-sectional imaging including CT & MRI can now produce high resolution tissue imaging. These techniques allowed both excellent tumour visualisation and HIFU treatment monitoring, thus providing the impetus to bring HIFU into clinical practice. Complete tumour treatment requires the placement of multiple lesions of HIFU adjacent to one another in a systematic fashion to ensure the entire tumour is covered. Given the typical size of a HIFU lesion outlined above, complete tumour ablation can be time-consuming. However, successful ablation has been achieved in the context of liver, breast, pancreatic, prostate, renal and bone cancer, as well as soft tissue sarcomas and uterine fibroids [32-39].

2.4 Acoustic cavitation

2.4.1 Principles

In the presence of a high amplitude sound wave propagating through a medium, the peak rarefactional pressure (PRFP) may be sufficiently high to cause cavities to form within the medium which rapidly fill with gas or vapour. The process is known as acoustically driven nucleation [40-42]. The likelihood of nucleation is a function of the insonication pressure and the properties of the medium itself. With continued exposure to sound, these gas/vapour cavities (bubbles) will oscillate about their equilibrium radius – known as acoustic cavitation

[43]. The frequency of oscillation will be that of the propagating wave; the amplitude of oscillation will be greatest at the resonant frequency of the bubble.

2.4.1.1 Stable cavitation

At relatively low amplitudes with small changes in bubble size, linear behaviour will dominate resulting in a scattered wave of identical frequency to the driving signal. At higher amplitudes, non-linear effects are seen, with the subsequent generation of multiple sub-harmonics and ultra-harmonics of the driving signal generated. When this process is sustained over hundreds of cycles, it is termed stable (non-inertial) cavitation – see Figure 4.

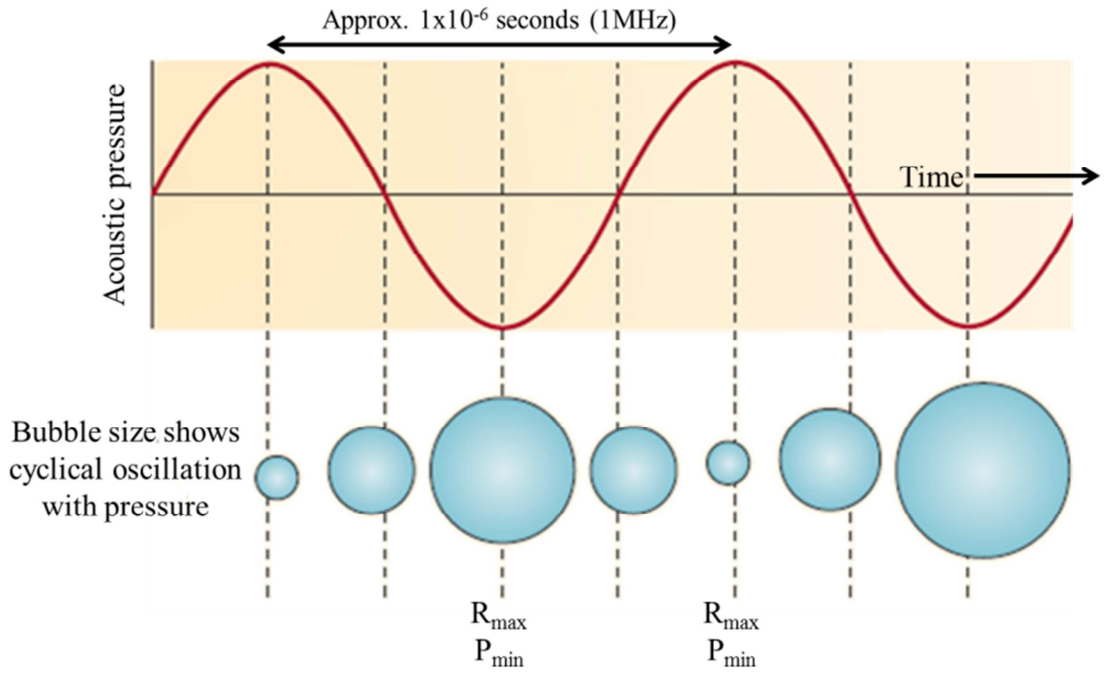

Figure 4 – Schematic diagram of acoustic cavitation activity, demonstrating bubble expansion during the rarefaction phase and bubble collapse during the compressional phase. When sustained over many cycles, it is known as stable cavitation; R=radius; P=pressure (adapted from [16])

2.4.1.2 Inertial cavitation

With further increases in the sonication amplitude, bubbles formed as a result of acoustic nucleation may expand to many times their initial radius over a number of acoustic cycles. Above a certain threshold pressure, a bubble may subsequently collapse violently during the

compressional half-cycle [44]. The collapse continues beyond that expected during stable cavitation to a radius many times smaller than the initial radius, driven by the inertia of the medium surrounding the collapsing bubble [45]. Complete bubble dissolution may result. This process, known as inertial cavitation result in a significant transfer of energy and is thus of considerable interest in the context of biomedical ultrasound.

2.4.2 Cavitation-enhanced heating

Acoustic cavitation is proposed as the mechanism responsible for a number of bio-effects including acoustic haemostasis, acoustically-driven opening of the blood-brain barrier and sonoporation [46]. Inertial cavitation is undoubtedly a key mechanism of urinary tract stone fragmentation using extracorporeal shockwave lithotripsy [47]. However, with relation to HIFU ablation, its ability to significantly enhance local heating, well above that expected due to linear & non-linear effects, warrants most attention. This is shown clearly in Figure 5 where a modest rise in insonication amplitude leads to a significant increase in heat deposition, beyond what would be expected with linear heating [48].

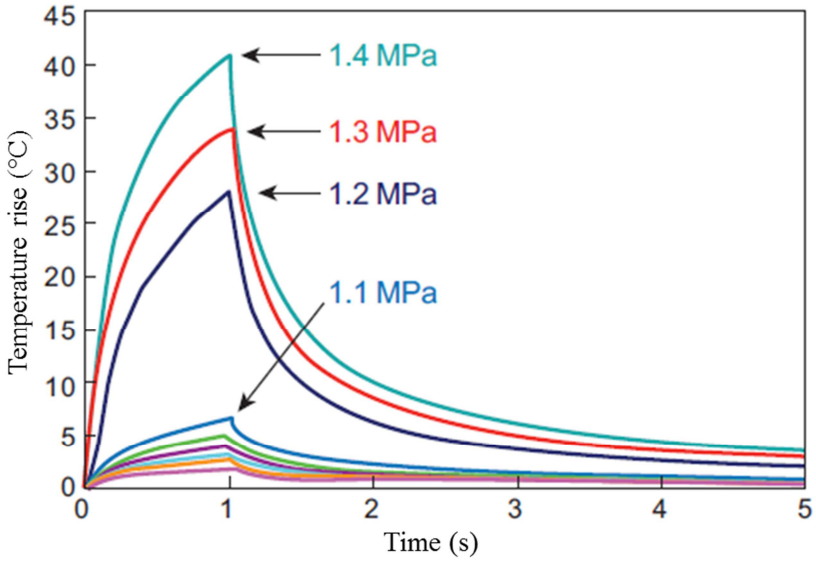

Figure 5 – Measured temperatures rises in a tissue phantom exposed to HIFU of increasing amplitude; a significant increase in heating is seen at 1.2MPa, beyond that expected with linear heating, due to cavitation activity (adapted from [46])

The mechanism of cavitation-enhanced heating is thought to be multi-factorial [46] Cavitating bubbles act as secondary sources of sound, emitting a scattered spherical wave. At low pressures, the emission spectrum consists purely of the driving frequency. At higher pressures, bubble behaviour is increasingly non-linear and the emission pattern will contain varying multiples or submultiples of the fundamental, collectively known as harmonics. At even higher pressures bubble behaviour becomes chaotic, producing the characteristic broadband noise seen in the emission spectrum of inertially cavitating bubbles. The frequency of this broadband signal is generally higher than the driving frequency, resulting in an increased rate of heating due to the frequency-dependence of absorption. This is shown graphically in Figure 6 – at 1.65MPa a modest temperature rise is noted with no broadband signal detected using a passive cavitation detector (PCD); at 1.8MPa an initial modest temperature rise is seen followed by a rapid temperature rise temporally associated with a strong PCD signal. At 1.9MPa, a strong PCD signal is seen from the outset with a simultaneous large temperature rise [46]. This significant increase in heat deposition is attributable to cavitation activity, the only source of broadband noise emissions [43]

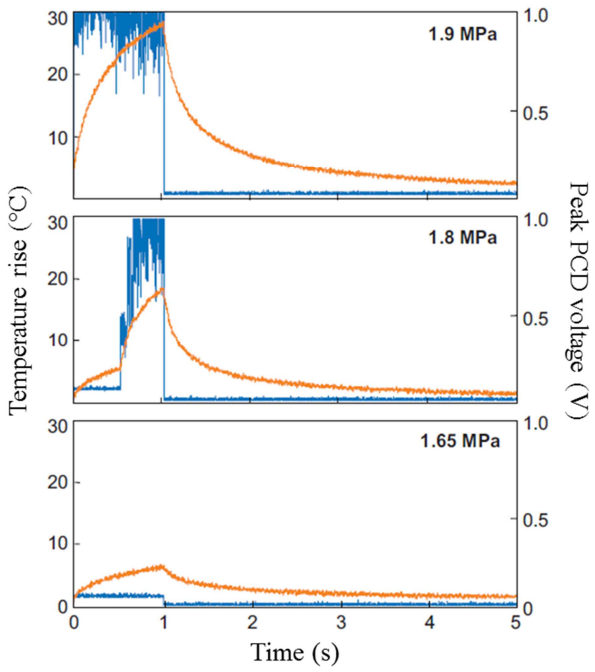

Figure 6 – Measured temperature rises and received PCD emissions in a tissue phantom during HIFU exposure of three differing amplitudes. Despite only a modest rise in amplitude, a significant increase in heating is seen which is temporally and quantitatively associated to the PCD signal voltage (adapted from [46])

Cavitation activity may also harness local heating through a process of energy trapping. Bubbles acts as strong scatterers, significantly increasingly the propagation path length whilst maintaining the energy within the region of cavitation activity. In addition, the presence of bubbles leads to energy transfer through viscous damping in the boundary layer of the bubbles [46].

Cavitation enhanced heating could be harnessed to vastly improve HIFU treatment. Its occurrence allows lower HIFU output powers to be used as the transfer to high frequencies emissions occurs only at the focus. This reduces the risk of pre-focal damage to tissues. Additionally, the energy trap serves to spatially localise the heat deposition to the region of cavitation activity thus improving the accuracy of ablation.

Finally, the acoustic signature from cavitation activity opens up a new opportunity to monitor the progress of HIFU ablation remotely without the need for focally-positioned temperature

or pressure probes. This extracorporeal approach is vital to maintain the minimally-invasive nature of HIFU therapy – a key feature which distinguishes HIFU from other energy ablative modalities.

2.4.3 Safety issues with cavitation during HIFU ablation

Initial studies into acoustic cavitation stemmed from concerns that bubble formation during diagnostic ultrasound imaging may impact on its safety [49-52]. Indeed, even in the context of HIFU therapy, cavitation was often considered undesirable [22, 53, 54]. The mechanical effects of cavitation on tumours in-vivo also led to concerns about the risk of metastasis. Studies have demonstrated increased gaps and disruption of connective tissue between muscle fibres and between parenchymal cells and extracellular matrix in tumours, with the potential for tumour cell dissemination [55, 56]. Early, animal studies also raised concerns about an increased metastatic burden from cavitation-inducing sonications [57, 58]. However, multiple other pre-clinical and clinical studies have failed to corroborate these findings [59, 60].

Further studies into cavitation bio-effects have determined that acoustically induced bubble formation may be considered beneficial in a controlled setting. The potential for enhanced, localised heat deposition is now widely accepted and results in accurate lesion formation without pre-focal migration or the need to cause tissue boiling [46, 48, 61, 62]. Moreover, HIFU may also lead to be a beneficial immune response which may prevent tumour recurrence or metastasis. Animal studies have demonstrated that HIFU treatment results in reduced primary tumour growth, reduced metastasis rates, provided protection against tumour re-challenge and improved survival [63-65]. Further work assessed the immune response in a mouse model using either a thermal or mechanical (cavitation) HIFU treatment regime.

Histology of the lesions produced during the mechanical revealed extensive cellular fragments and debris as a result of cell lysis. Increased dendritic cell stimulation, immunostimulatory cytokine levels and cell damage markers were with both treatment types but the effect was significantly greater in the mechanical HIFU group [66]. It is postulated that the release of cellular debris results in a specific immune response to tumour components which would otherwise remain undetectable by the normal immune system. Clinical studies in hepatocellular carcinoma, metastatic liver cancer, cholangiocarcinoma, osteosarcoma, breast carcinoma, pancreatic carcinoma and renal cell carcinoma have also demonstrated the development of anti-tumour immunity following HIFU including activation of antigen presenting cells and decreases in tumour-secreted immunosuppressive cytokines [34, 67-69].

2.5 Monitoring of HIFU treatment

Any ablative therapy intended for clinical use requires an effective monitoring technique in order to observe treatment progress, ensure the entire target is treated and to prevent damage to adjacent vital structures such as the intestine. By necessity these techniques must be remote image-based modalities – to attempt any assessment by direct visualisation of the target would immediately remove the non-invasive nature of these treatments. Indeed, if direct tumour visualisation is required, a strong argument can be made for surgical excision at the same time. Some form of pre-treatment cross-sectional imaging of the intended target is mandatory for ablation to facilitate a careful assessment of the surrounding structures. Traditionally, this has been in the form of a contrast enhanced CT, but may also be MRI, or positron-emission tomography (PET). In the context of HIFU, MRI imaging has often been used due to its superior imaging of soft tissues, particularly those that lies in the acoustic path of the HIFU beam. During HIFU treatment, it is necessary to register these pre-treatment

images, either manually or electronically, with the image-guidance modality on the clinical device. Currently, US-guided and MR-guided HIFU clinical devices are available – these are discussed in Chapter 2.9.2. MR-guided HIFU devices use thermometry (temperature estimates) whereas US-guided detect thermal lesion formation by detecting changes in ultrasound echogenicity associated with ablation.

2.5.1 MRI Monitoring

MRI is a non-ionising imaging modality in widespread clinical use in diagnostic radiology. It provides excellent anatomical resolution and has a high sensitivity for tumour localisation. MR-guided HIFU is in general clinical use and is arguably the gold standard technique for monitoring ultrasound therapy [70-78].

The human body is largely water and thus contains hydrogen nuclei (protons, ^{1}H) throughout. These unpaired protons mean the nucleus has a non-zero net magnetic field. Summed across an area, the random alignments of these protons cancel each other out, resulting in a zero net magnetic field in the region of interest. Application of a strong magnetic field results in the alignment of these nuclei along the axis of the field, flipping between alignment with or against the direction of the field at its proton resonant frequency (PRF).

A second intermittent electromagnetic field is then applied, perpendicular to the static magnetic field at the PRF. This secondary field is able to flip the spin of the nuclei thus reducing the net magnetisation along the static axis and producing a net magnetisation along the secondary axis. When the secondary field is switched off, the nuclei revert to alignment with the static field. The re-alignment (known as relaxation) process results in the emission of a radiofrequency signal. The time taken for relaxation of the magnetic fields along the static and secondary axis is called T1 & T2 respectively. Protons in different tissue types have

different relaxation times, as well as different spin densities and flow and spectral shift patterns, resulting in the excellent contrast resolution seen in MRI images.

Non-invasive estimates of in-situ temperature are possible using the T1 relaxation time, the diffusion coefficient or the PRF of tissue water. These techniques are well reviewed by Quession *et al.* [79]. At present the PRF shift method is favoured; this method provides accurate thermometry for a temporal resolution of 1 second and mm spatial resolution. Use of MRI thermometry circumvents the need to cross-register images from different modalities – pre-operative, intra-operative and post-operative imaging can all be MRI-based. However, MRI thermometry is very sensitive to motion artefact due to the necessary image subtraction – this requires careful correction to prevent erroneous measurements [80]. In addition, the CEM_{43} thermal dose estimates (discussed in Chapter 2.2.4) on which the temperature estimates are based, has inaccuracies at the temperatures associated with ablation.

MRI elastography attempts to counter the difficulties associated with MR thermometry by quantifying the mechanical properties of tissue [81]. In the context of HIFU monitoring, elastography aims to detect the change in stiffness of tissue as it is heated beyond a threshold for irreversible coagulative necrosis [81, 82]. This technique is attractive but currently suffers from long acquisition time (>5s) which prevent true real-time monitoring of HIFU pulses which typically last 2-3 seconds [83, 84].

2.5.2 Ultrasound monitoring

The use of an ultrasound-based technique to monitor HIFU therapy is logical. Both the diagnostic and HIFU ultrasound must propagate along the same path to allow successful imaging or treatment respectively. Any difficulties in obtaining good quality diagnostic

images imply that similar difficulties will be encountered when undertaking HIFU. Ultrasound is also non-invasive, non-ionising, cheap, mobile and readily available.

2.5.2.1 B-mode hyperecho

Diagnostic ultrasound fires sequential A-lines (pulsed ultrasound) and then receives the echo back to that transmitting element. Multiple A-lines from successive elements are then displayed next to each other to create the B-mode ultrasound image which is familiar to many.

The assessment of greyscale changes following HIFU exposure is the only form of treatment monitoring currently in use in ultrasound-guided HIFU. The formation of an intense hyperechoic region within the ablation zone was first described by ter Haar *et al.* using pig liver [85]. Further observations by Vaezy *et al.* demonstrated hyperecho to be a threshold phenomenon the appearance of which was inversely proportional to the duration of HIFU exposure [86]. At the threshold intensity, no immediate cellular damage was seen. The hyperecho results from scattering of the incident ultrasound due to the formation of bubbles.

Despite the widespread clinical adoption of hyperecho monitoring, the exact mechanisms of its formation are not well understood. Bubbles produced as a result of cavitation activity are small (order of microns) in comparison with boiling bubbles (order of millimetres). Hyperecho is thus much more likely to result from scattering from boiling bubbles than cavitation bubbles. Rabkin *et al.* demonstrated this in pig muscle – hyperecho appeared a significant time period (0.48 seconds) after focal temperatures reached 100C [87]. It should be noted from Chapter 2.2.4 that cell death occurs following a one second exposure at 56C and is immediate following a temperature rise to 80C. Boiling temperatures should thus be considered overtreatment in the context of HIFU ablation – as a general principal in clinical

practice the minimum input dosage necessary should be used to achieve the desired effect in order to minimise side-effects. This study also demonstrated that cavitation was initiated before hyperecho formation – an important finding in the context of cavitation monitoring. Khokhlova *et al.* also demonstrated that hyperecho formation was most likely due to boiling bubbles and further noted lesion distortion with migration towards the transducer and shielding of the focal zone when temperatures exceeded 100C [48]. This is a particular concern in the clinical setting – lesion migration increases the risk of injury to vital structures and focal shielding prevents damage at the intended target. It has also been demonstrated that hyperecho may occur in the absence of any histological tissue damage [87].

B-mode analysis is also an active process – sufficient time is required for the device to send and receive the signal on each element to create a complete image. HIFU intensities are several orders of magnitude greater than diagnostic ultrasound and therefore interfere with image construction when both are active simultaneously. This prevents true real-time monitoring of treatment. In the pre-clinical setting, it is possible to interlace the diagnostic and therapeutic pulses to prevent interference, by forming images during a quiescent period in HIFU excitation. However, in the clinical setting, currently available devices simply wait until after the HIFU exposure (typically 2-5 seconds) is completed before taking a further B-mode image.

2.5.2.2 Other US-based monitoring techniques

A variety of other ultrasound-based monitoring techniques are available, although all currently remain experimental. As tissue is heated, its compressibility and density change leading to shifts in ultrasonic propagation speeds.[27] Echo-shift thermometry uses these local changes in the speed of sound as a surrogate for temperature changes.[88-90]

Measurement of changes in backscattered signal as a result of changes in tissue compressibility may also provide non-invasive temperature information.[91]

Ultrasound elastrography images tissue stiffness by tracking speckle shifts in the RF echo signal following application of a force to the tissue.[92, 93] This technique has been used in the clinical setting for the assessment of lesions produced in the prostate following HIFU. A mean 50% decrease in strain was seen following treatment although tumours were only occasionally seen on pre-operative elastograms.[94]

2.6 Cavitation monitoring

Acoustic cavitation may greatly enhance local heat deposition. However, in the context of monitoring HIFU ablation, its acoustic emissions signature is of more interest. The broadband signals produced as bubbles undergo inertial collapse in a chaotic fashion are thought to be the only source of broadband emissions in therapeutic ultrasound. Moreover, cavitation emissions quantifiably correlate with tissue heating and ablation during HIFU [62, 95]. The onset of cavitation occurs in advance of the appearance of hyperecho and therefore also has the potential to be a more sensitive marker of thermal ablation [46]. Cavitation emissions propagate in all directions and therefore can be detected remotely without the need for implantable detectors thus satisfying the non-invasive requirement.

Cavitation can be detected using either active or passive techniques. Active detection methods have been studied widely and have given reliable results [96-99]. Whilst accurate, active cavitation detection functions through the use of an active diagnostic pulse similar to B-mode ultrasonography. This signal must be carefully synchronised with the high-amplitude HIFU signal to avoid saturation during HIFU exposure and data acquisition. This eliminates active detection as a real-time monitoring technique – it may provide feedback *after* an

exposure but is unable to monitor or modulate *during* the exposure. However, using an acoustic receiver in passive mode (without any active pulse) it is possible to receive cavitation emissions in real-time without interference and determine the temporal, spatial and amplitude parameters of the source.

Previous work conducted at the University of Oxford has demonstrated that the local heating rates are proportional to the signal power received using a PCD [100]. Further work carried out at Boston University demonstrated that cavitation was initiated some 25 seconds before a hyperecho bright-up was visible using active B-mode imaging during a 1.1MHz insonication of an agar-graphite phantom [46]. A single element PCD provides valuable information about the onset, duration and amplitude of cavitation activity. Whilst informative, little spatial information is obtained about the location of cavitation activity. The absence of an active signal prevents the use of time-of-flight data to calculate the cavitation source location unless the PCD is scanned across the zone of ablation. However, if an array of PCDs is used, source localisation becomes feasible [101].

2.7 Passive beamforming

The technique of using passive beamformed data to create spatial maps of acoustic cavitation was first described by Gyöngy and Coussios [102, 103]. They used a commercially available ultrasound system (z.one, Zonare, Mountain View, CA) as a linear array of PCDs to produce a novel cavitation mapping system [103]. This device, when operated in a specific research mode, can be made to function purely as a passive acoustic receiver, eliminating any interference from the driving signal. This allows true real-time cavitation detection. The device also gives access directly to the unprocessed RF data which allows the use of a passive beamforming algorithm. The principles underlying this beamforming method are derived

from the development of a technique for imaging underground acoustic sources using a process called Time Exposure Acoustics first derived by Norton *et al* [104, 105]. As discussed in Chapter 2.4, the collapse of a bubble results in the creation of a spherical wave propagating out from the point of collapse. As such, these emissions can be considered as discrete point sources. Using a single receiver, the time at which a cavitation signal is received is meaningless as there can be no distinction between events occurring further from the transducer at an earlier timeframe and those occurring closer to the transducer but at a later time point. Using an array of receivers however, will give a unique time of arrival at each element for a fixed source point. By applying the appropriate time delay to the signal received by each element of the array and then summing the signal across the entire array, a source intensity map can be constructed for the entire region of interest.

For an in-depth review of the beamforming algorithms associated with passive cavitation mapping, the reader is directed to the doctoral thesis entitled “Passive cavitation mapping for monitoring ultrasound therapy” by Miklós Gyöngy (available at ora.ox.ac.uk) [102].

2.8 Linear array

Most conventional ultrasound scanners function in active mode. Some devices will function in a receive only mode but do not allow full access to the unbeamformed RF data but rather employ a dynamic beamforming technique which limits the amount of post-processing that can be undertaken. Custom built research machines have previously been designed which allow access to channel data but are hugely expensive and beyond the means of most institutions. However, a commercially available ultrasound system, (z.one, Zonare, Mountain View, CA) allows access to this RF data for an acceptable cost. By placing this transducer co-

axial to the therapy transducer, it is possible to passively receive emission data to create accurate source maps in real-time with high temporal and spatial resolution.

2.9 Current Clinical HIFU

Clinical HIFU has expanded significantly since the first attempts to create thermal lesions in the central nervous system. Attempts have been made to treat many different tumour types including intra-cranial, intra-abdominal, pelvic, bone and soft tissue tumours. Extracorporeal, trans-rectal and laparoscopic devices have been designed with such tumours in mind and whilst numerous prototypes exist, only a small number are commercially available and approved for clinical use.

2.9.1 Uses

2.9.1.1 Kidney cancer

Renal cancer is a common tumour in adults; over 7,000 new cases are seen each year in the UK. The majority are organ confined and potentially curable with local therapy. Surgical resection for renal cancer is highly efficacious but morbid. HIFU is one of a number of minimally-invasive therapies to be used for renal masses. The evidence for the role of HIFU in renal cancer is discussed in detail in Chapter 2.11.5.

2.9.1.2 Prostate cancer

HIFU was first used in the prostate in the early 1990s. It was proposed that HIFU would be a suitable non-invasive alternative to trans-urethral resection of the prostate (TURP) – a surgical procedure for benign prostatic hyperplasia (BPH). Results were unsatisfactory [106, 107]. However, HIFU has proved a more effective option in the treatment of prostate cancer (PC) and is licensed for clinical use for this purpose. Early results demonstrated proof of

concept and outcomes were encouraging [108]. However, there were significant concerns about the rate of recto-urethral fistulae and the need for supra-pubic bladder drainage [109].

Since then, numerous groups have published case series demonstrating lower complication rates with more modern HIFU devices together with post-treatment negative biopsy rates of 82-94% [110]. However, the quality of evidence for the use of HIFU in PC is poor, with no randomised controlled trials (RCT) published [110, 111]. Consequently, the current role of HIFU is unclear.

What may be of significantly more interest in the management of PC is the use of focal therapy. It has long been recognised that radical prostate therapy (radical surgical excision, radical radiotherapy, whole gland ablation) may represent overtreatment – excessive treatment with its incumbent morbidity – for disease that is often localised to a zone or side of the prostate gland. Focal prostate HIFU treatment protocols, targeted only at clinically significant PC within the gland have been developed [112]. Early results are promising – after treatment 89% of men had cancer control together with pad-free continence and sexual potency at 12 months, the two major side-effects of radical therapy [113]. Longer term outcomes from RCTs are awaited with interest.

2.9.1.3 Liver tumours

Worldwide, primary liver cancer (hepatocellular carcinoma (HCC)) is one of the commonest cancers due to the high incidence of Hepatitis. In the Western world, hepatic metastases are a common cause of death in patients suffering from various cancer including colorectal, breast, pancreatic and stomach primary malignancies. Surgical resection of liver tumours is often challenging due to the anatomy of the liver and cure rates are relatively low. Minimally-

invasive treatments, including RFA, cryotherapy (CRY) and HIFU can have an important role.

Histological evidence of liver tumour ablation was demonstrated in the Chinese population using the Model JC HIFU device in Chongqing, China. Patients underwent HIFU followed by surgical resection [18]. Illing *et al.*, using the same device, subsequently demonstrated safety and feasibility in a Western population [32]. Most recently, two studies have reported oncological outcomes of patients with unresectable HCC who underwent HIFU [114, 115]. Acceptable morbidity was noted together with reasonable technical success. The exact role of this therapy is difficult to establish – many patients died from disease progression suggesting that sub-total ablation occurred.

One randomised control trial (RT) of liver HIFU has been published and, to date, is the only RCT of any HIFU device. Although seminal, note should be taken of the potential bias in the method of randomisation which merely alternately allocated patients to either treatment group [116]. Trans-arterial chemoembolization (TACE) was compared with TACE and HIFU in 50 patients; the median survival time was 11 *vs.* 4 months in favour of the combined treatment (p=0.004). No major complications occurred. This study suggests a promising role for liver HIFU although supporting data from other studies is lacking.

2.9.1.4 Pancreas

Pancreatic cancer is a common tumour in the Western world and has a dismally poor prognosis in most patients. Symptoms begin late in the disease and surgical resection is often impossible. HIFU can have a significant analgesic effect in those suffering from the chronic, unrelenting back pain often experienced in locally-advanced pancreatic cancer [117]. Wu *et al.* also treated patients with pancreatic cancer and found a reduction in pain together with

involution of both the tumour and its blood supply [118]. Currently, there is no high quality evidence for the use of HIFU in pancreatic cancer.

2.9.1.5 Uterine fibroids

Uterine fibroids are common benign pelvic tumours which are found in the uterus. Histologically they are muscle tumours – leiomyomas. They can be associated with pelvic pain, menorrhagia, inter-menstrual bleeding and pressure symptoms including lower urinary tract symptoms. Much of the commercial activity in extracorporeal HIFU is now aimed at the management of uterine fibroids. This may well be due to the benign nature of the disease – sub-total tumour ablation is entirely acceptable in this condition.

A number of studies have reported tumour ablation, shrinkage of treated leiomyomas and symptomatic relief following HIFU [70, 71]. Minimal morbidity occurs with uterine HIFU and treatment is possible even when overlying bowel appears in the acoustic window [119].

Fibroid HIFU is a promising treatment and may represent a niche market for HIFU manufacturers. However there is a lack of both RCTs and long-term outcome data which currently hinder its wider adoption.

2.9.1.6 Bone

HIFU has been used in both the curative treatment of primary bone tumours and the palliation of symptomatic bone metastases. HIFU is proposed as one component of a limb-sparing strategy for the treatment of osteosarcomas, chondrosarcomas and other primary tumours [120, 121]. It has been used effectively with low morbidity, reduction in pain scores and good long term survival figures. However, no comparative studies or RCTs exist. Bone pain is an extremely common symptom in patients with metastatic disease and the management of its

complications place a huge burden on health resources [122-124]. Symptomatic relief from bone pain has been achieved with HIFU in small case series [125, 126]. HIFU represents an additional option for the treatment of metastatic bone disease however in the absence of comparative studies there is no convincing evidence for its use over existing standard therapies.

2.9.1.7 Breast cancer

The non-invasive nature of extracorporeal HIFU makes a strong case for use in breast cancer, where cosmetic outcome is of considerable importance to many patients. Breast cancer was one of the first solid tumours to be treated with HIFU in published reports [18]. Subsequently, an RCT of radical mastectomy *vs.* HIFU followed by radical mastectomy was performed. This study demonstrated that breast HIFU was safe and that HIFU-treated breast tumour cells had lost their ability to proliferate, invade and metastasis, based on immunohistochemical analyses [33]. No long term follow-up or survival data was published. Since then a number of case series have been published but no comparative studies.

2.9.1.8 Brain tumours

There is a potential role for HIFU in the management of intra-cranial tumours. Surgical excision of tumours may be feasible but is associated with complications and the risk of significant neurological deterioration. Trans-cranial focusing of HIFU is challenging due to the significant phase and amplitude aberrations introduced by the skull which grossly distort the beam shape. However, using 3D-CT tomography, time-reversal algorithms can direct an ultrasound array to produce HIFU which is focused within the skull [127]. Since then, animal studies have demonstrated the feasibility of intra-cranial tumour ablation [128, 129]. To date, there are no published clinical studies.

2.9.2 Devices

Existing clinical HIFU devices are extracorporeal, trans-rectal or laparoscopic. Extracorporeal are most commonly used for HIFU treatment of intra-abdominal and intra-pelvic tumours; their transducers are large and have relatively long focal lengths (10-16cms). Both US-guided and MR-guide devices are in clinical use. Trans-rectal devices are specifically designed for the treatment of PC, are inserted into the rectum and have small transducers with short focal length (3-4cms). Similarly, laparoscopic HIFU devices are inserted into the abdominal cavity and applied directly to the tumour surface – their transducers are also small with a 3-4cm focal length.

2.9.2.1 Extracorporeal HIFU

2.9.2.1.1 Model JC/JC200, Chongqing HAIFU

The Model JC HIFU device (HAIFU™ Technology Company, China) was the first commercially available extracorporeal device. The first UK installation, shown in Figure 7, was at the Churchill Hospital (Oxford, UK). It uses PZT transducers of varying sizes (10-20cm) which are focused using an aluminium alloy lens. The focal length and HIFU frequency is transducer-specific but varies from 10-16cm and 0.8-1.2 MHz respectively. The moveable treatment head comprises the therapeutic transducer and a co-axially mounted 3.5MHz diagnostic ultrasound transducer used for imaging and treatment monitoring. This device holds a CE mark (Conformité Européene; 2005) awarded following proof of safe use in humans.

Figure 7 – The Model JC HIFU device installed at the Churchill Hospital (Oxford, UK). This was the first UK – installed clinical HIFU device (2002)

The Model JC200, from the same company, is an upgraded version of the original JC device. It was awarded a CE mark in 2007. The first UK installation was again at the Churchill Hospital, as shown in Figure 8. Both the software and hardware are similar, but the device has considerably smaller physical dimensions. A variety of HIFU transducers are available which are mounted around a modern 3.5MHz diagnostic ultrasound probe.

Figure 8 - The Model JC200 HIFU device installed at the Churchill Hospital (Oxford, UK). This was the first UK installation of this device (2011)

2.9.2.1.2 ExAblate 2000/2100, GE Insightec

The ExAblate 2000 (Insightec, Haifu, Israel) was the first commercially available MR-guided HIFU device. It uses a 10cm, 1.5MHz focused transducer which is compatible with either

1.5T or 3.0T MRI machines. The device received a CE mark in 2002 for the treatment of uterine fibroids and further CE marks in 2007 & 2010 for the palliation of bone metastases and adenomyosis respectively. The updated ExAblate 2010 device, shown in Figure 9, is marketed as the ExAblateOR & ExAblateOne. They are licensed for use in uterine fibroids and are currently being assessed in clinical trials for use in various other tumours.

Figure 9 – The GE Insightec ExAblate MR-guided HIFU device (image taken from http://www.insightec.com/ExAblate-OR.html)

2.9.2.1.3 Sonalleve, Philips

The Sonalleve MR-HIFU device (Philips, USA) is compatible with 1.5T or 3.0T MRI machines and is shown in Figure 10. It comprises a 256-element phased array which can operate at either 1.2 or 1.5MHz. Its focal zone size can be adjusted from 4-16mm (transverse) and 10-40mm (axial). It is licensed for use in the treatment of uterine fibroids and the palliation of bone metastases.

Figure 10 – The Philips Sonalleve MR-HIFU device (image taken from http://www.healthcare.philips.com/gb_en/products/mri/systems/sonalleve)

2.9.2.2 Trans-rectal HIFU

Two commercially available trans-rectal devices exist for the treatment of PC. Both are ultrasound-guided and require positioning in the rectum under general anaesthesia.

2.9.2.2.1 Ablatherm, Ablatherm

The Ablatherm (Ablatherm,, Technomed International, France) system consists of a treatment bed, probe positioning system, cooling system and a diagnostic scanner. The therapeutic focused transducer functions at 2.25-3.0MHz and has a focal length of 4cm. The diagnostic probe has a 7.5MHz centre frequency. The device software creates an automated treatment once the treatment boundaries are defined. The Ablatherm received its CE mark in 2000 for the treatment of PC.

2.9.2.2.2 Sonablate-500, Focus Surgery

The Sonablate-500 (Focus Surgery, USA) has a 4MHz curved PZT transducer with a selectable focal length of 3/4cm. It has a central diagnostic imaging transducer and the software requires the manual input of treatment parameters. It was originally used in the treatment of BPH but was subsequently awarded a CE mark in 2001 for the treatment of PC.

2.9.2.3 Laparoscopic HIFU

The Sonablate device (Focus Surgery, USA) was also available as a laparoscopic device as well as a trans-rectal device. The system consisted of a mountable arm together with a probe which could be inserted through a standard laparoscopic port. A 4MHz PZT transducer or 3/4cm focal length produced the therapeutic signal with a centrally-positioned diagnostic transducer for imaging. The device was used in Phase I clinical trials at the Churchill Hospital (Oxford, UK) with modest success [130]. Further device development is currently in progress.

2.9.3 Safety & Limitations

In the research setting, HIFU has been extensively investigated and can be used to create repeatable, accurate and controlled ablation without damage to surrounding regions outside the focal zone. However, it is of paramount importance that similar principles can be carried through to a clinical setting.

Concerns about the risk of metastasis have been addressed in Chapter 2.4.3. Clinical studies of HIFU treatment of a variety of solid tumours have demonstrated an acceptable side-effect profile.[32, 35, 131-133]. Pain following treatment is common, and is usually mild and transient, requiring only oral non-opiate analgesia in the vast majority of cases. A post-ablation syndrome has been described, consisting of fever, malaise and constitutional upset following various thermal therapies.[134] This occurs following release of intra-cellular debris and the probability of its occurrence is proportional to the volume of ablated tissue. It is uncommon and temporary, although symptoms may persist for up to seven days after treatment.

Skin toxicity is the most frequently occurring side effect other than pain. In the vast majority of cases, this is limited to small, superficial burns analogous to mild sunburn – these occur in one third of patients [32]. Whilst common, the frequency of skin toxicity should be taken in context of the non-invasiveness of the therapy; both open surgery and other thermally ablative treatments require skin incision or puncture. Significant full thickness burns have rarely been reported and are avoidable if attention is been paid to intra-operative examination and imaging [135]. Injury to adjacent vital structures following HIFU has also been reported, although is rare and avoidable.

In the context of trans-rectal HIFU, procedure-specific complications may occur. Trans-rectal devices ablate prostate tissue through the rectal wall and as a result rectal injury has been reported. The consequential recto-urethral fistula can be very serious for the patient and is difficult to treat, usually requiring major surgery. Early studies reported fistula rates of 6% - unacceptable to the majority [136]. However with the use of rectal wall cooling and technique development, reported fistula rates are now less than 1% [137]. Both urinary incontinence and impotence are both side-effects seen in all surgical treatments for PC. At the very least, they seem to occur less commonly than with radical prostatectomy.

To date, HIFU remains an experimental treatment for many solid tumours except PC where acceptable oncological outcomes have been achieved [138]. The attenuation of the rib cage, abdominal wall and intra-abdominal fat has not been entirely overcome and difficulties with image and target registration due to respiratory motion require further investigation. Treatment times remain lengthy and it is remains difficult to treat tumours through bone and those within hollow organs.

2.10 The Kidney

2.10.1 Anatomy

The paired kidneys lie in the retroperitoneum and occupy a cranial position within the abdomen, as shown in Figure 11. They are partially covered by the ribs posteriorly and are closely related to the small and large intestine, stomach, pancreas, diaphragm, spleen (left) and liver (right). The kidneys receive a sizeable proportion of the cardiac output (20-25%; 1-1.25l/min) via the paired renal arteries which are direct branches of the abdominal aorta arising at the L3 vertebral level. Both renal arteries separate into anterior and posterior branches which branch to supply individual segments of the kidney. Paired renal veins formed from the amalgamation of venous tributaries which then drain into the inferior vena cava.

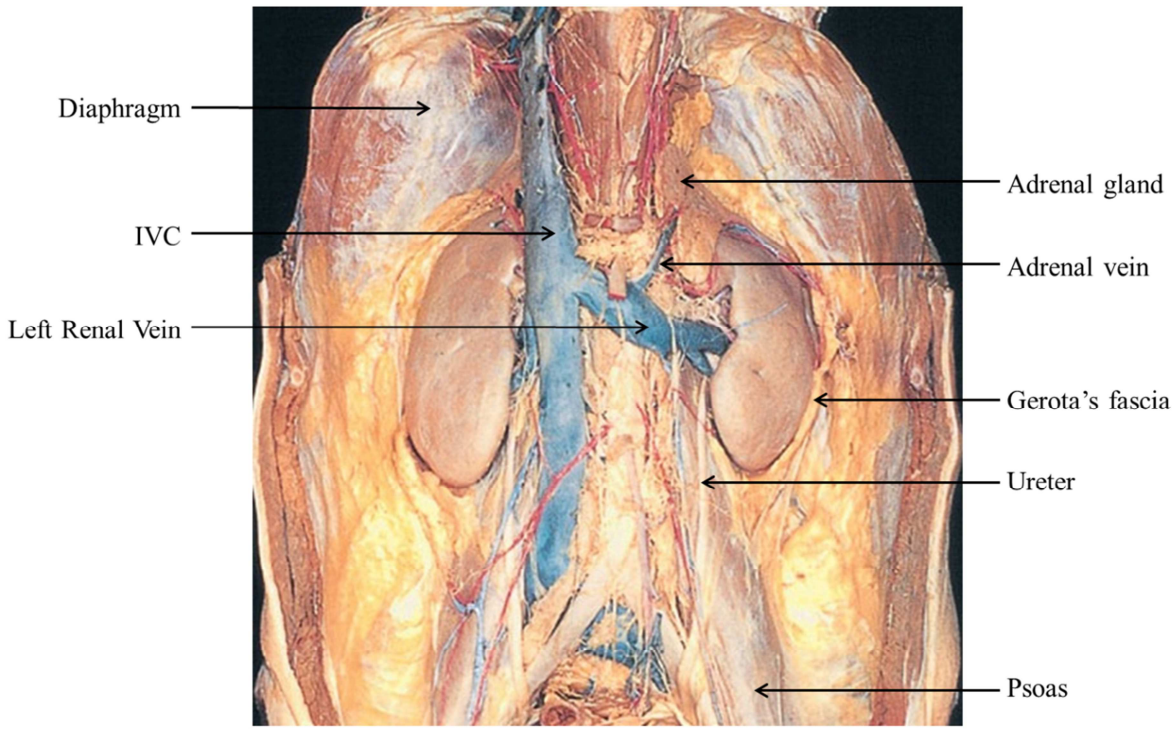

Figure 11 – Gross anatomy of the kidney demonstrating their cranial and posterior position within the abdomen

2.10.2 Function & physiology

The kidney has numerous vital functions in the maintenance of homeostasis. It functions to excrete the waste products of protein catabolism, principally urea as well as maintaining the acid-base balance by the reabsorption of bicarbonate and the excretion of H^+ ions. The kidney also regulates osmolality via the re-absorption of sodium ions, chloride ions and water. Through this mechanism it also regulates the long-term control of blood pressure. Finally, the kidney produces erythropoietin which stimulates the production of red blood cells, renin which is a key component of the renin-angiotensin system which help to maintain salt and water homeostasis and activates Vitamin D which leads to the renal reabsorption of phosphate.

2.11 Renal Cancer

2.11.1 Epidemiology & biology

Renal cancer is the eighth most commonly occurring cancer in the UK, with over 8,000 new diagnoses annually – see Table 2 [139]. It represents three percent of all UK cancers and results in over 3,000 deaths per year.

Table 2 – Number of new cases and rates of kidney cancer (UK 2007)

	England	**Wales**	**Scotland**	**N.Ireland**	**UK**
New Cases (2007)					
Males	4,236	315	463	151	5,165
Females	2,465	182	334	82	3,063
Persons	6,701	497	797	233	8,228
Crude rate per 100,000 population					
Males	16.9	21.7	18.6	17.5	17.3
Females	9.5	11.9	12.6	9.1	9.9

Persons	13.2	16.9	14.9	12.5	13.5

2.11.2 The changing face of renal cancer

There has also been a notable increase in the incidence of kidney cancer over the last 30 years [139]. This rise can be partly attributed to the more widespread use of abdominal imaging (ultrasound, CT, MRI) but there has also been a real increase in the occurrence in renal tumours. Changes in UK kidney cancer incidence over this time period are clearly demonstrated in Figure 12 [140-142].

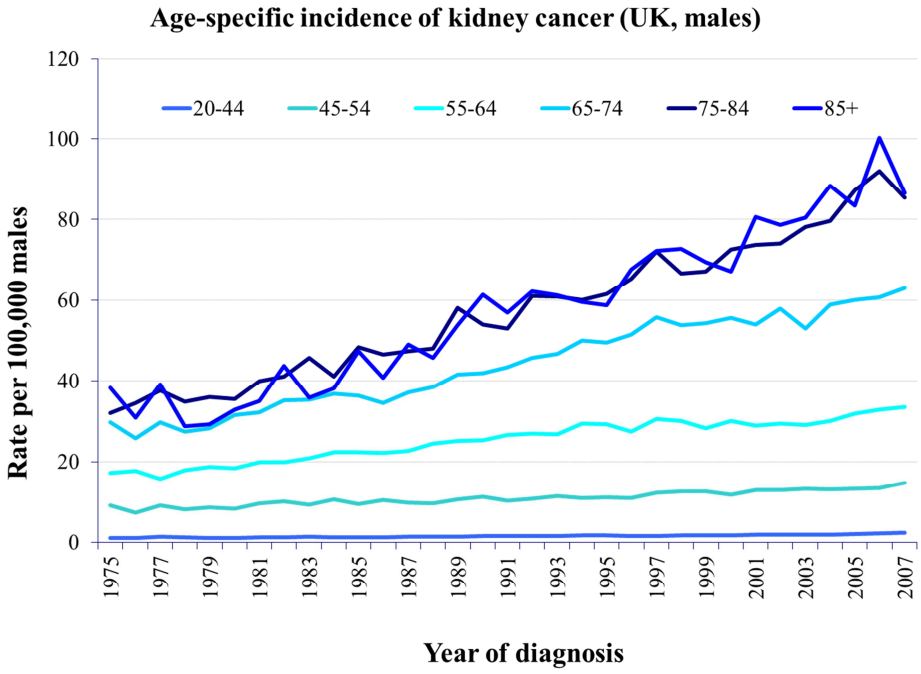

Figure 12 – Age-specific kidney cancer rates (UK males)

A similar increase in incidence is seen in females. Renal cancer remains a highly lethal disease, and survival statistics demonstrate this with just 50% of patients alive five years after diagnosis – see Figure 13 [139].

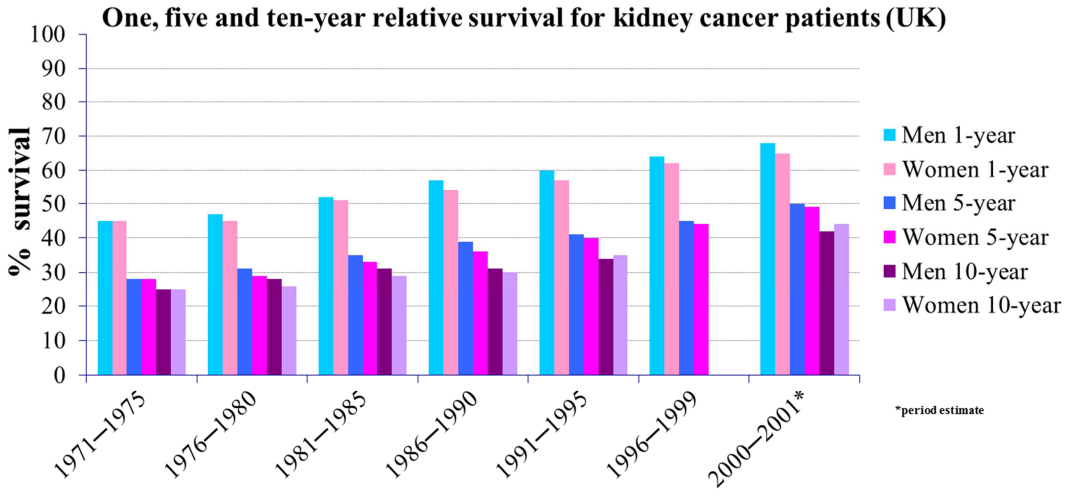

Figure 13 – UK kidney cancer survival statistics

Further analysis of Figure 12 reveals that the increase in incidence has occurred mostly in the older population. Observational studies have demonstrated a doubling in incidence over a 15 year period in those aged 65 and over [142]. A further consequence of the increase in abdominal imaging is earlier diagnosis during the asymptomatic phase. Many renal tumours are now discovered incidentally during the investigation of other symptoms – these tumours are often small (<4cm) at the time of diagnosis. Small renal masses often grow slowly and usually do not pose a threat to life [143, 144]. Observations on the small renal mass (SRM) show metastatic disease is rare in tumours <3cm in maximum diameter [145]. Active surveillance of the SRM is a potential treatment option, however radiographic imaging alone cannot determine high-risk tumours and thus it is only recommended when surgery is not safe or feasible [146].

2.11.3 Current treatment strategies

Surgical excision is the gold standard treatment for locally confined renal cancer if the patient is fit for the procedure. Open radical nephrectomy (RN) has been the traditional procedure for decades and associated with high cure rates. The advent of laparoscopic surgery led to shift

towards laparoscopic RN over open procedures. No RCTs are available that adequately compare oncological outcomes for these two procedures. However, oncological equivalence was demonstrated in two non-randomised studies [147, 148]. Laparoscopic surgery was also associated with a shorter hospital stay [149]. Whilst laparoscopic RN was increasingly used, there was an enlarging body of evidence of nephron-sparing surgery (NSS) primarily in the management of the small (<4cm) renal tumour. Preservation of normal renal parenchyma using partial nephrectomy (PN) preserves renal function and is associated with a lower risk of subsequent development of renal failure [150-152]. Open PN achieves similar oncological outcomes as RN [153-156]. PN is a more challenging procedure and therefore associated with a greater risk of complications [157]. Laparoscopic PN is an even more challenging procedure, with significant complication rates. Despite this, oncological outcomes appear broadly equivalent to both open PN and RN [157].

The current standard is that PN should be undertaken for small (<4cm, T1s) localised renal tumours, given the similar oncological outcomes. This is based in no small part on data which suggest that RN is associated with higher overall mortality rates due to chronic renal insufficiency resulting in higher risk of cardiovascular disease [158-162]. However, it should be noted that an RCT comparing oncological outcomes of NSS with RN demonstrated NSS to be *less* effective than RN in terms of overall survival which is not explained by death from renal cancer [163].

2.11.4 Minimally invasive therapy for renal cancer

In terms of oncological outcome, there is no requirement for an alternative treatment option. Surgery is highly effective. However, it is also morbid. Complication rates are significant with all forms of PN [157]. In particular, surgery is especially risky in the elderly age group

who have the highest incidence of renal cancer. In a series of 35 nephrectomies in patients aged over 80, the transfusion rate, early complication rate, re-hospitalisation rate and peri-operative mortality rate was 46%, 31%, 11% and 9% respectively [164].

It is evident that there may be a role for a less-invasive treatment for kidney cancer which commands good oncological efficacy together with a low morbidity. A number of thermally ablative therapies have the potential to fulfil this role.

Both radiofrequency ablation and CRY have developed into clinically acceptable treatments for small tumours – medium term data demonstrates reasonable oncological control from over 1,300 cases.[165] Complication rates with both procedures are low although tumour puncture is required in all cases, resulting in a risk of haemorrhage, urine leak and tumour seeding in the abdominal cavity. Oncological control with CRY is superior but is the procedure is usually performed via the laparoscopic approach requiring surgical incision and significant dissection around the kidney.[165]

2.11.5 History of HIFU in renal cancer

The first published studies on the use of HIFU in the kidney date back for the early 1990s. Chapelon *et al.* used two transducers (1MHz, 2.25MHz) to create HIFU lesions in healthy rat and canine kidneys [166]. The first clinical reports appeared soon after this – using both light and microscopy, histology demonstrated clear evidence of coagulative necrosis with sharply defined margins produced in healthy kidney tissue [167]. Renal tumour ablation was first reported in rabbits – a VX-2 renal tumour suspension was injected into the renal arteries or directly into the renal parenchyma. Open direct contact HIFU and transcutaneous HIFU were undertaken; histological evidence of ablation was seen in most animals [168]. Interestingly, transcutaneous HIFU was limited by poor quality diagnostic imaging of the small tumours, a

problem which continues to hinder renal HIFU in the present day. The clinical case report of HIFU treatment of renal tumours was published in 2002 – three general anaesthesia HIFU sessions were undertaken in three separate tumours in one patient. Necrosis and tumour involution was seen at a six month MRI in two cases; a third upper pole tumour showed no evidence of ablation due to absorption of HIFU by the overlying ribs [169]. To counter the difficulties of HIFU due to the abdominal wall and rib cage, a laparoscopic HIFU probe was designed and tested in animals, demonstrating successful ablation in 12/13 porcine renal units [170].

Using the Model JC HIFU device, Wu *et al.* treated 13 Chinese patients with advanced symptomatic renal malignancy. Haematuria resolved in 7/8 patients and metastatic flank pain resolved in 9/10 patient. In addition, a reduction in tumour perfusion together with tumour involution was noted in all patients [131]. This was the first study to report any clinically relevant outcomes in renal HIFU. Using the same device, renal HIFU was undertaken in non-metastatic renal tumours at the Churchill Hospital (Oxford, UK). The purpose of this study was to assess the feasibility of treating typical patients in the Western world who have larger abdomens and thicker fat layers. Renal tumour ablation was found in two-thirds of patients although imaging was challenging [32]. Clinical safety studies demonstrated that renal HIFU was associated with low morbidity [32, 171].

The first clinical reports of renal HIFU using a laparoscopic probe came from a multi-centre study conducted in Oxford (UK), Turin (Italy) and Vienna (Austria). Successful ablation was achieved without morbidity in patients after a number of modifications to the device. However, viable tumour was noted within regions of ablated tumour and at the probe-tumour

interface [36, 130]. Significant peri-nephric fat ablation was also noted if this was not removed from the tumour surface prior to treatment [130].

2.11.6 Current clinical role of renal HIFU

To date, the only published report of renal HIFU with follow-up was published in 2010, from patients recruited into the Phase I/II feasibility study conducted in Oxford discussed in Chapter 2.11.5 [172]. In total 15/17 recruited patients were treated, with two abandoned treatments. No major complications occurred in any patients although minor skin burns and pain were common. MRI evidence of ablation was seen in 7/15 patients. By six months, mean tumour cross-sectional area (CSA) had decreased by 12%. However, five patients had irregular persistent enhancement within their tumour and underwent alternative treatments (RFA, surgery). At a mean of 36 months after treatment, ten patients remained under follow-up with a mean 30% reduction in tumour CSA and central loss of enhancement in all.

This study generated a number of unanswered questions which are fundamental to understanding the future role of clinical HIFU:

i) What was the tumour pathology – did all patients have renal cancer?
ii) Why was MRI ablation seen in less than half of patients?
iii) Do the ten patients under follow-up have a benign or malignant tumour?
iv) Does viable tumour remain in the ten patients under follow-up?

The need for a further Phase I/II clinical trial of HIFU in kidney cancer is evident. Of paramount importance is the pathological diagnosis – all patients should undergo biopsy or resection to establish whether the tumour is benign or malignant. Additionally, the extent of tumour ablation should be established using histological *and* radiological assessments.

2.12 Contributions of the current work

Ultrasound is a versatile modality and can be used both diagnostically and therapeutically. This chapter has demonstrated that ablation is possible in both ex-vivo, animal and clinical settings. In the context of kidney cancer, the need for a safe, effective, minimally-invasive treatment has been proven and previous studies, whilst interesting, have lacked conclusive data to determine the role of HIFU in this disease. The need for a further clinical renal HIFU study with pathological analysis has been demonstrated.

It is also clear that little is known about demographics and tumour characteristics of those most suitable for renal HIFU. Patient selection criteria should be defined to improve outcomes. Similarly, features of different renal tumours may make their treatment easier – these criteria should be explored and defined to allow the appropriate treatment of those who might benefit and the protection of those who will not.

The lack of a truly effective real-time monitoring system for HIFU treatment is evident given the sub-optimal efficacy of existing methods. There is undoubtedly a role for a new technique which can be integrated with existing devices. Laboratory-based work has already established that PAM could achieve this aim and ex-vivo and clinical studies are required to confirm this.

3 Clinical results of extracorporeal renal HIFU

This chapter outlines the design, implementation, conduct and results of an ethically approved clinical trial of HIFU treatment of stage T1a renal cancer.

3.1 Introduction

3.1.1 Rationale

Ultimately, the effectiveness of a new cancer treatment can only be determined from carefully conducted clinical trials. Laboratory and animal studies establish proof of concept and determine treatment parameters but oncological outcomes can only be determined in human trials. Pre-clinical research in renal HIFU demonstrated promising results and suggested an important role in the context of managing the small renal mass. However, disappointing early clinical results limited enthusiasm for further trials, thereby depriving the medical community of the opportunity to assess the improved results that often accompany the evolution of new technologies.

A number of centres investigated the efficacy of renal HIFU as the technology was brought into the Western world, discussed in Chapter 2.11.5. Subsequently, the first clinical study with significant follow-up came from the Oxford Clinical HIFU Unit – see Chapter 10.6. At a mean three year follow-up, stable or involuting renal lesions were seen in two-thirds of

patients. Serial radiology over this time period provides vital information on the evolution of tumour size and morphology. However, the absence of histological outcomes limits the impact of the study. A significant proportion of SRMs may be benign (10-20%) and tumour stability or involution is not definitive proof of the absence of viable tumour cells. Moreover, successful surgical outcomes for renal tumours are determined by the completeness of excision, with emphasis placed on the presence or absence of viable cancer at the tumour margin. Such an assessment, in the absence of post-treatment biopsy, is not possible with ablative therapies.

The aforementioned trial also included a small surgical arm, comprising six patients who underwent surgical resection following HIFU treatment. Whilst informative, the results are limited by the small heterogeneous group of patients treated. As such, and given the above limitations of previous work, a trial protocol was designed by the author, to provide both radiological and histological outcome of renal HIFU.

3.1.2 Aims & objectives

i) To conduct an ethically approved clinical trial of HIFU treatment of small renal tumours, with combined radiological and histological follow-up.
ii) Improve patient selection of future treatments through the analysis of HIFU treatments and their outcomes.
iii) Define specific limitations of current renal HIFU treatment in order to define areas requiring further research.

3.1.3 Hypotheses

i) Extracorporeal HIFU can consistently and accurately be used to ablate small renal tumours successfully, assessed using post-resection histology
ii) Contrast-enhanced MRI can accurately predict the size and location of the zone of ablation following renal HIFU

iii) Results from this clinical study of renal HIFU can be used to define patient selection parameters and future research to improve clinical outcomes

3.2 Patients & methods

All patients with newly diagnosed stage T1a (<4cm) renal tumours on cross-sectional imaging were identified and screened for inclusion in the trial. Currently, diagnosis of a renal tumour suspicious for malignancy requires evidence of contrast-enhancement following administration of an intravenous contrast agent (Omnipaque^{TM} for CT; gadolinium for MRI). Diagnosis was made by a one of a number of radiologists. It is not currently considered standard practice to obtain histological evidence of malignancy in renal cancer, although pre-treatment biopsy, particularly in the context of minimally-invasive ablative therapies, is becoming increasingly common. To this end, some patients in this clinical study had pre-treatment biopsies.

3.2.1 Protocol design

The protocol design is summarised in a flowchart in Figure 14. Patients were identified through a combination of a) urology outpatient clinic visits, b) uro-oncology multi-disciplinary meetings & c) uro-oncological radiology meetings. A formal referral was made by the clinician-in-charge to the HIFU research team. All referred patients were reviewed by the lead research fellow (author) to discuss inclusion in trial. Trial information leaflets were distributed and further contact was made with the patient between 24 hours and seven days following initial contact. Following agreement to participate in the trial, informed consent to take part in the trial was gained recorded in the case report form (CRF).

Fundamental to the protocol design is the inclusion of both radiological and histological follow-up. Traditionally, the Oxford Clinical HIFU Unit has used CE-MRI to assess the zone

of ablation following HIFU treatment, primarily due to its greater soft tissue contrast in comparison with contrast-enhanced CT. However, the accuracy of CE-MRI in renal HIFU is not known. Equally, as discussed, oncological outcomes in renal HIFU are not certain. Formal surgical resection after renal HIFU therefore offers a number of benefits: a) provides definite evidence of the extent of ablation, b) provides a reference standard for assessing CE-MRI and crucially, c) ensures the patient receives the current best possible treatment with the aim of a complete cure.

Figure 14 – Protocol flowchart demonstrating steps in renal HIFU clinical trial

3.2.2 Ethical & trust management approval

An application for ethical approval to conduct this clinical trial was made (by the author) to the Oxfordshire Research Ethics Committee (OxREC) C. The application was to screen, enrol and treat 20 patients with newly diagnosed non-metastatic T1a renal tumours over a 24 month period. This period was subsequently extended to 36 months due to slow patient recruitment. The application covered treatment at a single centre (Churchill Hospital, Oxford) in a non-commercial clinical trial. Ethical approval was granted by OxREC C on 18th May 2009 under approval number 09/H/0606/42. Approval confirmation from the committee can be viewed in Chapter 10.1.1.

Simultaneously, an application for trust management approval was made to the Oxford Radcliffe Hospitals NHS Trust. This covered use of NHS property and resources for all aspects of the trial conduct. Approval confirmation can be viewed in Chapter 10.1.2. Prior funding for the trial had been previously sought and granted by the Oxford Biomedical Research Centre, which itself is funded by the National Institute for Health Research. Trial funding covered all aspects of the trial considered to be outside of routine care for patients with newly diagnosed non-metastatic T1a renal cancer. Confirmation of funding from the Oxford Biomedical Research Centre can be viewed in Chapter 10.1.3.

3.2.2.1 Substantial amendment

An application for a substantial amendment to the trial protocol was made to OxREC C ethics committee in June 2010 to request use of both the original extracorporeal HIFU device (Model JC) and the new device (Model JC 200). Approval for the protocol amendment was given on 30th July 2010. Approval confirmation from the committee can be viewed in Chapter 10.1.4.

3.2.3 Inclusion & exclusion criteria

The trial enrolment inclusion and exclusion criteria can be viewed in full in Chapter 10.1.5. The key requirements were the presence of at least one newly diagnosed non-metastatic T1a (<4cm) renal tumour suspicious for malignancy on cross-sectional imaging. The tumour identified for HIFU was suitable for surgical resection in the opinion of one of two urological surgeons (Mr David Cranston & Mr Mark Sullivan). Surgical resection was performed via the open, laparoscopic or robotic approach and either a radical or PN was undertaken. Each participant's general health and blood parameters was clinically acceptable for general anaesthesia and renal surgery. The index tumour demonstrated adequate visualisation on diagnostic B-mode ultrasonography, including clear identification of tumour boundaries and surrounding vital structures. No children, pregnant women or prisoners were recruited.

3.2.4 Enrolment procedure

3.2.4.1 Initial Screening

All patients identified with T1a renal tumours underwent initial screening which included a formal review of their most recent cross-sectional imaging (usually CT; occasionally MRI) to assess their suitability for HIFU and a review of medical history, recent blood results and referral letter. A review of recent radiological imaging was conducted by the research team in conjunction with the operating surgeon. Those considered appropriate for trial enrolment were then formally referred to the research team for review at the same outpatient visit. This review consisted of an invitation to participate in the trial, together with clear verbal and written explanations of the trial conduct and its benefits & side-effects. Potential participants were then given a period of time (24 hours to 7 days) to consider the invitation. A mutually agreed time for further telephone contact was arranged at which time potential participants

were asked to accept or reject the invitation. Those that declined participation were returned to standard NHS care. Those that agreed participation were invited to final screening.

3.2.4.2 Final Screening

Final screening began with the taking of informed consent to enrol in the trial. This was recorded through the signing of the trial consent form which can be seen in Chapter 10.1.6. The purpose of this process was to ensure that the renal tumour was adequately visualised using B-mode ultrasound using both a handheld ultrasound probe (Toshiba™ for Model JC; Esaote™ for Model JC-200) and the extracorporeal device probe (same manufacturers). The initial handheld scan involved a formal ultrasound of the affected kidney and then careful localisation of the tumour with the aid pre-existing CT/MRI images. Successful handheld ultrasound required visualisation of the tumour, its boundaries and surrounding vital structures.

The subsequent ultrasound scan using the co-axial diagnostic ultrasound mounted within the treatment head was a vital component of final screening. This process involved placing the patient in the position required for formal treatment. In the context of renal HIFU, this was either left lateral or right lateral depending on the side of the tumour. Often patients were rolled up to 45° towards the supine position to improve the acoustic window, particularly for posterior tumours. During screening patients were asked to hold this position; during treatment cushioned supports and straps were used to immobilise the patient during anaesthesia. The water reservoir was filled with degassed water (warmed during screening; chilled during treatment to reduce skin burns). The additional stand-off between probe and patient meant that imaging deteriorated compared with handheld imaging. It was therefore vital to undertake the device ultrasound scan meticulously to again ensure that the tumour

could be visualised adequately for treatment. A number of patients failed final screening despite satisfactory handheld ultrasound imaging due to the deterioration in image quality using the HIFU device – this is discussed in detail in Chapter 3.4.1.2.

Following successful final screening, a HIFU treatment date was arranged. This required recruitment of an anaesthetist and anaesthetic nurse for general anaesthesia and reservation of the appropriate anaesthetic equipment and drugs. Treatments were arranged within four weeks of final screening (often sooner) unless the patient or surgeon requested otherwise. If final screening was unsuccessful, patients were returned to standard NHS care.

3.2.5 HIFU treatment

3.2.5.1 HIFU Device

HIFU treatment was performed under general anaesthesia using either the Model-JC or Model JC-200 Focused Ultrasound Tumor Therapeutic System (HAIFU™, Chongqing, China). The treatment head is mounted on a positioning system in a flexible rubber bath filled with degassed water. Three orthogonal movements and three rotational movements are possible. The treatment head comprises both a therapeutic and diagnostic transducer aligned co-axially – see Figure 15.

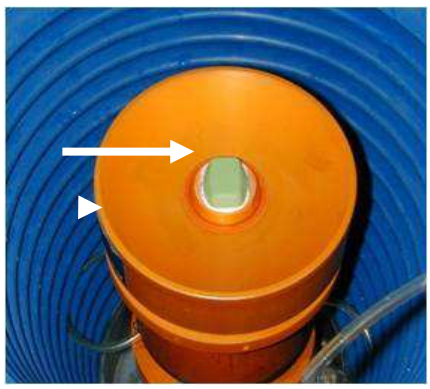

Figure 15 – Picture of treatment head from Model-JC HIFU device showing therapeutic transducer (arrow head) mounted co-axially with the diagnostic transducer (arrow)

3.2.5.2 Anaesthesia & Positioning

The skin overlying the tumour was cleaned, shaved and degassed with a suction device to maximise image quality and minimise bubble entrapment. The screening ultrasound was repeated to ensure treatment remained feasible. General anaesthesia was induced and the patient carefully positioned using a combination of (inflatable) cushions, pillows and straps. It was essential to ensure complete immobilisation to facilitate safe treatment. Pressure points were carefully protected using cushions & padding. Endotracheal intubation was performed with a dual lumen tube to allow single lung ventilation if required – this prevented any lung excursion on the side of treatment thereby minimising respiration movement of the kidney – see Figure 16. Where necessary, the isolated lung was also inflated or deflated to provide either caudal or cranial shift of the kidney respectively, if the imaging was obscured by an intervening rib. Intravenous hydrocortisone was administered to reduce the risk of tissue swelling during treatment as this can significantly limit imaging quality.

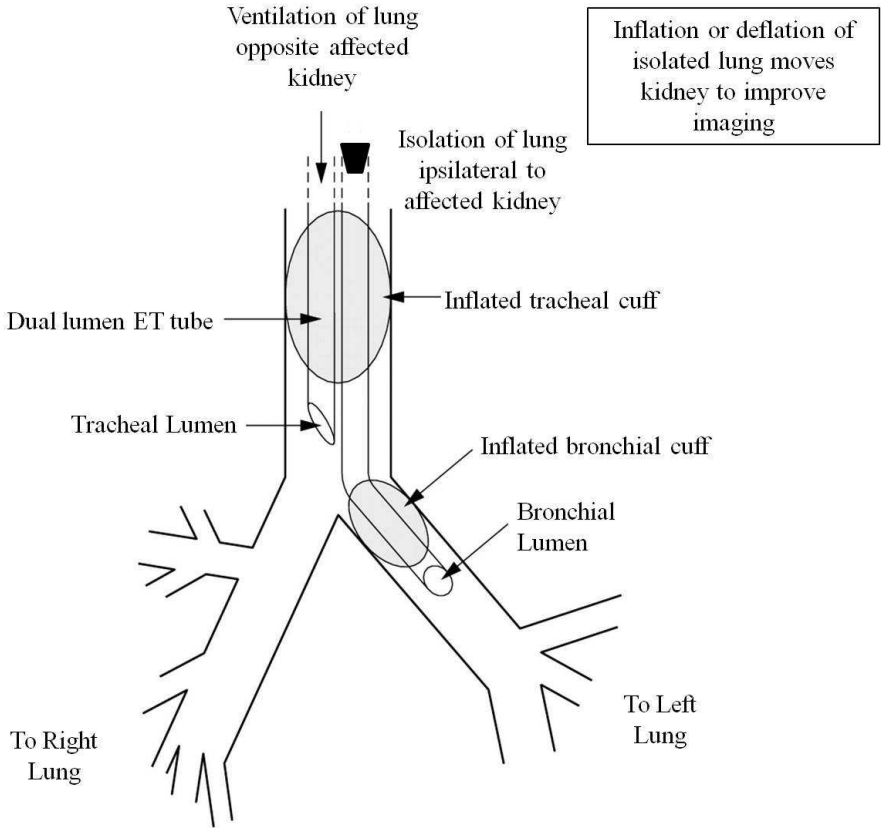

Figure 16 – Use of a dual lumen endotracheal tube facilitates single lung ventilation, thereby minimising respiratory excursion of the kidney during HIFU treatment (adapted from http://thorax.bmj.com/content/58/9/814.extract)

3.2.5.3 Treatment planning

The operator console houses the computer systems which control movement and activation of the treatment head, shown in Figure 17.

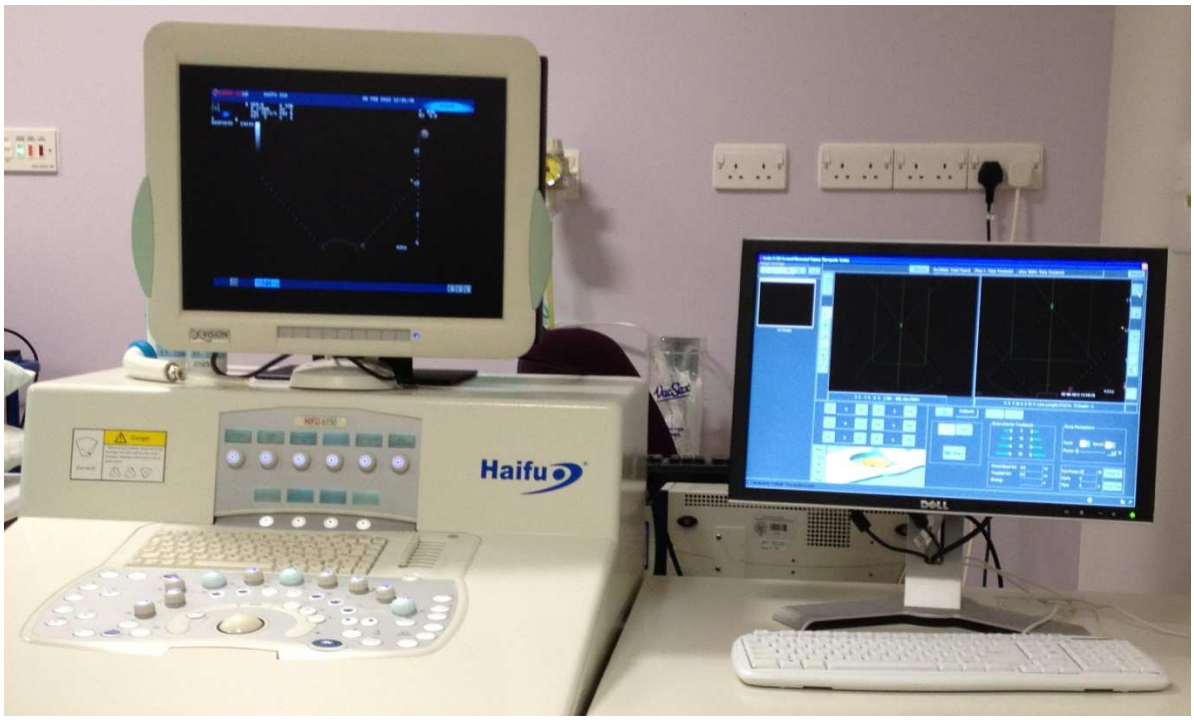

Figure 17 – Photograph of operator console from JC200 HIFU device. The left screen displays the diagnostic image from the integrated diagnostic ultrasound probe within the treatment head. The right screen display the operator console to control the degassing, water reservoir and HIFU output functions.

The treatment head controls are integrated with the diagnostic imaging device and the degassed water controls. After positioning, the tumour was located using B-mode ultrasound by moving the treatment head. The kidney was imaged in both the transverse and sagittal plane and the co-ordinates of the boundaries of the tumour were programmed into the planning software. Serial images were then created between these co-ordinates by selecting a slice separation – usually 2-3mm – thus ensuring that the entire tumour volume was mapped. Using on-screen images, the boundaries of the tumour were demarcated on each treatment slice to facilitate treatment of the entire tumour. These features are shown in a screenshot photograph in Figure 18.

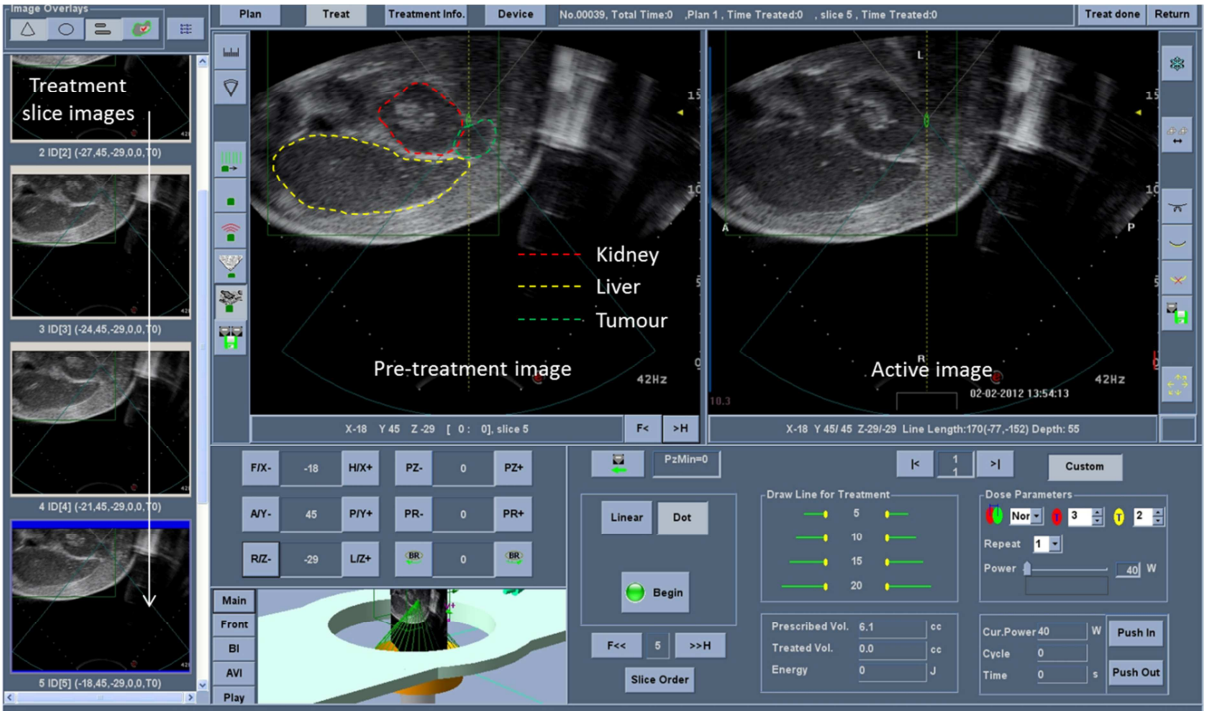

Figure 18 – Screenshot of HIFU treatment operator console. On the left hand side the serial treatment slices are shown. The left hand image of the main screen shows the pre-treatment image of the selected slice; the right hand image is the active image which displays any image change including the appearance of hyperecho. The controls for transducer movement and HIFU output are shown below these images.

3.2.5.4 HIFU therapy

Two therapeutic transducers were used during treatments – 0.8MHz for Model JC and 1.0MHz for Model JC-200. The ultrasound beam was produced by a plane disc situated behind an aluminium lens moulded together to produce the moveable treatment head. Each therapeutic transducer contained a circular hole through which a diagnostic ultrasound head passed – see Figure 19.

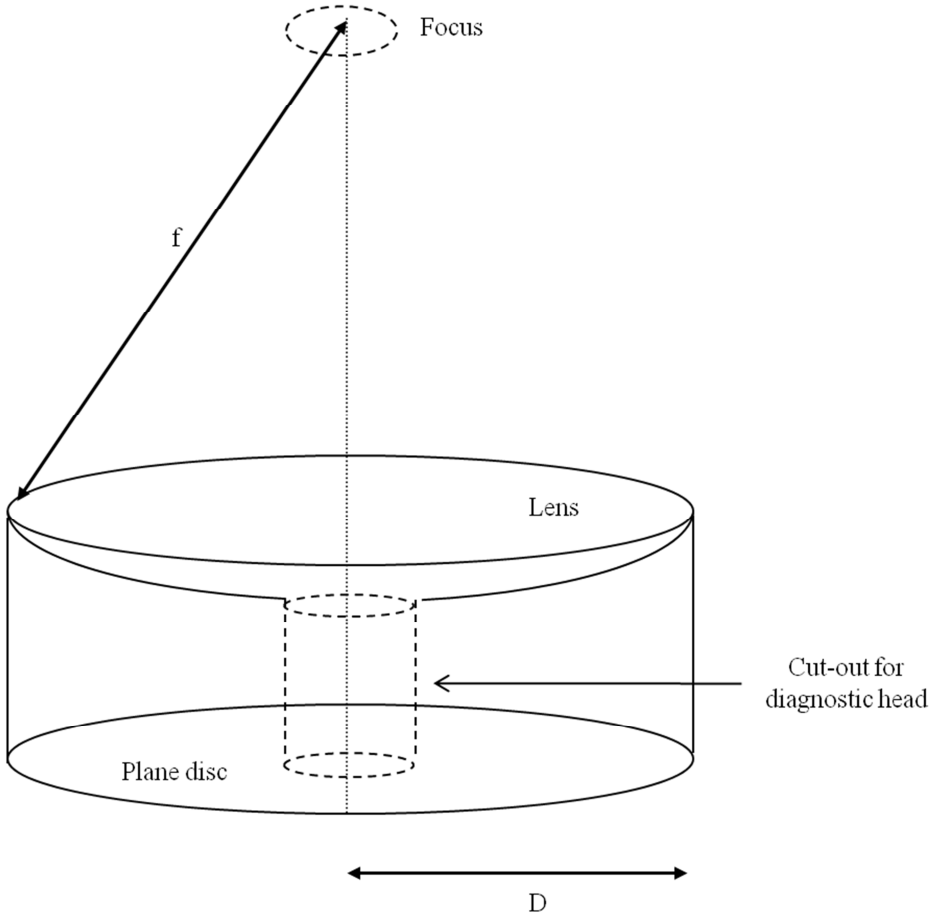

Figure 19 – Schematic diagram of HIFU treatment head demonstrating plane disc ultrasound transducer moulded to aluminium lens; f=focal length, d=transducer diameter

Device movements were controlled by the operator console and allowed 13cm of movement in the z, y or z plane and ±11°, ±30° & ±90° in the ψ-, γ- & θ-axis respectively. The characteristics of the transducers used are summarised in Table 3.

Table 3 – Summary of transducer characteristics used during HIFU treatment

Transducer	Frequency (MHz)	Focal length (f) (mm)	Outer diameter (D) (mm)	f-number f/D	Dimensions of focus (mm)	
					FWHM (transverse)	FWHM (axial)
20010A3 JC	0.84	128	150	0.85	1.9	15.0
20099-44 JC-200	0.95	135	202	0.67	1.2	9.5

HIFU treatment was undertaken in each of the imaging slices in which tumour (and its margin) was clearly visible. Tumour further from the transducer was treated first so as to limit the impact of image degradation caused by heating & swelling of tissues proximal to the focus. HIFU treatment was commenced with a single pulse of 2-3 seconds duration at low power. Further pulses of gradually increasing power were applied to the same region until a visible change was seen on B-mode ultrasound. Treatment was then undertaken at this power level using 5-20mm lines of multiple pulses with 50-66% overlap. This was continued until the entire visible tumour was covered. This is demonstrated in the schematic diagram in Figure 20. In the absence of visible ultrasound changes during treatment at different regions of the tumour, the power level was increased as required. Both the Model-JC & Model-JC200 allow scanned track insonication; however this was not used during renal HIFU treatment.

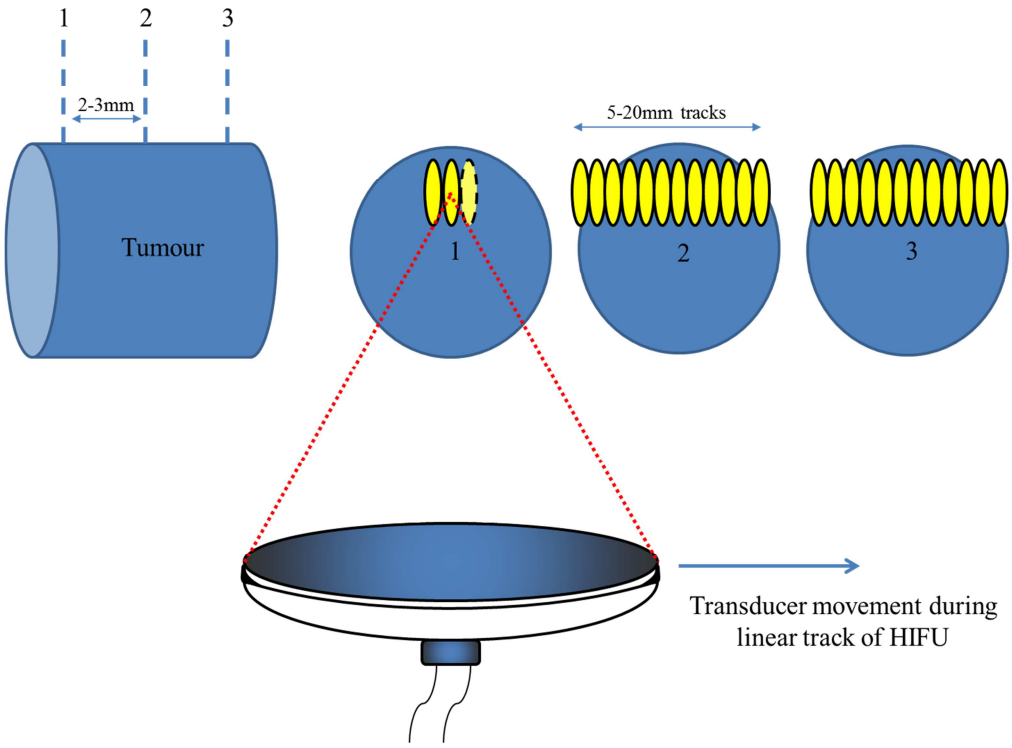

Figure 20 – Schematic of HIFU treatment. The entire volume is divided into multiple slices of 2-3mm thickness. Treatment is then undertaken in each slice by placing side-by-side HIFU exposures (2-3s) to cover the entire tumour. By treating multiple 2-D slices, an entire 3-D tumour volume is exposed to HIFU to ensure complete ablation.

During treatment, the water reservoir was automatically recycled every 15 minutes to ensure that the bath remains cold and degassed, thus helping to reduce the risk of skin burns. The skin overlying the treatment site was regularly inspected for injury throughout the treatment. Occasionally during treatment it was necessary to alter the patient position to improve tumour targeting.

After treatment of the entire tumour, or as much of the tumour as could safely be seen, the patient was transferred off the HIFU device. An immediate skin assessment was made and anaesthesia was reversed. Intravenous analgesia was administered as required.

3.2.5.5 HIFU therapy monitoring

As discussed in Chapter 2.5.2, hyperecho monitoring is the only method of ultrasound-guided HIFU monitoring in current clinical use. Hyperecho has been shown to correlate with the extent of coagulative necrosis [86, 87]. Both HIFU devices provide side-by-side ultrasound images, with the pre-treatment scan shown adjacent to the immediate post-exposure scan. This allowed a visual comparison of any grayscale change due to HIFU, as shown in Figure 21. The software also allows a quantitative assessment of grayscale change by subtracting the two images and providing a value of change in arbitrary HIFU units; in practice this method was rarely used as any image changes were immediately apparent on the treatment console after completion of a HIFU insonication. Grayscale change was used to determine both the necessary power level and the extent of treatment.

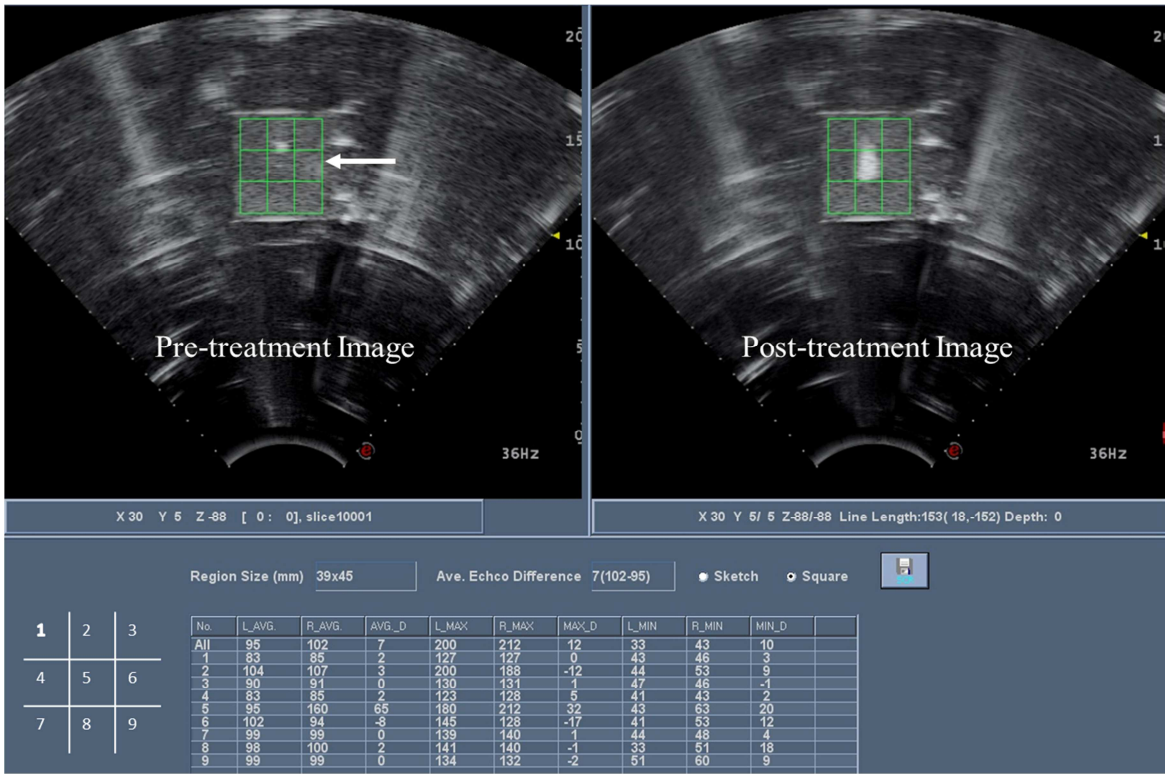

Figure 21 – Screenshot of grayscale analysis software. The pre- (left) and post-treatment (right) images are compared by dividing the volume into nine ROIs. A quantitative comparison is made between each ROI and shown in the table. A significant grayscale change has occurred at the focus in this tissue phantom cause a 65U increase in grayscale.

3.2.5.6 Post-HIFU care

Following treatment, patients were extubated and transferred to theatre recovery. Further analgesia was occasionally required. Patients were then transferred to a hospital ward for a single overnight stay. All patients were reviewed at approximately 6 & 24 hours following HIFU; this assessment including a careful skin examination. Blood was taken to analyse i) full blood count, ii) renal function, iii) serum electrolytes, iv) liver function & v) inflammatory markers. If clinical assessment and blood parameters were considered satisfactory, patients were discharged home with oral analgesia if required.

3.2.5.7 Clinical & trial follow-up

All patients were reviewed at 12±3 days following HIFU for a clinical assessment and CE-MRI to assess the tumour response – see Chapter 3.2.6. Further blood was analysed for the same parameters outlined in Chapter 3.2.5.6.

All patients subsequently underwent PN approximately 2-3 weeks after HIFU treatment. Surgery was performed using the most appropriate approach as decided by their surgeon – this was open, laparoscopic or robotic. The peri-nephric fat was inspected for macroscopic signs of ablation and sampled if required. The excised tumour was immediately transported (unfixed) to the pathology department. Patients were discharged when considered fit, usually 3-7 days following surgery.

Two further follow-up visits were arranged within the trial protocol. All participants had further cross-sectional imaging (CT or MRI) and clinical review at six & 12 months following surgery.

3.2.5.8 Trial Completion

Trial involvement was complete at 12 months; patients were returned to standard NHS care – this usually involved six or 12 monthly CT/MRI and clinical review for at least a further four years. The frequency of follow-up was determined by the surgeon.

3.2.6 Treatment morbidity

Any morbidity occurring during the trial conduct was graded according to the Common Toxicity Criteria for Adverse Events (CTCAE v4.03, 14th June 2010; available at www.ctep.cancer.gov, last accessed 26th August 2011). This is a descriptive terminology which is utilised for AE reporting. An AE is defined as "any unfavourable and unintended

sign, symptom or disease temporally associated with the use of a medical treatment or procedure that may or may not be considered related to the medical treatment or procedure". AEs are broadly classified in System Organ Class (SOC) which identifies event by anatomical or physiological system. Within each SOC, AEs are listed and accompanied by descriptions of severity. The severity of the AEs is classified through Grade 1-5. There are individual descriptions of the grade for each AE, but a general pattern is followed which is described in Table 4.

Table 4 – Common Toxicity Criteria for Adverse Events (CTCAE) grading guidelines

Grade	Description
Grade 1	Mild; asymptomatic or mild symptoms Clinical or diagnostic observations only Intervention not indicated
Grade 2	Moderate Minimal, local or non-invasive intervention only Limiting age-appropriate instrumental ADL
Grade 3	Severe or medically significant; not life-threatening Hospitalisation or prolonged hospitalisation Disabling; limiting self-care ADL
Grade 4	Life-threatening consequences Urgent intervention indicated
Grade 5	Death related to AE

All AEs were reported using this classification. As defined above, all events temporally related to the trial were reported. However, an assessment was also made of whether these AEs were related to HIFU treatment itself to allow a formal evaluation of the technology.

3.2.7 Assessment of tumour response

3.2.7.1 Radiological

Assessment of B-mode hyperecho response to HIFU treatment was performed using a semi-quantitative analysis by the clinicians performing the procedure (author & Tom Leslie; both HIFU surgeons). The HIFU software installed on both the Model JC & Model JC-200 was not designed to provide access to raw ultrasound data nor provide a measurement of the size

of the hyperecho region, preventing a formal quantitative measure. Pre-, intra- and post-treatment B-mode images of each tumour slice were provided and enabled an assessment of grayscale response using a standardised scoring system – see Table 5.

Table 5 – Scoring system for assessment of hyperecho response to HIFU treatment

Hyperecho Response	Description
Nil	No visible grayscale change seen throughout No evidence of successful treatment
Minimal	Occasional grayscale change seen in limited regions Evidence of very limited treatment effect
Moderate	Grayscale change seen frequently but not throughout Evidence of sub-total treatment
Significant	Widespread grayscale change seen throughout Consistent with successful tumour ablation

Magnetic resonance imaging (MRI) imaging of the abdomen (with IV gadolinium) also took place prior to HIFU treatment and at day 12±3. Prior to the study, an intravenous cannula was placed in an arm vein and attached to an MRI compatible power injector (Medrad, Cambridgeshire). Patients underwent imaging on a 1.5T or 3T MRI system (Twinspeed GE, Amersham) with high performance gradients and a torso phased array coil.

All patients underwent MR imaging using breath-hold techniques and comprising coronal T2W, T1W in phase and out of phase gradient-echo, fat-suppressed T2W and fast short inversion time inversion recovery sequences according to our routine protocol. All subsequently also underwent a breath-hold fat-saturated volumetric interpolated breath hold examination using a 3D-spoiled gradient-echo acquisition (LAVA – Liver acquisition volume acceleration) before, during and after injection of gadolinium (Prohance, Bracco, Amsterdam). The LAVA sequence allows thin section imaging with sequential enhanced image acquisition and also allows isotropic spatial resolution to demonstrate arterial, venous and delayed contrast enhancement. Due to the precise timing of data acquisition during

selected periods of enhancement, detection and characterisation of all lesions was possible. Subsequent subtraction imaging was performed to demonstrate the enhancement in isolation.

Three dimensional measurements of the tumour were recorded at baseline and at 12 ± 3 days. The sizes of the zone of coagulative necrosis and the tumour were measured. These were given both as short-axis diameters (the minimum requirements according to the International Working Group on Image Guided Tumour Ablation [173, 174]) and also as volume estimates derived from antero-posterior (AP), transverse (trans) and cranio-caudal (CC) dimensional measurements assuming a uniform ellipsoid shape, using the formula:

$$\frac{4}{3}.\pi.\left(\frac{AP}{2}\right).\left(\frac{trans}{2}\right).\left(\frac{CC}{2}\right)$$

All images were reviewed by the same, single consultant radiologist (Dr Rachel Phillips, Churchill Hospital, Oxford), who has a specialist interest in tumour ablation imaging.

3.2.7.2 Histological

The tumour specimen was sent unfixed for immediate photography and cut-up. The tumour was formally measured and then cut into 2-3mm slices perpendicular to the plane of the HIFU axis based on images recorded at the HIFU session. A macroscopic assessment was made of tumour ablation and photography obtained. Subsequently the tissue was fixed in formalin and stained with haematoxylin & eosin to assess for tumour size, grade, margin status and ablation volume. Immunohistochemistry was also undertaken to confirm tumour type using stains including, but not limited to, cytokeratins 7/8/9/19, vimentin and E-cadherin.

All specimens were examined by a consultant pathologist with a specialist interest in renal cancer (Drs Gareth Turner, Ian Roberts, Lisa Browning & Ran Perera). The pathologist

undertook a semi-quantitative assessment of the effectiveness of HIFU using a grading system adapted from a study of histological response to chemotherapy in Ewing sarcoma – see Table 6 [175]:

Table 6 – Grading of effectiveness of HIFU as determined by histological evidence of necrosis in treated tumour

Technique Effectiveness	Histological Findings
Grade 1	Necrosis of ≤50% of treated region
Grade 2	Necrosis of 50-90% of treated region
Grade 3	Necrosis of 90-99% of treated area
Grade 4	Necrosis of 100% of treated area (endpoint)

A formal histology report was issued by the pathologist which was used for both NHS care and research purposes.

3.2.8 Clinical trial outcomes measures and endpoints

3.2.8.1 Primary Outcome Measure

- Volume of tumour ablation on final histology expressed as a percentage of pre-treatment tumour volume

3.2.8.2 Primary Endpoints

- Complete (100%) tumour ablation on final histology

3.2.8.3 Secondary Outcome Measures

- Volume of tumour ablation on day 12 imaging expressed as a percentage of pre-treatment tumour volume
- Number and severity of AEs / toxicity following EC-HIFU based on CTC criteria; assessed at the following points:
    - C3 (day 1 post-HIFU)
    - C4 (day 2 post-HIFU)

  - C5 (day 12 post-HIFU)
  - C6 (Day 30 post-HIFU is surgery has not occurred)
- Evidence of cavitation during EC-HIFU expressed as a 'map' of cavitation activity
- Levels of general & specific immunological markers; assessed at the following points:
  - C2 (pre-HIFU)
  - C3 (day 1 post-HIFU; 6 hours following commencement)
  - C4 (day 2 post-HIFU; 24 hours following commencement)
  - C5 (day 12 post-HIFU)
  - C9 (6 months post-HIFU)
- Tumour volume (if any) at radiological follow-up; assessed at the following times:
  - C10 (6 months post-HIFU)
  - C12 (12 months post-HIFU)
- Tumour uptake (if any) of intravenous contrast on digital-subtraction MRI imaging; assessed at the following times:
  - C10 (6 months post-HIFU)
  - C12 (12 months post-HIFU)

3.2.8.4 Secondary Endpoints

- Complete (100%) tumour ablation on day 12 MRI imaging
- AEs / toxicity following EC-HIFU treatment
- Cavitation map correlation with histological damage assessed post-operatively.
- Anti-tumour immunity following EC-HIFU treatment

Oncological outcome (assessed radiologically) following HIFU & surgery up to 1 year post treatment

3.3 Statistical Analysis

3.4 Results

3.4.1 Trial recruitment

Trial recruitment began in August 2009 with an anticipated annual recruitment rate of 10. Funding was available to treat 20 patients in two years. Due to slower than expected

recruitment, enrolment was continued beyond two years and was on-going as of February 2012 with a total of 13 patients formally enrolled.

3.4.1.1 Initial screening

Through a combination of outpatient attendances, MDT meetings and uro-oncology radiology meetings, patients with T1a renal tumours appropriate for surgical intervention were identified. As a result 39 patients were put forward for initial screening. Following initial screening, described in Chapter 3.2.4.1, 11 patients were eliminated. The reasons for elimination at this stage are outlined in Table 7.

Table 7 – Reasons for failure to recruit at initial screening

Criteria	Number of patients
Unfit for major surgery	3
For non-operative management	1 (after final screening)
Cystic tumour	1
Declined enrolment	5
Benign tumour (biopsy)	1

The decision regarding fitness for surgery was made by the operating surgeon – the risk of surgical excision being far greater than the risks encountered during renal HIFU treatment. Patients considered fit for PN were invariably considered fit for HIFU treatment. A number of patients chose to pursue a non-operative management strategy, also known as active surveillance. The strategy is appropriate for a significant proportion of T1a tumours given their natural history – discussed in detail in Chapter 2.11.1. Small renal tumours often grow slowly; symptoms and/or metastatic disease are rare in tumours less than 3cm in maximum dimension and remain uncommon in tumours less than 4cm. In older patients or those with co-existing medical problems, the risks of surgery may therefore significantly outweigh any intended oncological benefit.

The majority of renal tumours are solid lesions, containing no significant fluid component. Fluid-filled cysts of the kidney are very common. Morphologically they are predominately lined by a thin-walled lining and contain serous fluid only – these are known as simple cysts. More rarely, the cyst lining contains malignant cells and is thus thicker, often with septations within the cyst itself; the fluid may contain blood as well as malignant cells. A previous study conducted in Oxford using a laparoscopic HIFU device, demonstrated that these cystic tumours responded poorly to HIFU [130]. Difficulties were encountered for two reasons; firstly boiling within the fluid of the cyst lead to significant hyperecho change on ultrasound imaging resulting in misleading feedback; secondly strong scattering from bubbles in the cyst fluid shielded the malignant cyst wall from ablation thus preventing successful treatment. Patients with cystic tumours were therefore excluded from the trial.

3.4.1.2 Final Screening

After initial screening, 28 patients were invited to attend final screening for formal renal ultrasound and treatment planning – see section 3.2.4.2. Consent for trial participation was obtained from all patients; no patients declined involvement after agreeing at initial screening. Using handheld ultrasonography the affected kidney and tumour was locatable in all patients.

The diagnostic transducer centred in the moveable treatment head has similar characteristics to the handheld probe. During device ultrasonography, the patient was placed in the lateral position resulting in some lateral movement of both the bowel and kidney towards the surrounding ribcage. The diagnostic transducer was moved vertically towards the target so that the probe was close to or touching the skin to allow the best possible imaging quality. With this strategy, it was possible to locate the kidney in all patients. However, in 16 patients,

the tumour itself could not be adequately visualised to allow safe treatment to proceed. It is noteworthy that for safe treatment, the tumour must be clearly visible not only with the treatment head positioned ideally for imaging, but also with it positioned appropriately for treatment. The focal length of the transducers used was approximately 12-13cm and with the treatment head placed at this depth a significant loss of image quality was noted. Moreover, with the depth of stand-off between the transducer and body wall, it was considerably more difficult to image between the ribs, often leading to a marked acoustic shadow which further limited tumour visualisation. Inadequate imaging was a significant cause of recruitment failure during this trial and remains a major limitation of current extracorporeal ultrasound-guided HIFU, particularly for organs lying in close proximity to the rib cage.

In the remaining 12 patients tumour visualisation with the device ultrasound was satisfactory and completed final screening. It was ensured that all limits of the tumour could be seen and that no portion of the tumour lay outside the limits of the focal length of the transducer to be used. Measurements were made of the tumour and colour Doppler was performed.

3.4.2 Patient demographics & tumour characteristics

All patients underwent CE-MRI of the upper abdomen using the protocol described in Chapter 3.2.7.1. This imaging provided the transverse, AP and coronal dimensions of the tumour as well as its location within the kidney. The maximum tumour dimension together with patient demographic and tumour location are shown in Table 8.

Table 8 – Demographics and tumour characteristics from all patients attending final screening; those highlighted in yellow passed final screening and were treated. Missing trial numbers represent those who failed initial screening or declined trial inclusion.

Trial No.	Age	Site	Location	Maximum Tumour Dimension (mm)
5.01	73	Left	Upper	18
5.02	66	Right	Upper	25
5.03	71	Left	Interpolar	30
5.05	50	Left	Interpolar	19
5.06	60	Left	Interpolar	25
5.07	41	Right	Interpolar	33
5.08A	49	Left	Upper	27
5.08B	49	Left	Lower	27
5.08C	49	Right	Upper	26
5.09	53	Left	Interpolar	30
5.10	82	Right	Interpolar	28
5.11	75	Right	Lower	28
5.12	71	Right	Upper	35
5.13	64	Left	Interpolar	38
5.14	79	Right	Interpolar	35
5.15	59	Right	Upper	22
5.16	52	Right	Lower	27
5.17	70	Right	Interpolar	30
5.19	56	Right	Interpolar	21
5.20	44	Left	Upper	25
5.21	71	Right	Lower	24
5.22	70	Right	Upper	30
5.23	36	Right	Lower	22
5.27	74	Left	Interpolar	31
5.29	35	Left	Upper	30
5.31	71	Right		20
5.34	69	Right	Upper	56
5.35	68	Left	Upper	37
5.38	60	Left	Lower	21
5.39	67	Right	Lower	18

The mean age of patient attending final screening was 61 (±2.3, SEM) years. 17/31 of tumours were right-sided and 11/31 (35%), 13/31 (42%) & 7/31 (23%) were located in upper pole, interpolar & lower pole regions respectively. The mean maximum tumour dimension was 27.9mm (±1.4mm, SEM).

3.4.3 Treatment according to protocol

Ten out of 13 patients were treated with HIFU according to the trial protocol. Three patients who had been enrolled in the trial did not receive any HIFU treatment. Patient 5.05 underwent general anaesthesia; despite repeated efforts it was not possible to accurately visualise the tumours and its margins to enable safe treatment. The screening visit, including handheld and device ultrasound had been undertaken satisfactorily. It was felt that muscle relaxation encountered during anaesthesia led to tumour occupying a position directly behind a rib, making imaging challenging. Patient 5.07 attended for treatment but was unwell with abdominal pain and vomiting; general anaesthesia was not undertaken. Subsequently, the patient was found to have co-existing intra-abdominal pathology (caecal carcinoma with metastases) – treatment for the renal tumour was not appropriate given this finding. Patient 5.19 underwent general anaesthesia but became unwell before HIFU could be commenced – this complication is discussed in detail in Chapter 3.4.4.

3.4.4 Complications & adverse events

Twelve of the 13 patients underwent general anaesthesia and were evaluated for adverse events (AE). Patient 5.07 did not undergo anaesthesia and was not therefore not included in the analysis. Renal HIFU was generally safe. All AEs during trial conduct were reported – see Table 9. No life-threatening consequences (Grade 4) or deaths (Grade 5) occurred during the trial conduct so they columns are eliminated from the table.

Table 9 – All AEs during trial conduct according CTCAE Grading; *=both related to post-operative haemorrhage after partial nephrectomy; **=severe hypertension related to anaesthesia, no HIFU used

System Order Class	AE	Grade 1	Grade 2	Grade 3	HIFU related
Skin & subcutaneous tissue disorders	Pain of skin	9/12	1/12	0/12	Yes
	Skin induration	9/12	0/12	0/12	Yes
Injury, poisoning & procedural complications	Post-operative haemorrhage	0/12	0/12	2/12*	No*
Renal & urinary disorders	Urinary retention	0/12	1/12	0/12	No
Vascular disorders	Hypertension	0/12	0/12	1/12**	No**

Mild skin pain and skin induration occurred in almost all patients; one patient had moderate pain. One patient (trial number 5.19) developed severe hypertension during general anaesthesia before any insonication was undertaken. This patient had Von Hippel-Lindau (VHL) syndrome and had an associated cerebellar haemangioblastoma which was under surveillance. In the context of this tumour, there were concerns that the hypertension was related to intra-cranial oedema or haemorrhage and a decision was made to promptly end the procedure. The patient was not found to have any neurological deficit following anaesthesia and made a full recovery without intervention. One patient developed urinary retention after the procedure and required temporary urethral catheterisation; a successful trial without catheter was undertaken soon after treatment. Finally, two patients (trial numbers 5.01 & 5.03) had significant post-operative haemorrhage following PN. Both patients required hospitalisation and required blood transfusion. Both underwent renal angiography and an arterio-venous fistula was found in both cases. In one patient (5.01) the bleeding was managed non-operatively and spontaneously ceased following a period of observation. In the remaining patient (5.03) the bleeding continued despite selective renal artery embolisation. The patient underwent a completion nephrectomy from which a full recovery was made. None of the Grade 3 AEs were felt related to the HIFU treatment – in the case of hypertension no HIFU treatment had been undertaken. In the two cases of haemorrhage, the

AEs occurred over two weeks after HIFU treatment and were temporally related to PN. Haemorrhage is a known complication of PN. Moreover, haemorrhage has never previously been reported in the context of HIFU treatment of any intra-abdominal organ; indeed ablated tissue is avascular and necrotic.

3.4.5 Laboratory follow-up

Serum haematological and biochemical indices were measured in all patients at three separate time-points – pre-HIFU treatment; 24 hours and 12 days after treatment. These are summarised in Figure 22 & Figure 23. There was no statistically or clinically significant change in serum sodium, potassium or creatinine concentration after treatment. There was a statistically significant rise in urea at day 12 which is considered to be clinically insignificant. There was a statistically significant rise in serum C-reactive protein (CRP) at 24 hours following HIFU (10.8 *vs.* 3.6; $p<0.05$), which had returned to pre-treatment levels at day 12. CRP is an acute-phase protein found in blood and is a non-specific marker of inflammation. During an acute-phase response, CRP begins to rise two hours after onset of the insult and peaks at 48 hours; its half-life is 18 hours. The transient rise in CRP noted following HIFU treatment was consistent with an inflammatory response to tissue necrosis following thermal ablation.

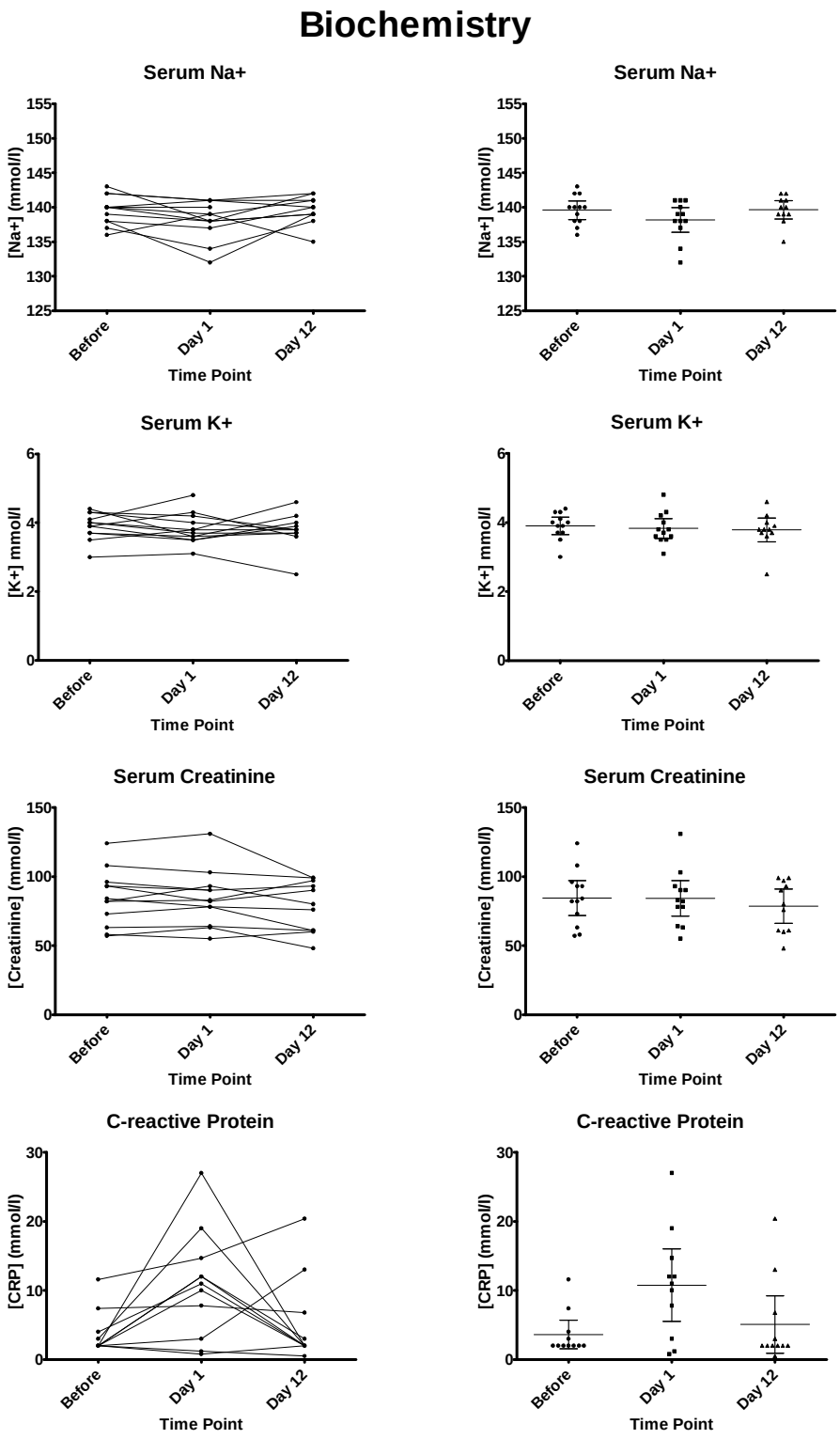

Figure 22 – Biochemical profiles of trial patients assessed before HIFU and at day 1 & day 12. Left hand graphs show change in each patient; right hand graphs show mean & 95% CIs at each time point.

A statistically significant rise in serum white cell count was observed at 24 hours (11.0 *vs.* 7.4; $p<0.01$) after treatment, which fully resolved by day 12. This was again consistent with

an inflammatory process due to thermal ablation. There was no change in serum haemoglobin or platelet count at either 24 hours or 12 days following HIFU.

These results demonstrate that HIFU treatment was not associated with major electrolyte or haematological disturbances. Significantly, indicators of renal function were not altered despite renal ablation. Evidence of acute inflammation following treatment was an expected finding and was consistent with cell death due to thermal necrosis.

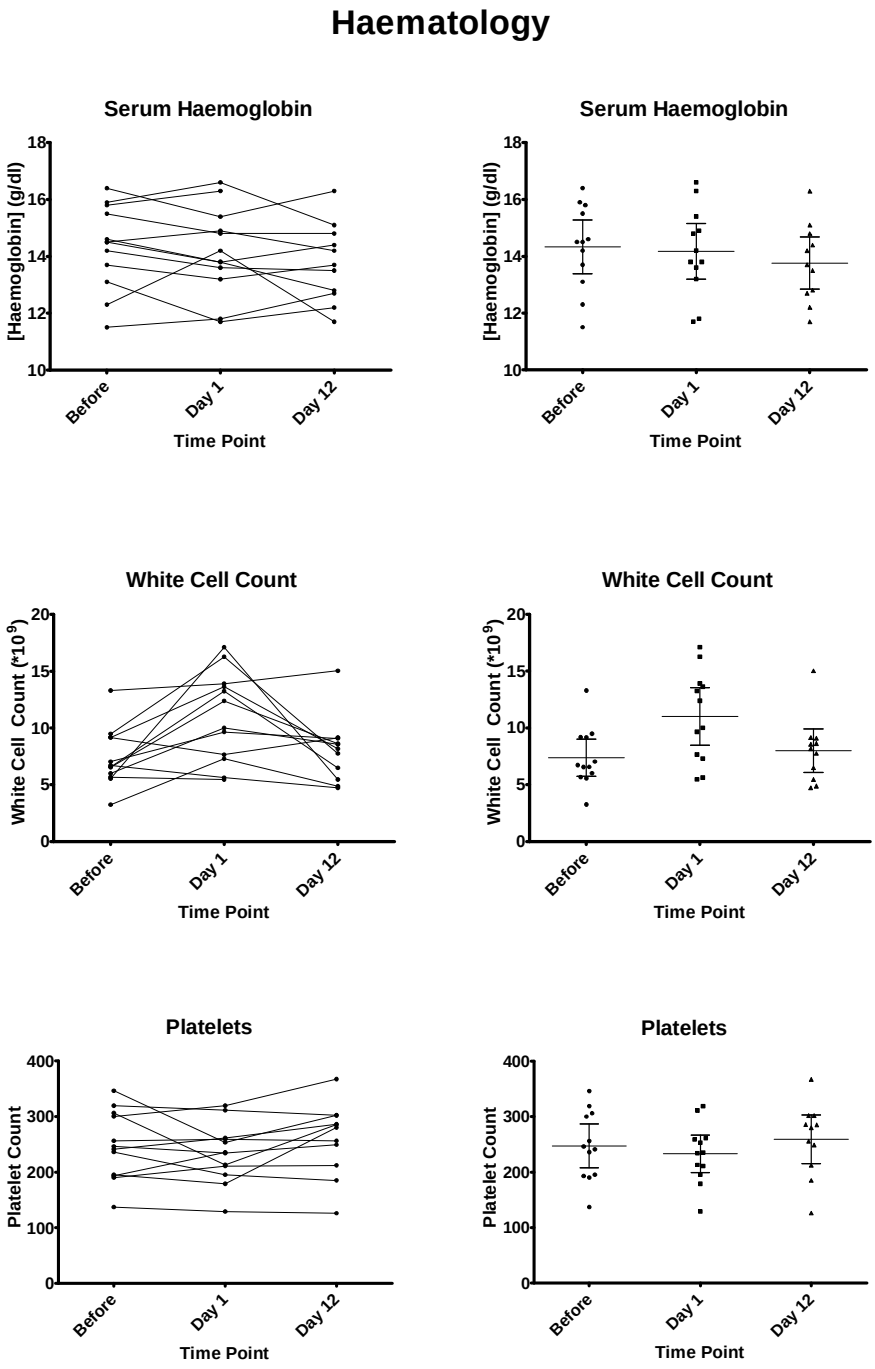

Figure 23 – Haematological profiles of trial patients assessed before HIFU and at day 1 & day 12. Left hand graphs show change in each patient; right hand graphs show mean & 95% CIs at each time point

3.4.6 Radiological follow-up

All treated patients underwent follow-up CE-MRI 12±2 days after HIFU as described in Chapter 3.4.6. This was compared directly with the pre-treatment CE-MRI. Patients who were not treated with HIFU, as discussed in Chapter 3.4.3, did not undergo further cross-

sectional imaging as part of the trial. Table 10 outlines the pre-treatment tumour volume, together with estimates of the volume of ablation, ablation to tumour ratio and the location of any residual enhancement suggesting viable tumour.

Definite radiological evidence of tumour ablation was seen in three patients in the trial. This was despite intra-operative ultrasound evidence of moderate or significant hyperecho appearing after treatment in five cases. Persistent visible tumour enhancement was seen both centrally and peripherally in all but three cases. Loss of central enhancement is considered to be the hallmark of successful tumour ablation, indicating that the tumour has been successfully devascularised [174]. Conversely, persistent peripheral enhancement after ablative therapy may not necessarily represent viable tumour, rather a benign peri-ablational halo indicative of a fibrotic response to thermal injury [174].

Table 10 – Radiological characteristics of zone of ablation in each trial patient according to post-HIFU MRI

Trial No.	Pre-HIFU tumour volume (mm^3)	Intra-op grayscale changes	MRI evidence of ablation	Volume of zone of ablation (mm^3)	Ablation : tumour ratio	Location of residual enhancement
5.01	2214	Moderate	No	0	0	Throughout
5.03	10824	Minimal	No	0	0	Throughout
5.05	3969	No R_x	N/A	N/A	N/A	Throughout
5.07	17649	No R_x	N/A	N/A	N/A	Throughout
5.10	9500	Significant	No	0	0	Throughout
5.13	24134	Minimal	No	0	0	Throughout
5.16	8814	Significant	Yes	10688	1.21	Peripheral
5.19	5309	No R_x	N/A	N/A	N/A	Throughout
5.21	6618	Significant	No	0	0	Throughout
5.23	4596	Significant	Yes	5189	1.12	Nil
5.29	10999	Minimal	No	0	0	Throughout
5.38	4376	Minimal	Yes	6142	1.40	Nil
5.39	2876	Significant	Yes	3046	1.06	Nil

3.4.7 Histological follow-up

All treated patients underwent surgery 2-4 weeks after HIFU treatment. Nine patients underwent open PN; two patients underwent robotic-assisted PN. Renal arterial clamping when required was used to minimise bleeding during tumour excision. The specimen was photographed fresh and then sliced and fixed for formal microscopy as described in Chapter 3.2.7.2. PN was also undertaken in patient 5.05 who was not treated due to a failure to adequately visualise the tumour. Patients 5.07 & 5.19 did not undergo surgery due to other co-existing health problems.

Following fresh specimen cut-up, both the margins of the tumour and the margins of ablation were evident on gross examination – an example is shown in Figure 24. Ablated tumour appears haemorrhagic under direct vision, whilst residual viable tumour often appears similar, although less homogenous, to normal renal parenchyma.

Figure 24 – Serial sections of partial nephrectomy specimen from patient 5.16. Normal renal parenchyma is seen superiorly. The tumour margin is clearly visible (black arrows) and contains predominately haemorrhagic ablated tissue. A small area of viable non-ablated tumour is seen (white arrow heads).

In order to fully treat a renal cancer, a rim of normal renal parenchyma must also be excised or ablated to ensure a safe tumour margin. This is clearly demonstrated in Figure 25 which shows a photograph of the treated tumour from Patient 5.40. The tumour has been sectioned in half (bi-valved) – it demonstrated widespread haemorrhagic tissue consisted with coagulative necrosis. Thermal ablation also extends a small distance into the adjacent normal renal parenchyma.

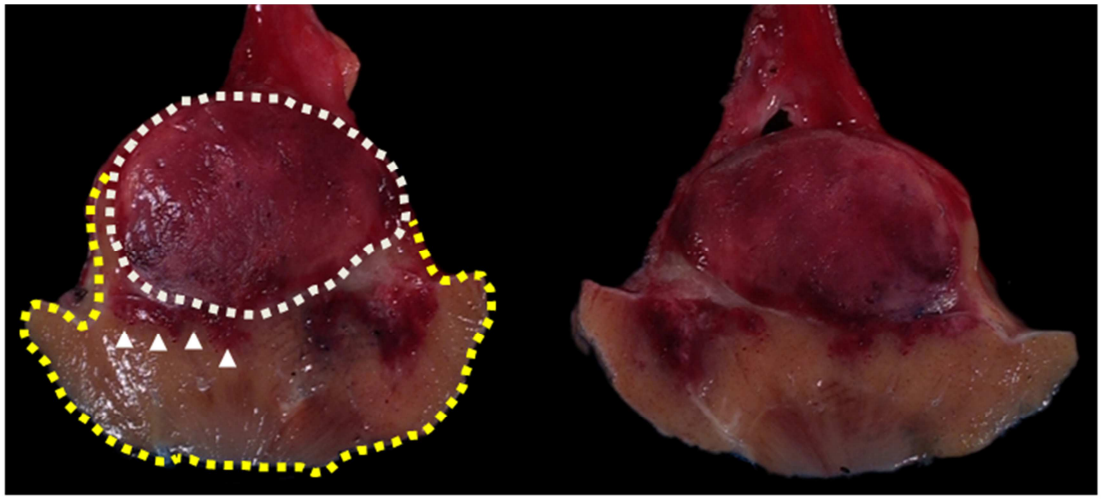

Figure 25 – Macroscopic pathology of bi-valved ablated tumour from Patient 5.40. Widespread haemorrhage consistent with necrosis is seen (white dashed line), A margin of normal renal parenchyma has been removed with the tumour (yellow dashed line) with also demonstrates some thermal damage (arrowheads).

The pathological analysis of the treated tumours and the zones of ablation is shown in Table 11. In 8/10 patients who had HIFU treatment the tumour was shown to be a renal cancer (4 clear cell, 4 papillary cell). In the remaining two patients benign tumours were found – one oncocytoma and one angiomyolipoma. Evidence of HIFU ablation was seen in all ten patients who were treated with HIFU. In two patients (patient 5.03 & 5.29) evidence of HIFU ablation was seen in both the surrounding peri-nephric fat and in the adjacent normal renal parenchyma; no ablation was seen in the tumour itself – classified as Grade 1 (see Chapter 3.2.7.2). In two other patients very limited tumour ablation (Grade 1) was seen, with less than 5% of total tumour volume destroyed. In three patients Grade 2 tumour ablation was seen

with approximately 60-70% of the total tumour volume showing evidence of thermal damage. In the remaining three patients Grade 3 ablation was seen – in each patient however, a thin rim of viable tumour was seen demonstrating that complete tumour destruction has not occurred.

The significance of small volumes of residual viable tumour remains uncertain. Positive surgical margin following PN is well documented but does not seem to be associated with poorer survival outcomes [176-178]. Additionally, follow-up in patients undergoing alternative image-guided ablation (CRY, RFA) is predominately radiology which has limited ability to detect very small areas of viable tumour. Histological follow-up in the form of a post-treatment biopsy cannot conclude that complete ablation has occurred and therefore even biopsy follow-up cannot be considered definitive evidence of complete tumour destruction.

3.4.7.1 Examples of histological evidence ablation

An example of histological ablation within a renal tumour is shown in Figure 26. Thermal ablation is characterised histologically by some or all of the following features [130]:

a) Erythrocyte homogenisation
b) Variation of shape, size and lysis of red cells within blood vessels
c) Endothelial damage
d) Granular protein deposits on vessel walls
e) Homogenisation of vascular smooth muscle
f) Shrinkage and loss of cell membrane detail of tumour cells
g) Pyknosis of nuclei

In tissue which has been immediately excised following ablation the margin between normal and damaged tissue is sharp, measuring merely a few cells in thickness. In cases where the

ablation target is left in-situ for a period of time following ablation, the healing process starts at the periphery of the lesion where the vasculature remains intact. The influx of inflammatory cells leads to the gradual formation of a fibroblastic scar. Given sufficient time (weeks to months) this process occurs throughout the zone of ablation leading ultimately to a permanent area of scar tissue at the site of treatment.

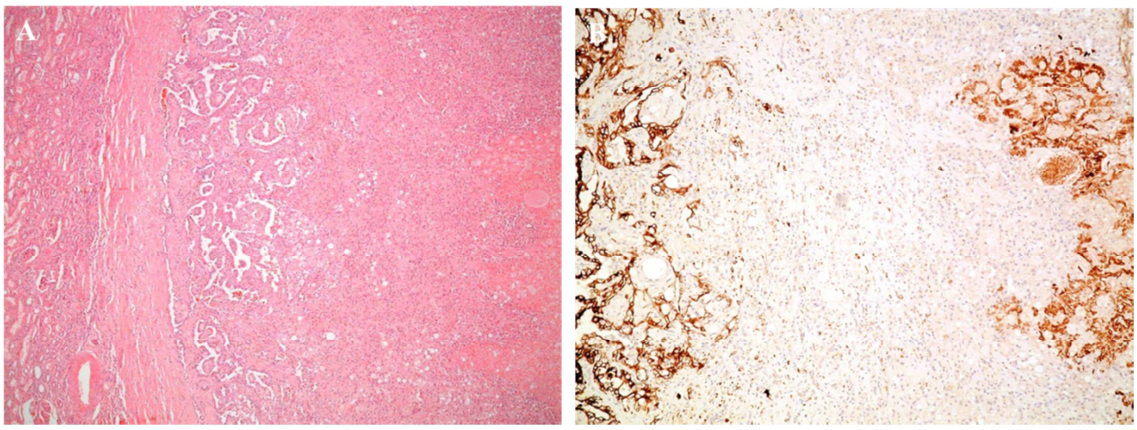

Figure 26 – Evidence of thermal ablation in Patient 5.21 demonstrated with H&E (A) and CK7 (B) stains. Ablated tumour is seen on the right in both images; a band of fibroblastic scar consistent with the healing process in seen centrally and non-ablated tissue is seen on the left of each image

It is noteworthy that in Patient 5.03, there was no evidence of tumour ablation but evidence of thermal damage to normal kidney. Figure 27A demonstrates normal renal parenchyma found within the surgical margin of the tumour specimen. Contrastingly, Figure 27B shows evidence of thermal ablation of normal renal parenchyma lying outside the tumour. Clear evidence of interstitial and intra-glomerular haemorrhage is demonstrated. This finding suggests inaccurate targeting of the tumour most likely due to poor quality imaging at the time of treatment. It is important to note that although the thermal damage lies outside the tumour, it also lies entirely within the surgical specimen with no evidence of thermal ablation at the margin of the resection.

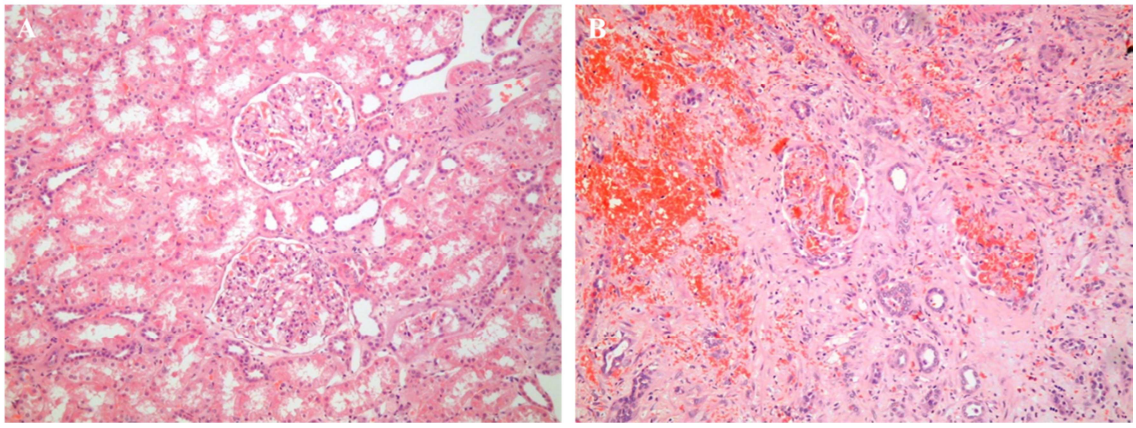

Figure 27 – H&E stain of surgical specimen from Patient 5.21 demonstrating normal kidney within the resection specimen (A) and evidence of thermal ablation in normal kidney (B). Two normal glomeruli are visible centrally (A); in contrast interstitial and intra-glomerular haemorrhage and cellular necrosis is seen in the ablation specimen (B)

Previous studies have shown that cavities or 'holes' are often seen in ex-vivo tissue following HIFU ablation [48]. It is likely that these cavities form as a result of tissue boiling rather than acoustic cavitation as the name might suggest, given their size (0.1-2mm). Cavities such as these were found within the resection specimens, as demonstrated in Figure 28. It is boiling 'bubbles' such as these, acting as strong scatterers, that are responsible for the hyperecho formation seen using standard monitoring of ultrasound-guided HIFU treatments.

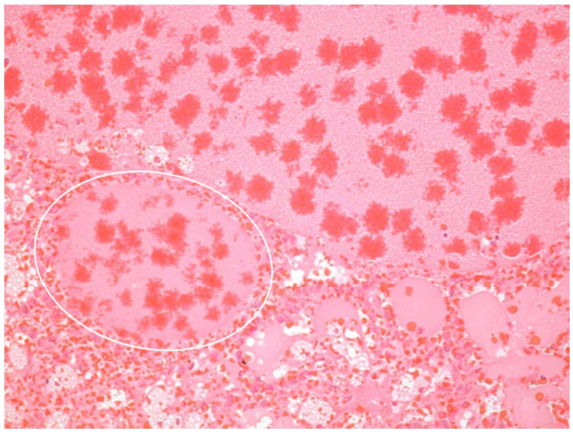

Figure 28 – H&E stain of ablated tumour from Patient 5.21 demonstrating the formation of cavities (circled) within tissue due to the formation of boiling bubbles. *In vivo* these cavities fill with fluid from the surrounding interstitium

In all treated patients, radiological and/or histological evidence of peri-nephric fat ablation was seen. In some cases (Patients 5.03 & 5.10) extensive fat ablation was seen without evidence of tumour ablation, suggesting the majority of HIFU energy was deposited in the

tissues immediately proximal to the expected focal region. This finding was previously noted in both an extracorporeal and laparoscopic renal HIFU trial and was the motivation for further work on the acoustic properties of peri-nephric fat described in Chapter 4 [130, 172].

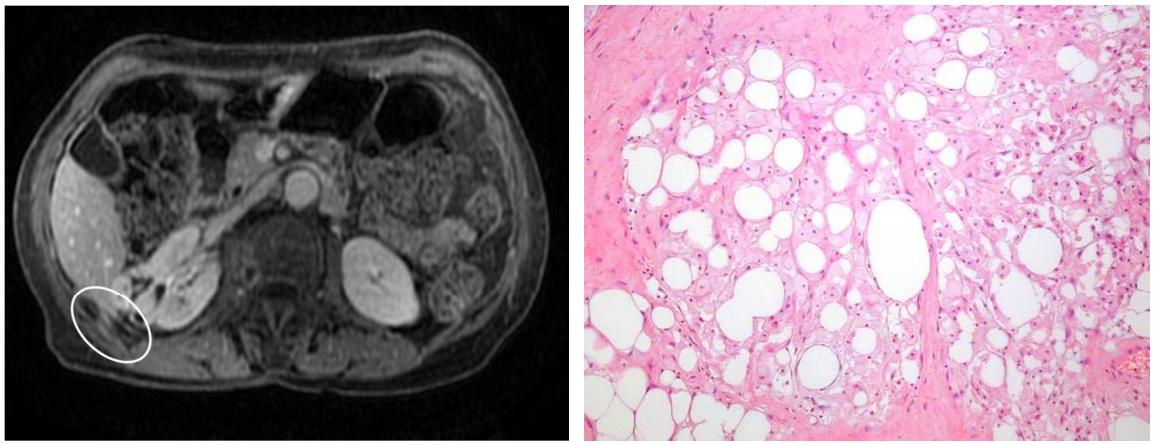

Figure 29 – Post-HIFU MRI (left) and histological examination (right) of the peri-nephric fat specimen of Patient 5.10; limited ablation was seen within the tumour but significant ablation (circled) of pre-focal fat tissue was evident

Table 11 – Microscopic characteristics of tumour and zone of ablation according to post-resection histology; O=open surgery, R = robotic surgery

Trial No.	Tumour Type	Maximum tumour dimension (mm)	Evidence of HIFU ablation[1]	Evidence of tumour ablation[2]	Ablation : tumour ratio	Grade of ablation	Location of viable tumour	Comments	Surgery O/R
5.01	Papillary RCC	15	Yes	Yes	0.95	Grade 3	Peripheral		O
5.03	Chromophobe RCC	34	Yes	No	0	Grade 1	Throughout	Fat & kidney ablation	O
5.05	Papillary RCC	25	No R_x	N/A	N/A	N/A	N/A	No R_x	O
5.07	Not known	N/A	No R_x	N/A	N/A	N/A	N/A	No R_x	N/A
5.10	Clear cell RCC	21	Yes	Yes	<0.05	Grade 1	Throughout	Biopsy related?	O
5.13	Oncocytoma	37	Yes	Yes	<0.05	Grade 1	Throughout		O
5.16	Clear cell RCC	30	Yes	Yes	0.95	Grade 3	Peripheral		O
5.19	Not known	21	No R_x	N/A	N/A	N/A	N/A	No R_x	N/A
5.21	Papillary RCC	25	Yes	Yes	0.95	Grade 3	Peripheral		R
5.23	Clear cell RCC	35	Yes	Yes	0.6	Grade 2	Peripheral		O
5.29	Clear cell RCC	30	Yes	No	0	Grade 1	Throughout	Fat only Part cystic	O
5.38	Papillary RCC	21	Yes	Yes	0.6	Grade 2	Central		R
5.39	AML[3]	18	Yes	Yes	0.7	Grade 2	Peripheral		O

[1] – Indicates whether thermal ablation was seen anywhere in the resection specimen (including fat & normal renal parenchyma)
[2] – Indicates whether thermal ablation was seen *within* the tumour itself
[3] – AML = angiomyolipoma

3.4.8 Correlation between intra-operative, radiological and histological monitoring

The use of immediate post-exposure B-mode ultrasound images as a surrogate marker for tissue ablation was first proposed by ter Haar *et al.* [85]. The authors demonstrated a correlation between the lesion size measured on ultrasound images using electronic callipers and that measured directly following tissue sectioning. Since then, a number of studies have been published examining the biological mechanisms of hyperecho formation [86, 87, 179]. Furthermore, clinical studies have demonstrated successful use of hyperecho monitoring in liver, breast, renal, pancreas and bone tumours [16, 18, 120, 130, 172, 180, 181]. Despite its widespread acceptance, quantitative proof of its effectiveness is lacking. Yu *et al.* found hyperecho to have poor sensitivity, specificity, positive predictive value (PPV) and negative predictive value (NPV) as an indicator of tissue necrosis in HIFU exposure of in vivo rabbit liver and kidney [182]. To date no other work has assessed the correlation between intra-operative hyperecho imaging and the volume of tissue necrosis.

The correlation between the three methods of assessing treatment outcome is presented in Table 12. In the majority of cases (6/9), minimal or significant hyperecho change correlates with Grade 1 or Grade 3 ablation respectively (see Table 12). However, two give cause for concern – firstly in Patient 5.10 there was widespread hyperecho throughout the treatment but very little of ablation at surgical resection; secondly patient 5.23 demonstrated approximately 60% ablation when a much higher level would have been expected given the widespread intra-operative hyperecho change. It is possible to speculate that the hyperecho change seen occurred in the kidney outside of the tumour as a result of inaccurate targeting. However, no evidence of ablation of normal renal parenchyma was seen on follow-up MRI (Patient 5.10) or within the completion nephrectomy specimen (Patient 5.23). It is more likely that the poor quality ultrasound imaging combined with the poor sensitivity and specificity of hyperecho

monitoring led to misleading intra-operative feedback. The difficulties seen with B-mode ultrasound based imaging and monitoring techniques in this trial are the motivation for further research on imaging and monitoring presented in Chapters 5 & 6 respectively.

Table 12 – Correlation between intra-operative monitoring, post-HIFU radiology and histology evidence of ablation

Trial No.	Intra-operative hyperecho	Ablation : tumour ratio		
		Radiology	Histology	
5.01	Moderate	0	0.95	Grade 3
5.03	Minimal	0	0	Grade 1
5.05	No R_x	N/A	N/A	N/A
5.07	No R_x	N/A	N/A	N/A
5.10	Significant	0	<0.05	Grade 1
5.13	Minimal	0	<0.05	Grade 1
5.16	Significant	0.96	0.95	Grade 3
5.19	No R_x	N/A	N/A	N/A
5.21	Significant	0	0.95	Grade 3
5.23	Significant	1.12	0.6	Grade 2
5.29	Minimal	0	0	Grade 1
5.38	Minimal	1.4	0.6	Grade 2
5.39	Significant	1.06	0.7	Grade 2

The correlation between post-HIFU MRI and histology was poor. Previous clinical work from HIFU treatment of liver tumours suggests that MRI evidence of ablation infers successful tumour ablation [183]. In three cases, MRI demonstrated no evidence of ablation and no histological ablation was seen. In two cases, significant ablation was demonstrated on MRI and correlated with widespread histological ablation. However, in two cases the post-treatment MRI demonstrated no changes consistent with ablation despite almost complete tumour ablation on subsequent histological analysis.

3.5 Summary

An ethically-approved trial of renal HIFU with combined radiological and histological follow-up has been successfully performed using two clinical HIFU devices. Enrolment into the trial was slow and approximately two-thirds of patients initially approached were found to

be unsuitable for treatment after a formal ultrasound imaging assessment, primarily as the tumour and its margins were not clearly visible. In those suitable for treatment, there was very little morbidity and no serious adverse events attributable to HIFU. Haematological and biochemical serum markers returned to normal soon after treatment.

Treatment was challenging in many cases primarily due to poor ultrasonic visualisation of the tumour, particularly when using the co-axially aligned imaging probe in the treatment head. This lengthened many treatments and significantly diminished operator confidence in the accuracy of any treatment. Additionally, thermal energy was deposited in the pre-focal tissues in many cases, particularly in the peri-nephric fat. This resulted in two significant consequences – a further deterioration of image quality and a reduction in energy delivery to the actual focus and intended target.

Successful ablation was achieved in over half of treated patients based on post-excision histology. MRI did not predict the degree of ablation well – this is a significant concern. It was not possible to completely ablate any treated tumours – areas of viable tumours were visible in all cases.

This trial has highlighted a number of significant issues in renal HIFU which are further investigated in this thesis:

i) The role of peri-nephric fat in energy delivery
ii) Patient and tumour selection to optimise outcomes
iii) Diagnostic ultrasound imaging quality during HIFU
iv) Quality of treatment feedback & monitoring during HIFU

Each of these issues is examined and discussed in the following chapters. The overall implications for patient care as a result of this work in explored in detail in Chapter 8.

4 Effect of peri-nephric fat on HIFU ablation

In this chapter the acoustic properties of peri-nephric are presented together with its aberration effect on renal HIFU. The use of pre-HIFU fat imaging to predict clinical outcomes is also examined to help select those most appropriate for treatment.

4.1 Peri-nephric fat

The kidney differs from many other abdominal organs in that it is surrounded by a dense layer of fat – known as peri-nephric fat. Anatomically, this adipose tissue is fixed to the renal capsule, which is the outer most component of the kidney itself. It is enclosed almost entirely by Gerota's fascia, which has both an anterior and posterior leaf – see Figure 30. The anterior leaf of Gerota's fascia passes medially across the midline to enclose the contralateral kidney, where it fuses with the posterior leaf. Clinically, peri-nephric fat together with Gerota's fascia, plays an important role in protecting the kidney from physical trauma as well as limiting the spread of renal haemorrhage, infection and neoplasia.

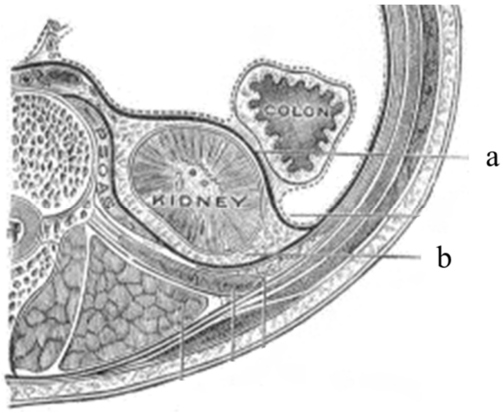

Figure 30 – Diagram of the right kidney and retroperitoneum in transverse section demonstrating Gerota's fascia (a) enclosing the peri-nephric fat (b); (adapted from www.urology-textbook.com; accessed 2/11/2011)

Peri-nephric fat is physically similar to other fat within the body and can vary in thickness – being almost absent in anorexic patients and several centimetres thick in the obese. It is often particularly thick in obese men – demonstrated clearly in Figure 31. Interestingly, the lack of peri-nephric (and other retroperitoneal fat) in underweight patients results in very poor quality cross-sectional imaging of the kidneys (CT/MRI) as there is minimal contrast between them and nearby structures.

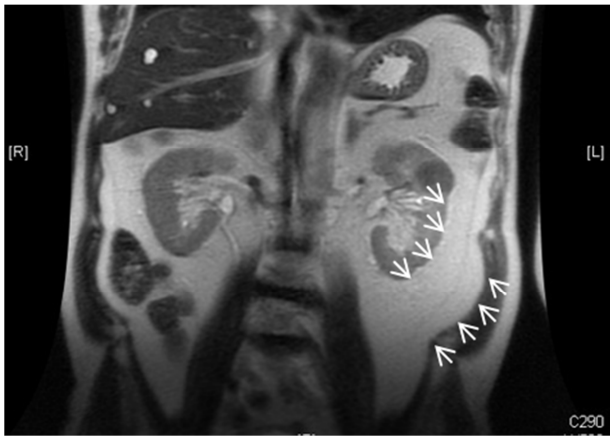

Figure 31 – Coronal MRI of patient 5.03 (BMI 34kgm^{-2}; clinically obese) demonstrating significant amount of peri-nephric fat (white arrow heads)

4.1.1 The role of peri-nephric fat in renal HIFU

There is scanty research examining the impact of the peri-nephric fat on renal HIFU. Various authors have looked at the acoustic properties of fat and its effect on ultrasound propagation. Table 13 outlines the reported attenuation coefficients from a variety of studies of human and

porcine fat compiled by Goss *et al.* and Chivers & Parry [184, 185]. It is noteworthy that although seemingly comprehensive, there are few reports of fresh human fat tested at 37°C and none used peri-nephric, intra-abdominal or retroperitoneal fat. The values for attenuation vary significantly between studies but are universally substantial when considered in the context of the typical thickness of human peri-nephric fat.

Table 13 – The attenuation of human and porcine fat as reported by a=Goss *et al.* [184] and b=Chivers & Parry [185]. NR = not reported.

Species	Location	Preparation	Temperature (°C)	Frequency (MHz)	Attenuation (dB/cm)	
					dB/cm	Np/cm
Human[a]	NR	Fresh	NR	0.8	0.44	0.051
Human[a]	Subcutaneous	Fresh or refrigerated	37	1	0.6 ± 0.2	0.07 ± 0.02
				3	1.6 ± 0.2	0.18 ± 0.02
				5	2.3 ± 0.7	0.27 ± 0.08
Human[a]	NR	Melted	15-18	0.87	0.39	0.045
				1.7	0.8	0.09
				3.4	1.4	0.16
Human[a]	NR	Formalin	18.2 ± 2	1	0.8	0.09
				2	1.7	0.2
				4	4.2	0.48
				5.6	6.1	0.70
Human[b]	Orbit	Fresh	37	5.9	20	2.3
				7.5	28.7	3.3
				9.8	37.3	4.3
Human[b]	Orbit	In-vivo	NR	6	15.6	1.8
Pig[a]	NR	Fresh	32 ± 0.1	1	1.8 ± 0.1	0.21 ± 0.01
Pig[a]	NR	Fresh	37	1.6	0.6	0.07
				2.5	1.5	0.17
				4	3	0.3
				6	4.9	0.56
Pig[a]	NR	NR	NR	2	10	1.2
				4	16	1.8
				7	32	3.7
NR[a]	NR	NR	37	1	0.3	0.04
				2	0.9	0.10
				4	2.6	0.30
				6	4.8	0.55

Damianou looked at both in-vitro and in-vivo ablation of porcine renal tissues with the aim of understanding some of the issues in renal HIFU [186]. The peri-nephric fat was noted to be highly attenuating and HIFU lesions created in kidney were significantly smaller in the

presence of a fat layer in the intervening acoustic path. Bubbles were sometimes noted at the kidney-fat interface and in the presence of these it was not possible to create HIFU lesions within the renal parenchyma.

From a more clinical perspective, findings in two renal HIFU trials from Oxford provided further insight into the role of peri-nephric fat. In a Phase I trial of a novel laparoscopic HIFU device, it was not possible to create HIFU ablation within the vascularised kidney if the peri-nephric was not removed from the kidney before treatment [130]. Histology revealed significant fat necrosis but no evidence of thermal necrosis within the kidney. Similarly, in a Phase I/II extracorporeal HIFU trial, both radiological and histological follow-up of unsuccessful renal HIFU treatments revealed evidence of fat ablation suggesting that much of the acoustic energy was deposited in the pre-focal fat tissues [172].

4.1.2 Motivation for work & hypotheses

Despite the above, it is evident that there is a lack of research into both the acoustic properties of peri-nephric fat and the impact that its thickness and location has on clinical treatments. This evidence gap motivates the work presented in this chapter which seeks to test the following hypotheses:

i) The attenuation of human peri-nephric fat is clinically significant
ii) Typical thicknesses of peri-nephric cause significant focal intensity loss
iii) The inhomogeneity of fat tissue (and its relative position) cause focal aberrations
iv) Pre-operative fat imaging analysis can help predict renal HIFU outcomes

Work presented in this chapter was undertaken jointly with Jamie Collin who assisted with the experimental measurements of fat (both human & animal) and with data processing.

4.2 The impact of peri-nephric fat attenuation on renal HIFU

Studies on in-vivo peri-nephric fat attenuation are challenging – relative estimates can be obtained by measuring back scatter reflections, but absolute measurements are most accurately performed using an ultrasound source and detector placed in front and behind a known distance of tissue. However, the perfusion of fat tissue (including peri-nephric fat) is relatively poor and changes very little after excision if maintained at 37°C in physiological conditions. Recently excised, unfixed, human peri-nephric fat held at 37°C in isotonic saline therefore provides an acceptable surrogate for in-vivo tissue.

A large number of methods exist for the measurement of ultrasonic attenuation [45]. These can be broadly categorised as follows:

i) Narrow band
   a. Phase insensitive
   b. Resonance
   c. Pulse transmission

ii) Broad band
   a. Spectrum analysis
   b. Swept frequency

The pulse transmission method represents a convenient technique which eliminates standing waves and limits sample heating due to the short pulse lengths used. Both variable and fixed path methods have been described [187, 188]. Using a variable path method, the change in amplitude of the received signal with varying positions of the receiver provides the attenuation coefficient but is difficult to use with solid tissues. Fixed path methods are more suited to the measurement of solid tissues and the insertion technique is the most widely used [188]. The received signal is measured from a source signal propagated through a tissue sample or through an identical distance of a reference medium (usually water). A comparison

between the (log) amplitudes of the two signals give the insertion loss which, when divided by the propagating distance gives the sample attenuation. The original narrow band method requires the use of different transducers to measure the attenuation across a frequency range. However, spectral analysis allows the use of the received time-domain signal to be transformed using the fast Fourier transform (FFT) into the frequency domain to obtain the attenuation coefficient as a function of frequency without the use of multiple transducers.

4.2.1 Clinical trial protocol

A trial protocol was designed to test the first two hypotheses using human tissue. Patients who were scheduled to undergo renal cancer surgery (partial or RN) were eligible for inclusion provided they were willing to give informed consent to participate in the trial. Participants were asked to donate a sample of their peri-nephric fat tissue for use in experiments and then discarded thereafter. Peri-nephric fat is routinely removed in the course of a standard RN or PN and all patients had previously been scheduled for surgery. As such, there was no additional burden to the participant. No other tissue or fluid was required from any patient and no further follow-up or hospital contact was necessary.

4.2.2 Ethical & trust management approval

Simultaneous applications were made for ethical and trust management approval to OxREC A and the Oxford Radcliffe Hospitals NHS Trust in a similar fashion to that described in Chapter 3.2.2. Ethical approval was granted by OxREC A on 17th June 2010 under approval number 10/H0604/34 (Chapter 10.2.1). Trust management approval was granted on 25th June 2010 (Chapter 10.2.2).

4.2.3 Trial conduct

Ten patients were recruited into the study having given informed consent to donate tissue. All had a pre-operative diagnosis of renal cancer on cross-sectional imaging and/or histology. The surgical procedure was performed in a standard fashion and was not altered for the purpose of this trial. For patients undergoing RN, peri-nephric fat was excised from the tumour immediately after the specimen was removed from the patient. Fat was removed from the entirety of the kidney with the exception of the fat located near to the tumour. This allowed a full histological assessment of the tumour stage. For patients undergoing PN, peri-nephric fat was removed with the kidney in-situ and fully vascularised. The fat was immediately placed into a saline-filled container at 37°C and transported to the laboratory on the hospital site for experimentation.

4.2.4 Experimental methods

4.2.4.1 Tissue handling

All measurements were made within one hour of excision. The excised tissue was transferred from the container to water bath (47cmx26cmx26cm; 27 litre capacity) containing isotonic phosphate-buffered saline (PBS) at 37°C. The PBS solution was made using 192g PBS powder dissolved in 20 litres of degassed, deionised water obtained fresh from the Model JC clinical therapy device. An immersion heater (GD 100, Grant Instruments, Shepreth, UK) was used to maintain a constant temperature of the water bath. After the tissue was placed in the water bath it was continuously held under the surface of the water to limit gas bubbles accumulating on the surface.

The excised peri-nephric fat was relatively malleable and therefore could be manipulated into different positions to allow variable path lengths to be measured. This property allowed the

measurement of multiple different propagation paths within the same tissue sample, thus serving as a control for intra-sample variations due to intrinsic inhomogeneities.

4.2.4.2 Experimental apparatus

Two identical unfocused 2.25MHz immersion transducers (Olympus NDT, Rotherham, UK) each with a 12.5mm aperture were inserted into a custom-built holder comprising two vertical blocks mounted on horizontally-positioned rods. The transducers were positioned into circular cut-outs within the vertical blocks which allowed both transducers to be moved in the horizontal plane – see Figure 32.

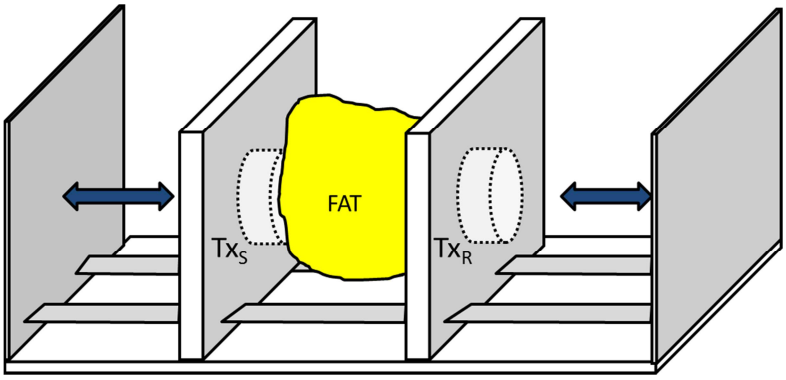

Figure 32 – Experimental apparatus for measurement of peri-nephric fat attenuation; source and receiver transducers (Tx_S, Tx_R) mounted on moveable blocks to fix fat sample at varying path lengths

A personal computer (PC) running LabView (National Instruments, UK) software was connected to a signal generator (Agilent Technologies, Santa Clara, USA) which controlled the output of the source transducer and to a digital oscilloscope (LeCroy, USA) which received the signal from the receiving transducer – see Figure 33.

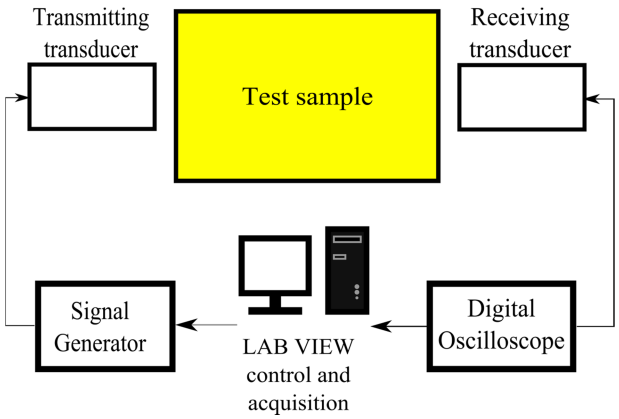

Figure 33 – Schematic diagram of experimental setup for attenuation measurement

4.2.4.3 Attenuation measurement

The fat sample was positioned between the transducers and the vertical blocks moved towards each other so as to fix the sample in place. This process served two functions, firstly to prevent movement of the sample during data acquisition and secondly to ensure that a planar surface was presented to each transducer to minimise reflections. For each measurement a 10-cycle pulse of ultrasound was transmitted (central frequency 2.25MHz) and the time-domain signal (P_F) recorded on the PC. Signal was captured with a sampling frequency of 100Ms/s. After successful acquisition, the sample was removed from between the vertical blocks using surgical forceps, ensuring that their position was not altered in the process. The received signal from propagation through the reference medium alone (P_S) was then recorded.

The fat sample was manipulated into an alternative shape whilst underwater and re-positioned between the transducer such that the path length was different. This was easily performed due to the size and consistency of the fat sample. The above process was repeated to acquire ten samples of varying path length through each sample. Ten measurements were taken in each of ten different patients (n_{total}=100).

After completion of data acquisition for each sample, the tissue was immediately placed into clinical waste for incineration to comply with the trial protocol and ethical approval. No human tissue was retained after completion of the attenuation measurements.

4.2.4.4 Data Processing

The received data was transferred to PC running Matlab software (Version R2009b, Mathworks, USA) and converted to the frequency domain using the FFT. Using an in-house Matlab script, the frequency-domain data was used to calculate the attenuation coefficient across a range of frequencies, based on the following equation:

$$\alpha_F = \frac{1}{d}\left(\ln\frac{P_S}{P_F}\right) + \alpha_S$$

Equation 1 – α_F = attenuation coefficient of fat; α_S = attenuation of saline; d = path length; P_F = amplitude of received signal through fat; P_S = amplitude of received signal through saline

The propagation path length was calculated from the time-of-flight data measured from the time difference between the first zero crossings of the received waveform and the source waveform.

4.2.5 Results

The speed of sound in fat was measured to be 1464.1m/s (±7.2ms, SEM). The attenuation coefficient of human peri-nephric across the range of 0.5-4.5MHz and is shown in Figure 34. A power law fitted attenuation was also plotted with yielded an attenuation function of 15.6 Nepers/metre/$MHz^{1.2}$. At a clinically relevant 0.8 & 1.0MHz frequency range for HIFU, this represents an attenuation coefficient of 11.9Np/m (±0.9Np/m, SEM) and 15.6Np/m (±1.0Np/m, SEM).

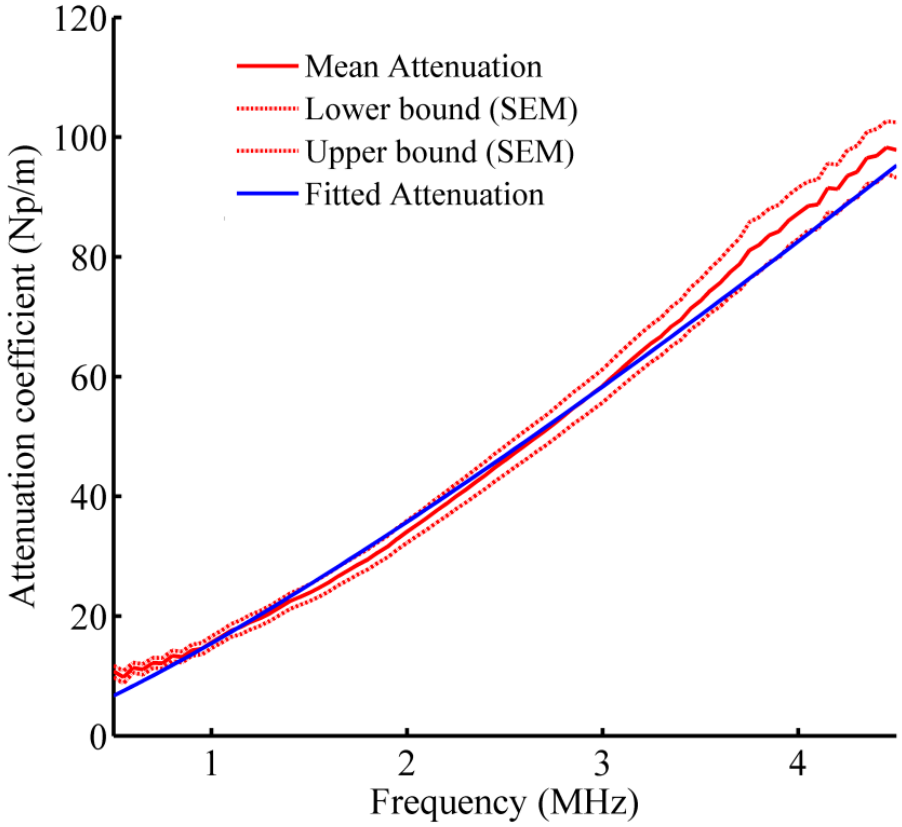

Figure 34 – Graph of attenuation coefficient of human peri-nephric fat across a range of frequencies plotted with upper and lower limits of the standard error of the mean (SEM).

4.2.6 Discussion

The attenuation calculated from human peri-nephric fat is significant. The values are generally higher than those reported for fat from other locations from humans or pig (see Table 13) although within the same order of magnitude. This degree of attenuation of ultrasound may cause significant loss of focal intensity during a clinical treatment depending on its thickness. A graph of focal intensity as a function of thickness of tissue is shown in Figure 35 using the measured attenuation coefficients.

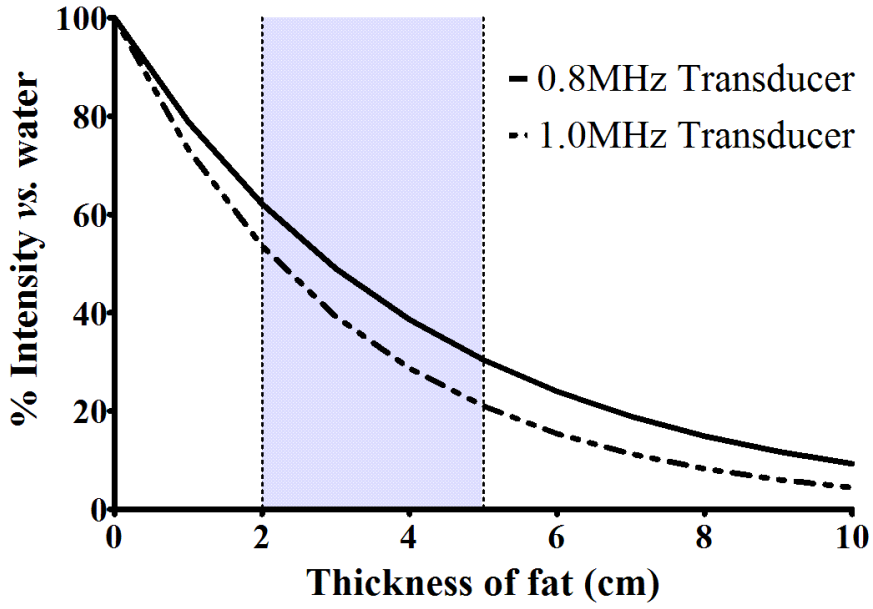

Figure 35 – Graph of focal intensity as a function of tissue thickness (% versus water) calculated for two HIFU frequencies using measured attenuation coefficient of fresh human peri-nephric fat

Typical peri-nephric fat is approximately 2-5cm thick. It varies between individuals and maybe significant in the obese. Using these typical values, the derated focal intensity of an ultrasound propagating through fat, given as a percentage of intensity through pure water, is shown in Table 14.

Table 14 – Derated focal intensity for typical thicknesses of peri-nephric fat using measured attenuation

Fat Thickness (cm)	Intensity (% vs. water)
2	62%
3	49%
4	39%
5	30%

The high attenuation of peri-nephric fat in comparison with other tissue in the HIFU propagation path also mean that a relatively small thickness of fat can have a significantly greater effect on focal energy delivery than a much larger thickness of abdominal wall structures, for example skin and muscle. It is likely that the thickness of peri-nephric fat will

better predict the outcome of renal HIFU than an assessment of the abdominal wall thickness or the total propagation distance through tissue.

4.3 Measurement of aberrations due to fat

The significant impact of the attenuation of pre-focal peri-nephric fat has been clearly demonstrated in Chapter 4.2. The estimates for derated intensity based on typical human peri-nephric fat thickness assumed the layer was uniformly thick and homogeneous in structure. The measurement technique used was optimised to ensure parallelism of the surfaces and a uniform propagation distance for the entire ultrasound beam. The technique also minimised error by using variation in path lengths; this included very short distances to minimise the errors due to beam diffraction.

Tissue, no matter what its origin, is never truly homogenous. Structural variation including blood vessels, scarring, calcifications and lymphatic glands or vessels can result in local variations in the speed of sound, resulting in phase aberrations in the propagating signal. Likewise, local variations in tissue thickness, even if the speed of sound is unchanged, will result in similar affects. A schematic diagram illustrating this is shown in Figure 36. In the context of a focused incident ultrasound beam, this aberration produces an apparent attenuation due solely to phase cancellation.

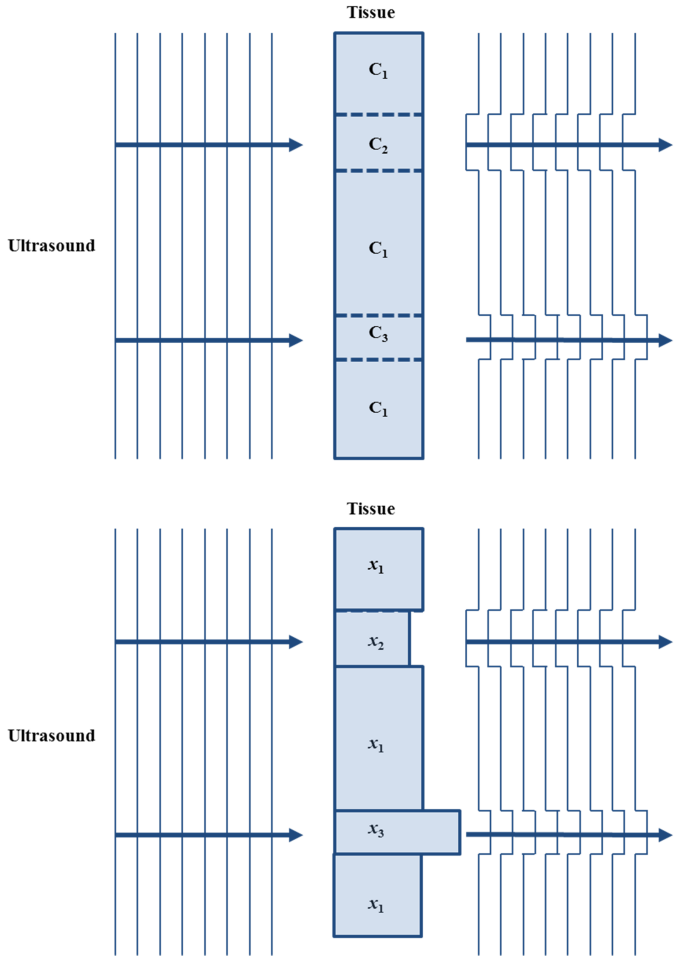

Figure 36 – Schematic demonstrating aberration due to variation in tissue homogeneity or thickness ($C_{1\text{-}3}$ & $x_{1\text{-}3}$ – different speed of sound or thickness of tissue) which produces an apparent attenuation due solely to phase cancellation (adapted from [45])

It is known that relatively minor differences in the speed of sound can result in significant apparent attenuation due to phase cancellation. These phase aberrations cause significant loss of both spatial and contrast resolution, particularly in those with a thick abdominal wall due to a muscular physique or, more commonly, obesity. In clinical practice, image blurring is the noticeable consequence.

The loss of image quality due to the abdominal wall is apparent in diagnostic imaging of the kidney. It hinders localisation of kidney tumours, particularly small tumours and makes visualisation of tumours margins and surrounding structures difficult. Image degradation progresses during renal HIFU as pre-focal tissue damage leads to further alterations in the

speed of sound and even greater loss of spatial and contrast resolution. This problem is discussed in a clinical context in Chapter 5.3.

However, phase aberrations may also impair the focusing of the HIFU beam due to phase cancellation. The impact of this is potentially more serious than a loss of diagnostic image resolution – inadvertent beam 'steering' may lead to heat deposition outside the targeted region resulting in misplaced zone of ablation and possible damage to vital structures.

A HIFU beam encounters two distinct layers of fat as it propagates towards a targeted renal tumour. The superficial layer is in the subcutaneous tissue deep to the dermis & epidermis – see Figure 37. In thin individuals it may be just a few millimetres thick; in the obese it may measure several centimetres.

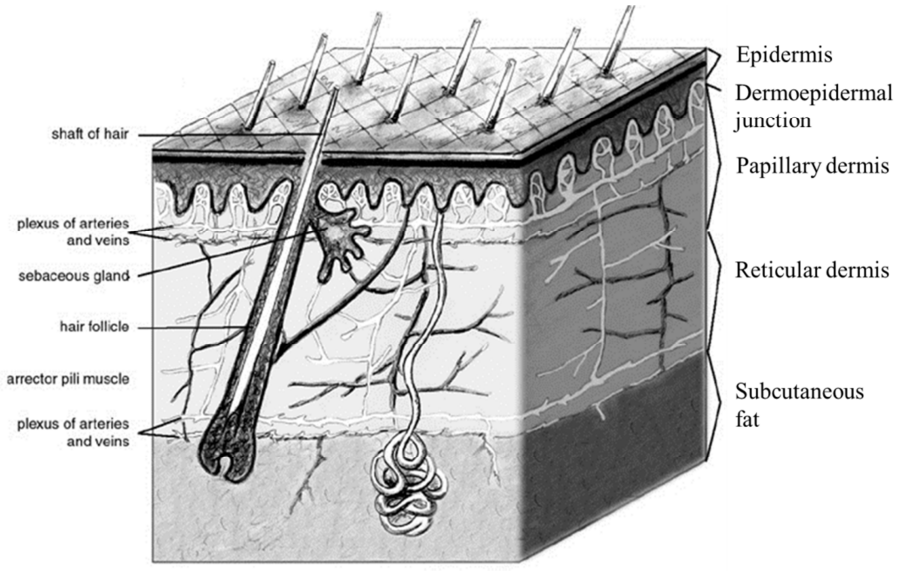

Figure 37 – Diagram of skin anatomy demonstrating location of subcutaneous fat later (adapted from [189])

The deep layer is peri-nephric fat as described in Chapter 4.1. This layer may vary in size considerably.

4.3.1 Experimental method

An experiment was designed to test the third hypothesis outlined above (Chapter 4.1.2) that fat tissue causes focal aberrations due to its inherent regions of inhomogeneity. A key aim was to assess whether the position of the two fat layers relative to the transducer was significant.

For the purpose of this work it was not possible to obtain sufficient quantities of fresh human fat to conduct the necessary measurements. Therefore, porcine fat was obtained which has a similar macro- and microscopic structure to human fat. To maintain maximum clinical applicability, porcine fat was obtained from freshly (within 1 hour) slaughtered pigs used for research purposes (Northwick Park Institute for Medical Research, Northwick Park Hospital, Harrow). Sections of skin and subcutaneous fat down to muscle, approximately 30-40cm x 30-40cm, were excised from the back and belly. The tissue was then immediately covered with 0.9% saline, wrapped in saline soaked swabs, transferred to self-sealing tissue bags and transported to the BUBBL lab in Oxford. Despite their size (60-80kg) pigs are generally lean animals; the sections of excised fat were approximately 3-5mm thick. Identical experiments were conducted on tissue from two separate pigs.

An initial set of experiments were conducted to measure the acoustic properties (speed of sound; attenuation) of subcutaneous porcine fat. The aim was to ensure that porcine fat was a suitable surrogate for human fat when compared with reported literature values. The method used was identical to that used for measurement of the same properties in human peri-nephric fat, described in Chapter 4.2.4. Varying thickness of porcine fat were placed between the two 2.25MHz transducer to allow measurements over a range of propagation path lengths.

For the aberration measurements, two sections of tissue were cut from the fat, each approximately 15cm x 15cm to ensure that the entire cone of the HIFU beam from the transducer passed through the sample. Each sample was then positioned in a custom built holder which allowed the tissue to be held horizontally without impeding the ultrasound – see Figure 38. Each holder was then attached to a positioning system in a large water tank which allowed each holder to be moved relative to the other in the axial plane of the transducer. The water within the tank was freshly filtered, degassed and heated using an immersion heater to 37°C; the tissue was given sufficient time in the tank to reach thermal equilibrium.

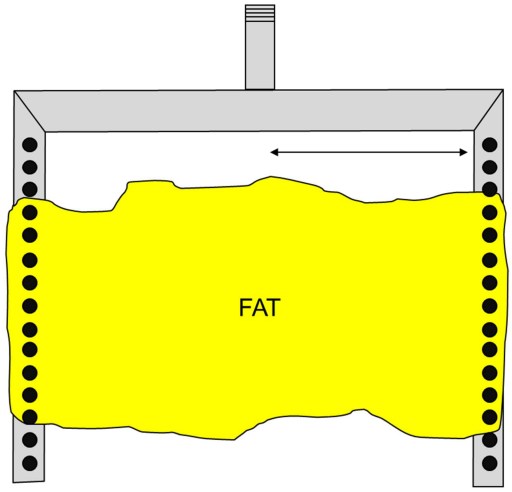

Figure 38 – Diagram of customer-built fat holder; fat held in place with sharp spikes place through tissue. Vertical supports (left and right) can be moved to accommodate different sizes of tissue

To maintain clinical applicability, the transducer from the Model JC-200 (20099-44; 0.95MHz, focal length 135mm) was used. The transducer was positioned on the floor of the tank, with the propagating surface facing vertically upwards towards the surface of the water.

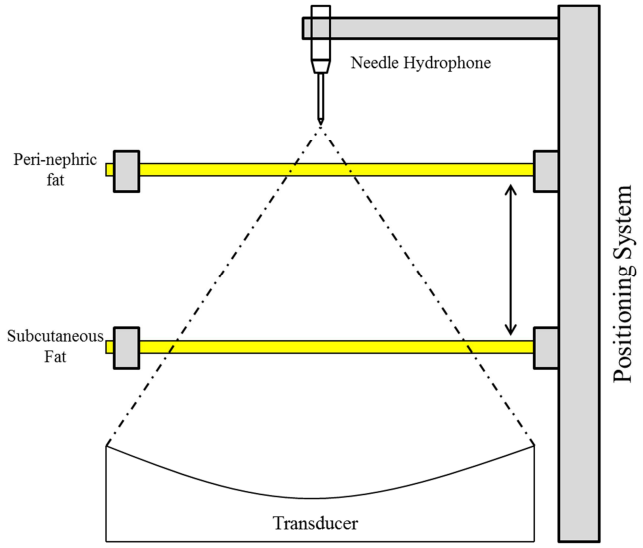

Figure 39 – Diagram of experimental setup with HIFU transducer facing upwards within water tank; needle hydrophone is attached to a positioning system to enable exact location at the transducer focus

A 0.5mm hydrophone (HPM05/3, Precision Acoustics, UK) was positioned at both the planar & axial focus of the transducer by scanning to find the beam maximum using a positioning system controlled by computer software (UMS, Precision Acoustics, UK) written in LabView (National Instruments, USA) on a desktop PC (Hewlett Packard, USA; Windows Vista). Twenty-five cycle bursts of ultrasound at $10V_{peak\text{-}to\text{-}peak}$ were transmitted by the transducer via a signal generator (33250A, Agilent Technologies, Santa Clara, CA, USA). The hydrophone signal was received on a digital oscilloscope (LeCroy Waverunner) with a synchronised trigger from the signal generator and acquired on the desktop PC – see Figure 40.

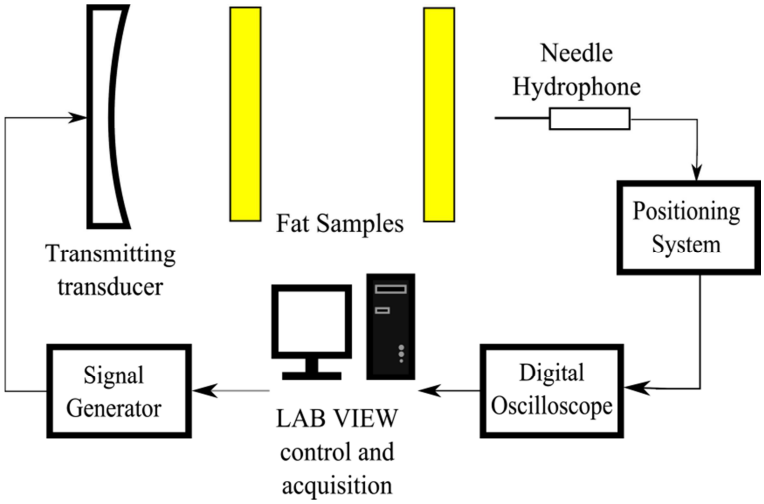

Figure 40 – Schematic diagram of experimental setup for fat aberration experiments

During an axial scan, data was acquired at 51 points separated by 0.5mm centred over the focus i.e. 12.5mm pre- and post-focal. During a planar scan, data was acquired at 31 x 31 points separated by 0.2mm centred over the focus i.e. 3mm either side of the focus in each of the two planes. Axial & planar scans were undertaken as follows:

i) Reference scan – no fat; propagation through pure water (37°C) alone
ii) Fat sample A placed 12.5mm in front of focus (cf. peri-nephric fat)
iii) Fat sample B placed 100mm in front of focus (cf. subcutaneous fat)
iv) Fat sample A & B placed together (cf. renal HIFU treatment)

The raw data was transferred to a PC computer running MATLAB software (Version 2011b; Mathworks, USA). Using in-house MATLAB scripts, transverse planar and axial plots were plotted for all fat positions. In addition, all scans were normalised to each other and scans ii), iii) & iv) were digitally subtracted from the reference scan i).

4.3.2 Results

The measured speed of sound in porcine fat was 1492m/s (±15m/s, SEM) average across all measurements (n=20). The measured attenuation coefficient was 9.6 Np/m at 1MHz. The attenuation plot over a range of frequencies (0.5-4MHz) is shown in Figure 41. This compares well with reported values for porcine fat and human fat [184].

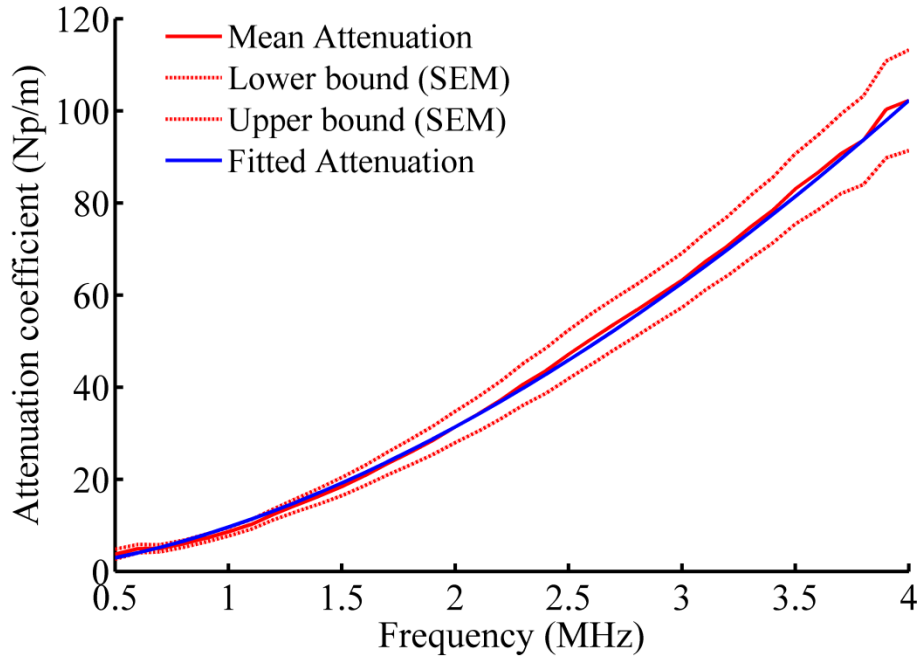

Figure 41 – Graph of attenuation coefficient of porcine subcutaneous fat across a range of frequencies plotted with upper and lower limits of the standard error of the mean (SEM).

The presence of fat layers in all positions had a significant defocusing effect, as well as an expected amplitude attenuation effect. An example set of aberrations images is shown in Figure 42 plotted as both absolute and difference transverse beam profiles. A progressive shift of the focus can be seen due to each layer of fat. The defocusing effect of both layers appears to be synergistic. The same layer of fat was used to create the transverse profiles in both images ii) and iii). It is evident that the presence of fat further from the focus – closer to the transducer cf. subcutaneous fat – had a greater defocusing effect than the same layer placed nearer to the focus. This is due to the dimensions of the HIFU beam cone as it passes through the fat layers. Close to the transducer, the beam cone is wide and therefore encounters a greater surface area of the inhomogeneities within the fat layer resulting in greater aberrations. Closer to the focus, the beam cone is narrow, the fat surface area encountered smaller and the aberrations less pronounced.

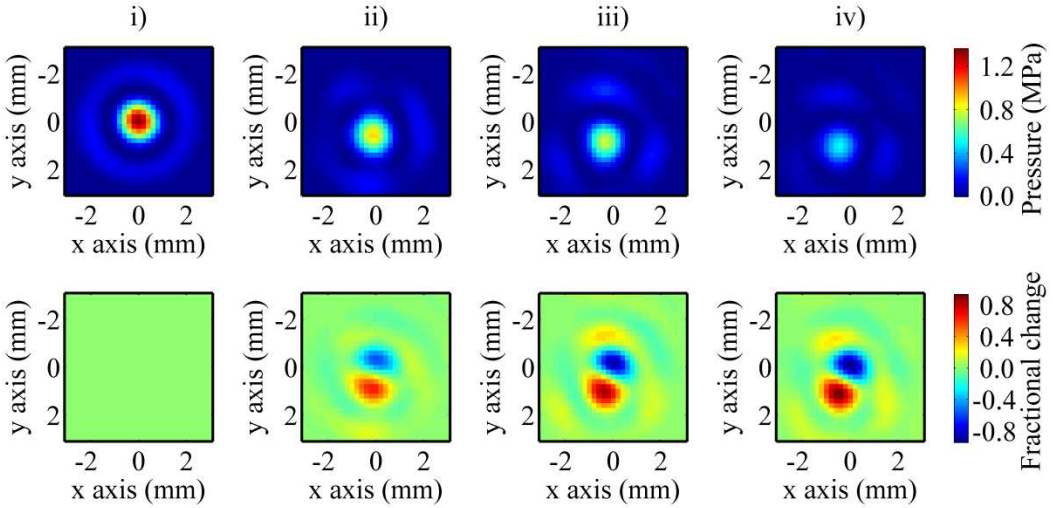

Figure 42 – Example aberration introduced by porcine fat layers using clinical HIFU transducer (20099-44, 0.95MHz, focal length 135mm, Model JC200) for various fat positions. Top row – transverse beam profile; bottom row – normalised difference images. Images i) water only, ii) fat sample 12.5mm pre-focal iii) fat sample 100mm pre-focal iv) both fat sample together

The defocusing effect of fat layers was performed using fat from two separate pigs. A compiled table of these results can be seen in Table 15. The axial shift in focus is small in comparison with the axial focal dimensions of the transducer. Equally, an axial shift in focus is less clinically significant. However a 0.5-1mm transverse focal shift was seen in both experiments. This effect was most pronounced with the fat layer close to the transducer.

Table 15 – Beam distortions introduced by the insertion of fat layers into the acoustic path of a clinical HIFU transducer

Sample name	Axial Offset (mm)	Transverse Offset (mm)	Ratio of maximum
Set 1			
No fat	0	0	1
Fat near hydrophone	0	0.6	0.66
Fat near transducer	0	0.89	0.57
Two fat layers	0.5	1.08	0.37
Set 2			
No fat	0	0	1
Fat near hydrophone	-0.5	0	0.71
Fat near transducer	1.5	0.45	0.68
Two fat layers	1.5	0.45	0.46

4.3.3 Discussion

It has been demonstrated that even very thin sections of fat tissue can cause significant focal aberrations as a result of local variations in the speed of sound, variations in the local thickness or a combination of the two. A 1mm offset in the focus, although small in absolute terms, is significant in relative terms. It represents an entire focal beam-width of a standard clinical HIFU transducer. Additionally, these aberrations were found with very thin tissue sections. In clinical practice, both subcutaneous and peri-nephric fat can reach many centimetres in thickness, particularly in the obese, leading to substantially greater focal distortions.

4.4 Predicting clinical outcomes using pre-treatment fat measurements

4.4.1 Methods

The thickness of peri-nephric fat was carefully analysed in those screened for trial inclusion to test the fourth hypothesis (Chapter 4.1.2). Whether its dimensions affected the quality of renal ultrasonography and successful final screening was a matter of some interest as it has not previously been investigated. Using pre-operative MRI/CT images, the transverse and AP depths of peri-nephric fat were measured using electronic callipers. The depths were measured from the periphery of tumour to the innermost layer of the abdominal wall. In those circumstances where the liver or spleen lay lateral to the tumour, the depth was measured from the periphery of the tumour to the liver – this ensured that only the impact of peri-nephric fat was taken into consideration. The Body Mass Index (BMI) of all patients who attended for HIFU treatment was calculated using the formula:

$$BMI\ (kg.m^2) = \frac{Weight}{(Height)^2}$$

4.4.2 Results

The peri-nephric fat and BMI measurements are presented in Table 16. The list includes all patients completing initial screening and therefore considered on the basis of pre-operative cross-sectional imaging. Those patients highlighted in yellow are those successfully completing final screening who went on to be treated with HIFU. The trial protocol dictated that only those formally treated in the trial had their BMI measured.

Table 16 – Peri-nephric fat and BMI measurements for all patients attending for final screening. Those highlighted in yellow successfully completed final screening; missing trial numbers correspond to those failing initial screening

Trial No.	Tumour Dimension (mm)	Peri-nephric Fat (trans; mm)	Peri-nephric Fat (AP;mm)	Body Mass Index ($kg.m^{-2}$)
5.01	18	20	11	22
5.02	25	21	20	-
5.03	30	29	5	34
5.05	19	10	2	28
5.06	25	26	9	-
5.07	33	8	1	Not known
5.08A	27	21	1	-
5.08B	27	22	11	-
5.08C	26	22	2	-
5.09	30	42	22	-
5.10	28	1	3	21
5.11	28	53	57	-
5.12	35	15	19	-
5.13	38	10	20	28
5.14	35	25	22	-
5.15	22	5	48	-
5.16	27	34	3	28
5.17	30	48	34	-
5.19	21	20	8	23
5.20	25	28	14	-
5.21	24	4	19	28
5.22	30	48	38	-
5.23	22	8	3	25
5.27	31	40	50	-
5.29	35	14	4	27
5.31	21	45	45	-
5.34	56	38	39	-
5.35	37	12	10	-

5.36	24	8	7	-
5.38	21	32	17	31.5
5.39	18	1	1	18

The overall mean peri-nephric fat thickness was 22.9mm (±15.0mm, SD) & 17.6mm (±16.5mm, SD) in the transverse and AP plane respectively. The mean peri-nephric fat thickness was greater in patients who failed screening than in those who passed – 28.1mm *vs.* 14.8mm (transverse) and 23.8mm *vs.*7.8mm (AP). These results are summarised graphically in Figure 43.

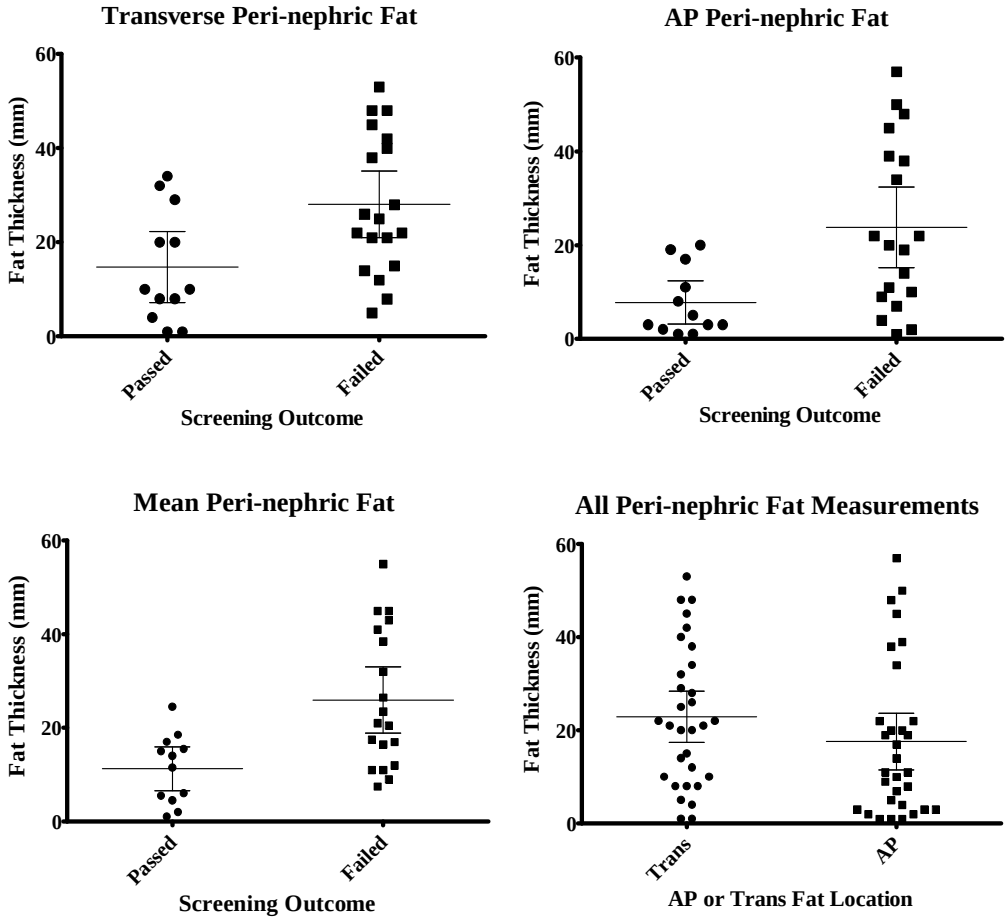

Figure 43 – Measured peri-nephric fat thickness in patients screen for trial inclusion. The mean fat represents the average of the trans & AP measurements. Error bars represent 95% CI of each data set.

These differences were statistically significant ($p<0.05$) when analysed using a Mann-Whitney U test(non-parametic) with a null hypothesis of there being no difference between the two groups. The mean peri-nephric fat thickness was also calculated from the average of

the transverse and AP measurements (12.2mm *vs.* 25.9mm). Comparison using a similar statistical analysis demonstrated a highly significant (p=0.007) difference between the fat thickness. These results are summarised in Table 17.

Table 17 – Comparison of peri-nephric fat thickness between patients who passed & failed final screening (standard deviation in brackets; unpaired two-tailed T-test)

	Passed Screening	Failed Screening	P-value
Transverse fat thickness (mm)	14.8	28.1	0.014
AP fat thickness (mm)	7.8	23.8	0.008
Mean fat thickness (mm)	11.2	25.9	0.005

4.4.3 Discussion

Despite the small sample size, it is evident that patients with large depths of peri-nephric fat are more likely to fail screening for trial inclusion. Effectively, this means that patients with significant peri-nephric fat are unlikely to be suitable for HIFU. This is plausible – it limits both diagnostic ultrasound imaging and the delivery of therapeutic ultrasound to its intended target. This is not surprising as surgery is generally more challenging in the obese – patients undergoing abdominal surgery for cancer have a higher post-operative complication rate [190]. In the context of HIFU, the peri-nephric fat poses a very specific problem unique to this minimally-invasive treatment.

The implications for patient care, specifically patient selection are discussed in detail in Chapter 8.1.1. However the management of the HIFU treatment of obese patients require considerable care. There is a risk of introducing a viscous cycle of events – pre-focal oedema due to fat attenuation resulting in poor imaging and reduced focal heating which necessitates an increase in HIFU output and an exacerbation of the problem. Rather than increasing HIFU output, it is more sensible to allow time-outs for tissue cooling, to use steroids to limit tissue oedema and to regularly move to treat different areas of the tumour.

However, peri-nephric fat is a necessary obstacle if extracorporeal HIFU is pursued. It is possible to eliminate its impact through the use of laparoscopic HIFU – a HIFU probe is introduced into the abdominal cavity and applied directly to the surface of the kidney [36, 130, 191]. This is feasible but significantly reduces the non-invasive of HIFU which remains the key feature which drives its use.

4.5 Summary

Work in this chapter has demonstrated, using fresh human tissue, that peri-nephric fat has a significant acoustic attenuation which is considerably greater than other human abdominal tissues. It has been demonstrated that it significantly limits focal energy delivery and that the inhomogeneities in fat tissue can cause considerable defocusing. From a clinical perspective, this can have a significant effect on the accuracy and likelihood of thermal ablation. It has been demonstrated using data from the aforementioned clinical trial that peri-nephric fat thickness correlates with the likelihood of being suitable for HIFU treatment. This measurement could therefore be used to predict treatment outcomes and this is discussed further in a later chapter on implications for patient care (Chapter 8). Finally, the heat deposition in pre-focal peri-nephric fat leads to tissue swelling and a further increase in attenuation. This results in a deterioration in diagnostic imaging quality of the renal tumour being treated – this is investigated quantitatively in the following chapter.

5 Improving imaging during renal HIFU

The use of renal nephrometry to predict clinical outcomes before HIFU treatment is presented together with an assessment of the deterioration in diagnostic imaging quality during HIFU

5.1 Introduction

5.2 Nephrometry scoring in renal HIFU

It is generally accepted that PN for certain renal tumours is more challenging than others. Surgery for larger tumours is associated with longer warm ischaemia time (WIT), increased rate of collecting system repair and greater blood loss, blood transfusions, operative time and urinary fistulae [192, 193]. Similarly, centrally located tumours are associated with longer WIT during PN [194] and complications rates were lower for exophytic masses compared with endophytic or hilar masses [195]. However, until recently no validated scoring system existed to categorise renal mass complexity. Without such a system, comparison of complications rate and oncological outcomes for different tumour types and for different surgical centres was not possible.

The RENAL nephrometry scoring system (available at http://www.nephrometry.com [196]) was first described by Kutikov & Uzzo and was designed to provide a structured, reproducible and quantitative assessment of key anatomical features of solid renal tumours

[197]. The scoring system describes the mass according to its size, exophytic component, nearness to the collecting system and location within the kidney - Table 18. It is evident from the scoring system that small, exophytic tumours located well away from both the collecting system and the renal hilum achieve the lowest complexity score. Total nephrometry scores (NS) of 4-6, 7-9 & 10-12 are classified as low, moderate and high complexity tumours respectively. Since its introduction, a positive correlation between NS and complication rates following surgery has been demonstrated [198-201]. The use of NS has therefore been proposed as a method of improving decision making in management of the SRM [202]. However, to date NS has not been shown to correlate with oncological outcome following renal cancer surgery. Additionally NS has not been used in the assessment of any ablative therapy for renal cancer. Despite this, the criteria used in the NS are fundamental in the decision whether to pursue an ablation modality and its assessment is therefore of considerable interest.

Table 18 – Renal nephrometry scoring system used to classify complexity of surgery for renal tumours [196]

	Criteria	**1 points**	**2 points**	**3 points**
R	Radius (maximum; cm)	≤4	>4, <7	≥7
E	Endo/exophytic	≥50%	<50%	Entirely endophytic
N	Nearness of tumour to collecting system or sinus (mm)	≥7	>4, <7	≤4
A	Anterior/posterior	No points; assigned a, p or x		
L	Location relative to polar lines	Entirely above upper or below lower	Crosses polar line	>50% across polar line' across axial midline or entirely between polar lines

The location and size of the renal tumour may significantly impact on the ability to visualise it using ultrasound. Larger tumours are inevitably easier to see; exophytic tumours may be easier to locate as their margins are clearly seen as a distortion to the normal contour of the kidney. Right-sided tumours may be easier to locate due to lower position of the right kidney which is pushed caudally by the liver. Likewise, upper pole tumours may be harder to

visualise as they may be partially obscured by the overlying rib-cage. Lower pole tumours can be examined from below the lowest ribs and may be easier to see.

5.2.1 Methods

All tumours in patients who successfully completed initial screening were analysed and their NS calculated. The most recent cross-sectional imaging available was used in the assessment – either CT or MRI. All patients were recruited through outpatients clinics where management decision were being made therefore recent (within 3 months) imaging was available in all cases.

The maximum tumour dimension was determined by measuring the size in an AP, trans & CC direction using electronic calipers within the Churchill hospital PACS (Patient Archive and Communication System) software. The exophytic component was determined by drawing an imaginary line of the normal renal outline through the tumour and measuring what percentage of the tumour lay within this outline. The closeness to the collecting system was measured using electronic calipers; finally the location was determined by viewing the tumour in the coronal plane and assessing its relation to the polar lines.

5.2.2 Results

The calculated NS for each tumour is presented Table 19 together with the tumour site, size and maximum dimension based on the pre-operative MRI.

Table 19 – Tumour site, location, maximum dimension & nephrometry score for all patients attending for final screening. Those highlighted in yellow successfully completed final screening; missing trial numbers correspond to those failing initial screening

Trial No.	Site	Location	Tumour Dimension (mm)	Nephrometry Score
5.01	Left	Upper	18	7
5.02	Right	Upper	25	7
5.03	Left	Interpolar	30	8
5.05	Left	Interpolar	19	5
5.06	Left	Interpolar	25	9
5.07	Right	Interpolar	33	8
5.08A	Left	Upper	27	8
5.08B	Left	Lower	27	7
5.08C	Right	Upper	26	8
5.09	Left	Interpolar	30	10
5.10	Right	Interpolar	28	7
5.11	Right	Lower	28	7
5.12	Right	Upper	35	8
5.13	Left	Interpolar	38	5
5.14	Right	Interpolar	35	8
5.15	Right	Upper	22	6
5.16	Right	Lower	27	4
5.17	Right	Interpolar	30	10
5.19	Right	Interpolar	21	6
5.20	Left	Upper	25	4
5.21	Right	Lower	24	4
5.22	Right	Upper	30	7
5.23	Right	Lower	22	6
5.27	Left	Interpolar	31	6
5.29	Left	Upper	30	10
5.31	Right	Interpolar	20	9
5.34	Right	Upper	56	9
5.35	Right	Upper	37	9
5.36	Right	Interpolar	24	4
5.38	Left	Lower	21	4
5.39	Right	Lower	18	4

The overall mean renal NS was seven; 18, 10 & 3 tumours were classified as low, moderate & high complexity respectively. The distributions of tumour site, location, maximum dimension and NS are shown in Figure 44.

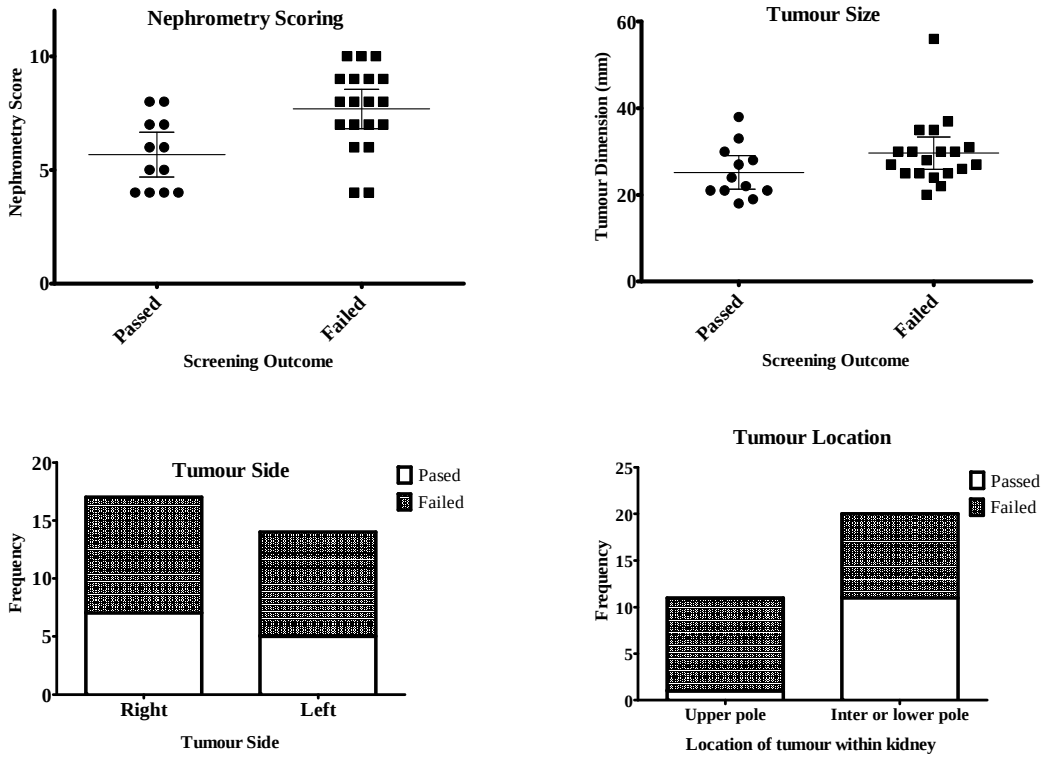

Figure 44 – Outcome of final screening categorised by tumour nephrometry score, size, side and location.

A comparison of tumour size, location and renal NS between patients who passed and failed final screening was undertaken – this is shown in Table 20. Statistical analysis was performed using an unpaired t-test for continuous data and Fisher's exact test for categorical data.

A significantly lower NS (5.7 *vs.* 7.7; p=0.003) was seen in those patients successfully completing final screening – tumours considered more complex in the context of PN were also more difficult to visualise sonographically. The mean tumour size was also smaller in the group who passed screening (25.2mm *vs.* 29.6mm; p=0.103) however this difference did not reach statistical significance. It is also noteworthy that a single outlier in the 'failed' group has significant skewed the mean tumour size. Just one upper pole tumour was judged suitable for HIFU treatment after screening, whereas 10 were considered untreatable (1/12 *vs.* 10/19; p=0.020), a statistically significant difference. There was no difference between right and

left-sided tumour with respect to their suitability for HIFU treatment (6/12 *vs.* 10/19; p=1.000).

Table 20 – Comparison of tumour size, location and nephrometry score between patients who passed & failed final screen (95% CI in brackets; *=unpaired two-tailed T-test, ^=Fisher's exact test)

	Passed Screening	Failed Screening	P-value
Maximum tumour size (mm)	25.2 (21.2-29.1)	29.6 (25.9-33.4)	0.103*
Nephrometry score	5.7 (4.7-6.7)	7.7 (6.8-8.6)	0.003*
Upper pole tumour	1/12	10/19	0.020^
Right-sided tumour	6/12	10/19	1.000^

5.2.3 Discussion

Tumour size alone was always likely to be insufficient as a predictor of HIFU outcome – there is little room for manoeuvre as tumours <20mm are usually not treated at all and tumours >40mm are generally not suitable for any ablative modality primarily because it has rarely been performed. However, it is also likely that a more detailed assessment of tumour complexity could be more successful. In this study, NS is significantly less in those who passed final screening compared with those who failed. The NS was devised to assess renal tumours in the context of partial nephrectomy. However, tumours with a strong exophytic component and those far from the collecting system are likely to be easier to visualise with diagnostic ultrasound and therefore be easier to treat. In the future, it may be possible to predict suitability for HIFU and treatment outcomes using NS and this is discussed in detail in the Chapter 8 on implications for patient care.

It is also evident from this study that upper pole tumours are extremely difficult to visualise and treat with HIFU. Just 1/12 upper pole tumours assessed for trial inclusion could be successfully treated; this compared with 10/19 interpolar or lower pole tumours. This is highly likely to be due to the synergistic impact of the lower lobe of the lungs, the liver or

spleen and the rib cage on the quality of diagnostic imaging. If the tumour and its boundaries are difficult to visualise then the operator has little confidence that HIFU can be undertaken safely and accurately and this will often lead to sub-total treatment or early cessation of treatment on safety grounds.

5.3 B-mode scoring

Evidence from previous extracorporeal HIFU trial has shown that quality of the intra-operative B-mode ultrasound may deteriorate with time [32, 172]. To allow successful treatment of an entire tumour volume, clear visualisation of all tumour margins and surrounding structures is required. In the absence of either or both these criteria, the operator is unable to confidently apply HIFU leading inevitably to residual viable tumour.

Some pre-focal heat deposition is expected during HIFU treatment. The attenuation is the skin, abdominal wall and fat tissue is not negligible and therefore some absorption will occur. Non-linear propagation of the incident ultrasound may also lead to increased absorption of the ultra-harmonics created during distortion of the ultrasound wave. This pre-focal damage causes tissue swelling, resulting in increased propagation distances and increased ultrasound reflections and absorption (see Figure 45).

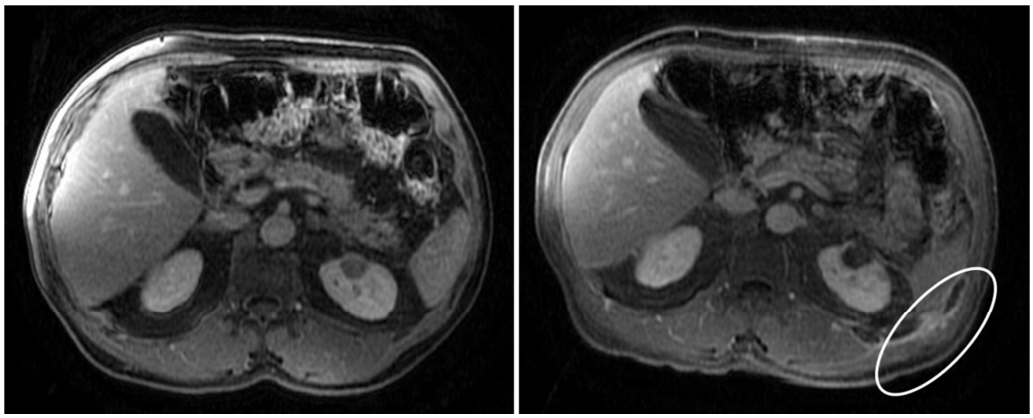

Figure 45 – Pre-HIFU (left) and post-HIFU (right) MRI of Patient 5.01 demonstrating extensive abdominal wall swelling (circled) still present 12 days after treatment

These factors combine to degrade imaging quality and may lead to a vicious cycle as increased HIFU power are used to achieve sufficient focal intensity for ablation resulting in further pre-focal damage. During clinical treatments, four techniques are used to prevent or minimise pre-focal tissue oedema:

i) Distal tumour targeted first leaving proximal structures easier to see
ii) Short rest periods taken during treatments to allow cooling
iii) Minimum HIFU power necessary used to achieve ablation
iv) Intravenous steroid (dexamethasone) administered to limit inflammation

5.3.1 Methods

To analyse the degree of image degradation during treatment, a scoring system was devised to quantify the imaging quality. Image quality was assessed at three time points – before commencement of treatment, at the mid-point of treatment and at the end of treatment. The scoring system is outlined in Table 21.

Table 21 – B-mode scoring system for intra-operative ultrasound imaging quality

B-mode Score	Description
1/5	Tumour margins/vital structures not visible Unsafe for HIFU treatment
2/5	Tumour margins/vital structures difficult to see HIFU treatment difficult; caution required
3/5	Blurring of margins/structures but remain visible Careful HIFU treatment safe
4/5	Some contrast loss but margins/structures obvious Safe for HIFU treatment
5/5	Tumour margin/vital structures perfectly clear Ideal for HIFU treatment

The purpose of devising a scoring system was to provide a quantifiable assessment of ultrasound images which are often criticised for being a subjective diagnostic tool. This assessment was created by the author and was carefully applied to images from trial patients; it is not an externally validated measure of ultrasound-image quality in the context of HIFU.

Examples of ultrasound images pre-HIFU, during HIFU and post-HIFU are shown in Figure 46 along with their B-mode score. Each patient was assessed at these three time points. The assessment was made after HIFU treatment but before any radiological or histological follow-up was available. A summary of the B-mode scores for each treated patient is shown in Table 22. The B-modes scores were compared with the baseline (pre-operative) score using a repeated measure ANOVA test to assess for differences between the means at different time points. Dunnett's multiple comparison post-test was applied, using pre-operative imaging score as the control group to determine statistical significance.

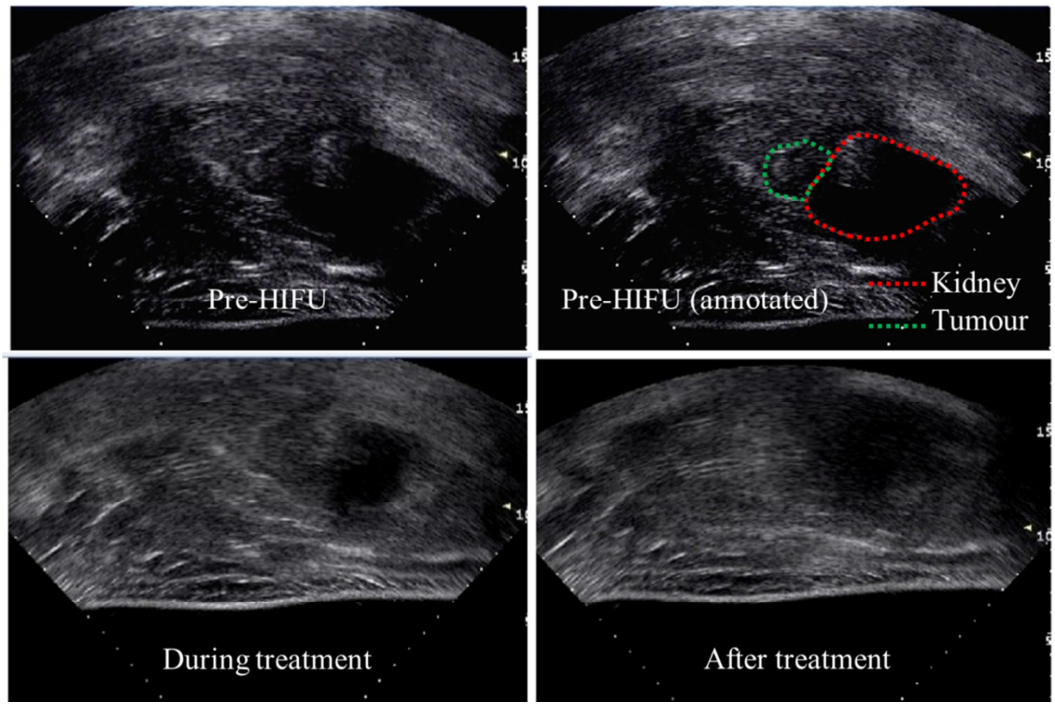

Figure 46 – Ultrasound images from Patient 5.21 demonstrating change in image quality during treatment (Model JC-200 HIFU device). Pre-HIFU image quality is good but deteriorates during treatment (3/5 during; 2/5 after). After treatment, the kidney and tumour are completely obliterated due to tissue oedema.

5.3.2 Results

The results of the B-mode scoring for all patients at the three time points are shown in Table 22. These results are also summarised in graph form in Figure 47. The mean pre-operative B-mode score was significant higher than both the intra-operative (3.2 *vs.* 1.9; $p<0.001$) and the post-operative (3.4 *vs.* 1.6; $p<0.001$). Notably, even the mean pre-operative B-mode score is

such that blurring of the tumour margins & surrounding structures. The post-operative imaging was poor in all but two cases. Indeed, at the end of treatment, eight of the cases were deemed to score 1/5 indicating that the tumour, its margins or its surrounding structures were no longer visible.

Table 22 – B-mode score for each patient before, during and after HIFU treatment. The T-test (paired, two-tailed) is used to compare intra-operative and post-operative with the baseline (pre-operative) score

Trial No.	**B-mode Score**		
	Pre-operative	Intra-operative	Post-operative
5.01	2	1	1
5.03	4	2	1
5.10	3	2	1
5.13	3	1	1
5.16	5	4	4
5.19	2	1	1
5.21	5	3	2
5.23	3	1	1
5.29	2	1	1
5.38	2	1	1
5.39	5	4	4
Mean (95% CI)	3.3 (2.4-4.1)	1.9 (1.1-2.7)	1.6 (0.8-2.5)
ANOVA (vs. pre-op)	-	p<0.001	P<0.001

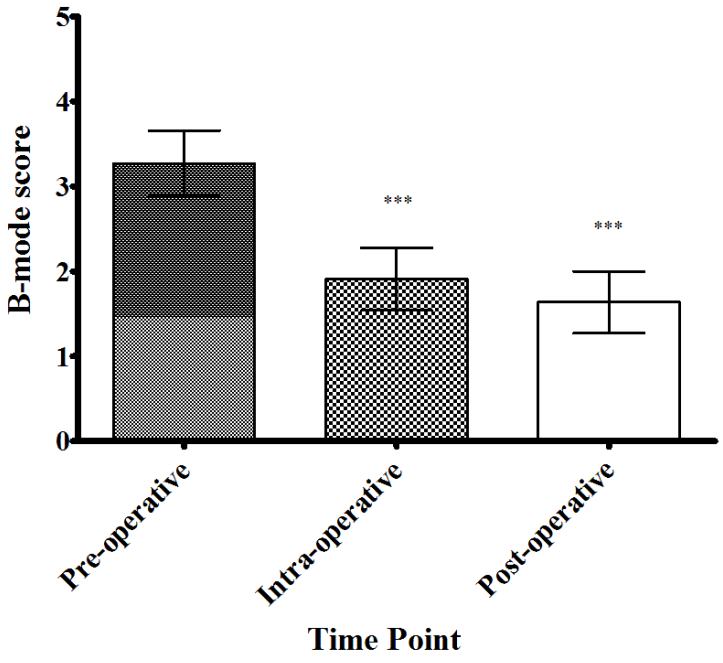

Figure 47 – Graphical representation of the mean (shaded) and SEM (whiskers) B-mode score at the three treatment time points. Data compared with repeated measures ANOVA (*=p<0.001 *vs.* pre-op)**

5.3.3 Discussion

A number of striking features are evident from the above results. Firstly, even before the HIFU treatment commenced, the imaging was far from ideal. The initial tumour imaging was considered ideal in only two patients (Patient 5.16 & 5.39). In the majority of patients the imaging was sub-optimal and caution was required during HIFU treatment. Secondly, the quality of tumour imaging declined in **all** patients during treatment. In only two treatments was the deterioration in imaging determined to be minor. Finally, the imaging was so poor in seven patients that this factor played a significant role in the decision to end the treatment. Only three treatments (Patients 5.16, 5.21 & 5.39) were ended by the HIFU clinicians because they were satisfied that the entire tumour had been ablated based on the intra-operative hyperecho B-mode imaging.

The reasons for the poor imaging quality are multiple and cannot be attributed to the quality of the ultrasound machines themselves – both devices have modern scanners that are in current clinical use. The focal lengths of the clinical transducers mean that there is a significant stand-off between the transducer and the abdominal wall during treatment. It is possible to move the diagnostic probe in a vertical direction, whilst maintaining the position of the therapeutic transducer, such that the diagnostic probe lies in contact with the skin – this leads to a significant improvement in image quality. However, it is not possible to maintain the probe in that position for treatment – the probe must be retracted so as not to interfere with the HIFU field.

It is noteworthy that in four patients the initial pre-operative imaging was deemed difficult. This can only be attributed to the imaging modality itself as HIFU treatment had not commenced. The diagnostic accuracy of ultrasonography in renal cancer is variable. Whilst tumours greater than 30mm in diameter can be detected with near 100% accuracy, tumours of

0-25mm are correctly detected in 0-79%, with tumours less than 10mm detected in less than one quarter of cases [203]. By comparison, CT diagnosis has a higher detection rate. In this clinical trial, the inclusion criteria required tumours to be less than 40mm; however many tumours were considerably smaller than this making US detection more challenging. Renal cancers less than 30mm may also be iso-echoic in up to 50% of cases – diagnosis in these circumstances relies on detection of bulging of the renal contour alone [204]. This finding can be subtle even with handheld diagnostic probes; the renal outline is often difficult to visualise clearly with the clinical HIFU devices.

The subsequent deterioration in imaging noted in all patients as HIFU treatment progressed predominately due to pre-focal heating and tissue swelling. The attenuation of the skin, abdominal wall musculature, subcutaneous fat and peri-nephric fat is significant, leading to substantial heat deposition. The consequent tissue swelling lengthens the propagation path and further increases the attenuation which limits energy delivery to the focus and impedes imaging. The standard clinical response is to allow cooling time and administer anti-inflammatory medication. However, in addition, higher output energies are often used to maintain focal heating which ultimately leads to a cycle of further image degradation and pre-focal damage.

Difficulties with ultrasound imaging have also been encountered using other ablative therapies for small renal masses. Park *et al.* assessed various factors which contributed to difficulties in performing ultrasound-guided RFA [205]. Of 31 renal masses, just 13 were considered sufficiently visible on ultrasound to allow US-guided RFA. Five masses were also deemed ultrasound-visible but subsequently required CT-guided RFA due to incomplete ablation or recurrence. A key difficulty cited during US-guided RFA was the formation of

steam bubbles which obscured diagnostic imaging – similar to the obscuration of imaging by pre-focal heating in renal HIFU.

Finally, imaging difficulty is also encountered with renal masses due to the rib cage and respiratory motion. Anatomically the kidney lies high in the retroperitoneum, surrounded posteriorly and laterally by the ribs. The lower pole of the kidney projects below the line of the rib cage but imaging of the interpolar and upper polar regions is often limited by bone. From a diagnostic perspective, inter-rib imaging using modern handheld transducers is relatively straightforward, allowing kidney visualisation in most circumstances. However, using the clinical HIFU device with its 10-12cm standoff means than ribs often impact on imaging. The kidney also moves with respiration, often by several centimetres. In this trial, single lung ventilation limited respiratory movement significantly but it is impossible to eliminate entirely. This also serves to limit imaging quality and makes treatment targeting more challenging.

5.4 Summary

In this chapter it has been demonstrated that there is a significant difference in NS between patient suitable for trial inclusion and those who are not. This is most likely due to the ease with which small, exophytic renal tumours located away from the upper pole can be seen. The importance of clear tumour visualisation is emphasised by the impact of the deterioration in imaging quality demonstrated in the second half of this chapter. Imaging became more challenging in all HIFU-treated patients and commonly led to premature cessation of the procedure. A number of clinically-relevant strategies to limit the extent and impact of image degradation were discussed.

In the following chapter, efforts to improve treatment guidance, feedback and monitoring during HIFU by spatially localising acoustic emissions from cavitation are examined using an ex-vivo animal tissue model.

6 Improving treatment guidance in HIFU

In this chapter the efficacy of an entirely novel method of monitoring HIFU using passive acoustic mapping in ex-vivo ox liver is presented, demonstrating its superiority over the existing ultrasound-based method in current clinical use

6.1 Motivation for work

Safe and effective ablation requires a reliable method of monitoring treatment progress and outcome in real-time. Current ultrasound-guided clinical devices use B-mode ultrasound images to display pre- and post-exposure image and enable the detection of hyperecho which corresponds with thermal necrosis [85]. Despite its position as the reference standard for monitoring ultrasound-guided HIFU, it is imperfect. True real-time monitoring is not possible as the magnitude of the therapeutic pulse is several orders of greater than the diagnostic pulse and thus interferes with image formation during HIFU on-time. The appearance of hyperecho does indeed correlate with thermal necrosis but they are temporally disparate. Histological ablation appears in tissue almost instantaneously when temperatures reach 60°C, yet hyperecho appears only when tissue boiling occurs and is associated with distorted lesion shape and pre-focal migration [16, 48, 206]. Statistical analysis also shows hyperecho to perform poorly as a diagnostic test for thermal ablation – sensitivity, specificity, PPV and NPV are 49-76%, 27-45%, 60-84% & 13-43% respectively [182].

Contrastingly, spatio-temporal passive acoustic mapping (PAM) is a truly real-time method of assessing thermal ablation. Its use is possible because cavitation-enhanced heating is a key method of energy deposition at the focus of a HIFU transducer [46] and emissions associated with its occurrence, received on a remote transducer, can be reconstructed to map cavitation activity [207]. It has previously been demonstrated, through both computational simulation and experiments in agar gel phantoms, that PAM can be used to map cavitation activity with high temporal and spatial resolution [103, 208].

This chapter presents work undertaken to assess PAM during HIFU ablation of ex-vivo ox liver, its performance in comparison to current clinical monitoring methods and its potential for translation into the clinical environment. Work in this chapter was undertaken jointly with Miklós Gyöngy & Carl Jensen who assisted with experimental conduct and data processing.

6.2 Hypotheses

The aim of this chapter is to present evidence to test the following hypotheses:

i) Applying thresholds to the integrated received power from PAM data can predict ex-vivo tissue ablation
ii) PAM outperforms conventional hyperecho detection of ex-vivo tissue ablation
iii) PAM is an accurate method for real-time spatial detection of ex-vivo tissue ablation
iv) Early PAM allows prediction of ablation location *before* heating occurs

6.3 Experimental Methods

6.3.1 Choice of tissue

Ox liver, rather than kidney, was chosen as the most appropriate tissue for experimentation for a numbers of reasons. The ox liver is large, measuring approximately 50cm x 40cm x 15cm, thus providing a suitable volume of tissue to conduct multiple, suitably spaced, HIFU

exposures. In contrast the kidney is a considerably smaller organ and is less easy to section and position as required. In addition the kidney is an inhomogeneous organ, containing both solid and fluid areas, which may lead to unpredictable ablation. The liver is relatively homogenous in architecture such that ablation occurs consistently, predictably and accurately in the target zone. The ox kidney is also surrounded by peri-nephric fat which further limits its suitable for HIFU experimentation. The acoustic properties of ox liver and kidney are similar [185].

6.3.2 Tissue Handling

This experimental protocol was designed to maximise clinical applicability. Fresh, whole ox livers were acquired from a local abattoir (Mutchmeat, Witney, UK) and used within four hours of slaughter. Ox liver has similar acoustic properties to many human tissues and has thus often been used for ex-vivo work [85, 89, 209-213]. The acoustic properties and cavitation thresholds for pure water and ox liver are shown in Table 23. The measurements in pure water were taken from work by del Grosso & Mader; ox liver measurements were conducted together with Miklós Gyöngy.

Table 23 – Acoustic properties and cavitation thresholds of degassed pure water & ox liver (at 1MHZ); attenuation of peri-nephric fat from Chapter 4 is included for interest.

Material / tissue @ 37°C	**Speed of sound (m/s)**	**Attenuation (Np/m)**	**Cavitation threshold (PRFP; MPa)**
Pure water **[7]**	1482	0.03	>8
Ox liver	1615	6.7	2.7
Peri-nephric fat	-	17.5	-

Using a tissue sectioning knife, samples of tissue were cut from the whole ox liver so as to fit in a Perspex holder of internal dimensions 90 x 90 x 40 mm^3. The holder was designed with hollow square sides that were then covered with 19μm-thick biaxially-orientated polyethylene terephthalate (boPET) sheets which served as acoustic windows – see Figure

48. Two similar holders were made; the second holder had a narrow central slit at the midplane (20mm from the front and back surfaces). The ox liver tissue was transferred to this second holder after experimentation to facilitate sectioning of tissue directly through this plane.

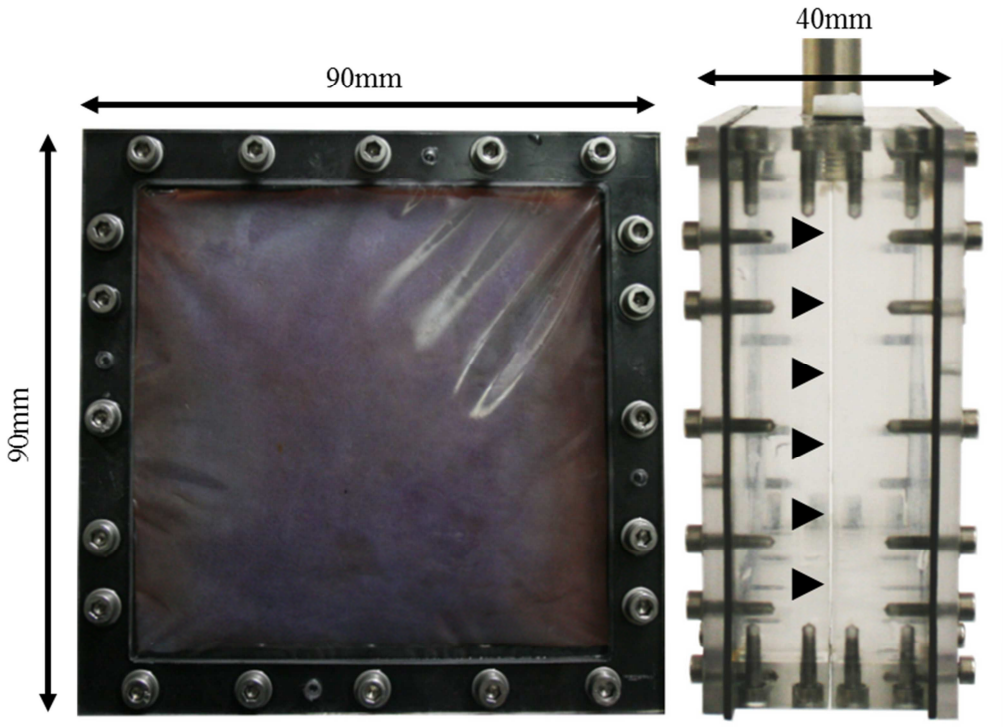

Figure 48 – Tissue holder for ox liver (90 x 90 x 40mm^3, sealed front and back by 19µm-boPET. The arrow heads indicate the mid-plane slit which facilitated tissue sectioning (picture courtesy of Miklós Gyöngy)

After any living tissue is excised, air begins to enter the tissues and raises its gas concentration. In the context of HIFU, this potentially lowers the cavitation threshold of tissue and may limit the clinical relevance of the results. Therefore, prior to insertion into the holder, each tissue sample was placed into a desiccating chamber (NALGENE® Labware, Rochester, NY, USA) with five litres of isotonic phosphate buffer saline solution (GIBCO®, Invitrogen, Paisley, UK) and degassed at -0.1 bar for 30 minutes using a vacuum pump (Model MZ2, Vacuubrand GMBH + CO KG, Wertheim, Germany). The isotonic saline solution served to prevent osmotic cell damage. After 30 minutes, the tissue was placed into the holder, maintaining the tissue under the saline solution level at all times to minimise air

entering the tissue. The holder was then transferred to a large tank of degassed, deionised water held at 37°C. The water within the tank was pumped through a flow loop containing filters (1μm & 0.2μm), a degassing membrane (connected to a vacuum pump) and an in-line heater to maintain water temperature.

6.3.3 Transducers

A custom-manufactured 1.06MHz transducer (H-102B SN22, Sonic Concepts, Bothell WA, USA) was used to ablate the ox liver tissue. A rectangular cut-out (18 x 45mm^2) in the transducer allowed co-axial placement of a 5-10MHz linear array (Model L10-5, Zonare Medical Systems, Mountain View CA, USA) which functioned as the multi-element passive cavitation sensor – see Figure 49. The HIFU transducer and the linear array placed co-axially using a custom-manufactured holder.

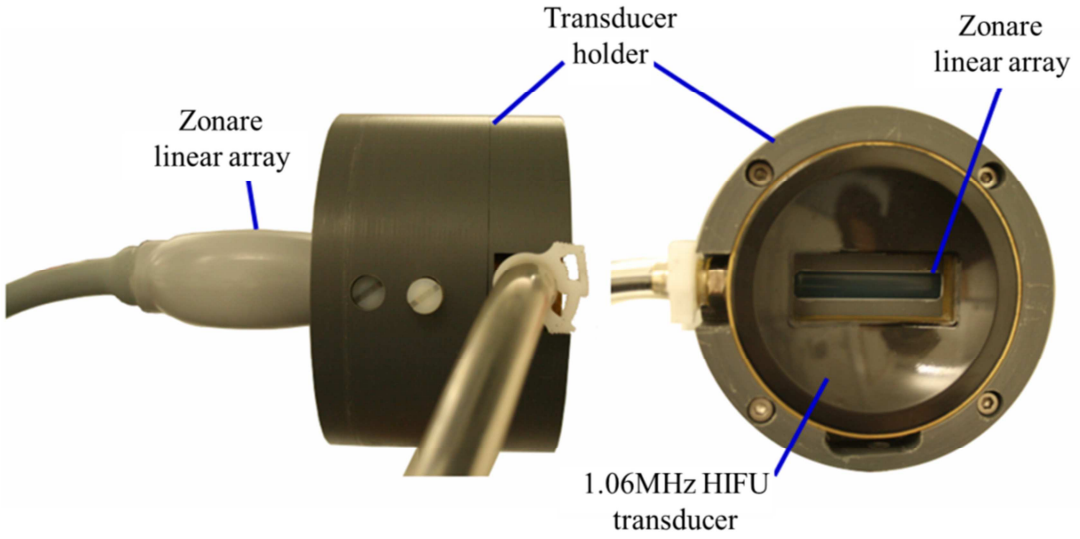

Figure 49 – 1.06MHz HIFU transducer mounted co-axially through the central rectangular cut-out with the Zonare 5-10MHz linear array (picture courtesy of Miklós Gyöngy)

The HIFU transducer was spherically focused with a 64mm active diameter. The transducer was calibrated in water using a 0.5mm needle hydrophone (SN 1203, Precision Acoustics, Dorchester, Dorset, UK). The absolute calibration was performed up to 1.1MPa only to avoid

damage to the hydrophone. The -6dB longitudinal, transverse and elevational beam widths were measured as 16mm, 2mm & 1mm respectively - see Table 24.

Table 24 – Characteristics of HIFU transducer used in PAM experiments

Frequency (MHz)	**Characteristics (mm)**		**-6dB Focal Width (mm)**		
	Focal Length	Aperture	Axial	Transverse	Elevation
1.06	64	63	16	1	2

The linear array consisted of 128 elements spanning an aperture of 38mm. Each element has a 0.3 width, 5mm elevational height and a nominal frequency response of 5-10MHz. The diagnostic ultrasound system connected to the array (z.one, Zonare Medical Systems) could operate in active or passive mode. In active mode, conventional B-mode images were acquired at a 10Hz frame rate. In passive mode, no active pulse was transmitted; instead 64 channels of down-modulated in-phase and quadrate (I/Q data; 4.6-9.6MHz) data were recorded at a frame rate of 30-100Hz depending on HIFU exposure length. The channels were connected to every other element across the array in order to maximise longitudinal resolution through use of the entire aperture.

The dual transducer assembly was placed into the large water tank such that the curved axis of the HIFU transducer was directed through one of the acoustic windows of the holder. The assembly was attached to a motorised positioning system which allowed control of movement in three axes to 0.1mm accuracy. The assembly was then aligned using B-mode ultrasound (active mode) such that its geometric focus coincided with mid-plane of the Perspex holder, at a depth of 20mm into the tissue – see Figure 50.

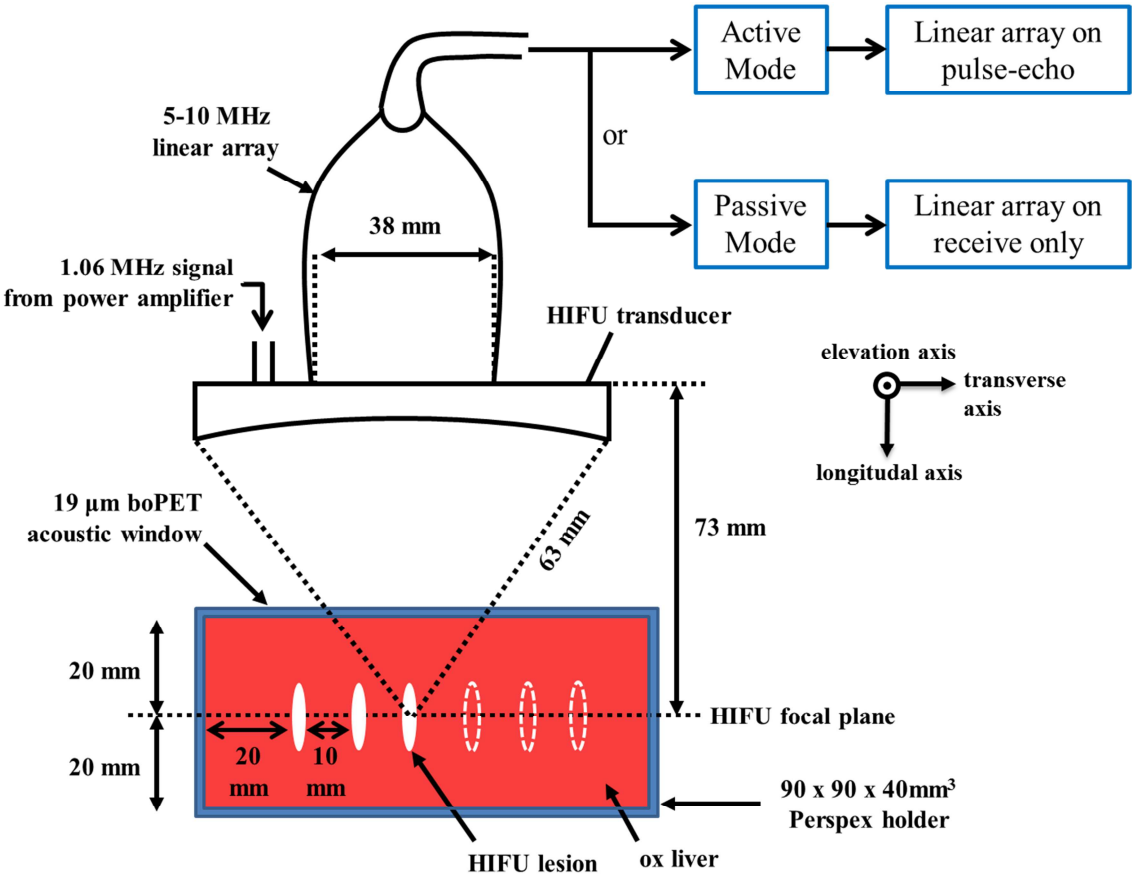

Figure 50 – Schematic of transducer assembly and tissue holder set-up; Zonare linear array can function in active (pulse-echo) or passive (receive only) modes

To generate HIFU a signal generator (Model 33250A, Agilent Technologies, Santa Clare, CA) was connected to a power amplifier (Model A300, ENI, Rochester, NY) which was in turn connected to a 50Ω matching network which was custom made for the HIFU transducer. Both the positioning system and HIFU signal output were controlled by LabVIEW software. A schematic of the electronics setup is shown in Figure 51.

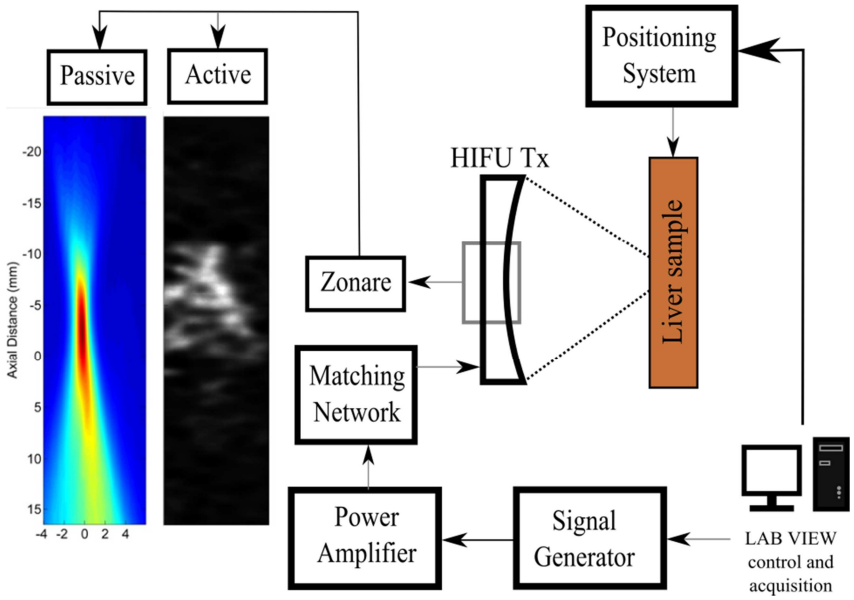

Figure 51 – Schematic of the electronics setup

6.3.4 HIFU Exposures

The 1.06MHz HIFU transducer was driven continuously at its operating frequency. Six different PRFP amplitudes, calculated from the transducer calibration over a tissue path length of 20mm (μ=6.7Np/m), were used for the HIFU exposures, increasing uniformly from 3.6MPa to 8.0MPa. The amplitudes were specifically chosen to provide monitoring information on these specific clinical relevant scenarios:

i) Sub-therapeutic range (at threshold for thermal ablation)
ii) Therapeutic range for safe thermal ablation (consistent ablation; no focal distortion)
iii) Supra-therapeutic range (focal migration and lesion distortion)

For the purposes of labelling, the sub-therapeutic range was referred to as low amplitude (3.6-4.5MPa), the therapeutic range as intermediate (5.4-6.3MPa) and the supra-therapeutic range as high (7.2-8.0MPa). The intensity values corresponding to these pressures are shown in Table 25.

Table 25 – PRFPs and corresponding intensity values used during HIFU exposures (SPTP – spatial-peal temporal peak; SPTA – spatial-peak temporal-average; SATA – spatial-average temporal-average)

PRFP (MPa)	Intensity Values (kW/cm^2)		
	I_{SPTP}	I_{SPTA}	I_{SATA} (Gaussian)
3.6	0.8	0.4	0.2
4.5	1.4	0.7	0.3
5.4	1.9	1.0	0.5
6.3	2.6	1.3	0.7
7.2	3.5	1.7	0.9
8.0	4.2	2.1	1.2

Exposure durations of 2, 5 & 10 seconds were used for each PRFP, giving 18 exposure configurations in total. The transducer characteristics outlined in Table 24 were used to give a -6dB focal volume:

$$Ellipsoid\ volume = \frac{4}{3}\pi(x.y.z) = \frac{4}{3}\pi(1.6 * 0.1 * 0.2) = 0.134cm^3$$

Using the I_{SATA} intensity values in Table 25, a measure of energy deposited for each exposure configuration was calculated and can be seen in Table 26.

Table 26 – Thermal dose values for each of the 18 exposure configurations based on absolute & spatial calibrations

PRFP (MPa)	Energy Deposited (kJ)		
	2 secs	5 secs	10 secs
3.6	0.05	0.13	0.27
4.5	0.08	0.20	0.40
5.4	0.13	0.34	0.67
6.3	0.19	0.47	0.94
7.2	0.24	0.60	1.21
8.0	0.32	0.80	1.61

To allow a comparison between the active and passive modes of monitoring HIFU, each exposure configuration was undertaken twice, thus creating a grid of 36 exposures in each liver sample. The exposures was placed 10mm apart in rows of six, with 10mm spacing between rows. Odd-numbered rows were monitored by active (B-mode ultrasound) imaging and even-numbered rows by passive (acoustic mapping) imaging, as shown in Figure 52.

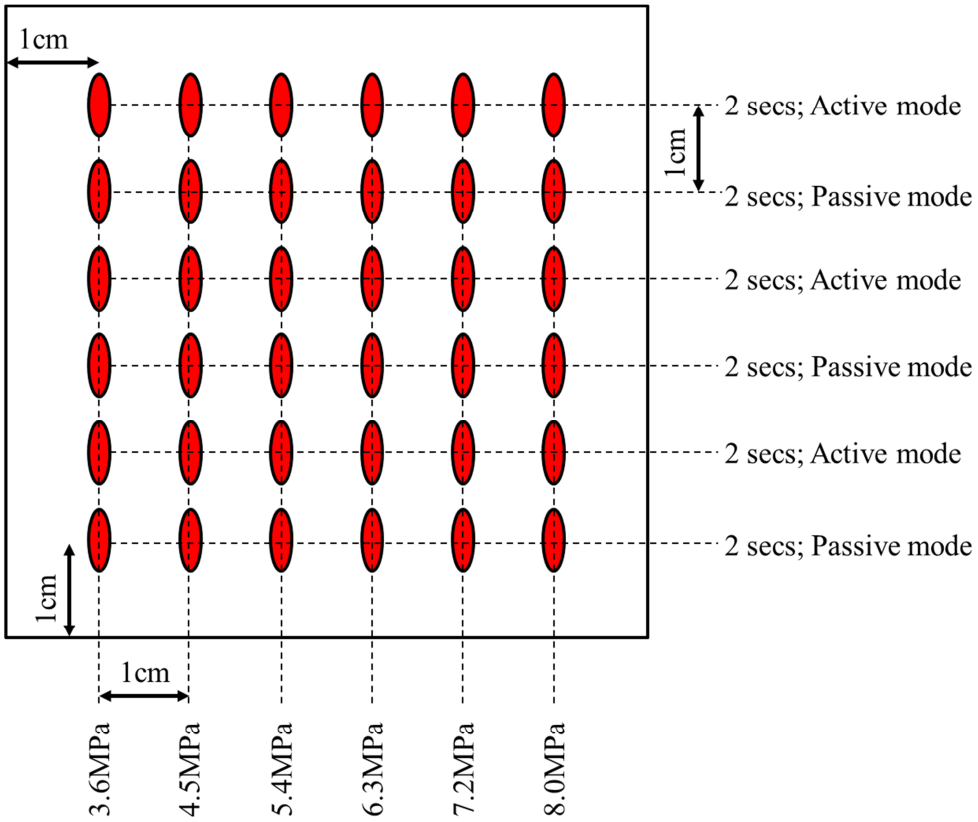

Figure 52 – Schematic demonstrating HIFU exposure configurations and use of monitoring techniques

In total, five samples of liver from five different animals were assessed, using both active and passive mode for each exposure configuration. In total, 180 exposures were conducted; however there was data loss for five exposures. Consequently, using the matched pair statistical analysis described later, there were 170 pairs available for comparison.

6.3.5 Data Processing

After all 36 HIFU exposures were completed the monitoring data were transferred to a personal computer and converted to Matlab (R2009b, Mathworks, Natick, MA) data files for further processing.

6.3.5.1 Active mode (B-mode ultrasound)

The active mode data were analysed on a frame-by-frame basis to locate the image immediately before and after HIFU treatment. The appropriate images were easy to identify as the HIFU signal causes significant interference during B-mode imaging. The pre-HIFU

image was then digitally subtracted from the post-HIFU image using the Matlab image processing toolbox. This processed created a differential B-mode image to analyse for evidence of hyperecho formation.

6.3.5.2 Passive mode (PAM)

The passively acquired I/Q was up-modulated to RF. A comb filter of 300KHz bandwidth was applied to each channel of RF data to separate the received signal into its broadband and harmonic components. Both signal components were then fed through a beamforming algorithm as previously described by Gyöngy & Coussios and discussed in Chapter 2.7 [103]. A region of interest (ROI) of 40mm (axial) by 10mm (transverse) centred around the focus was defined and the acoustic source power at each location within the ROI was reconstructed using the probe sensitivity [102, 208]. The produced individual frames mapping the source distribution every 10, 20 or 33ms (depending on frame rate) HIFU exposure, giving information on the onset, duration and location of activity. In addition, integration of the acoustic source power across of the frames during each exposure (2 secs – 200; 5 secs – 250; 10 secs – 333) yielded a measure of the radiated acoustic energy from each location.

6.3.6 Gross Pathology

After completion of all 36 exposures in each liver sample, the tissue was immediately sectioned for visual analysis and photography. The tissue was cut into two halves perpendicular to the direction of the HIFU propagation i.e. parallel to the acoustic windows of the holder. As discussed and demonstrated in Chapter 6.3.2 and Figure 48 respectively, to facilitate this process the tissue was transferred to an alternative holder with narrow slit located exactly at the mid-plane. A sharp tissue sectioning knife was used to accurately cut across this plane. The sectioned halves of tissue were placed side-by-side and photographed. The zone of ablation in tissue were easily identified as a sharply demarcated blanched region

due to protein denaturation and are termed ‘lesions’ for the remainder of this thesis [214]. The presence or absence of a lesion at each exposure location was determined by consensus opinion of two researchers (author & Carl Jensen) – see Figure 53.

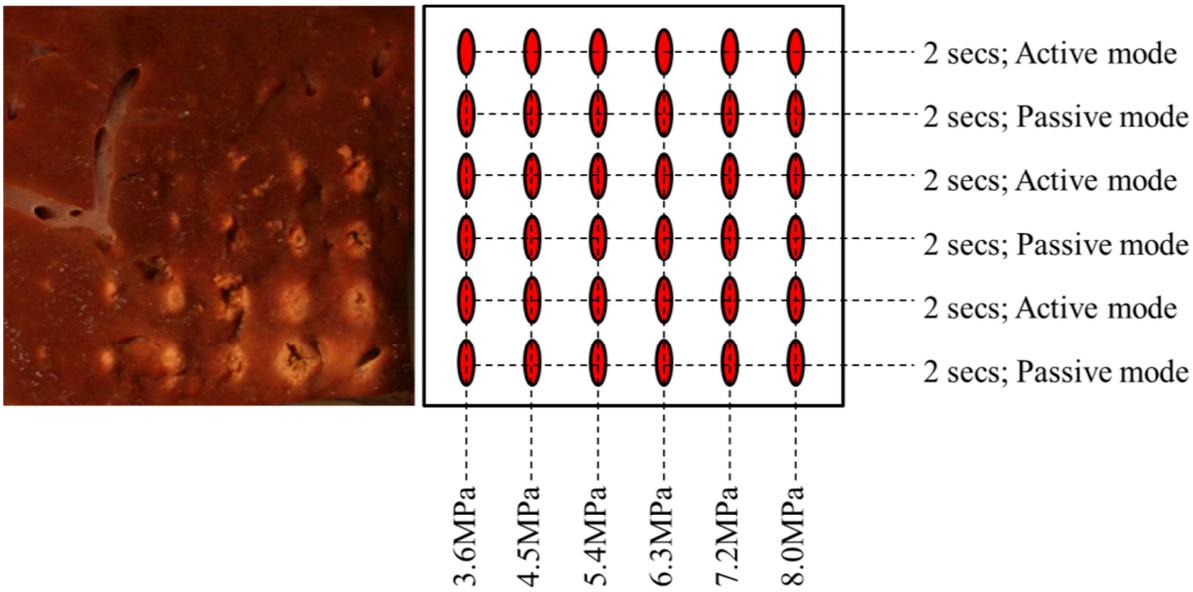

Figure 53 – Gross pathology photograph or exposure grid placed alongside schematic of HIFU exposure configurations. The presence of tissue blanching can be clearly seen indicating thermal ablation.

After photography, the tissue was then sectioned along the imaging plane and the two halves of tissue then placed next to each other to produce cross-sectional images of the lesion in the axial plane of the transducer – see Figure 54. The tissue cross-sectional images were used to perform a visual comparison of the location and shape of the thermal lesions relative to both the B-mode and PAM images.

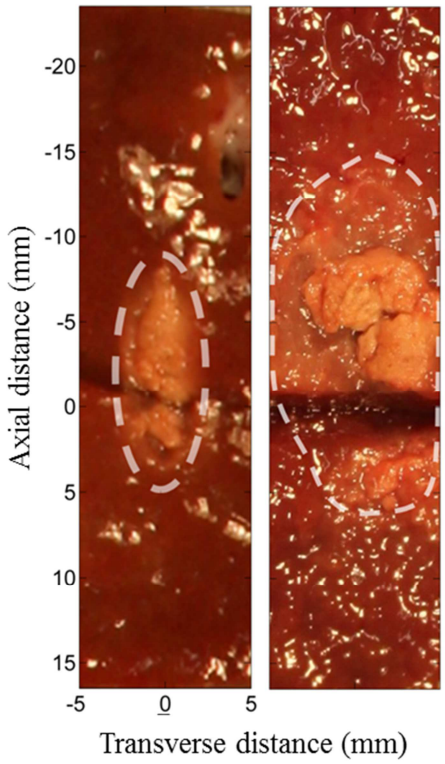

Figure 54 – Axial cross-section images of thermal ablation with two different HIFU exposure configurations. The plane of the tissue cut is centred at zero (axial). The left image demonstrates a non-distorted focally-positioned lesion; the right image demonstrates a tadpole-shaped pre-focal lesion.

6.3.7 Comparison of B-mode & PAM images with gross pathology

To facilitate a comparison of lesion location, the B-mode images and PAM were displayed side-by-side next to the gross pathology. The position of the focus within the imaging was aligned with the tissue which had been sectioned through the geometric focus as described in Chapter 6.3.6.

The difference B-mode images were assessed for the presence or absence of hyperecho by two research clinicians (author & Tom Leslie). Both assessors had experience in clinical ultrasound-guided HIFU treatment. The assessments were performed independently and were blinded to the exposure configurations and the outcome of the PAM imaging for the same configuration. Each assessor classified each image as either positive or negative for the presence of HIFU-related hyperecho; no differences in opinion were encountered.

The PAM data were assessed by first creating a 10mm x 10mm ROI centred on the focus. Within this window, the filtered broadband and harmonic data were integrated across all frames acquired during HIFU on-time producing a total received broadband and harmonic energy for each configuration. The total broadband energy is a measure of the energy of the noise produced by inertial cavitation during HIFU – this has been shown to correlate well with the temperature rise due to inertial cavitation [62]. Harmonic emissions during thermal ablation are primarily associated with non-linear scattering of the HIFU by large, boiling bubbles produced as temperatures approach or rise above 100°C [101, 215]. Exposures that lead to significant harmonic emissions can therefore be generally viewed as overtreatment i.e. as having an input energy significantly greater than the energy required to produce the desired effect.

To allow a quantitative analysis of the PAM data, the broadband and harmonic emission energies were compared with the presence or absence of a lesion at gross pathology. From this comparison, energy thresholds of simultaneously occurring emissions were defined. The broadband & harmonic energy levels that most accurately predicted lesion occurrence were 0.0137mJ & 1.17mJ respectively. These thresholds were used to categorise the PAM data as positive or negative for the presence of significant bubble-related emissions.

6.3.8 Statistical analysis

Eighty-five pairs of data were available for comparison with gross pathology data. For each monitoring method, the gross pathology result was compared with the presence or absence of hyperecho (active monitoring) or whether the emission thresholds were exceeded. A positive detector result with a positive gross pathology result was a true positive (TP). A negative detector result with a negative gross pathology result was a true negative (TN). Conversely, a positive detector result with a negative gross pathology result and a negative detector result

with a positive gross pathology result were a false positive (FP) and false negative (FN) respectively. The performance of each detector was initially assessed by calculating the test sensitivity, specificity, PPV & NPV, using the following formulae:

$$\text{Sensitivity (\%)} = \left(\frac{TP}{TP + FN}\right) * 100 \qquad PPV\ (\%) = \left(\frac{TP}{TP + FP}\right) * 100$$

$$\text{Specificity (\%)} = \left(\frac{TN}{TN + FP}\right) * 100 \qquad NPV\ (\%) = \left(\frac{TN}{TN + FN}\right) * 100$$

The overall accuracy of each detector was also calculated:

$$\text{Accuracy (\%)} = \left(\frac{TP + TN}{TP + TN + FP + FN}\right) * 100$$

A formal statistical comparison between the two detectors requires the use of a matched pair analysis. The accuracy, sensitivity & specificity were compared using McNemar's test with Yate's correction [216]. The PPV & NPV were analysed using a test statistic proposed by Leisenring *et al.* which compares matched pairs similar to McNemar's test but specifically conditioned on the test outcome [217]. The null hypothesis for these statistical tests was that the probability that the two tests disagree were the same, that is:

$$P(Hyperecho[+ve], PAM[-ve]) = P(Hyperecho[-ve], PAM[+ve])$$

Statistical significance was defined as $p<0.05$. Any $p<0.05$ thus gave reason to reject the null hypothesis and accept the alternative hypothesis:

$$P(Hyperecho[+ve], PAM[-ve]) \neq P(Hyperecho[-ve], PAM[+ve])$$

Acceptance of the alternative hypothesis means that any difference between the two probabilities was likely due to a true difference in the detectors' performance rather than due to chance.

6.4 Lesion size, shape & position

Gross pathology analysis & photography confirmed that lesion size, shape & position were consistent for both monitoring methods for all exposure configurations. Overall lesions were seen in 106/170 exposures; lesions were seen in 10/54 (19%), 40/58 (69%) & 56/58 (97%) exposures in the low, intermediate & high pressure categories respectively. Lesion size correlated with both increasing PRFP and increasing exposure duration – see Figure 55. At the higher exposure regimes pitting, located within the boundaries of the zone of ablation, was also evident – these cavities form during HIFU due to gas pockets arising as a result of tissue boiling [215].

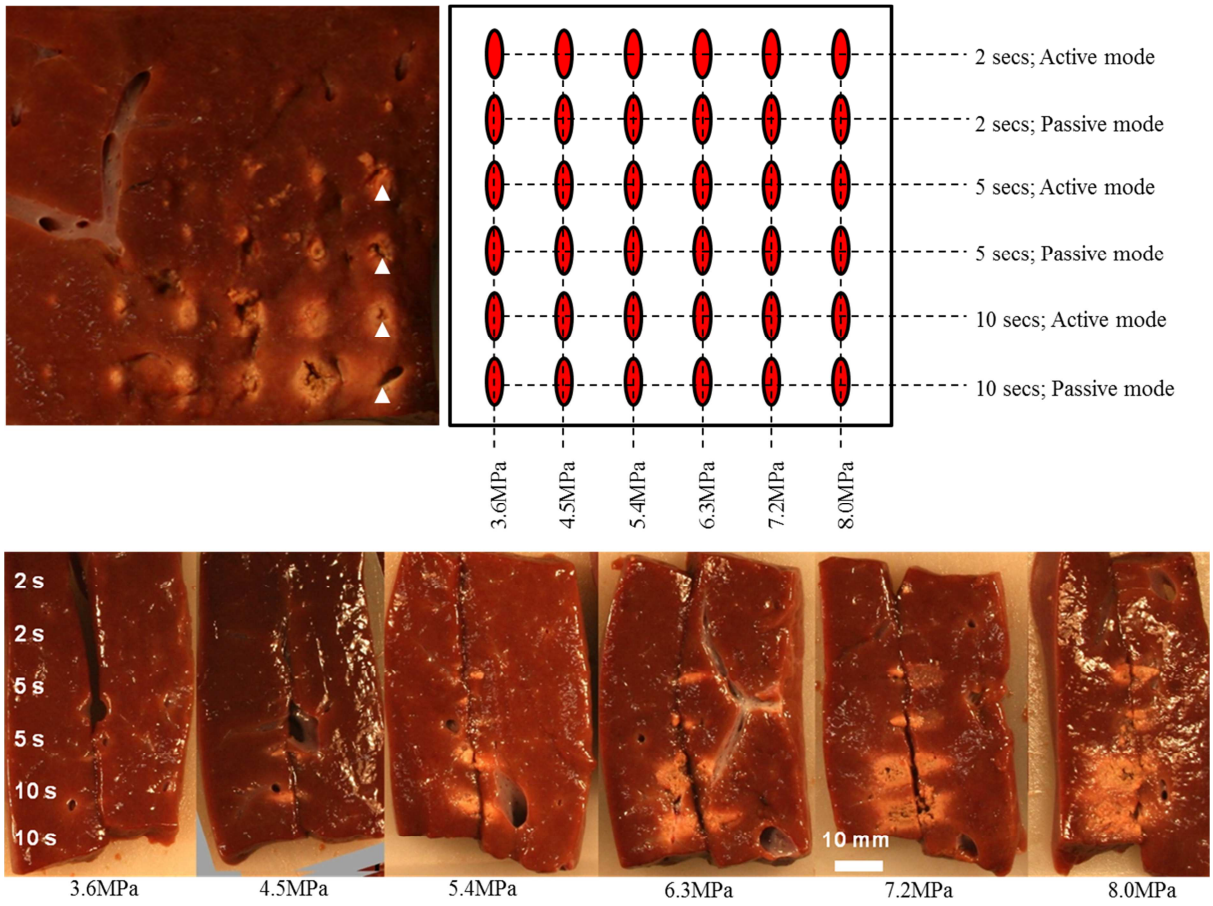

Figure 55 – Photograph showing transverse (top) & axial (bottom) cross-sections of lesions for one liver. Pits are visible (arrowheads) in the higher pressure and longer duration exposures due to boiling. Notice the oversized, distorted (tadpole-shaped) and pre-focally migrated lesions seen in the high pressure exposures.

Figure 55 also reveals that the majority of lesions in the high exposure configuration (7.2-8.0MPa) are oversized, distorted in shape (tadpole-shaped) and positioned pre-focal to the mid-plane cut. These lesion characteristics are again associated with tissue boiling and overtreatment [48]. It is evident that the most clinically relevant pressure range is the intermediate category where ablation is often seen and the lesions produced are positioned at the focus, uniformly-shaped and of a size consistent with the focal dimensions of the transducer. At the low pressure range, ablation is rarely seen (19%). At the high pressure range lesions are invariably seen; however they are often distorted in shape, size and position – not ideal for safe therapeutic use.

6.5 Predicting lesion occurrence – PAM versus hyperecho

The gross pathology, B-mode hyperecho images and PAM images were categorised into positive or negative for the presence of a lesion as discussed above. The thresholds for PAM were calculated using ROI curves to give the maximum accuracy possible. Table 27 outlines the rate of lesion occurrence seen (gross pathology) or predicted (B-mode hyperecho & PAM).

Table 27 – Rate of lesion occurrence (seen or predicted) from 170 HIFU exposures; exposures were monitored with B-mode hyperecho or PAM hence half (85) exposures are seen for each

	Number of lesions (seen[1] or predicted[2])		
	Low	Intermediate	High
Gross pathology[1]	19% (10/54)	69% (40/58)	86% (50/58)
B-mode hyperecho[2]	0% (0/27)	21% (6/29)	66% (19/29)
PAM[2]	7% (2/27)	55% (16/29)	93% (27/29)

The above offers some information on the monitoring techniques being assessed. However, a direct comparison using these figures is misleading as the data are paired and must be analysed using paired statistics as described in Chapter 6.3.8. A detailed breakdown of the performance of the two detectors is shown in Table 28. At the low pressure range true lesion occurrence based on gross pathology was uncommon i.e. sub-therapeutic from a clinical perspective. Both detectors performed similarly – both were usually negative and no statistically significant difference was seen between them. This is logical at sub-therapeutic exposures – neither the cavitation nor boiling threshold was reached. However, both detectors had poor specificity (0% vs. 20%) meaning they failed to detect the true lesions seen at this pressure which occurred only at the longer duration exposures. The single FP noted with PAM in this pressure range occurred as the focus lay over a large blood vessel which resulted in strong cavitation activity within the saline fluid.

At the intermediate pressure range, lesions were regularly produced without the features of overtreatment – this is the ideal therapeutic range. PAM significantly outperformed hyperecho. Hyperecho provided correct detection in less than half (13/29, 45%) of all exposures; PAM, in contrast, was accurate in 23/29 exposures (79%; p=0.011). Both returned similar specificity (8/9, 89%) and similar PPV (5/6, 84% *vs.* 15/16, 93%). The sensitivity (ability to detect TPs) of PAM is significantly greater than hyperecho (15/20, 75% *vs.* 5/20, 25%; p=0.0061) as is the NPV (8/13, 62% *vs.* 8/23, 35%; p=0.011).

At the high pressure range, lesions were invariably produced but were often distorted in shape, size and position. Hyperecho was more often accurate at this exposure level (18/29) due to high focal temperatures causing tissue boiling. However, PAM was again more accurate (26/29; p=0.018) with a higher sensitivity (18/28, 64% *vs.* 26/28, 93%; p=0.018).

The data is summarised graphically in Figure 56. Overall, across the entire pressure range, PAM accurately predicted lesion occurrence in 84% (71/85). The PPV & NPV, essentially measures of the confidence in a detector result, were 93% & 73% respectively.

Table 28 – Analysis of performance of B-mode hyperecho and PAM monitoring as detectors of lesion formation (reference standard = gross pathology)

	Low (3.6-4.5 MPa)			**Intermediate (5.4-6.3 MPa)**			**High (7.2-8.0 MPa)**			**Overall**	
Lesion[1]	19% (10/54)			69% (40/58)			97% (56/58)			106/170 (62%)	
	Hyperecho	Passive	*p*	Hyperecho	Passive	*p*	Hyperecho	Passive	*p*	Hyperecho	Passive
Accuracy	81% (22/27)	81% (22/27)	0.72	45% (13/29)	79% (23/29)	0.011	62% (18/29)	90% (26/29)	0.018	62% (53/85)	84% (71/85)
Sensitivity	0% (0/5)	20% (1/5)	0.62	25% (5/20)	75% (15/20)	0.006	64% (18/28)	93% (26/28)	0.018	43% (23/53)	79% (42/53)
Specificity	100% (22/22)	95% (21/22)	0.62	89% (8/9)	89% (8/9)	0.72	0% (0/1)	0% (0/1)	N/A	94% (30/32)	91% (29/32)
PPV[2]	N/A (0/0)	50% (1/2)	N/A	83% (5/6)	94% (15/16)	0.53	95% (18/19)	96% (26/27)	0.33	92% (23/25)	93% (42/45)
NPV[3]	81% (22/27)	84% (21/25)	0.43	35% (8/23)	62% (8/13)	0.011	0% (0/10)	0% (0/2)	N/A	50% (30/60)	73% (29/40)

[1] Lesion = Gross pathology analysis
[2] Positive predictive value
[3] Negative predictive value

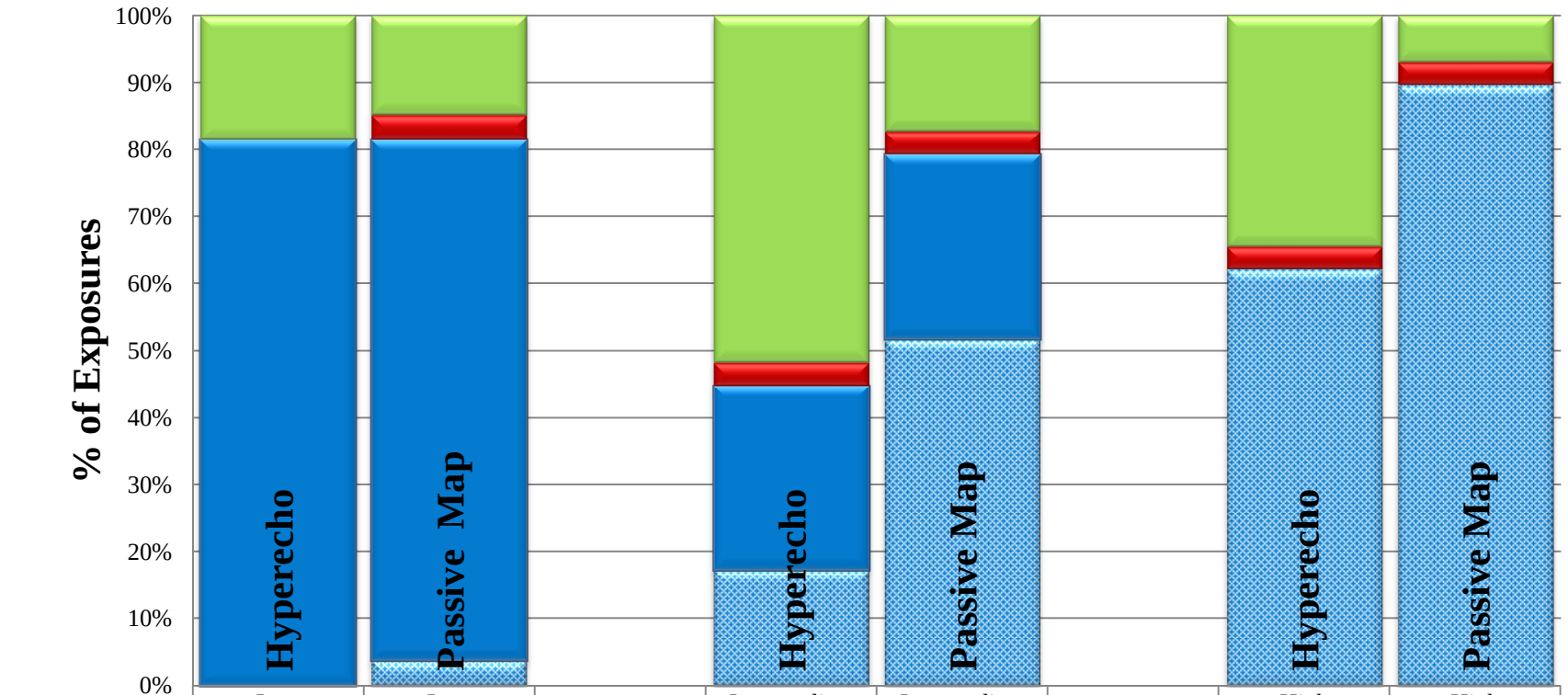

Lesions	Low 3.6-4.5 MPa 5/27	Low 3.6-4.5 MPa 5/27		Intermediate 5.4-6.3 MPa 20/29	Intermediate 5.4-6.3MPa 20/29		High 7.2-8.0 MPa 28/29	High 7.2-8.0 MPa 28/29
False Negative	5	4		15	5		10	2
False Positive	0	1		1	1		1	1
True Negative	22	21		8	8		0	0
True Positive	0	1		5	15		18	26

Figure 56 – Graphical summary of the performance of both detectors (hyperecho & PAM) according to low, intermediate & high insonation pressures. The blue sections (solid & patterned) represent all exposures where the detector prediction was accurate

6.6 Predicting lesion location

Current B-mode monitoring of HIFU therapy suffers greatly because of the biological origin of HIFU-induced hyperecho. Boiling temperatures are required to create the strong scattering required to produce significant grayscale changes. As such they only appear when a HIFU exposure has gone beyond its desired outcome. Hyperecho should truly be regarded as an indicator of overtreatment not as an indicator of successful treatment.

Prediction of lesion occurrence is possible with PAM. The same experimental data were used to assess whether PAM can also spatially detect lesions in real-time. Three snapshots of a PAM movie are shown below from an 8MPa, 10seconds exposure which led to an oversized, tadpole-shaped & pre-focal lesion. Figure 57, taken at t=2secs, demonstrates an early rise in broadband activity which is clearly localised to the focus. At this stage no significant harmonic activity is noted. Gross pathology demonstrated that the lesion formed after two seconds at the same pressure was small, uniformly-shaped and located at the focus. Figure 58, taken at t=4secs, demonstrates that harmonic activity has commenced and initially this is initially located at the focus. Gross pathology demonstrated that after t=5secs at the same pressure the formed lesion was again uniform and focal. Figure 59, at t=9secs, now demonstrates high-level harmonic activity occurring pre-focal as demonstrated on both the instantaneous and cumulative map. This change in location and level of harmonic activity is consistent with the onset of tissue boiling resulting in the distorted lesion seen at gross pathology at t=10secs.

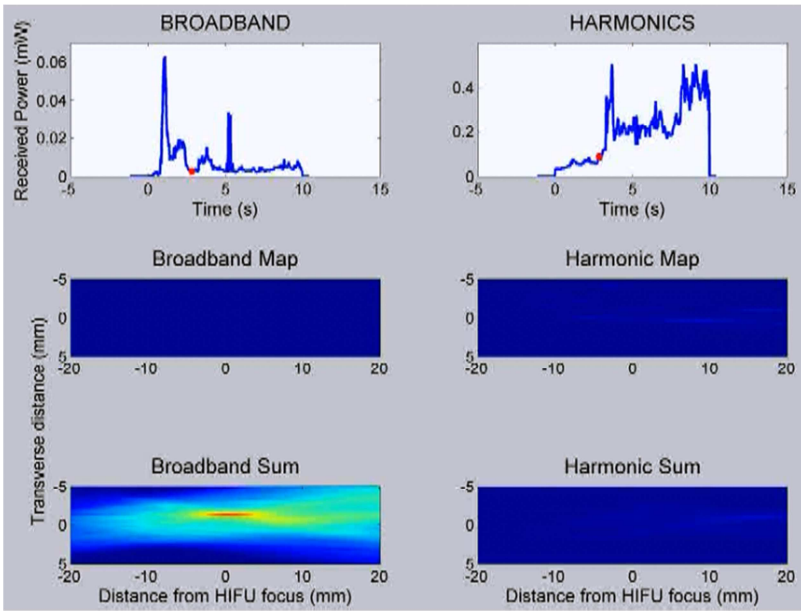

Figure 57 – Time trace (top), instantaneous (middle) and cumulative (bottom) PAM images at t=2secs of an 8MPa, 10 second duration HIFU exposure. Broadband activity occurred at the focus after early cavitation; no significant harmonic activity was seen at this stage

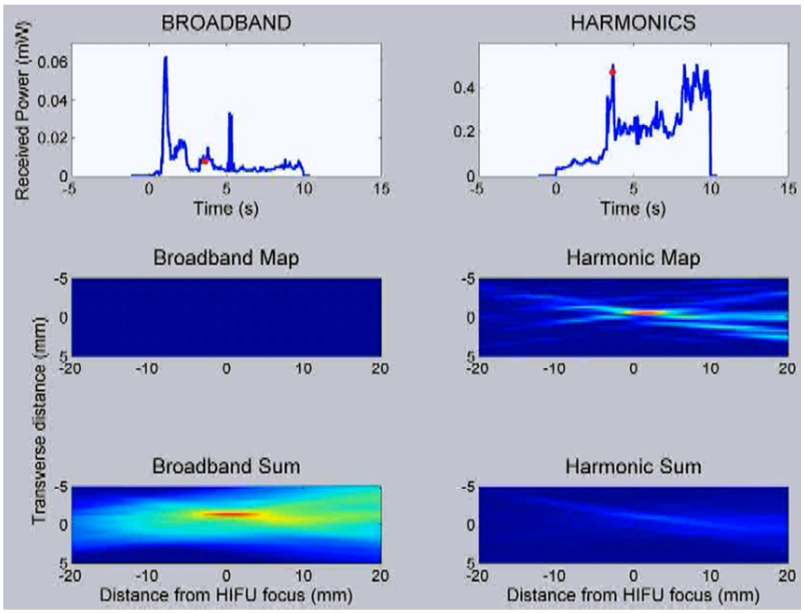

Figure 58 - Time trace (top), instantaneous (middle) and cumulative (bottom) PAM images at t=4secs of an 8MPa, 10 second duration HIFU exposure. Broadband activity was again localised to the focus and early harmonic activity was also seen located at the focus

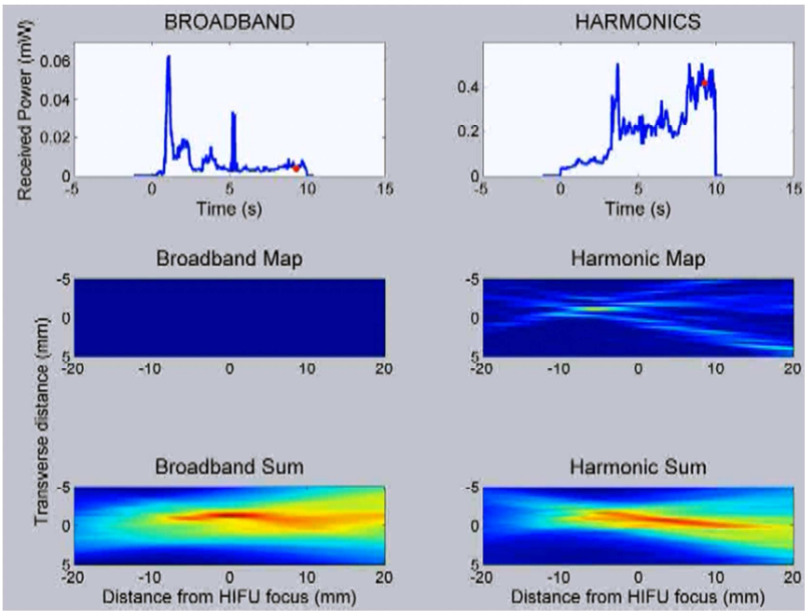

Figure 59 - Time trace (top), instantaneous (middle) and cumulative (bottom) PAM images at t=9.5secs of an 8MPa, 10 second duration HIFU exposure. Significant, sustained harmonic activity was seen located in the pre-focal regions, consistent with tissue boiling and overtreatment.

Comparison of PAM images from an exposure in the intermediate (therapeutic) range with one from the high (overtreatment) range demonstrates its superiority over B-mode hyperecho. Figure 60 demonstrates broadband & harmonic cumulative PAM maps, gross pathology and difference B-mode hyperecho images. Following the intermediate exposure (A;top), broadband activity accurately predicted lesion location. Low level, focal harmonic activity was also seen but no hyperecho change is seen. At the high exposure, pre-focal lesioning is predicted by both broadband and harmonic activity. The high level harmonic activity implies tissue boiling, which is confirmed by the strong hyperecho signal which is located in the pre-focal tissues.

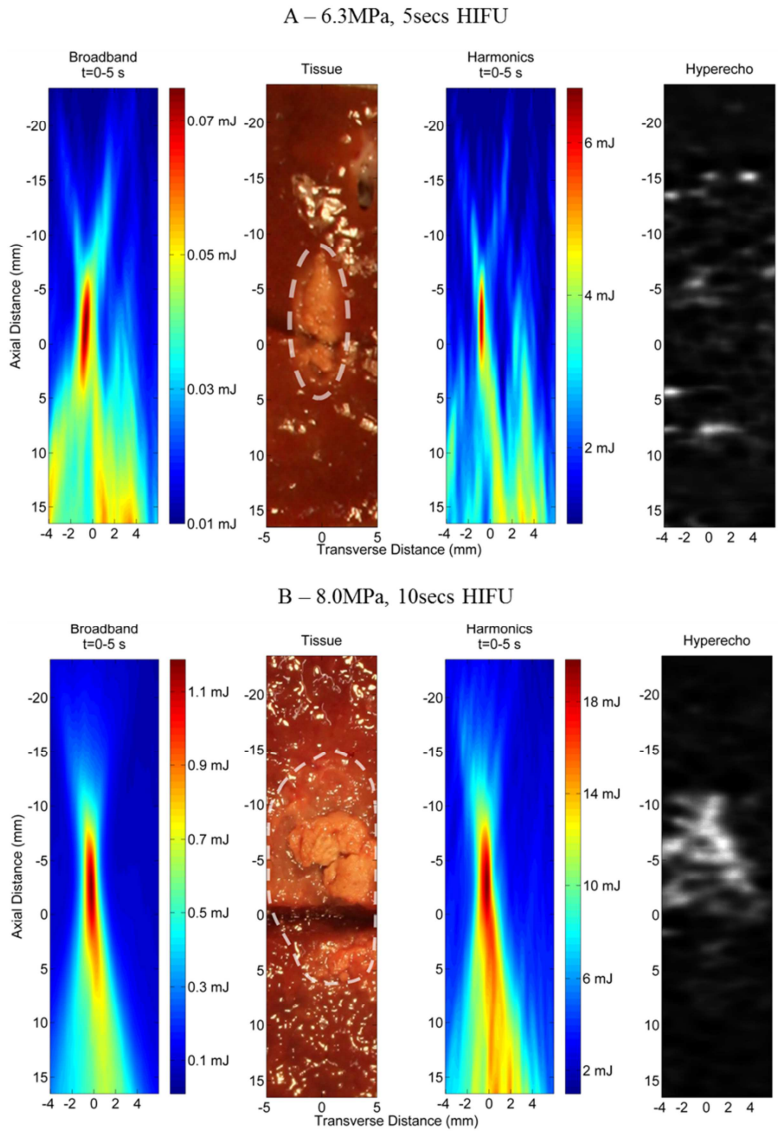

Figure 60 – Broadband & harmonic PAM images, gross pathology and hyperecho images for an intermediate pressure (A; top) and high pressure (B; bottom) exposure demonstrating accurate lesion location using PAM. Hyperecho is only visible in the overtreatment exposure (B).

6.7 Early focus registration using PAM

Current clinical devices use the free-field focus of the transducer to display the expected zone of ablation as an overlay on the B-mode diagnostic image of the treatment area. These parameters are measured by calibration in non-attenuating media and take no account of possible focal aberrations due to the attenuation and speed of sound in overlying tissues. Accurate targeting is absolutely vital during clinical HIFU to prevent damage to nearby vital structures such as bowel or ureter.

A more satisfactory approach would allow a non-destructive HIFU exposure to be undertaken *prior* to a therapeutic to confirm that the zone of ablation will occur at its intended position. B-mode hyperecho monitoring is unable to achieve as it appears upon tissue boiling when thermal ablation has already occurred. This was demonstrated by Rabkin *et al.* – hyperechoic regions were produced in rabbit tissue using short (30-60ms) pulses of HIFU. However tissue damage including cavities and blood congestion were observed, possibly due to millisecond boiling, rendering this method unsuitable for pre-treatment targeting [87, 213].

In contrast, a single cycle of HIFU may be sufficient to initiate cavitation activity at the focus provided that its amplitude is above the cavitation threshold for the tissue being insonated. Real-time imaging using PAM could then demonstrate the location of cavitation activity thus acting as a surrogate for the true thermal focus.

Cavitation maps were created for the first 100ms of HIFU exposure. Exposures of such duration are sufficiently short to avoid thermal tissue damage. Two representative examples of early cavitation activity can be seen in Figure 61. In both time traces, early onset cavitation activity was seen, which is localised to the -6dB transducer focus when reconstructed. Gross pathology confirmed that thermal lesion formed following the full exposure was located at the geometric focus.

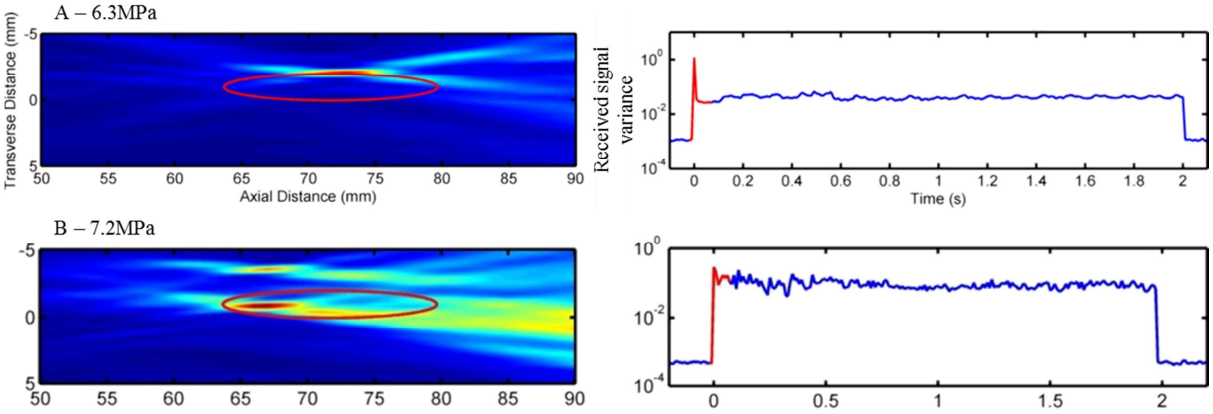

Figure 61 – Two exposure configurations demonstrating early (<100ms) cavitation activity used non-destructively to demonstrate predicted lesion position. PAM images (left) and presented alongside corresponding time trace of received signal power on array. Red ellipse represents -6dB focal zone.

The use of PAM for focus registration has two distinct requirements – firstly that the cavitation threshold is exceeded and secondly that the cavitation activity occurs *early* in the exposure. The first condition is nearly always met – this is demonstrated in the low FN rate of PAM discussed in Chapter 6.5. The second condition is more problematic as cavitation activity is not always predictable. A further example can be seen in Figure 62 where a high amplitude HIFU exposure was undertaken. No significant activity occurred in the first 100s; indeed it was absent until two seconds in the exposure. Beginning at two seconds, significant cavitation was detected which ultimately enable to formation of a precise PAM image. However, the PAM image formed from the first 100ms of the exposure gives no information to aid focus registration in this example.

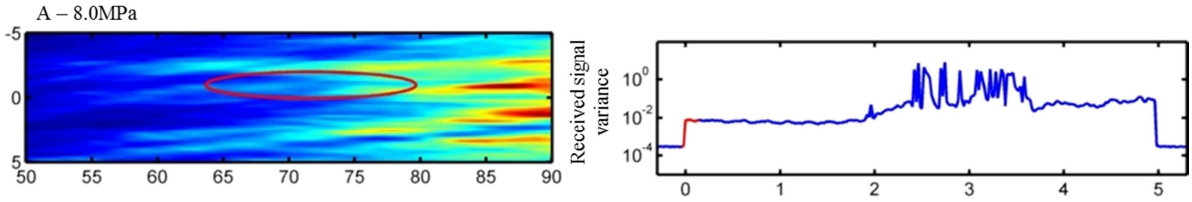

Figure 62 – PAM demonstrating absence of early cavitation activity despite the high insonating pressure. Significant cavitation activity is seen later in the exposure but no early focus registration can be performed in this example.

The examples shown in Figure 61 demonstrate that short non-destructive bursts of HIFU can be used as a feasible method for focus registration. The implementation of this technique into clinical practice with current HIFU devices is possible and relatively straight forward. It has

the potential to improve the safety of HIFU by reducing the risk of inadvertent damage to vital structures.

6.8 Discussion

The most striking feature of the results presented in this chapter is that the current method for method for monitoring HIFU exposure is poor. The transducer output required to produce thermal necrosis in any tissue is not fixed – it varies from patient to patient, organ to organ and tumour to tumour. HIFU clinicians rely on hyperecho treatment monitoring – it represents the only method of intra-operative assessment of thermal ablation – yet at clinically relevant exposures it gives correct results less than half the time. It is evident that its lack of accuracy stems from its poor sensitivity – thermal ablation has occurred but it has not been detected.

The results presented above demonstrate that PAM enables the localisation of tissue heating and ablation during HIFU, including any activity that occurs pre-focally. PAM also functions as an accurate and sensitive predictor of tissue ablation following a HIFU exposure and significantly outperforms current clinical hyperecho methods. Moreover, PAM can be used in a non-destructive fashion to spatially locate the zone of ablation *before* therapeutic HIFU is undertaken. In addition it has been shown that strong passive harmonic maps correlated with boiling and overtreatment, features which are typically detected by hyperecho, providing further feedback on the HIFU exposure.

Fundamental to the use of PAM to monitor HIFU is that it can be used in real-time. Hyperecho monitoring cannot be undertaken during HIFU on-time as the HIFU signal saturates the diagnostic image. The result of hyperecho monitoring is only available after the exposure has stopped when undertreatment or overtreatment may have occurred. It is theoretically possible to interleave the diagnostic ultrasound within a HIFU exposure by

lowering the HIFU duty cycle, which would enable quasi-real-time imaging. However this is not feasible with current clinical devices. In contrast, the passive nature of PAM means that monitoring is truly real-time – individual HIFU exposures could be modified in their amplitude or duration until the desired outcome is achieved using relatively simple feedback loops [218].

PAM did not perform perfectly in the above experiments. There were a number of false negatives, spread across all the exposure configurations. In these circumstances, too little (sub-threshold) cavitation activity was detected despite visible lesions at gross pathology. The tissue is heated by HIFU absorption and any generated harmonics but there are insufficient broadband emissions to reach the designated ablation threshold. This may occur for a number of reasons:

i) Focal pressure is too low to instigate cavitation activity
ii) Cavitation emissions are attenuated by overlying tissues
iii) Detector threshold is set too high

The likelihood of cavitation occurring in perfused tissue is a relative unknown with little research into cavitation thresholds in *in-vivo* human tissue. However the problem is potentially surmountable with the use of micro- or nano-bubbles which would provide the necessary nuclei necessary to initiate cavitation. Acoustic emissions from inertially cavitating bubbles are broadband but are usually of a higher frequency than the insonating HIFU. Given the frequency-dependence of absorption, attenuation of cavitation emissions may be problematic, particularly when treating depth. However, the use of ultra-high sensitivity receivers, appropriate pre-amplification and carefully filtering of the fundamental frequency will help to minimise this issue. Finally, the detector threshold can be manipulated – for example lowering the threshold improves the sensitivity at the expense of specificity.

Three FPs were seen using PAM – one at each exposure regime. In these circumstances, significant cavitation activity was seen in the absence of a lesion at gross pathology. Carefully inspection of the tissue in each case revealed a blood vessel at the focus leading to cavitation within the saline fluid.

6.9 Summary

In this chapter a novel method of spatially localising acoustic emissions from cavitation has been tested in an ex-vivo animal model. It has been shown that PAM enables non-destructive localisation of the HIFU focus, accurate spatial localisation of thermal ablation and quantitative prediction of thermal ablation which can be performed real-time in order to avoid boiling, overtreatment and pre-focal tissue damage. The translation of this technique into the clinical setting is possible without major modifications to existing clinical devices. The design, testing and clinical use of a PAM device for the Model JC & Model JC-200 HAIFU devices is discussed in the Chapter 7.

7 Design, testing & clinical use of a PAM device

Using the PAM techniques presented in the previous chapter, a novel device was designed and fully integrating into an existing clinical HIFU device. Safety and efficacy data of its use in renal HIFU are presented in this chapter.

7.1 Clinical Integration of Passive Acoustic Mapping

In Chapter 6 the use of a novel technique to passively monitor acoustic cavitation emissions was tested in *ex-vivo* tissue. It was demonstrated to be superior to the reference standard techniques used during ultrasound-guided HIFU, functioning as a better detector and locator of ablation as well as providing a method of pre-treatment targeting. The use of *ex-vivo* tissue enabled the conduct of a repeatable experimental protocol which in turn facilitated the development of accurate algorithms to process the passively received signals from HIFU exposures into meaningful geographic maps of cavitation activity. Proof of concept has been established. However, significant differences exist between laboratory-based *ex-vivo* tissue experimentation and hospital-based *in-vivo* perfused tissue clinical studies.

It is not known whether cavitation occurs during clinical HIFU treatments. If indeed it does, do cavitation emissions propagate sufficiently to be received using an extracorporeal detector? The paucity of evidence regarding cavitation during clinical HIFU is primarily due to the lack of a suitable detector – clearly intracorporeal detectors are unsuitable for non-invasive

treatments. Any cavitation detector must be remote from the patient and also must not interfere with the transmission of the therapeutic HIFU or with the movement of the therapeutic head.

7.2 Hypothesis

A custom-built PAM device can be applied to existing clinical HIFU machines (without impeding treatment) to allow PAM of *in-vivo* cavitation and other sources of acoustic non-linearity.

7.3 Design of passive cavitation detector

7.3.1 Principles

A fundamental principle of designing the PCD was to ensure that it could be used on the existing clinical HIFU device(s) without the need to alter the functionality of the device itself. In essence, the PCD was required to be entirely independent of the device and cause no significant interference to the production or transmission of the therapeutic beam, in order to not violate the CE mark of the device.

The design of the PCD was based on its application to the Model JC HIFU device which uses a 0.8MHz therapeutic transducer for renal HIFU. Given that treatments are conducted using mechanical translation of the HIFU transducer to target a tumour volume, it was desirable to have the PCD array mounted on the therapeutic head to maintain alignment throughout.

During the course of the clinical trial, a substantial amendment to the protocol was made to allow the use of the Model JC-200 HIFU device which uses a 0.95MHz therapeutic head. Design changes were required to the signal filtering on the receive electronics which are

discussed in more detail below. In addition, the following design issues were considered to be of fundamental importance

i) The receive array must be acoustically transparent at the HIFU drive frequency to minimise attenuation of the therapeutic HIFU.
ii) The receive array must be easily removable from the therapeutic head.
iii) The positioned receive array (including any cabling) must not interfere with the movement of the therapeutic head or with the positioning of the patient.
iv) Pre-amplifiers should be positioned as close as possible to the receive array to maximise the signal-to-noise (SNR) ratio but outside of the water reservoir.
v) High performance data acquisition is required to allow simultaneous multi-channel data at a suitably high frame rate.

The design, testing and clinical implementation of the PCD array described in this chapter was conducted with Dr Jamie Collin in the Institute of Biomedical Engineering (University of Oxford). Assistance with equipment design and manufacture was also supplied by Precision Acoustics (Dorset, UK) & DNV (Portland, UK).

7.3.2 PCD array

To maximise spatial resolution a large number of receiving elements were required. The Zonare array described in Chapter 6 uses 64 separates elements to record data. A trade-off was required between element size and number with the clinical array to ensure a sufficiently large receiving area without significant impact on the transducer output.

A compromise of 32 receiving elements arranged in four concentric rings was agreed. To conform optimally to the bowl-shaped therapeutic transducer, a dart-shaped design was adopted, orientated with the wide end towards the outside of the bowl. Eight darts each containing four receiving elements were to be arranged symmetrically around the transducer

with each pointed tip just abutting the diagnostic probe in the centre. A schematic diagram of this arranged is shown in Figure 63.

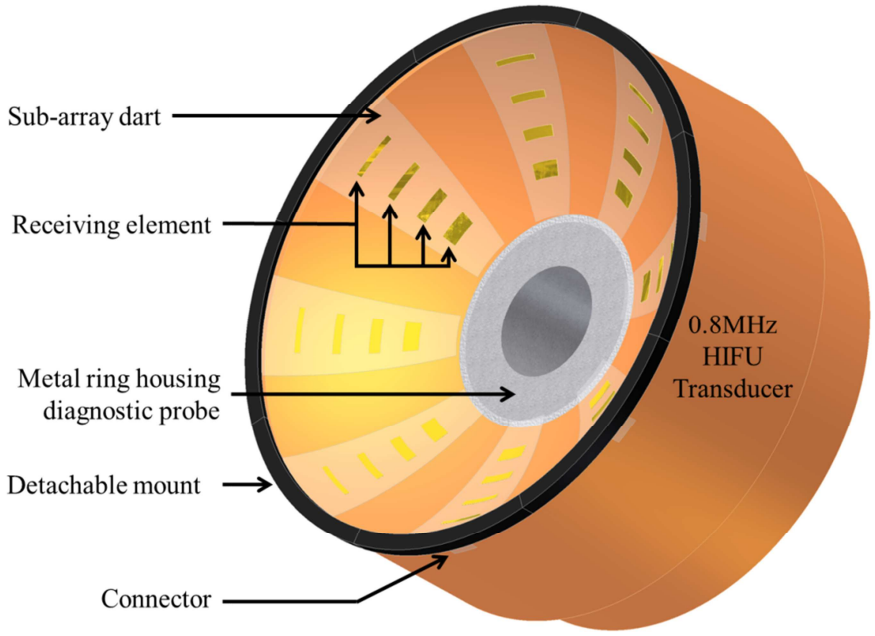

Figure 63 – Schematic of the PCD array in the form of eight symmetrically arranged darts arranged in four concentric rings (picture courtesy of Jamie Collin)

Each sub-array dart was manufactured from polyvinylidenefluoride (PVDF) which is the active element in many hydrophones. This PVDF material produces a voltage from the received acoustic signal via the piezo-electric effect. It is a suitable material as it has relatively low acoustic impedance and can be manufactured into thin, flexible sheets ideal for positioning over the transducer. The PVDF layer is sandwiched between a layer of gold and a layer of kapton applied to the back and front of each entire sub-array respectively. The layer of gold functions as the common ground electrode for all the elements. Each individual electrode is copper which is printed on to the kapton layer. Each channel therefore connects to the earth plane and its respective electrode. A photograph of a sub-array is shown in Figure 64.

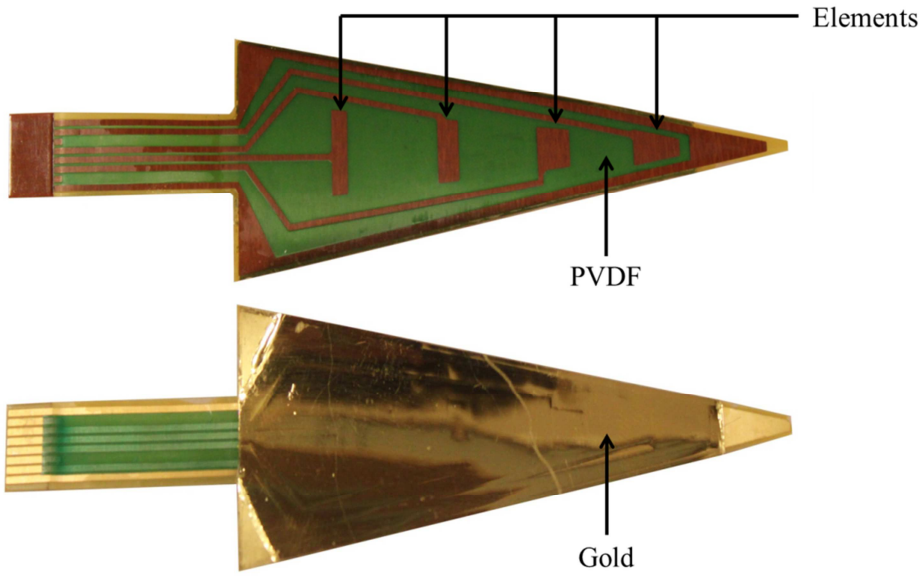

Figure 64 – Photograph of acoustically transparent sub-array demonstrating four elements printed on a PVDF sheet with a gold common ground electrode backing.

7.3.3 Detachable array mount

Appropriate equipment was required to ensure that the sub-arrays could be placed onto the surface of the clinical transducer in a repeatable and symmetric fashion. Without this, it would not be possible to be certain of the location of each individual receiving element relative to the others. However the sub-arrays were also required to be entirely removable to allow alternative transducers to be used and to allow machine servicing and calibration. A circular ring was custom-designed to fit around the lip of the transducer which does not transmit acoustic energy. The mount was designed with eight symmetrically-positioned holes in the outer surface to allow the sub-array connectors to pass through and connect on to the appropriate cabling. An aerial and side-on view of the mount is shown in Figure 65. The mount was designed such that there was minimal overlap onto the acoustic window of the HIFU transducer. The mount was safely secured onto the transducer by four circumferential screws. In order to ensure that the sub-arrays conformed accurately to the surface of the transducer, the tip of each sub-array was secured to the metal ring at the centre of the transducer which houses the diagnostic probe.

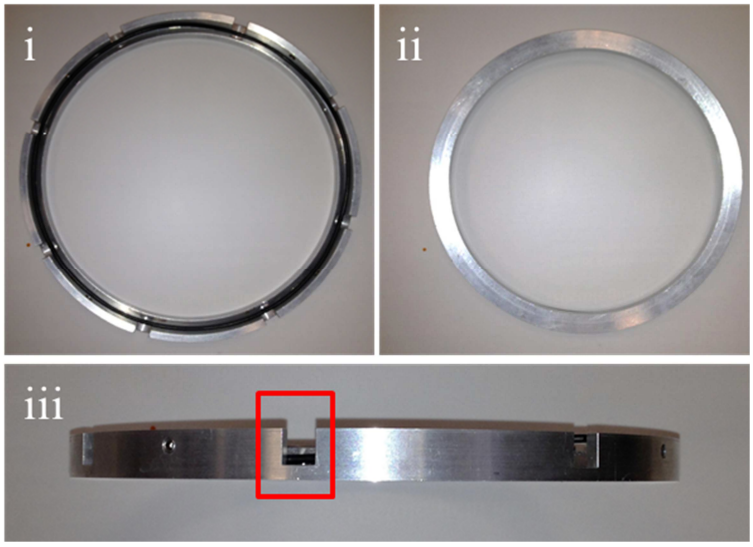

Figure 65 – Detachable mount for clinical PCD sensor for Model JC HIFU device photographed from i) underside, ii) above & iii) side. Red box demonstrates holes in mount to allow sub-array connectors to pass though

Due to differences in the size of the 0.95MHz transducer used on the JC-200 device, an additional mount was constructed of similar design to allow the array to be accurately positioned. The wider lip on this transducer meant that whilst the mount was required to position the sub-arrays, they could be satisfactorily secured such that the mount could subsequently be removed. This eliminated any impact the mount would otherwise have on the HIFU output.

7.3.4 Receive electronics

To achieve satisfactory PAM with the array, it was necessary to have suitably high impedance pre-amplifiers to maximise sensitivity whilst minimising electrical noise. Given that the array was mounted over the HIFU acoustic window, it was also necessary to filter the driving frequency to prevent saturation of any passively received signal. Custom-made pre-amplifiers were designed (DNV, Portland, UK) with in-built elliptical filters which gave a rejection of 60dB at the fundamental (0.8MHz) frequency – see Figure 66.

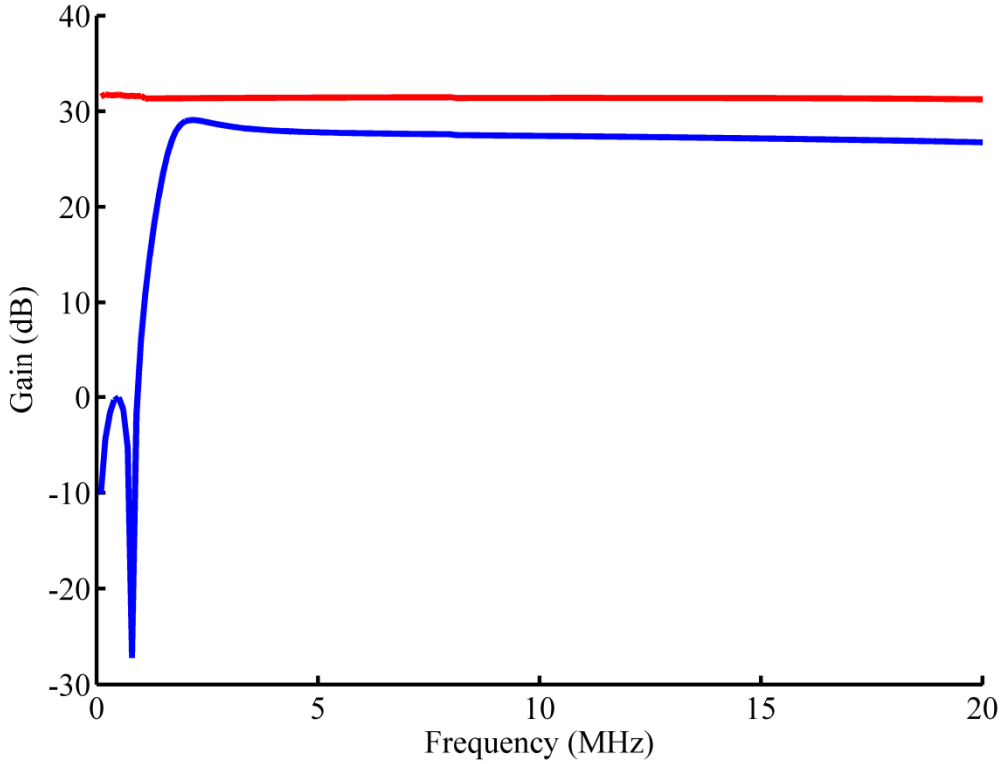

Figure 66 – Gain of pre-amplifiers without elliptical filter centred the HIFU driving frequency (graph courtesy of Jamie Collin)

Each pre-amplifier circuit board was designed to receive signal from one sub-array i.e. four elements. Eight pre-amplifier board were thus made and assembled into two banks of four to allow them to appropriately positioned as close to the array as possible. Cabling from the array to the pre-amplifiers was minimised to reduce electrical noise however the pre-amplifiers had to be positioned outside of the water reservoir and away from the patient bed.

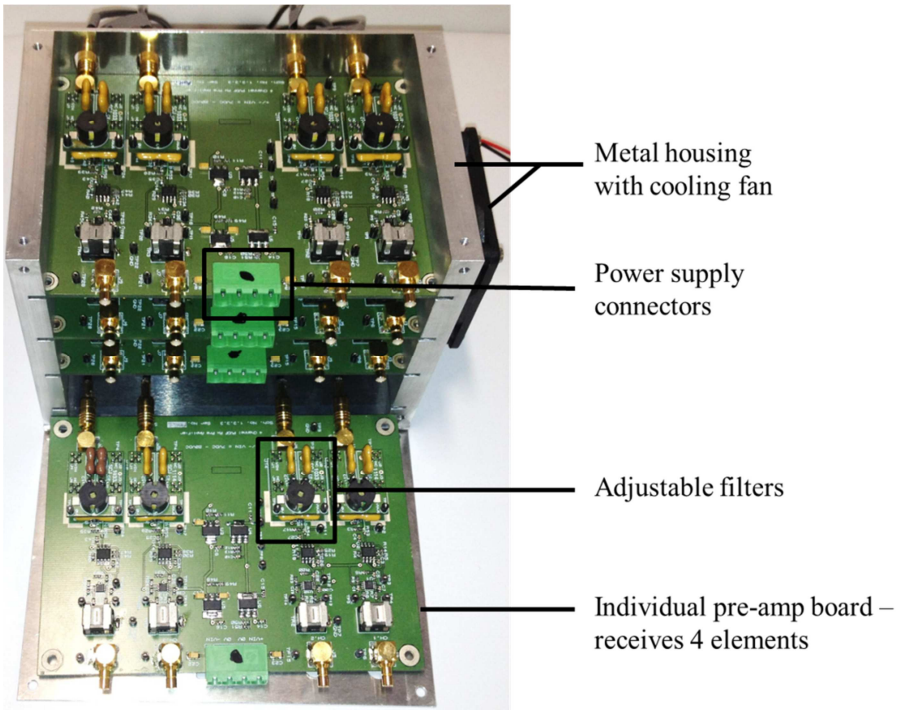

Figure 67 – Custom-built pre-amplifiers (1 of 2); each unit is cooled and houses 4 pre-amplifier board which each receive data from 4 elements (1 sub-array unit). Data is filtered to exclude the HIFU drive signal and amplified.

Using two different frequency transducers (2.25MHz & 7.5MHz) the sensitivity of one of the sub-array elements was assessed using a substitution calibration with a previously calibrated 0.5mm hydrophone (HPM05/3, Precision Acoustics). Each transducer was moved on a positioning system to the point of maximum signal on the element. The element signal was then recorded across the frequency bandwidth for each transducer, resulting in an assessment of the array sensitivity for a frequency range of 0.1-10MHz. This can be seen graphically in Figure 68 – consistently high sensitivity is seen across the frequency spectrum with effective filtering below 1.5MHz.

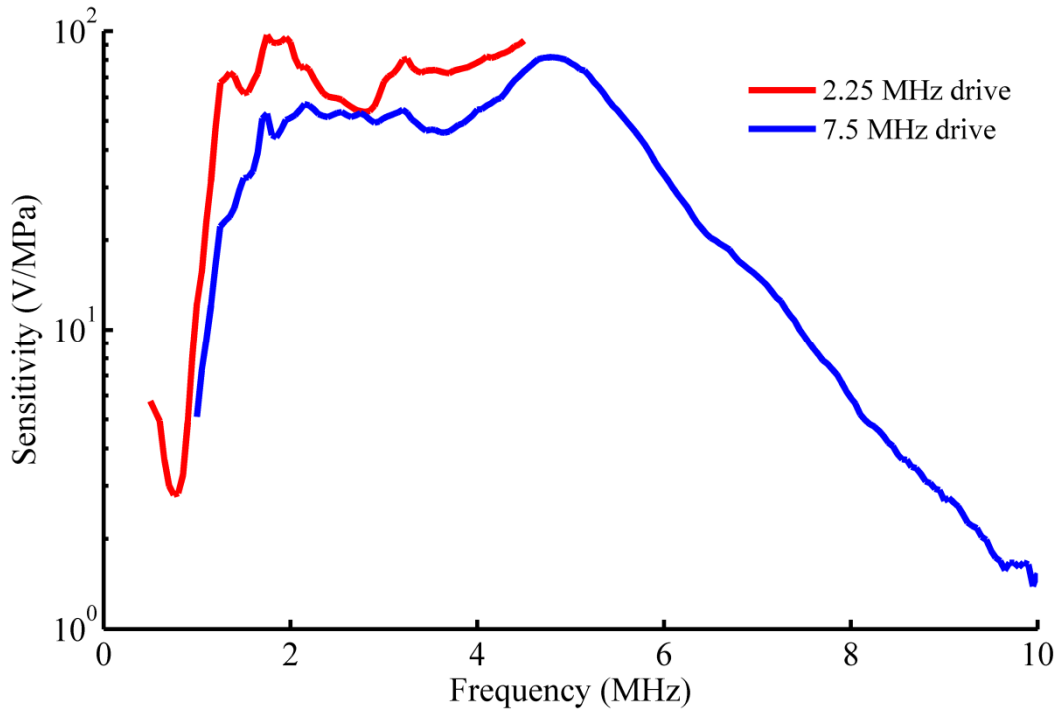

Figure 68 – Filtered and unfiltered sensitivity of one array element measured using a substitution calibration with a 2.25 & 7.5 transducer (graph courtesy of Jamie Collin)

The 32 channels of data were then acquired on Field-Programmable Gate Array (FPGA) based digitisers (NI5752, National Instruments) which allow simultaneous acquisition of data with high temporal resolution.

7.4 Clinical trial ethics

The design and testing of the clinical PCD array was a project to run concurrently with the clinical trial of HIFU in renal cancer discussed in Chapter 3. It was anticipated that the PCD array would be available for clinical use towards the later stages of the trial; the trial protocol and ethics submission was therefore designed to allow use of the array for clinical testing.

Ethical approval was granted to use the PCD array through the same ethics application described in Chapter 3.2.2. The approval was granted on the assumption that the device had been tested in the laboratory setting and proven to cause no significant impact on the acoustic field of the HIFU transducer. A maximum drop of 10% of the focal pressure was considered

acceptable. It was also required that the PCD array caused no interference with the normal functioning of the transducer positioning system, patient positioning system and the HIFU device software.

Finally, the purpose of clinical trial with regard to the PCD array was to establish the following:

i) A PCD array could be safely used during clinical HIFU without causing any interference with normal patient care.
ii) An appropriately filtered signal can be received during clinical HIFU.
iii) The received filter signal can be reconstructed post-treatment to provide a quantitative and spatial measurement of cavitation activity

The trial was designed to establish proof of concept, but not to allow PCD data to be used to modify the clinical treatment itself. Data were acquired in real-time during clinical HIFU but were not relayed to the operating team or used to influence treatment decisions. All data were analysed post-operatively when the entire clinical HIFU treatment was complete.

7.5 Clinical safety studies

A calibration experiment was undertaken with the clinical transducer to assess the total drop in focal pressure due to the PCD array. The 0.8MHz transducer was placed in a large water tank of degassed water. A 0.5mm hydrophone (HMP05/3, Precision Acoustics) was attached to a positioning system and aligned at the focus of the transducer. A signal generator was used to produce a $10V_{PP}$ burst of 25 cycles of HIFU at the transducer driving frequency. The signal was received on an oscilloscope (LeCroy Waverunner) and acquired using LabVIEW (National Instruments) software on a desktop PC. An axial scan over a range of 40mm centred and a planar scan over a 4mm range centred, both centred on the focus, were performed.

Identical scans were performed with the array mount alone *in situ* and with both the array mount and the array elements *in situ*.

The graph shown in Figure 69 demonstrates the axial profile of the transducer. The drop in pressure as a result of the detachable mount alone is negligible which is consistent with minimal overlapping of the acoustic field. With the mount and sub-arrays in position, the drop in pressure is approximately 5% which equates to a minimal and acceptable drop in intensity.

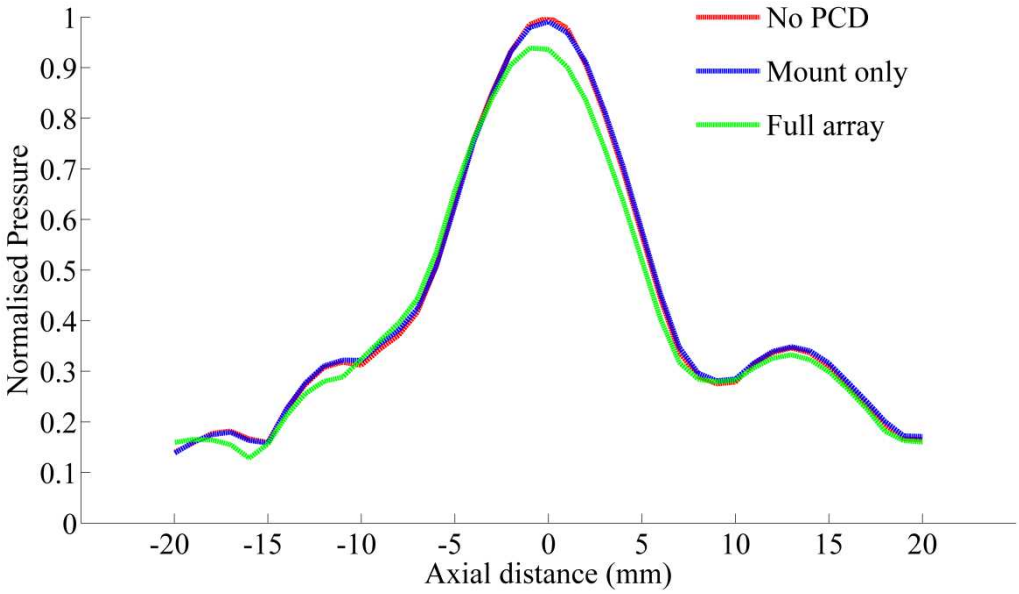

Figure 69 – Axial profile of 0.8MHz clinical transducer measured with a 0.5mm needle hydrophone over a 40mm range centred at the focus, taken with no PCD, the mounting ring only and the full PCD array *in-situ*.

The presence of inhomogeneities within the acoustic field has the potential to cause focal aberrations as demonstrated in Chapter 4.3. It was therefore equally important to ensure that the presence of sub-arrays within the acoustic field did not have any defocusing effect. Even small shifts in the focal position have the potential to cause significant harm if vital structures lie close to the intended zone of ablation. The three planar scans shown in Figure 70 demonstrate that no focal distortion occurred as a result of the array mount or sub-arrays.

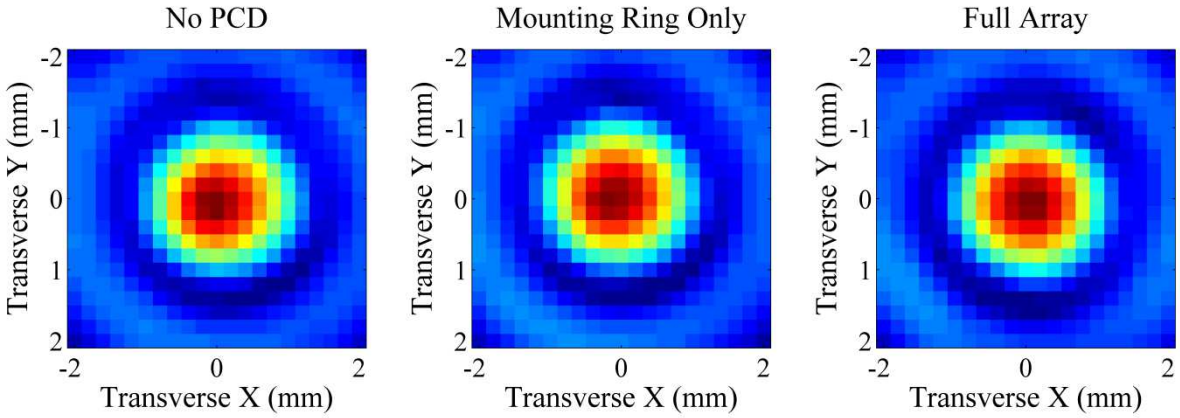

Figure 70 – Transverse profile of 0.8MHz clinical transducer measured with a 0.5mm needle hydrophone over a 4mm (X & Y) range centred at the focus, taken with no PCD, the mounting ring only and the full PCD array *in-situ*.

The final stage of ensuring clinical safety was to conduct a mock treatment. The PCD array was installed onto the clinical device and connected to the pre-amplifiers. The cabling from the sub-array connectors was attached to the base of the therapeutic head using a steel jubilee clip. This ensured that no tension was placed on the sub-arrays. The cabling was then brought together into two separate bundles deep in the water reservoir and secured together using cable ties. The two bundles were then brought out of the water reservoir at its corner so as not to interfere with either the patient position or transducer movement. The two banks of pre-amplifiers were placed adjacent to the patient bed. The cabling to the digitisers was run underneath the patient bed. A photograph of the PCD array fully installed on the JC-200 HIFU device can be seen in Figure 71.

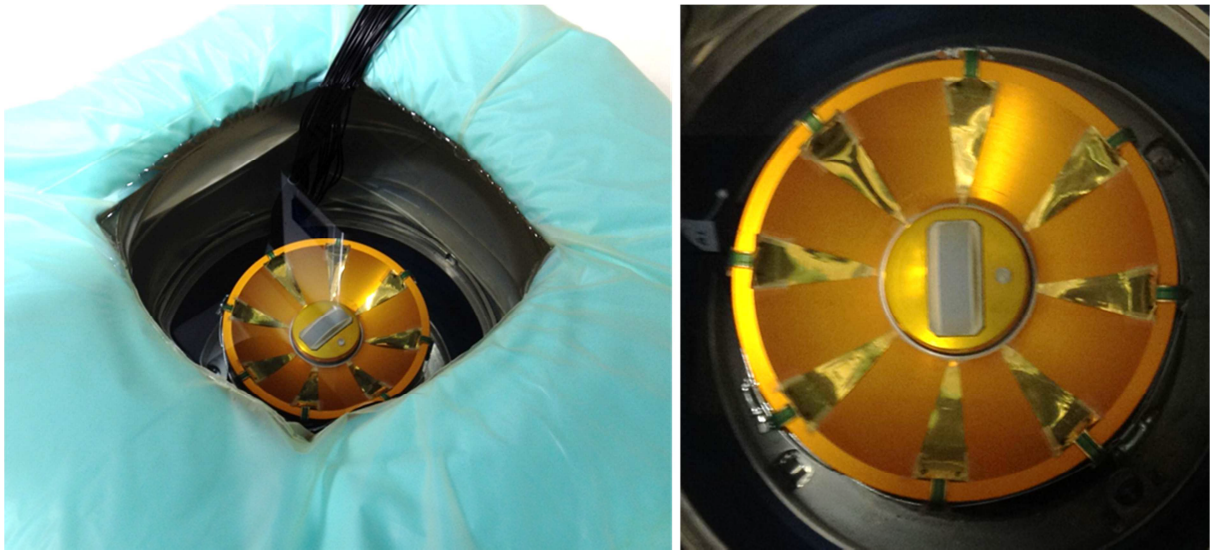

Figure 71 – Oblique (left) and overhead (right) photograph of PCD setup integrated with the JC-200 clinical HIFU device. The cabling from the elements is neatly collected at the base of the water reservoir and brought to the surface at the corner (see top left of oblique image).

The therapeutic head was moved throughout its entire range with the transducer at its highest, lowest and zero height. No interference with its movement was detected. The centrally-located diagnostic probe was also moved through its entire range without impediment. An absolute calibration was also conducted using a RFB and compared with measurements obtained from the manufacturers. This is described in detail in Chapter 7.6.1 & Chapter 10.5.

7.6 Clinical use of PCD array

The final stage of clinical integration of PAM was to test the array in the clinical setting. This testing was subject to the ethics agreement discussed in Chapter 7.4. The original pre-amplifiers were designed for use with the 0.8MHz transducer on the original JC HIFU device. As such the elliptical filter was centred on the driving frequency to eliminate the therapeutic signal from the PAM signal. The switch to the higher frequency JC-200 device meant that the filtering of the drive signal was inadequate with the existing filters. A change in filter was required which only became available at the very end of the clinical trial.

The preliminary stage of clinical testing (Phase I clinical trials) is always primarily aimed at safety and AE assessment. Therefore despite the absence of the appropriate filtering, the PCD

array was used in two clinical treatments to determine these outcomes. PAM data was also collected to determine whether the real-time acquisition was effective.

The elliptical filters on the pre-amplifiers were re-designed for the final patient in the trial. PAM data were acquired during this treatment and compared with intra-operative hyperecho, post-HIFU MRI and post-resection histology.

7.6.1 Safety

An absolute calibration was conducted using a radiation force balance (RFB) which are custom-built and provided by the device manufacturers. The design and use of the RFB is described in Chapter 10.5. The RFB was placed over the HIFU transducer and the radiation force was measured three times at input powers for 50-450W in steps of 50W, as shown in Figure 72.

Figure 72 – Photograph of RFB positioned over transducer with mount and sub-array in place. Radiation force measurements were taken at 50-450W output in 50W steps (3 measurements at each output)

The process was repeated with the PCD array in-situ. The results are summarised in Table 29, where the mean RFB value is shown for various power output with no PCD, only the

mounting ring and the full PCD array in place. Values are shown together with the SEM from the three measurements at each output. The percentage drop in radiation force due to the presence of the two components of the PCD is also shown. These results are also presented graphically in Figure 73.

Table 29 – Summary of RFB measurements with no PCD (left), mount only (middle) & full array (right) in place. Mean RFB value is shown over 3 measurements together with SEM and % drop *vs.* no PCD.

Power (W)	No PCD (g)	SEM	Mount only (g)	SEM	% diff.	Full array (g)	SEM	% diff.
50	3.20	0.00	3.30	0.06	+3.12	3.23	0.03	+1.04
100	6.47	0.03	6.30	0.00	-2.58	6.33	0.03	-2.06
150	8.93	0.09	8.83	0.13	-1.12	8.50	0.10	-4.85
200	12.50	0.00	12.13	0.03	-2.93	11.93	0.12	-4.53
250	16.17	0.03	15.57	0.27	-3.71	15.03	0.07	-7.01
300	19.70	0.00	19.30	0.00	-2.03	18.23	0.07	-7.45
350	22.90	0.12	22.23	0.09	-2.91	20.97	0.18	-8.44
400	26.00	0.10	25.47	0.03	-2.05	23.93	0.09	-7.95
450	28.83	0.03	28.07	0.03	-2.66	26.43	0.03	-8.32

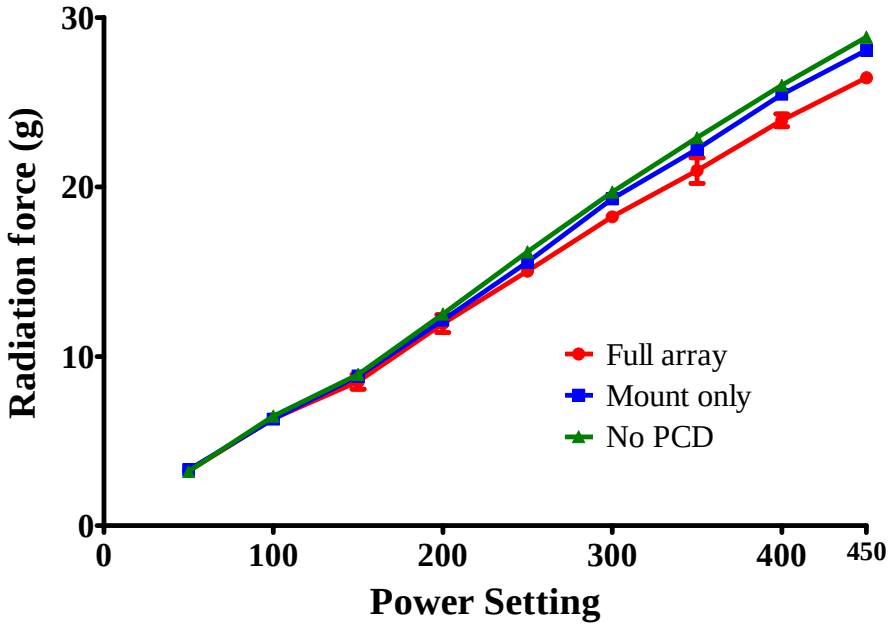

Figure 73 – Graphical representation of the radiation force recorded at various power outputs with no PCD, mounting ring only and the full PCD array in place. Each result is the average of three measurements; error bars (where visible) are SEM values.

The RFB measurements show that there is minimal and acceptable drop in the radiation force as a result of integration of the PCD with the clinical therapy head. Even at the highest

acoustic output the drop in radiation force was just 8%, approximately equivalent to a 4% drop in pressure.

Both clinical treatments were conducted in full with the PCD array in place. The array and cabling were all fully installed before commencement of the treatment. Both patients were placed on the HIFU device before induction of anaesthesia to reconfirm the tumour target and to ensure that there was no interference from the array. Both treatments progressed without complication. No problems as a result of the PCD array were encountered. Both patients required repositioning during treatment and no problems with this were noted. Transducer movements were required throughout and this occurred without limitation.

7.6.2 PAM results

The full PCD array was installed in full working order for the final treatment in the clinical trial (Patient 5.39). The signal received on one of the array elements was used as the trigger to commence data acquisition for each exposure. This ensured that data was acquired immediately after the HIFU transducer was switched on and for the entire duration of the exposure. In addition the trigger allowed temporal correlation between the received PCD signal and the time-point within the HIFU exposure. Data from each element was sampled at 50MS/s.

Following the standard technique a dose-escalation ramp was performed at the beginning of the procedure to determine the optimum treatment power. A central location with the tumour was selected for this process – this ensured that the energy was highly likely to be deposited entirely within the tumour rather than at a boundary between tumour and normal renal parenchyma or peri-nephric fat. Two-second HIFU exposures were undertaken at the same spot within the tumour using increasing output electrical powers of 40-270W in steps of 10W. Sufficient time between each exposure was left to allow both tissue cooling and an assessment

of the pre- and post-exposure ultrasound images. Using a screenshot dump program installed on the device computer, these images were stored before each exposure together with the treatment data. Data from the PCD array was recorded for each of these ramp exposures. Some real-time data was shown on the desktop PC used to record the PCD array data but this was not viewed by the HIFU operators or used to influence treatment parameters.

During the dose escalation no evidence of hyperecho change within the tumour was seen from 40-240W. Following the 250-270W exposures some temporary grayscale was demonstrated within the tumour; 250W was therefore selected as the optimum treatment power for the remainder of the procedure.

A number of difficulties were encountered with the technique after the data were post-processed with the PAM algorithms. Data were successfully recorded for the majority of the exposures. However electrical noise from the clinical therapy device resulted in saturation of the signal. This noise signal was broadband in nature, similar to that which PAM attempted to spatially localise, resulting in distorted or inconclusive maps. Analysis revealed that most of the filtered broadband passive acoustic maps were uninformative for this reason. Successful mapping of broadband emission during clinical HIFU exposures was therefore not possible during this treatment. However the filtered harmonic signal, given its significantly greater amplitude, was successfully mapped during certain HIFU exposures despite the widespread electrical noise. Broadband emissions during HIFU exposure are thought to be solely due to cavitation activity, however the generation of harmonics during HIFU may arise from non-linear propagation of the HIFU signal, scattering of the HIFU signal due to bubble formation due to tissue boiling or indeed low-amplitude cavitation where the emission spectrum has yet to become entirely broadband. In spite of the varying mechanisms responsible for the generation of the harmonic signal, successful mapping of its location can still provide useful

information on the acoustically-driven activity during HIFU. The filtered harmonic signal was mapped for each HIFU exposure during the dose escalation ramp. A coherent spatial map indicating the origin of activity was obtained in a number of cases.

In the absence of hyperecho change at the lower power levels it was not possible to determine the true position of the focus. The device software projects an overlay of the estimated focus position based on the free-field calibration of the transducer. However this does not take account of changes in the speed and aberrations introduced by the intervening tissues – these can be both numerically and clinically significant, as shown in Chapter 4. Knowledge of focal location before ablation occurs is highly desirable to limit the risk of damage to surrounding structures.

Examination of the PCD data demonstrated that spatial localisation of the focus was possible at lower acoustic power than that required to produce hyperecho. In Figure 74, a screenshot image after a 70W exposure is shown. In the middle image the pre-treatment B-mode image can be seen which a clear outline of the renal tumour. The estimated focal position calculated by the device is also presented as an overlay together with the estimated size of the focus. In the right hand image the immediate post-exposure B-mode exposure is demonstrated. No hyperecho change was seen following this exposure. The left hand image demonstrated the B-mode image together with an overlaid spatial map of the PCD data, analysed using the PAM technique discussed in Chapter 6.3.5.2.

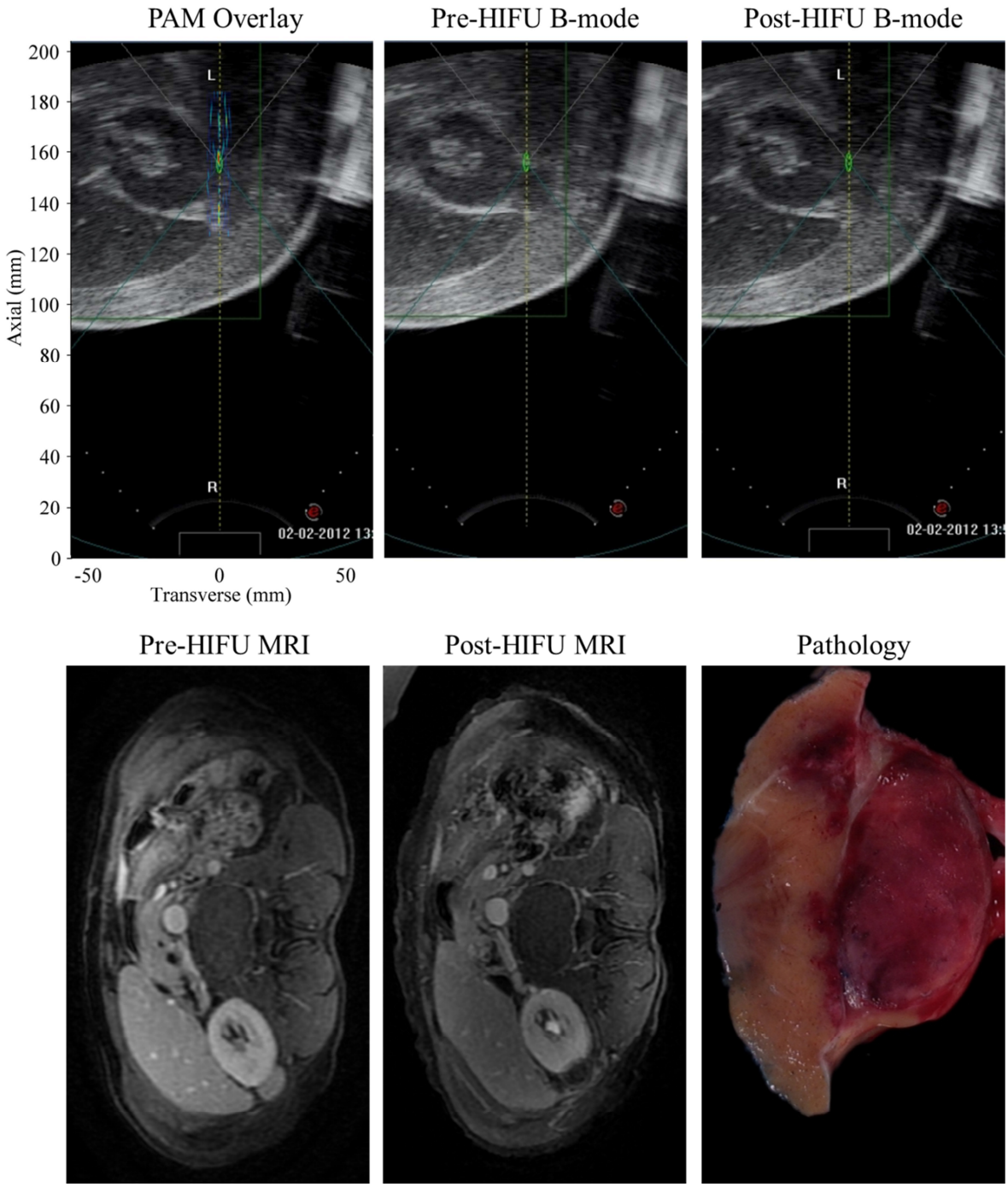

Figure 74 – Diagnostic imaging and pathology of HIFU-treated renal tumour from Patient 5.39. Top row: B-mode image of 70W 2 second HIFU exposure showing overlaid harmonic map (left), pre-treatment image (middle) and post-treatment (right). Bottom row: LAVA MRI showing pre-HIFU (left) and post-HIFU (right) images with photograph of surgical resection pathology (right).

The absence of hyperecho shown in the post-treatment B-mode is consistent with sub-boiling temperatures; indeed at this relatively low intensity exposure tissue ablation is unlikely. However the overlay PAM image demonstrates that harmonic activity occurred during the exposure. This was located within the estimated focus provided by the clinical device

software and therefore also located within the boundaries of the tumour being treated. Therefore even at the lowest acoustic output of the HIFU device PAM was able to confirm the true location of the HIFU focus before any significant heating or tissue damage has occurred.

This is a significant development in HIFU monitoring. At present, the operator has to assume that the predicted focus displayed over the B-mode is indeed the true acoustic focus. In addition, the operator is obliged to continually increase the power output until hyperecho is achieved before the true focal location can be confirmed. At this stage, when hyperecho is evident, tissue damage has already occurred. PAM has therefore been demonstrated to allow pre-destructive localisation of the focus in a clinical HIFU treatment of a renal tumour.

In addition to the spatial localisation of the harmonic data, the energy of the received harmonic signal was also averaged across the exposures. This was performed by creating a 20mm x 4mm (-10 to 10mm axial; -2 to 2 transverse) ROI centred on the focus. The total received filtered harmonic energy across the entire ROI was calculated for each frame and then averaged across all the frames recorded during the HIFU exposure (frame rate 20Hz). The value produced, due to various scaling factors, is in arbitrary units although it is proportional to the power of the received signal.

A line plot of the dose escalation ramp showing acoustic output power against mean received PCD power is shown in Figure 75. This demonstrates a near-linear relationship between HIFU drive power and the received harmonic power across all 32 elements. Temporary hyperecho was observed only at acoustic outputs of 250W or greater. This linear relationship suggests that, with further investigation of *in-vivo* tissue ablation thresholds, it may be possible to apply appropriate thresholds to the received PCD signal to detect tissue ablation. These threshold acoustic outputs are likely to be significantly below the output required to produce hyperecho change which is currently used to predict tissue ablation.

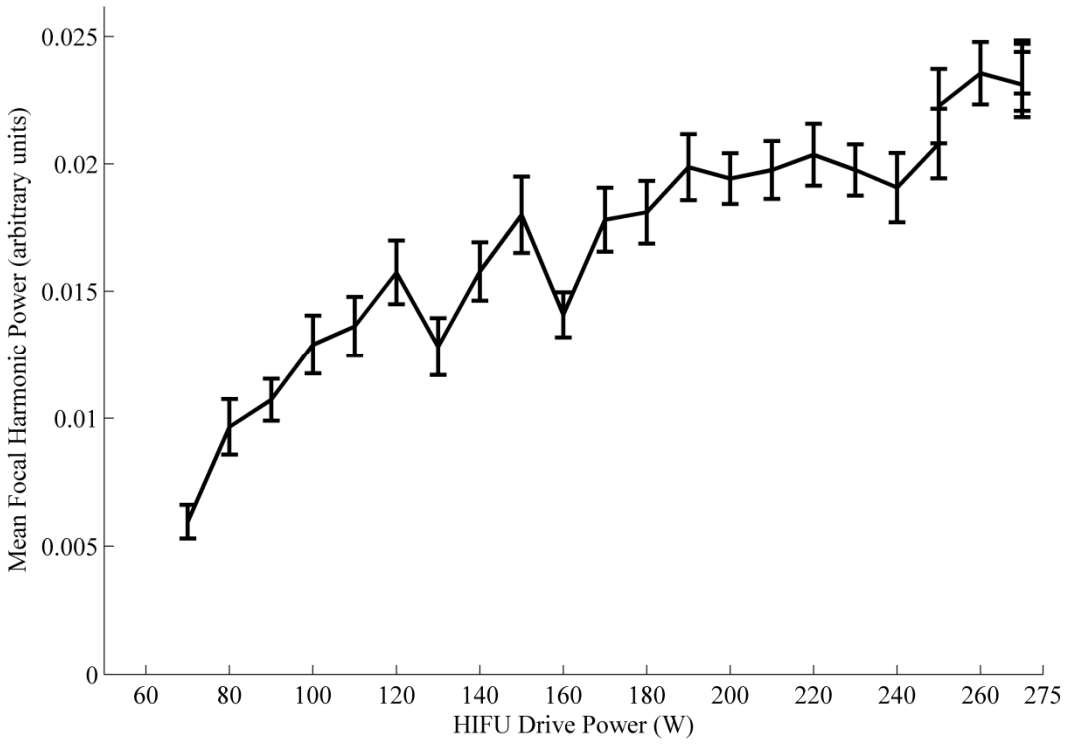

Figure 75 – Graph of HIFU acoustic output power *vs.* the mean harmonic power received across all 32 elements of the PCD during the dose escalation ramp of a clinical HIFU treatment of a small renal tumour (Patient 5.39). Error bars represent SD.

7.7 Discussion

Previous chapters have clearly outlined the need for new and improved monitoring techniques for ultrasound-guided HIFU. The novel technique of PAM was tested successfully in an *ex-vivo* model but its clinical translation is a far more complex task, particularly given the constraints of the existing clinical HIFU device and ethical clinical trial conduct. These factors were fundamental to the design of the PCD array. Replacement of existing components within the current clinical HIFU device would have been more straight-forward however this would have contravened the existing CE mark for the device. Such a change would have necessitated considerable pre-clinical testing, extensive safety investigations and a new medical device application for the Medicines and Healthcare Products Regulatory Authority (MHRA). This is both expensive and time-consuming. In contrast the addition of an entirely independent device can be undertaken with relative ease provided that the function of

the existing device is not affected and appropriate clinical trial ethics is obtained. The acoustic transparency of the array elements and the design of the array mount was therefore of considerable importance. The small drop in acoustic intensity as a result of installation of the PCD array is within the limits defined at the start of the trial – a less than 10% drop.

The receiving electronics, in particular the pre-amplifiers, posed a significant challenge. Ideally the pre-amplifiers should be positioned as close as possible to the receiving elements. However the size of the pre-amplifiers and that the therapeutic head is entirely submerged in water meant this was not feasible. A significant length of cabling (1.5m) was required to route the PCD signal to the pre-amplifiers which result in considerable electrical interference. This could be minimised by the design of miniaturised, waterproof pre-amplifiers which could be placed directly around the therapeutic head. Despite these difficulties it was possible to receive filtered harmonic PCD data with an acceptable SNR ratio.

The primary concern in the translation of any pre-clinical healthcare product or device into clinical practice is safety. It was therefore essential to confirm that the additional PCD array did not impact significantly on a standard clinical HIFU procedure. To confirm this extensive testing was undertaken prior to clinical use. Laboratory-based calibrations using highly sensitive hydrophone confirmed a minimal drop in acoustic intensity and no focal beam aberrations. An *in-situ* absolute calibration with an RFB also demonstrated a radiation force drop within acceptable limits. Mock runs of clinical treatments also successfully demonstrated the absence of impediment to the standard device function. These experiments successfully demonstrated clinical safety of the PCD array.

It is evident that the PAM of clinical renal HIFU was difficult. The primary underlying problem was electrical noise from both seepage of the drive signal and the electronic positioning system. This prevented the mapping of broadband activity associated with inertial

cavitation which is of low amplitude due to attenuation by the abdominal wall structures and peri-nephric fat. However, as discussed in the pre-clinical setting in Chapter 6.7, the PCD array was used to successfully register the focus location before tissue damage occurred. This function alone is extremely important – it could provide real-time feedback to the operator thus providing confidence that the targeted area is indeed the true location of acoustic focus. As previously discussed one of the key limiting factors in renal HIFU is poor imaging quality – the operator lacks confidence in the accuracy of the zone of ablation. These results demonstrate the PAM, acquired at sub-therapeutic exposure parameters, could be used to confirm the intended target prior to permanent tissue injury.

The poor SNR of the filtered broadband signal prevented the use of PAM to spatially localise inertial cavitation activity and to create thresholds to predict tissue ablation. The use of PAM in this fashion is particularly useful as broadband emissions are uniquely associated with the occurrence of inertial cavitation. The energy of these broadband emissions correlates linearly with the degree of heating [62]. However, the correlation between received harmonic power and acoustic drive power suggests that similar thresholds may enable prediction of tissue ablation. However, in the absence of gold standard pathological analysis of the exposed tissue after each individual exposure, it is not possible to establish this from these results.

7.8 Summary

In this chapter a PCD array has been integrated with an existing HIFU device in current clinical use with the use acoustically transparent PVDF elements. Laboratory-based studies demonstrated that it caused minimal attenuation and no aberration of the drive signal. Clinical studies demonstrated the array to be safe for use in patients without hindrance to the normal device function. The device was used in three patients with the array in-situ without complication. Despite difficulties with pre-amplification, low SNRs and low amplitude

emissions, it was demonstrated that harmonic PAM can predict the focal location even at low amplitude, non-destructive exposure levels. In addition a near linear correlation between received harmonic power and acoustic output was shown which may allow its future use to predict tissue ablation remotely with greater sensitivity that the currently used hyperecho methods.

8 Implications for patient care: Renal HIFU

The key aim of translational research is to improve outcomes that are important to patients. In this chapter, the impact of work in this thesis is applied to clinical practice with the aim of improving clinical outcomes in renal HIFU

8.1 Patient selection

One of long-standing challenges of HIFU to any body part has been to determine which factors determine whether the treatment is effective or not. This applies to both ultrasound- and MRI-guided HIFU. Many of these factors exist for all treatment modalities – tumour size, tumour location, surrounding structures, tumour vasculature. However, HIFU is unique amongst all surgical treatment options – including surgical resection, minimally invasive surgery, energy ablation – in that the treatment modality is passed through the body wall to its target without any skin puncture whatsoever. This, in many respects, approaches the ideal treatment – truly non-invasive. However, the method of energy delivery introduces an entire new group of parameters to consider which are unique to HIFU. These parameters include:

i) Acoustic properties of overlying structures including skin, muscle, parenchyma, fat
ii) Thickness of overlying structures
iii) Distance from transducer to tumour margins
iv) Tumour perfusion
v) Cavitation thresholds of different tissue types

vi) Tissue response/resistance to hyperthermia including intra-operative
vii) Respiratory excursion of organs and image registration during movement

To date, whilst there have been many case series reporting treatment outcomes of HIFU for many pathologies, very little effort has been made to determine which patients are most suitable for HIFU treatment. Should we avoid obese patients? Are certain types, size, or location more amenable to treatment? Is acoustic cavitation a help or a hindrance during HIFU? Is ultrasound- or MRI-guided HIFU more effective? In many situations, large patient numbers are required to answer these questions. However, given the wide range of treatment outcomes in this small study, it is inherently possible to draw some conclusions on which patients may be more suitable for renal HIFU.

8.1.1 Peri-nephric fat

It has been demonstrated that peri-nephric fat significantly attenuates ultrasound. Indeed, it is more attenuating that many other human tissues. This attenuation significantly limits the delivery of ultrasound to its intended target and results in pre-focal heating and resulting image deterioration.

Using the peri-nephric fat measurements from all patients considered suitable for the trial at initial screening, it has been demonstrated that patients with a greater thickness of peri-nephric fat are more likely to be excluded. Using this same data, it is possible to construct Receiver Operator Curves (ROC) to assess the likelihood of trial exclusion based on peri-nephric fat thickness. Three ROC curves are shown in Figure 76 – transverse, AP & mean fat thickness. Both transverse & AP thickness are acceptable measures to determine trial exclusion (AUC=0.746, p=0.027 & 0.773, p=0.014 respectively). However, the mean thickness gives an even better measure (AUC=0.787, p=0.010).

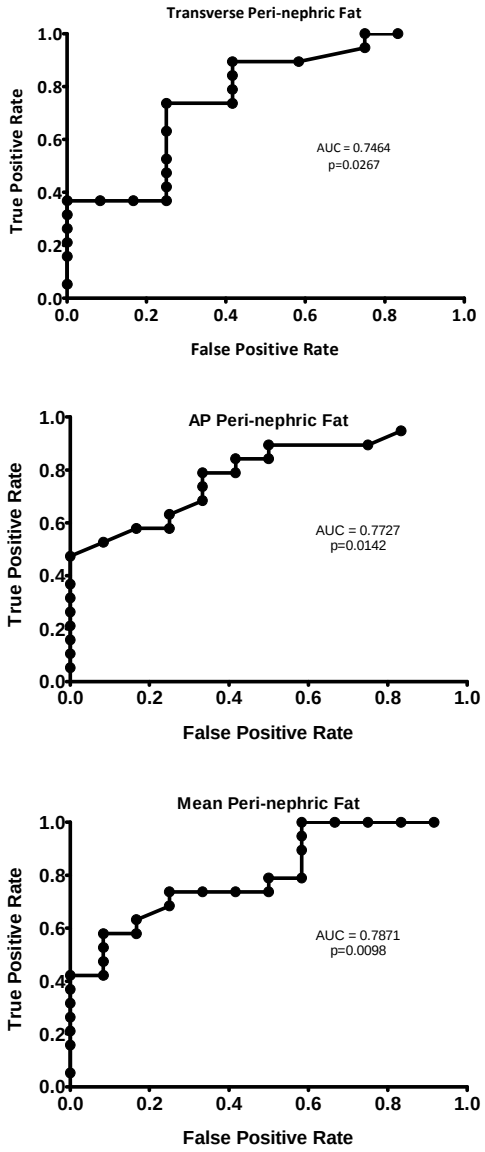

Figure 76 – ROC curves of transverse, AP and mean peri-nephric fat thickness for a successful outcome of final screening (trial inclusion); AUC=area under curve

A table of sensitivity and specificity at different cut-off values can also be constructed to determine the most appropriate threshold. This table for mean fat thickness is shown in Table 30. A threshold fat thickness of 19.5mm gives a likelihood ratio (LR) of 7.0 – this means that probability of the screening outcome for patients with a fat thickness of greater than 19.5mm is 7.0 times higher than the same outcome for patients with a fat thickness of less than 19.5mm. Values above this threshold lead to a higher specificity at the expense of sensitivity and vice versa. This is a statistically significant and clinically plausible finding.

Unfortunately due to the small number of patients actually treated within the trial, it is not possible to use fat thickness to determine the outcome of HIFU treatment itself. No statistically significant differences were noted between the patients who had effective or ineffective HIFU treatment. It is likely that a larger sample size would yield a more meaningful result.

Table 30 – Table of sensitivity & specificity demonstrating likelihood ratio (LR) of positive outcome (successful final screening) for varying values of mean peri-nephric fat thickness

Cutoff	Sensitivity	95% CI	Specificity	95% CI	LR
> 1.500	1.000	0.8235-1.000	0.08333	0.002108-0.3848	1.09
> 3.250	1.000	0.8235-1.000	0.1667	0.02086-0.4841	1.20
> 5.000	1.000	0.8235-1.000	0.2500	0.05486-0.5719	1.33
> 5.750	1.000	0.8235-1.000	0.3333	0.09925-0.6511	1.50
> 6.750	1.000	0.8235-1.000	0.4167	0.1517-0.7233	1.71
> 8.250	0.9474	0.7397-0.9987	0.4167	0.1517-0.7233	1.62
> 10.00	0.8947	0.6686-0.9870	0.4167	0.1517-0.7233	1.53
> 11.25	0.7895	0.5443-0.9395	0.4167	0.1517-0.7233	1.35
> 11.75	0.7895	0.5443-0.9395	0.5000	0.2109-0.7891	1.58
> 13.00	0.7368	0.4880-0.9085	0.5000	0.2109-0.7891	1.47
> 14.50	0.7368	0.4880-0.9085	0.5833	0.2767-0.8483	1.77
> 15.25	0.7368	0.4880-0.9085	0.6667	0.3489-0.9008	2.21
> 16.00	0.7368	0.4880-0.9085	0.7500	0.4281-0.9451	2.95
> 16.75	0.6842	0.4345-0.8742	0.7500	0.4281-0.9451	2.74
> 17.25	0.6316	0.3836-0.8371	0.8333	0.5159-0.9791	3.79
> 18.00	0.5789	0.3350-0.7975	0.8333	0.5159-0.9791	3.47
> 19.50	0.5789	0.3350-0.7975	0.9167	0.6152-0.9979	6.95
> 20.75	0.5263	0.2886-0.7555	0.9167	0.6152-0.9979	6.32
> 22.25	0.4737	0.2445-0.7114	0.9167	0.6152-0.9979	5.68
> 24.00	0.4211	0.2025-0.6650	0.9167	0.6152-0.9979	5.05
> 25.50	0.4211	0.2025-0.6650	1.000	0.7354-1.000	-
> 29.25	0.3684	0.1629-0.6164	1.000	0.7354-1.000	-
> 35.25	0.3158	0.1258-0.5655	1.000	0.7354-1.000	-
> 39.75	0.2632	0.09147-0.5120	1.000	0.7354-1.000	-
> 42.00	0.2105	0.06052-0.4557	1.000	0.7354-1.000	-
> 44.00	0.1579	0.03383-0.3958	1.000	0.7354-1.000	-
> 50.00	0.05263	0.001332-0.2603	1.000	0.7354-1.000	-

8.1.2 Tumour Size

The mean tumour size in those who passed final screening was less than in those who failed (25.2mm *vs.* 29.6m; p=0.103). However this difference was not statistically significant. Unsurprisingly, tumour size alone is not an ideal predictor of the final screening outcome. An ROC curve, shown in Figure 77, for tumour size demonstrates its limited effectiveness as a discriminator (AUC=0.695) which was not statistically significant (p=0.071).

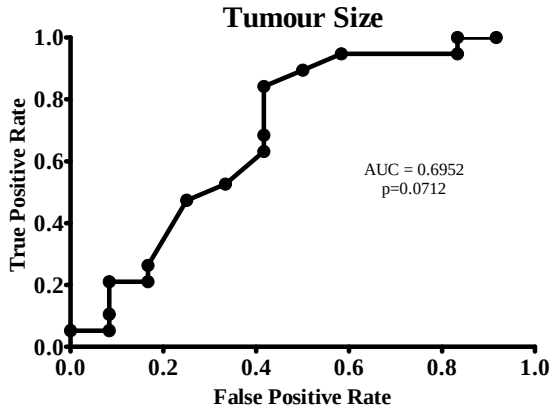

Figure 77 – ROC curve of tumour size for a successful outcome of final screening; AUC=area under curve

It is recommended that tumour size alone should not be used to determine suitability for renal HIFU.

8.1.3 Renal Nephrometry

As discussed in Chapter 5.2, recently it has been recognised that renal NS can predict the risk of complications. Some surgeons recommend its use to aid treatment decision. Most recently, Simone *et al.* have demonstrated the PN can be performed with zero ischaemia – no isolation or clamping of the hilar vessels – safely in patients with a low NS [219].

It has been shown that tumour size alone is not an ideal measure of suitability for HIFU treatment. However, it has also been demonstrated that a higher NS is strongly associated with a failure to successfully complete final screening, rendering HIFU treatment unsuitable.

An ROC curve constructed for NS demonstrates it to be a highly useful discriminator in predicting screening outcome (AUC=0.798; p=0.006). This is shown in Figure 78.

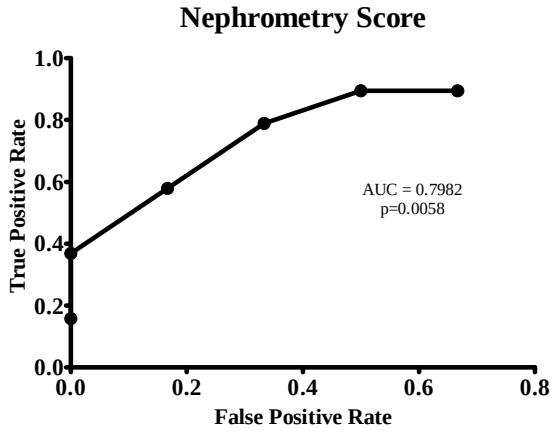

Figure 78 – ROC curve nephrometry score for a successful outcome of final screening; AUC=area under curve

The table of threshold values, shown in Table 31 demonstrate that the LR for a NS of >6.5 (LR=2.37) & >7.5 (LR=3.47). NSs can only be integer values; the threshold for nephrometry scoring would be appropriately set at 7.

Table 31 – Table of sensitivity & specificity demonstrating likelihood ratio (LR) of positive outcome (successful final screening) for varying nephrometry scores.

Cutoff	Sensitivity	95% CI	Specificity	95% CI	LR
> 4.500	0.8947	0.6686-0.9870	0.3333	0.09925-0.6511	1.34
> 5.500	0.8947	0.6686-0.9870	0.5000	0.2109-0.7891	1.79
> 6.500	0.7895	0.5443-0.9395	0.6667	0.3489-0.9008	2.37
> 7.500	0.5789	0.3350-0.7975	0.8333	0.5159-0.9791	3.47
> 8.500	0.3684	0.1629-0.6164	1.000	0.7354-1.000	-
> 9.500	0.1579	0.03383-0.3958	1.000	0.7354-1.000	-

The nephrometry scoring was designed to provide a quantifiable method of defining the complexity of surgery. It was based on the long-standing belief that larger tumours are more challenging to excise because they require greater dissection and more incision into the renal parenchyma leading to a greater risk of haemorrhage and blood transfusion. It also assesses the exophytic nature of tumours – those that are predominately exophytic are easier to find and again require less incision in the kidney. Tumours that lie close to the collecting system

are also higher risk as the likelihood of entering the collecting system is greater, potentially resulting in urine leaks & urinary sepsis which in turn may require ureteric stenting, percutaneous drainage or surgical intervention. Finally, tumours lying close to the interpolar regions are also associated with complications due to their proximity to the renal hilum, the segmental arteries & the collecting system.

It is entirely plausible that these same factors should result in difficulties in visualising and treating similar tumours with HIFU. It is accepted that small renal tumours are difficult to locate with ultrasound. Endophytic tumours may demonstrate no mass effect and those located near to the collecting system and renal hilum may also be difficult to distinguish from normal renal parenchyma. In contrast, the larger, purely exophytic tumour located at the extreme upper or lower pole are easily identifiable with ultrasound.

It is recommended that a renal NS is calculated for all patients being considered for renal HIFU. Almost all patients with a NS of ≥8 will be unsuitable for HIFU treatment and therefore could reasonably be excluded before final screening is undertaken. All those with a NS of <8 should be undergo final screening although only those with a score of ≤6 are ultimately likely to be suitable for HIFU.

8.2 Treatment morbidity

The search for novel minimally-invasive treatments for small renal cancers is fuelled predominately by a desire to avoid treatment morbidity rather than poor oncological outcomes of existing treatments. Formal tumour excision, performed as a PN, confers an excellent long term survival rate which has not been replicated by any alternative treatment modality [157, 220-222]. However, renal surgery can be associated with significant complications; many of these are directly related to incision of the renal parenchyma, however high rates of

complications associated with surgery in general are seen [157, 164, 223, 224]. In a meta-analysis of the largest series of patient undergoing PN, Porpiglia *et al.* found an overall complication rate of 21.3% & 21.4% for open and laparoscopic surgery respectively [157]. Significantly approximately half the complications seen following PN are medical, for example myocardial infarction, deep vein thrombosis, pulmonary embolism and pneumonia – this is a reflection of the patient population who are often elderly and suffer from co-morbidity [157, 164]. Renal cancer surgery is particularly risky in those aged 80 and over – Liguori *et al.* found a peri-operative mortality rate of over 11% (4/35 patients) in octogenarians undergoing open RN. In the same series, nearly half of patients required blood transfusion and the early complication rate was over 30% [164]. The presence of more than two co-morbidities at the time of surgery was an independent risk factor for post-operative morbidity.

Surely a conservative approach towards small renal cancers is therefore appropriate, particularly in the elderly and co-morbid? This approach certainly minimises the risk of surgical complications and follow-up studies have shown benign histology in 46%, 22% & 20% of renal masses of less than 1cm, 1 to 2.9cm & 3 to 3.9cm respectively [225]. Moreover, small renal masses grow slowly, typically at 2-4mm/year [226]. In this same growth study of over 200 renal masses, no growth was noted in 30% over a 2-3 year period and progression to metastases occurred in just one patient. However, currently cross-sectional imaging and/or clinical characteristics cannot predict growth rates or the risk of metastatic disease. Despite high rates of benignity, over 25% of 3.1-4cm renal masses are high grade (Fuhrman grade G3/4), 36% are stage T3a or greater and distant metastases occur in 8% [227]. More recently, a study of over 2,000 renal cancers less than 7cm demonstrated distant metastases were occurred in 4%, 5% & 10% of tumours of 1.1-2.0cm, 2.1-3.0cm & 3.1-4.0cm respectively [228]. Renal cancer remains the most lethal urological cancer, with overall 1-year, 5-year &

10-year UK survival rates of 65-68%, 49-50% & 42-44% respectively [139]. Notably, the 5-year survival rate for those with distant metastases is dismal (10%).

Minimally-invasive therapies for renal cancer were developed to provide active treatment whilst avoiding surgical risks. Whilst a number of different energy ablative therapies have been proposed and tested in Phase I/II clinical trials, only CRY & RFA have provided medium-term follow-up in sufficient numbers to warrant comparison with HIFU. The morbidity statistics for RFA and CRY from selected larger series are summarised in Table 32 & Table 33.

Table 32 – Morbidity statistics of renal CRY from selected studies; EBL = estimated blood loss

Study	**n**	**Complications* (n,%)**					**EBL (mls)**	**Tranfusion (n,%)**	**Hospital stay (hours)**
		Total	Grade 1	Grade 2	Grade 3	Grade 4			
Gill [229]	32	2 (6.2)	0	2 (6.2)	0	0	67	0	43
Cestari [230]	37	6 (16.2)	4 (10.8)	1 (2.7)	1 (2.7)	0	165	1 (2.7)	91
Gill [231]	56	4 (7.1)	4 (7.1)	0	0	0	87	1 (1.8)	41
Hegarty [232]	164	11 (6.7)	2 (1.2)	4 (2.4)	5 (3.0)	0	N/A	4 (2.4)	N/A
Davol [233]	48	7 (14.6)	5 (10.4)	2 (4.1)	0	0	N/A	2 (4.1)	72
Schwartz [234]	85	5 (5.9)	1 (1.2)	3 (3.5)	1 (1.2)	0	58	2 (2.4)	72
Permpo. [235]	23	5 (21.7)	5 (21.7)	0	0	0	N/A	0	N/A
Aron [236]	80	8 (10.0)	2 (2.5)	5 (6.3)	1 (1.3)	0	111	1 (1.3)	48
Guazzoni [237]	131	32 (24.4)	25 (19.1)	6 (4.6)	1 (0.8)	0	210	6 (4.6)	113
Sidana [238]	162	38 (23.4)	19 (11.7)	8 (4.9)	5 (3.1)	6 (3.7)	N/A	1 (0.6)	N/A
Total	818	118 (14.4)	67 (8.2)	31 (3.8)	14 (1.7)	6 (0.7)	129 Av.	18 (2.2)	44 Av.

* - Complications graded according to the Clavien-Dindo classification of surgical complications (available at www.surgicalcomplication.info; accessed 21/20/2011)

Table 33 – Morbidity statistics of renal radiofrequency ablation from selected studies; EBL = estimated blood loss, T_x = transfusion

Study	n	Complications (n,%)					EBL (mls)	T_x (n,%)	Hospital stay (hours)
		Total	Grade 1	Grade 2	Grade 3	Grade 4			
Gervais [239]	100	12 (12.0)	6 (6.0)	2 (2.0)	4 (4.0)	0	N/A	2 (2.0)	N/A
Park [240]	94	13 (13.8)	9 (9.6)	1 (1.1)	3 (3.2)	0	12	0	N/A
Hegarty [232]	82	8 (9.8)	5 (6.1)	1 (1.2)	2 (2.4)	0	N/A	1 (1.2)	N/A
Zagoria [241]	125	8 (6.4)	5 (4.0)	2 (1.6)	0	1 (0.8)	N/A	1 (0.8)	<24
Breen [242]	105	5 (4.8)	1 (1.0)	0	4 (3.8)	0	N/A	0	N/A
Veltri [243]	87	10 (11.5)	6 (6.9)	0	4 (4.6)	0	N/A	0	N/A
Total	593	56 (9.4)	32 (5.4)	6 (1.0)	17 (2.9)	1 (0.2)	12	4 (2.8)	N/A

* - Complications graded according to the Clavien-Dindo classification of surgical complications (available at www.surgicalcomplication.info; accessed 21/10/2011)

It is evident from the above morbidity statistics that even minimally-invasive procedures carry a significant risk of complications. Most RFA procedures are performed percutaneously with imaging guidance whereas most CRY procedures are performed via the laparoscopic approach, thus requiring either retroperitoneal or transperitoneal access, dissection of the kidney and resection of overlying fat. It is therefore inevitable that CRY carries a higher complication rate. Both modalities also require skin incision (CRY greater than RFA) and whilst not considered a complication, should not be ignored in a comparison with renal HIFU.

A direct numerical comparison between RFA, CRY and HIFU is misleading. Minor skin erythema and swelling occurs invariably with renal HIFU as the propagating ultrasound passes from the non-attenuating degassed, deionised water reservoir into the attenuating skin. By definition this is an undesired effect and is thus considered a complication of treatment;

however it is rare for this to be of clinical significance and should not be considered any more detrimental to a patient's health than the skin incision required for other minimally-invasive therapies. If the occurrence of mild skin injury is eliminated from the morbidity statistics, just one patient suffered a complication directly related to HIFU therapy – this was moderate pain following treatment which required short term treatment with strong opioid analgesia in peri-operative period. It did not delay discharge and should be considered in the context of the pain expected with RFA or CRY.

The length of hospital stay is a key measure in assessing treatment options – it has health, social and financial implications for both patients and hospitals. Little information has been reported in the literature about hospital stay following renal RFA; it is likely that these are performed as day-case or 23 hour hospital stay procedures in the majority of cases. Renal CRY by comparison, results in a mean hospital stay of almost two days, reflecting the more extensive nature of the surgery. All patients were discharged within 24 following renal HIFU; most requiring minimal or no analgesia during their hospital stay.

8.3 Treatment imaging

It is evident that diagnostic ultrasound imaging of renal tumours using existing clinical HIFU devices is problematic. The loss of spatial and contrast resolution due to the stand-off between the transducer and the target region using therapeutic transducer with long focal length (>10cm) is the main contributing factor. This is compounded by the deterioration in imaging due to pre-focal heating & swelling, a factor which is not unique to HIFU ablation, as discussed in Chapter 5.3.

The administration of pre-treatment intravenous dexamethasone seems, albeit anecdotally, to limit the impact of intra-operative oedema. This should be considered routine practice for all trans-abdominal HIFU.

The use of shorter focal length transducers should be considered. This may be suitable for superficially placed renal tumour that are positioned lateral or posteriorly within the kidney. However, for the majority of patients, the combined thickness of skin, subcutaneous fat, abdominal musculature and peri-nephric fat make this unfeasible. This is compounded by the effect of gravity when patients lie in the lateral position – the abdominal tends to sag towards to the transducer thereby increasing the propagation path length through the tissues.

Similarly, it is unlikely that any change to the diagnostic imaging machines themselves will lead to a significant improvement. The majority of the renal tumours in the clinical study were easily visible using a handheld ultrasound probe when closely applied to the skin. Likewise, when the diagnostic probe on the clinical device was elevated to the skin surface, most renal tumours were easily located. However, when the probe is retracted for treatment, the issues with poor resolution arise invariably. The development of image registration software which are able to display pre-operative CT/MRI imaging overlaid with intra-operative ultrasound images, if performed in real-time with motion compensation, will provide a significant step towards improving imaging in ultrasound-guide HIFU [244].

A more fundamental question is whether an alternative imaging modality should be used. MR-guided HIFU devices are in current clinical use. A number of feasibility studies in animals have been performed which establish proof of concept [83, 245, 246]. However, to date no clinical studies of MR-guided renal HIFU have been published. MRI does not suffer from the loss of resolution and pre-focal attenuation seen with renal ultrasound imaging and it is possible to non-invasively monitor temperature change although not truly in real-time.

Motion tracking algorithms to compensate for respiratory movement during abdominal HIFU have also been developed [80, 247, 248]. However, MR-guided HIFU remains an ultrasound-driven therapy – no change in the diagnostic image modality can alter the delivery of ultrasound to the focus. MR-guided HIFU will almost certainly improve the targeting of renal tumours and will identify tumour margins and surroundings structures more readily. MRI thermometry may even provide a more objective measure of tissue heating. However, there remains a very strong argument for US-guided HIFU – if the diagnostic ultrasound imaging is poor then the delivery of therapeutic ultrasound to the focus is also likely to be ineffective.

The use of water balloons to aid HIFU treatment is controversial. Their use allows the abdominal wall to be mechanically deflected away from the HIFU transducer thereby reducing the propagation distance and also displacing mobile intra-peritoneal viscera. In doing so, it is possible to improve imaging, reduce the amount of pre-focal heating and move vital structures away from the target. This has been done with success in the HIFU treatment of uterine fibroids where there is overlying bowel in the acoustic path [119]. However, the Oxford experience with the use of a water balloon in the treatment of kidney tumour in a renal transplant was unsatisfactory – a significant skin burn resulted which required formal surgical excision [249]. Similarly, anecdotally a number of HIFU operators at European HIFU centres have also reported skin burns with the use of water balloons. At present water balloons should be used with caution in trans-abdominal HIFU and should not be considered standard remedy for poor quality imaging.

8.4 Treatment monitoring

It has been demonstrated that the current methods for monitoring ultrasound-guided HIFU are unsatisfactory. Indeed, it would not be unreasonable to conclude that hyperecho monitoring is unsafe. Its ability to detect thermal ablation is insensitive and poorly predictive. This is not

surprising given the mechanism by which it functions. It is not however, entirely redundant – the formation of hyperecho following HIFU ablation provides strong evidence of boiling, supra-therapeutic temperatures and also provides acceptable spatial information.

A PCD array provides significant additional information. Cavitation activity can be mapped with high spatial and temporal resolution, in real-time. Thresholds applied to PAM data can provide a quantifiable measure of energy delivery which can be successfully used to predict cavitation. Significantly, a PCD array can be fully integrated into existing devices without the need for extensive hardware or software changes.

The use of PAM has the potential to significantly improve the monitoring of HIFU treatment. It should be used in combination with current methods and PAM results could be displayed on the same screen as the B-mode images used for therapy planning. More importantly, PAM can be used to modulate HIFU exposure in real-time, increasing its power or duration until a desired threshold achieved. The temporal resolution of PAM can be such that such information is available in milliseconds and when integrated into feedback loops, may significantly lower the input energy and as a result, lower the risk of pre-focal tissue damage.

The most elegant solution to full PAM integration is to replace the existing diagnostic imaging probe on the HIFU devices with an ultrasound imaging device capable of accessing & processing pre-beamformed RF data. The PAM data can then be used to modulate the HIFU exposure directly. Ultrasound devices are commercially available but their integration into existing devices would be extremely challenging, if not impossible without re-assessment of the device use regulations. Despite this, the existing PCD array tested herein could be used to obtain useful feedback on treatment progress. At present the PAM process for a two second HIFU exposure takes several minutes to produce high resolution mapping and further time again to integrate the power across all the frames to produce a ‘dose’ estimate. However, it is

entirely possible, with existing technology, to develop software to perform this function quickly enough so as to influence the power, duration and location of the next HIFU exposure. This could be performed using PAM data from the existing clinical PCD array designed for the JC-200 HIFU device.

There are still a large number of unknowns with regard to cavitation monitoring of clinical HIFU. It is expected but not proven that cavitation occurs in vivo. In the presence of supra-threshold negative pressure it is logical that bubbles will form yet there is little evidence for this. It is also not clear whether any cavitation-enhanced heating effect is the dominant heating process in clinical HIFU. This may not be necessary in the context of PAM but whether accurate thresholds can be applied to PAM data if linear & non-linear heating processes predominate is unclear.

8.5 Imaging follow-up

The correlation between post-operative MRI and histology was poor in this clinical trial. The reason for this is not obvious. The decision to use CE-MRI as both pre-HIFU and follow-up imaging in this trial was based on a number of factors. MRI gives superb soft-tissue contrast resolution as well as excellent spatial resolution, particularly with newer three tesla MRI machines. This allowed examination not only of the target region but also a careful assessment of the pre-focal tissues including abdominal musculature and peri-nephric fat. In addition, the Churchill Hospital has the benefit of an MRI radiologist (Dr Rachel Phillips) who has extensive experience in the assessment of MRI in ablative therapies. Dr Phillips research training at New York University Hospitals was based on MRI follow-up of small renal parenchymal masses. Finally, CE-MRI involves no ionising radiation. The clinical trial protocol (Chapter 3.2.1) required an additional post-operative scan to assess the outcome of

ablation thus MRI follow-up eliminated the risk of additional exposure to radiation as a result of voluntary participation in the trial.

In the context of HIFU-based ablation, much of the follow-up imaging has been performed with CE-MRI. PC, renal cancer, breast cancer, uterine fibroids & liver cancer HIFU have all been undertaken using MRI follow-up [172, 183, 250-253]. In the majority of these studies, MR-guided HIFU devices have been used; consequently, MRI follow-up is clearly the most appropriate for baseline and future imaging. However, even after US-guided HIFU, MRI follow-up has been recommended as the sequence of post-ablative changes are consistent and correlate well with the completeness of ablation [254].

Contrastingly, there is no consensus on the follow-up modality using ablative therapies other than HIFU, with both CT & MRI recommended [165, 229, 231, 232, 255-257]. The excellent soft tissue resolution is a strong factor in favour of ablation follow-up which may hinge on subtle changes in soft tissue densities particular at the periphery of the zone of ablation [258]. However, much of the diagnostic work in imaging the small renal neoplasm is based on high-resolution CT. The current European Association of Urology guidelines on renal cancer recommend CT for the diagnosis of renal cancer, with MRI reserved for cases where CT is indeterminate, where there is an allergy to iodine-based contrast agents and in pregnancy [259].

There appears to be no fundamental reason to exclude MRI as the imaging modality in renal HIFU, although the paucity of clinical research in this specific condition gives little support to this argument. The strength of MRI follow-up in other ablative modalities suggests that MRI this stance is acceptable. However the poor correlation with histological findings seen in this trial is clearly concerning.

8.6 Treatment outcomes

The treatment options for renal cancer are numerous and the gold-standard treatment of surgery is associated with very high cure rates when tumours are diagnosed <4cm in size. As previously discussed, there are a number of ablative therapies available whose evidence base is beginning to mature towards five- and ten-year survival figures. In this context, the benchmark for alternative treatment modalities is set high. The purpose of this clinical study was to obtain definitive histological evidence of ablation – a finding distinctly lacking amongst other studies of ablative therapies.

Renal HIFU is effective in approximately half of patients based on histology. Histological ablation is generally either Grade 1 (ineffective) or Grade 3 (significant but not complete ablation). However, no Grade 4 (100%) ablation was seen – some viable tumour was demonstrated in all cases. Given the lack of histological data from RFA & CRY studies, it is not possible to compare this finding to other ablation treatment. However, it is known that the positive margin rate with PN for T1a tumours is low (5.5%; 77/1390) and does not impact of prognosis [176, 178]. At present HIFU does not compare favourably with surgery in terms of oncological outcome; however this must be viewed in the context of the invasiveness of the procedure. Whilst HIFU treatment is truly non-invasive & safe, surgery is invasive and potentially morbid. Moreover, HIFU is a repeatable therapy in those who have residual viable tumour. No effort was made in this trial to repeat HIFU – the primary aim was to determine the outcomes of a single treatment after surgery. However no clinical issues would have prevented any of the trial patients from undertaking a second session of HIFU treatment.

8.7 Future role of renal HIFU

It is evident from this trial that it is possible to safely ablate significant proportions of a small renal tumour without major side effects. However, the significance of any residual viable tumour after HIFU is not known but must be assumed to be a risk factor for tumour recurrence. Currently, the widespread use of HIFU in the primary treatment of renal cancer cannot be justified. Furthermore, renal HIFU should continue to be deemed an experimental treatment which should only be conduct within a clinical trial. This is so that the appropriate data is assimilated, analysed and published in the public domain.

It is evident that the results of tumour ablation improved as the trial progressed. Significant ablation was seen in 4/5 patients treated following the switch to the new JC-200 HIFU device. It is possible that the device upgrade can account for the improvements in results. Technology evolution is often a problem in medical device trials and can make data evaluation and comparison challenging. The overall upgrade in the JC-200 is relatively limited – there is undoubtedly an improved diagnostic imager, but the treatment software, positioning system and therapeutic transducer are essentially unchanged.

It is more likely that the improved results were due to the learning curve for the HIFU surgeons. A gradual improvement in outcomes and complications rate with repetition is widely expected and there is little reason to doubt that such improvements should occur in renal HIFU.

It is absolutely clear that an improvement in patient selection has the potential to dramatically improve clinical outcomes. A combination of the use of renal nephrometry and careful measurement of peri-nephric fat dimensions will help to exclude those who treatment is likely to be challenging and/or sub-optimal. Simultaneously an improved method of monitoring

HIFU treatment will ensure that those suitable for treatment achieve complete tumour ablation.

9 Conclusions & Future Work

9.1 Conclusions

The aim of the present work was to study the patient selection, treatment technique, treatment monitoring and follow-up for renal HIFU with the overall purpose of improving future clinical outcomes. A number of hypotheses were proposed and tested.

In Chapter 3, the design, implementation and results of a clinical renal HIFU trial with combined radiological and histological follow-up were discussed. Despite no significant changes in the trial protocol, there was a clear improvement in ablation outcomes which is attributable to better patient selection and treatment technique. It was evidently possible to ablate significant proportions of small renal tumours with exceptionally low morbidity, even compared with the morbidity associated with CRY or RFA. However it was not possible to completely ablate an entire tumour in a single treatment. The low complication rate associated with renal HIFU lends itself to repeated treatment and this may achieve improved outcomes.

As a result of the trial a number of patient selection factors were examined. It was established that renal tumours with low complexity scores (according to NS), located away from the upper pole with thin surrounding peri-nephric fat were the most appropriate for treatment. Investigations into the acoustic properties of peri-nephric fat, discussed in Chapter 4

demonstrated that the attenuation of this tissue was significant, particularly when compared with other tissue types in the propagation path during renal HIFU. Notably, up to two-thirds of the energy of a HIFU exposure may be deposited in the pre-focal fat tissue. In addition, fat tissue was also shown to have a significant de-focusing effect on the HIFU beam, resulting in transverse shifts of the focus of 1-2mm. These combined results strongly suggest that peri-nephric fat has a significant influence of renal HIFU outcomes.

It was further demonstrated in Chapter 5 that the quality of diagnostic ultrasound imaging invariably deteriorated throughout the course of a HIFU treatment such that it was often a determining factor in the early cessation of treatment. This in no small part is due to the energy deposition in the fat layers discussed previously – pre-focal fat heating causes tissue swelling, propagation path lengthening, additional phase aberrations and increased attenuation. A number of techniques to limit its impact were discussed and were implemented in the course of the clinical trial.

Chapter 6 introduced the use of an alternative method of monitoring the progress of and feedback obtained during HIFU therapy. It was demonstrated that PAM outperformed conventional hyperecho monitoring in the detection of lesions at clinically-relevant insonation amplitudes in *ex-vivo* ox liver. It was further demonstrated that hyperecho is a poor determinant of lesion formation and corresponds with boiling and overtreatment rather than the appearance of tissue ablation itself. Thresholds were applied to the PAM data and were shown to successfully predict lesion formation with both high sensitivity and specificity. In *ex-vivo* liver PAM data was also able to accurate predict the location of thermal lesions and it was also demonstrated that early broadband and harmonic emissions could be used to localise the zone of ablation prior to significant heating.

The concepts introduced in PAM are of significant interest because they can be integrated into existing clinical ultrasound-guided HIFU devices with ease, without affecting the performance of the therapy. In Chapter 7 the design and testing of a clinical PCD sensor was presented – highly sensitive acoustically transparent receive elements were placed around the therapy head of commercially available HIFU machines. With suitable filtering and pre-amplification, acoustic emissions could be received and localised accurately and without impeding the delivery of therapeutic ultrasound to the focus. The device was safely tested in in patients within the confines of the clinical trial. Localisation of sources of non-linearity was feasible without compromising patient safety.

Finally, in Chapter 8 all the presented work was used to provide a detailed discussion of the implications for future patient care in renal HIFU. Appropriate patient selection parameters for NS, fat thickness and tumour size were analysed and suggested that NS and fat thickness could be used to determined suitability for HIFU. The low morbidity of renal HIFU was demonstrated, which supports its in-going use, but attention must be paid to maintaining the quality of intra-operative imaging. In addition, the use of PAM may vastly improve feedback and should be promptly investigated.

Renal HIFU to date has shown promising but ultimately sub-optimal results. Interest in its use will and should continue – it represents the most minimally-invasive cancer therapy currently available and is highly acceptable to patients and clinicians alike. However, the minimally-invasive market for renal cancer has many options and based on current results HIFU remains experimental. This will remain so until improvements in intra-operative imaging and feedback are adequately addressed.

9.2 Future work

Inevitably detailed clinical research often generates as many questions as it does answers. The following section provides some insight into the key issues in renal HIFU and suggestions as to how they should best be answered.

9.2.1 Clinical role of HIFU

Short term clinical studies are effective in establishing proof of concept, safety and efficacy using surrogate outcome data such as ablation percentages based on radiology or histology. However the true efficacy of any treatment should be assessed using the most clinically relevant outcome measures. In the context of renal HIFU these are progression-free survival, cancer-specific survival and overall survival. Of equal importance is the relative efficacy of renal HIFU in comparison to existing techniques. The comparison should include surgery (PN – open, laparoscopic or robot-assisted), active-surveillance and alternative ablative therapies (CRY & RFA). Without comparative studies of all relevant treatment options there will never be any conclusive evidence for their use.

The most appropriate study is an RCT which must be appropriately powered. A prospective study of this format helps to minimise selection bias, confounding factors and data errors associated with retrospective studies. It will not be possible to blind either the subjects or the clinicians to treatment; however both the histological and radiological assessments could easily be blinded and should also be centralised such that they are examined and cross-examined by a select group of assessors. An example of how such an RCT might be designed is suggested in Figure 79.

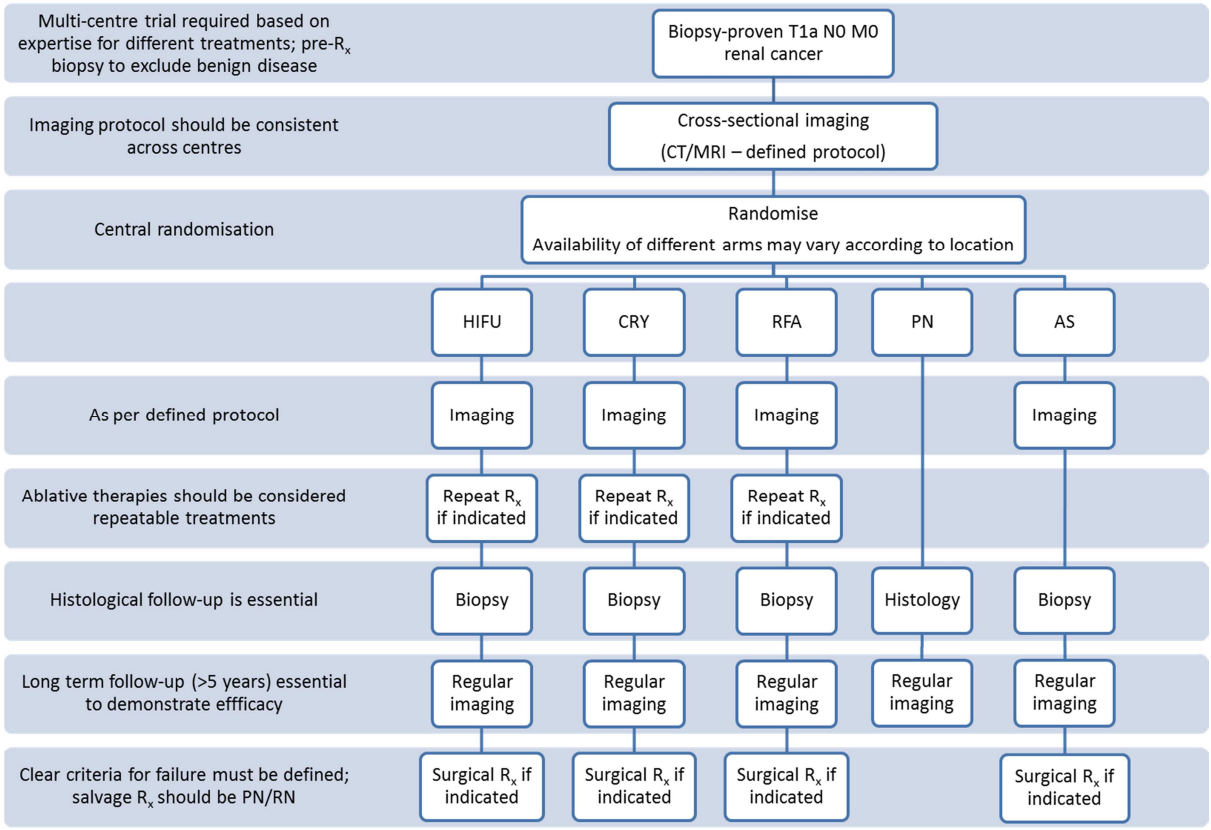

Figure 79 – Suggested design of an RCT to determine role of renal HIFU in the management of T1aN0M0 renal cancer; AS = active surveillance.

Any trial protocol should also ensure that appropriate tissue, blood and/or urine is obtained to allow assessment of the immunological response to tissue ablation. These samples should also be used to search for any biomarkers which may help select patients and tumours which are most likely to have successful outcomes in each treatment group.

An RCT such as this would require large patient numbers and would therefore require the co-operation of a number of centres with varying expertise in surgery and ablation. It would also be expensive to conduct. However it would answer issues that are currently fundamental to how we manage renal cancer and any cost would certainly be justifiable.

9.2.2 Patient selection

The work presented in Chapter 4 & 5 represents the first effort to improve patient selection for renal HIFU. It has demonstrated the tumour size, location, NS and fat dimensions are

important factors in determining whether a patient is suitable for HIFU. However, due to low patient number, it was not possible to determine whether these (or other) factors were able to predict a successful outcome of HIFU treatment itself. Further clinical studies should be directed towards assessing these factors.

9.2.3 Image registration & motion-compensation

It is evident from this work that ultrasound imaging of renal tumours is challenging. The rib cage, abdominal wall, fat tissues, respiratory motion, water stand-off with the clinical device and pre-focal tissue damage all contribute to the limited image quality. Many of these factors cannot be modified with the extracorporeal delivery route. However the ability to accurately register ultrasound images with pre-operatively obtained cross-sectional imaging would significant increase the confidence of the HIFU operator that treatment will be accurate. A number of groups are looking at image registration algorithms in the context of HIFU and if combined with motion tracking/compensation could significantly improve renal HIFU [244].

9.2.4 HIFU monitoring

In this work a novel monitoring method has been tested in the *ex-vivo* setting and integrated with a HIFU device in the clinical setting. Safety has been proved and preliminary monitoring results are promising. Further research should urgently look at the efficacy of PAM in comparison with existing hyperecho monitoring. Both should be compared with a histological assessment of ablation. This should initially be done using *ex-vivo* tissue and then could be further testing in perfused tissue models. Carefully designed *in-vivo* animal studies of ablation in a number of organs (both normal parenchyma and tumour) should then be undertaken to accurately determine the necessary thresholds to predict lesion formation. Finally, clinical studies of HIFU which use both monitoring formats should then be performed. There is no reason to eliminate hyperecho monitoring in its entirety - indeed it will always be visible in

US-guided HIFU. Its presence is a strong indicator of overtreatment and is thus a warning to lower the energy delivery.

9.2.5 Improving image quality

It is evident from the clinical trial data that tumour imaging was often of good quality when the diagnostic probe was placed directly in contact with the skin. The existing JC & JC-200 devices do not allow HIFU therapy to be delivered whilst the probe in elevated against the skin as it blocks the acoustic window. The problem can be overcome in two ways. The use of transducers with shorter focal lengths would enable the therapeutic head to be placed closer to the abdominal wall. This may allow the diagnostic probe to lie very close to the abdominal wall without interfering with HIFU delivery. Whilst feasible, the short focal length may prevent treatment of many renal tumours which can be up to 10-12cms deep the skin. Alternatively altering the therapeutic transducer design may allow the diagnostic probe to remain elevated without impacting of the HIFU beam. The use of a wider therapeutic transducer which has a larger inactive central component would allow focused ultrasound delivery whilst eliminating the HIFU beam from the inner area of the transducer which would be blocked by the diagnostic probe. In addition it may be possible to focus the HIFU beam using a lens placed further away from the therapeutic element closer to the abdominal wall. The unfocused HIFU beam could be produced by a planar element and focused only at the level of the diagnostic probe. This would allow focused ultrasound treatment as well as allowing high quality diagnostic ultrasound from the probe placed in contact with the skin.

10 Appendices

10.1 Clinical trial methodology – Renal HIFU

10.1.1 Ethics approval confirmation

Oxfordshire REC C
2nd Floor, Astral House
Chaucer Business Park
Granville Way
Bicester
OX26 4JT

Telephone: 01869 604062
Facsimile: 01869 604055
Email: scsha.OxfordRECC@nhs.net

18 May 2009

Mr David Cranston
Consultant Urological Surgeon & Senior Lecturer in Urology
Oxford Radcliffe NHS Trust
Urology Department
Churchill Hospital
Oxford
OX3 7LJ

Dear Mr Cranston

Full title of study: **Extracorporeal High Intensity Focused Ultrasound for Small Kidney Tumours: Phase I Pilot Histological Follow-Up Trial**
REC reference number: **09/H0606/42**

Thank you for your letter of 07 May 2009, responding to the Committee's request for further information on the above research and submitting revised documentation, subject to the conditions specified below.

The further information has been considered on behalf of the Committee by the Chair.

Confirmation of ethical opinion

On behalf of the Committee, I am pleased to confirm a favourable ethical opinion for the above research on the basis described in the application form, protocol and supporting documentation as revised.

Ethical review of research sites

The favourable opinion applies to all NHS sites taking part in the study, subject to management permission being obtained from the NHS/HSC R&D office prior to the start of the study (see "Conditions of the favourable opinion" below).

The favourable opinion applies to the following research sites:

Research site	*Principal Investigator / Local Collaborator*
Oxford Radcliffe Hospitals NHS Trust	Mr David Cranston

10.1.2 Trust management approval confirmation

Oxford Radcliffe Hospitals NHS
NHS Trust

JM/EC/5983

From the Medical Director
Dr James Morris, FRCPath
C/o R&D Office, Manor House
The John Radcliffe Hospital
Headley Way, Headington
Oxford OX3 9DZ

Tel: (01865) 222147
Fax: (01865) 222648
Email: Elaine.cherry@orh.nhs.uk

Mr David Cranston
Consultant Urological Surgeon
& Senior Lecturer in Urology
Urology Department
Churchill Hospital
Headington
Oxford OX3 7LJ

29th June 2009

Dear Mr Cranston

Re: Extracorporeal High Intensity Focused Ultrasound for Small Kidney Tumours: Phase I Pilot Histological Follow-Up Trial.

Research and Development Reference: 5983
Research Ethics Committee Reference: 09/H0606/42

Confirmation of Trust Management Approval

On behalf of the Oxford Radcliffe Hospitals NHS Trust, I am pleased to confirm Trust Management Approval and Indemnity for the above research on the basis described in the application, protocol and other supporting documents.

Conditions of Approval

The Approval is given provided that you have a contract of employment with the Trust and that you have obtained Ethical Approval. You should also comply with the conditions set out within the attached document. Please ensure that you read these conditions carefully.

Research Sponsorship

The Oxford Radcliffe Hospitals NHS accepts the role of Research Sponsor for this study in accordance with the Medicines for Human Use (Clinical Trials) Regulations 2004 and/or, the requirements of Department of Health Research Governance Guidelines.

Approved Documents

Protocol Flowchart, Version 1.0, 19 February 2009
Protocol, Version 1.0, 19 February 2009

10.1.3 Funding confirmation

DIRECTOR: Professor Keith Channon

Oxford Biomedical Research Centre
Room 4503, Level 4
John Radcliffe Hospital
Oxford
OX3 9DU
Tel: 01865 743341
Email: cora.reilly@orh.nhs.uk

16 Jan 09

To whom it may concern,

I hereby confirm funding for the amounts outlined below to support the research study 'Extra – corporeal High Intensity Focused Ultrasound for Small Kidney Tumours: Phase I Pilot Histological Follow up Study'

BRC Ref: A90104

Salaries	**% time**	**£**	**Employer**
Clinical Research Fellow (10 months)	100	42,683	NHS
Clinical Research Fellow (10 months)	100	42,683	NHS
Post Doc RA	100	25,610	UNI
Support Costs			
Hydraphones and stages		7,200	Uni
Data acquisition computer and cards		3,000	Uni
Passive cavitation detection transducers		1,800	Uni
Total Funding 2008/2009		**122,976**	

Further funding will be subject to annual review until 2012.

Yours sincerely

J Shanahan

Manager of Clinical Research Operations

10.1.4 Substantial amendment approval

Oxfordshire REC C
Room 002
TEDCO Business Centre
Rolling Mill Road
Jarrow
NE32 3DT

Tel: 0191 428 3564
Fax: 0191 428 3432

03 August 2010

Mr David Cranston
Urology Department
Churchill Hospital
Oxford
OX3 7LJ

Dear Mr Cranston

Study title: **Extracorporeal High Intensity Focused Ultrasound for Small Kidney Tumours: Phase I Pilot Histological Follow-Up Trial**
REC reference: **09/H0606/42**
Protocol number: **N/A**
Amendment number: **2.0 (24th June 2010)**
Amendment date: **19 July 2010**

The above amendment was reviewed at the meeting of the Sub-Committee held on 30 July 2010.

Ethical opinion

Favourable Opinion

The members of the Committee taking part in the review gave a favourable ethical opinion of the amendment on the basis described in the notice of amendment form and supporting documentation.

Approved documents

The documents reviewed and approved at the meeting were:

Document	Version	Date	
Covering Letter	Rob Richie	19 July 2010	
Notice of Substantial Amendment (non-CTIMPs)	2.0 (24th June 2010)	19 July 2010	
Updated REC Application Form	IRAS Version 3.0 12641/13619/1/1	24 June 2010	
Protocol	Version 2.0	24 June 2010	

10.1.5 Trial inclusion & exclusion criteria

10.1.5.1 Inclusion criteria

Participant is willing and able to give informed consent for participation in the study.

Male or Female, aged 18 years or above.

Lesions suspicious for renal cell carcinoma on radiology that are < 4cm in maximum diameter and suitable for surgical resection

Participant must be in sufficiently good health to be suitable for general anaesthesia for both EC-HIFU treatment and subsequent surgical resection of tumour

Subjects must have ≥ 1 evaluable tumours which can be visualised on diagnostic ultrasound. If more than one tumour exists, an index tumour will be nominated and treated (uncommon)

Previous chemotherapy and / or biological therapy for cancer are permitted, but the subject should have recovered fully from the effects of these and any prior surgery.

Patients should not have received radiotherapy to the target area within the preceding 12 months.

Subject has clinically acceptable haematological, electrolyte and hepatic function as demonstrated by serum laboratory values within 14 days prior of EC-HIFU treatment:

Absolute neutrophil count (ANC) ≥ $1500mm^{-3}$

Platelet count ≥ $100,000mm^{-3}$

Haemoglobin ≥ $10gdl^{-1}$

Prothrombin time (PT) ≤ 1.5 * Upper Limit of Normal (ULN)

Activated partial thomboplastin time (APPT) ≤ 1.5 * ULN

Total bilirubin < 2.5 * ULN

Aspartate aminotransferase (AST) < 3 * ULN

Alkaline phosphatase (ALP) < 2 * ULN; unless arising from bone

Participant has a clinically acceptable ECG

Negative pregnancy test within 24 hours of EC-HIFU treatment (if appropriate)

Able (in the Investigators opinion) and willing to comply with all study requirements.

Willing to allow his or her General Practitioner and consultant to be notified of participation in the study.

An American Society of Anaesthesiologists (ASA) score of ≤ 2

A World Health Organisation (WHO) performance status of ≤ 1

10.1.5.2 Exclusion Criteria

The participant may not enter the study if ANY of the following apply:

Female participants who is pregnant, lactating or planning pregnancy during the course of the study (see pregnancy test note above)

Significant hepatic impairment.

Significant renal impairment as to mean surgical resection is unsuitable

Clinical or radiological evidence of metastatic disease

Subjects with tumours lying adjacent to vital structures such that EC-HIFU treatment would risk damage to these structures

Subjects currently taking anti-coagulant or immunosuppressive medication

Scheduled elective surgery or other procedures requiring general anaesthesia during the study.

Any other significant disease or disorder which, in the opinion of the Investigator, may either put the participants at risk because of participation in the study, or may influence the result of the study, or the participant's ability to participate in the study.

Participants currently involved in any medicinal trial (participants involved in the treatment phase of a clinical trial (observational or follow-up studies will be allowed)

10.1.6 Clinical trial consent form

Centre Number: 1 (of 1)

REC Reference No: 09/H0606/42 (Oxford REC C)

Patient Identification Number for this trial:

Consent Form

Extra-corporeal High Intensity Focused Ultrasound for small kidney tumours: Phase I pilot histological follow-up trial

Name of Researchers:

Mr. Robert Ritchie BM MRCS Academic Clinical Fellow in Urology
Tel: 01865 763100

Mr. Tom Leslie MB ChB MRCS Clinical Lecturer in Urology
Tel: 01865 763100

Mr. David Cranston DPhil FRCS Urol. Consultant Urological Surgeon
Tel: 01865 226145

Please initial box

I confirm that I have read and understand the information sheet version number……2.0….date……7/5/2009…… for the above study and have had the opportunity to ask questions. ☐

I understand that my participation is voluntary and that I am free to withdraw at any time, without giving any reason, without my medical care or legal rights being affected. ☐

I understand that sections of any of my medical notes may be looked at by responsible individuals from Central Clinical Research Services Partnership, from the regulatory authorities where it is relevant to my taking part in research. I give permission for these individuals to have access to my records. ☐

I understand that my GP will be informed about my participation in this study. ☐

☐

I agree to take part in the above study.

Samples of your blood will be taken and stored before and after your treatment to assess whether high intensity ultrasound treatment can stimulate the immune system. These samples will be retained after the end of the study for this purpose. We would also like to use these samples in future research on high intensity focused ultrasound.

Samples will **NOT** be used for any of the following
for research outside the UK,
for research involving animals, human embryos or stem cells
for research into the termination of pregnancy or contraception
for commercial research

Do you consent to blood samples being retained in this fashion?

☐ Yes ☐ No

Samples of kidney tissue will be taken and stored before and after your treatment to assess whether high intensity ultrasound treatment can stimulate the immune system. This tissue will be retained after the end of the study period for this purpose. Tissue for research purpose will also be stored in a tissue bank at the John Radcliffe Hospital for use in future research projects. Do you consent to kidney tissue being retained in this fashion?

Do you consent to tissue being retained in this fashion?

☐ Yes ☐ No

Your personal details will remain entirely confidential throughout the trial.

You are free to withdraw your consent for the retention of this tissue at any point and this will not affect your on-going participation in this trial or any subsequent care you may receive.

_____ _____ _____
Name of Patient Date Signature

_____ _____ _____
Name of Person taking consent (if different from researcher) Date Signature

_____ _____ _____
Researcher Date Signature

4 copies:

1 for patient
1 for researcher
1 to be kept with hospital notes
1 to be inserted into site file

10.2 Clinical trial methodology – Peri-nephric fat

10.2.1 Ethics approval confirmation

NHS
National Research Ethics Service
Oxfordshire REC A
2nd Floor, Astral House
Chaucer Business Park
Granville Way
Bicester
OX26 4JT

Telephone: 0191 428 3561
Facsimile: 0191 428 3432

17 June 2010

Mr Thomas Leslie
Clinical Lecturer in Urology
Oxford Radcliffe NHS Trust
HIFU Unit
Churchill Hospital
Oxford
OX3 7LJ

Dear Mr Leslie

Full title of study: **How do the properties of perinephric fat influence the outcome of high intensity focused ultrasound (HIFU) in the ablation of renal tissue and renal tumours?**
REC reference number: **10/H0604/34**

Thank you for your letter of 9 June 2010. I can confirm the REC has received the documents listed below as evidence of compliance with the approval conditions detailed in our letter dated 07 May 2010. Please note these documents are for information only and have not been reviewed by the committee.

Documents received

The documents received were as follows:

Document	*Version*	*Date*
Protocol	Version 2.0	09 June 2010
Protocol Flow Chart	Version 2.0	09 June 2010
Covering Letter	Rob Ritchie	09 June 2010
Summary/Synopsis	Patient Information Flow Chart Version 2.0	09 June 2010
Letter of invitation to participant	Version 2.0	09 June 2010
Participant Information Sheet: Patient	Version 2.0	09 June 2010
Participant Consent Form: Patient	Version 2.0	09 June 2010

10.2.2 Trust management approval confirmation

Oxford Radcliffe Hospitals NHS
NHS Trust

HH/JF/6170

Mr Thomas Leslie
Clinical Lecturer in Urology
HIFU Unit
Churchill Hospital
Oxford
OX3 7LJ

From the R & D Lead
Research & Development
Room 13, Manor House
The John Radcliffe Hospital
Headley Way, Headington
Oxford OX3 9DZ

Tel: (01865) 221930
Fax: (01865) 222648
Email: jo.franklin@orh.nhs.uk

25 June 2010

Dear Mr Leslie

Re: How do the properties of perinephric fat influence the outcome of high intensity focused ultrasound (HIFU) in the ablation of renal tissue and renal tumours?

Research and Development Reference: 6170
Research Ethics Committee Reference: 10/H0604/34

Confirmation of Trust Management Approval

On behalf of the Oxford Radcliffe Hospitals NHS Trust, I am pleased to confirm Trust Management Approval and Indemnity for the above research on the basis described in the application, protocol and other supporting documents.

Conditions of Approval

The Approval is given provided that you have a substantive or honorary contract with the Trust and that you have obtained Ethical Approval. You should also comply with the conditions set out within the attached document. Please ensure that you read these conditions carefully.

Research Sponsorship

The Oxford Radcliffe Hospitals NHS accepts the role of Research Sponsor for this study in accordance with the Medicines for Human Use (Clinical Trials) Regulations 2004 and/or, the requirements of Department of Health Research Governance Guidelines.
Site Specific Assessment

Site Specific Assessment

This Trust management Approval letter also incorporates site specific assessment for the Oxford Radcliffe Hospitals NHS Trust site

10.3 Summary of all clinical results

Presented below is a summary of the key demographic, tumour, treatment and follow-up characteristics for each individual patient. The before and after CE-MRI images taken during the LAVA phase of the imaging protocol are also shown.

10.3.1 Patient 5.01

Patient	Age (years)	73	BMI (kg/m^2)	22
Tumour	Size (mm)	18	NS score	7
	Fat (trans, mm)	20	Fat (AP, mm)	11
	Side	Left	Location	Upper pole
HIFU	Anaesthetic time[1]	305 mins	Treatment time[2]	214 mins
	HIFU on-time[3]	35 mins	B-mode score[4]	2-1-1
	Complications[5]	Post-operative acute urinary retention Haemorrhage post-surgery (required) embolisation)		
Follow-up[6]	Hb (g/dL)	12.3-14.2-11.7	WCC (*10^9/L)	3.3-7.3-4.9
	CRP (mmol/L)	3.0-19.0-2.0	Creatinine (mmol/L)	82-93-80
% ablation	MRI	0	Histology	95

[1] – Anaesthetic time represents total procedure time from induction to reversal of anaesthesia
[2] – Treatment time represents time from first HIFU exposure to last HIFU exposure
[3] – HIFU on-time represents total duration of HIFU exposures
[4] – B-mode scoring assessed at pre-, mid- & post-HIFU
[5] – Mild skin pain or burn (CTCAE Grade 1) not recorded
[6] – Laboratory follow-up assessed at pre-HIFU and days 1 & 12 post-HIFU

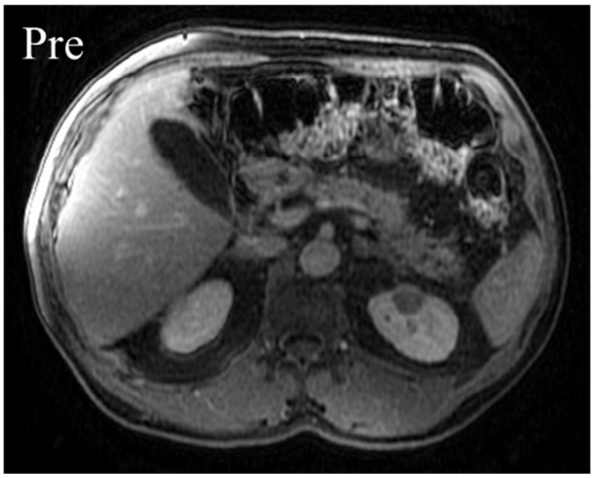

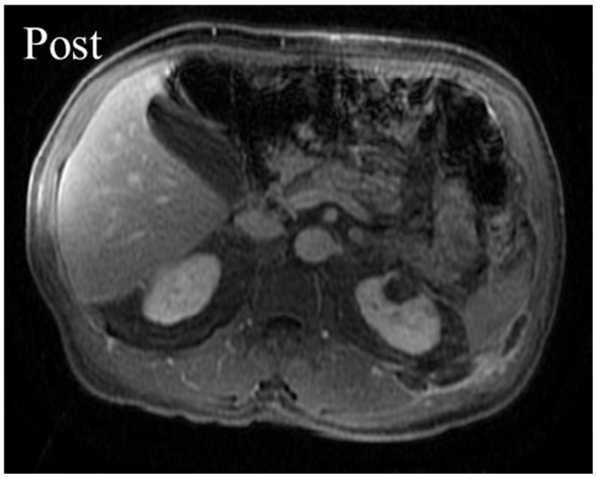

10.3.2 Patient 5.03

Patient	Age (years)	66	BMI (kg/m^2)	34
Tumour	Size (mm)	30	NS score	8
	Fat (trans, mm)	29	Fat (AP, mm)	5
	Side	Left	Location	Interpolar
HIFU	Anaesthetic time	270 mins	Treatment time	180 hours
	HIFU on-time	31 mins	B-mode score[1]	4-2-1
	Complications	Haemorrhage post-surgery (required nephrectomy)		
Follow-up[2]	Hb (g/dL)	14.5-13.8-14.4	WCC (*10^9/L)	5.6-17.1-5.5
	CRP (mmol/L)	2.0-12.0-2.0	Creatinine (mmol/L)	57-63-48
% ablation	MRI	0	Histology	0

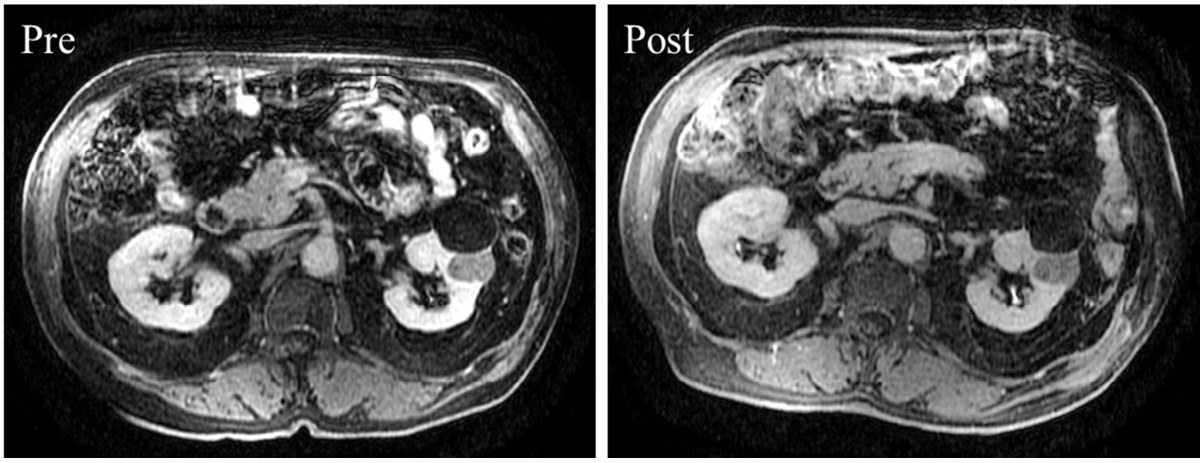

10.3.3 Patient 5.05

Patient	Age (years)	50	BMI (kg/m^2)	28
Tumour	Size (mm)	19	NS score	5
	Fat (trans, mm)	10	Fat (AP, mm)	2
	Side	Left	Location	Interpolar
HIFU	Anaesthetic time	180 mins	Treatment time	N/A
	HIFU on-time	N/A	B-mode score[1]	N/A
	Complications	No treatment		
Follow-up[2]	Hb (g/dL)	15.9-16.6-15.1	WCC (*10^9/L)	6.7-5.6-4.7
	CRP (mmol/L)	4.0-11.0-2.0	Creatinine (mmol/L)	73-78-61
% ablation	MRI	N/A	Histology	N/A

No imaging follow-up as no HIFU treatment took place.

10.3.4 Patient 5.07

Patient	Age (years)	41	BMI (kg/m^2)	Not known
Tumour	Size (mm)	33	NS score	8
	Fat (trans, mm)	8	Fat (AP, mm)	1
	Side	Right	Location	Interpolar
HIFU	Anaesthetic time	N/A	Treatment time	N/A
	HIFU on-time	N/A	B-mode score[1]	No treatment
	Complications	No treatment		
Follow-up[2]	Hb (g/dL)	14.2-13.6-13.5	WCC (*10^9/L)	13.3-13.9-15
	CRP (mmol/L)	N/A	Creatinine (mmol/L)	124-131-99
% ablation	MRI	N/A	Histology	N/A

No imaging follow-up as no HIFU treatment took place.

10.3.5 Patient 5.10

Patient	Age (years)	82	BMI (kg/m^2)	21
Tumour	Size (mm)	28	NS score	7
	Fat (trans, mm)	1	Fat (AP, mm)	3
	Side	Right	Location	Interpolar
HIFU	Anaesthetic time	235 mins	Treatment time	150 mins
	HIFU on-time	28 mins	B-mode score[1]	3-2-1
	Complications	Nil		
Follow-up[2]	Hb (g/dL)	13.1-11.7-12.2	WCC (*10^9/L)	9.5-16.3-7.8
	CRP (mmol/L)	2.0-27.0-2.0	Creatinine (mmol/L)	63-64-61
% ablation	MRI	0	Histology	<5

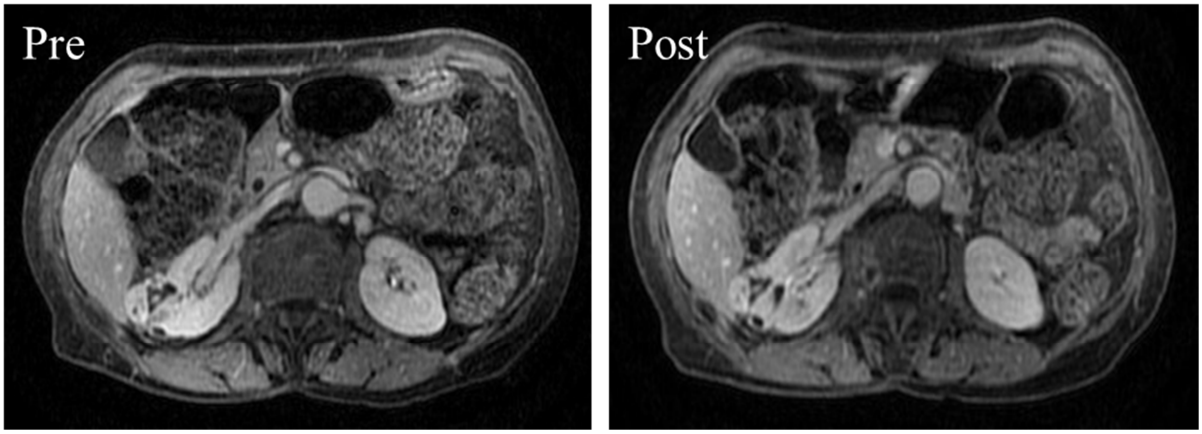

10.3.6 Patient 5.13

Patient	Age (years)	64	BMI (kg/m^2)	28
Tumour	Size (mm)	38	NS score	5
	Fat (trans, mm)	10	Fat (AP, mm)	20
	Side	Left	Location	Interpolar
HIFU	Anaesthetic time	245 mins	Treatment time	164 mins
	HIFU on-time	25 mins	B-mode score[1]	3-1-1
	Complications	Nil		
Follow-up[2]	Hb (g/dL)	15.5-14.8-14.8	WCC (*10^9/L)	6.6-13.2-6.5
	CRP (mmol/L)	2.0-12.0-3.0	Creatinine (mmol/L)	108-103-99
% ablation	MRI	0	Histology	<5

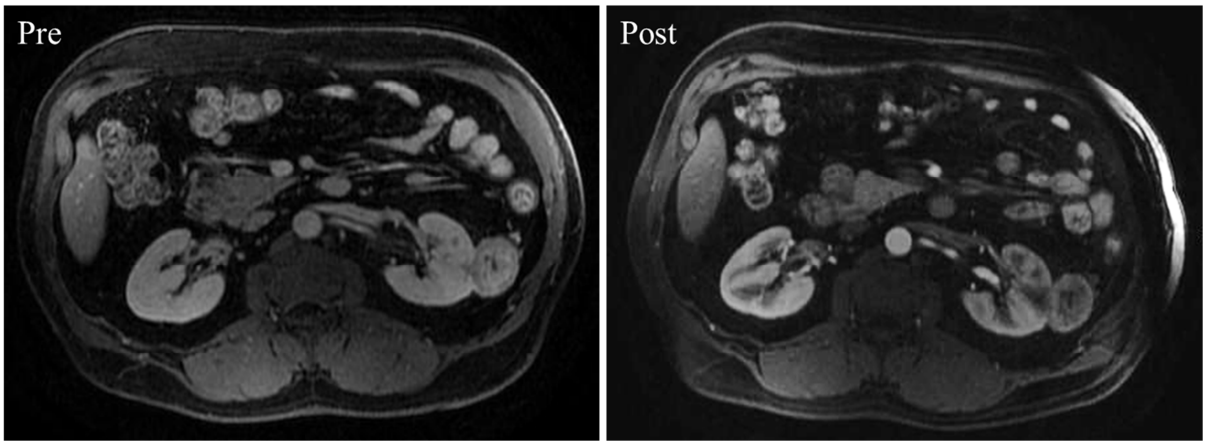

10.3.7 Patient 5.16

Patient	Age (years)	52	BMI (kg/m^2)	28
Tumour	Size (mm)	27	NS score	4
	Fat (trans, mm)	34	Fat (AP, mm)	3
	Side	Right	Location	Interpolar
HIFU	Anaesthetic time	235 mins	Treatment time	159 mins
	HIFU on-time	16 mins	B-mode score[1]	5-4-4
	Complications	Moderate skin pain		
Follow-up[2]	Hb (g/dL)	14.6-13.8-12.8	WCC (*10^9/L)	6.6-12.4-8.6
	CRP (mmol/L)	2.0-3.0-13.0	Creatinine (mmol/L)	82-83-97
% ablation	MRI	1.21	Histology	95

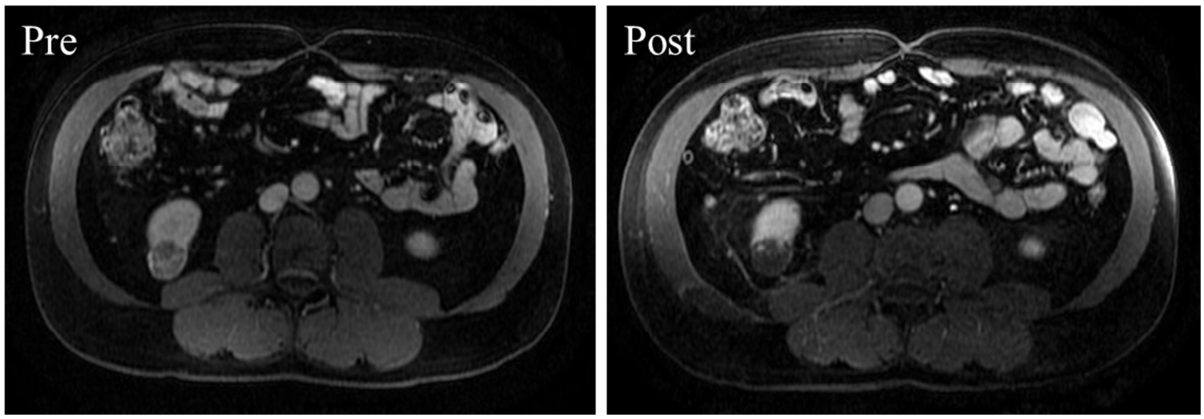

10.3.8 Patient 5.19

Patient	Age (years)	56	BMI (kg/m^2)	23
Tumour	Size (mm)	27	NS score	6
	Fat (trans, mm)	20	Fat (AP, mm)	8
	Side	Right	Location	Interpolar
HIFU	Anaesthetic time	183 mins	Treatment time	N/A
	HIFU on-time	N/A	B-mode score[1]	2-1-1
	Complications	Severe hypertension (treatment abandoned)		
Follow-up[2]	Hb (g/dL)	15.8-16.3-N/A	WCC (*10^9/L)	5.7-5.5-N/A
	CRP (mmol/L)	2.0-10.0-2.0	Creatinine (mmol/L)	93-90-N/A
% ablation	MRI	N/A	Histology	N/A

No imaging follow-up as no HIFU treatment took place.

10.3.9 Patient 5.21

Patient	Age (years)	71	BMI (kg/m^2)	28
Tumour	Size (mm)	24	NS score	4
	Fat (trans, mm)	4	Fat (AP, mm)	19
	Side	Right	Location	Lower pole
HIFU	Anaesthetic time	150 mins	Treatment time	77 mins
	HIFU on-time	9 mins	B-mode score[1]	5-3-3
	Complications	Nil		
Follow-up[2]	Hb (g/dL)	13.7-13.2-13.7	WCC (*10^9/L)	7.0-9.7-9.1
	CRP (mmol/L)	2.0-0.8-2.0	Creatinine (mmol/L)	96-90-93
% ablation	MRI	0	Histology	95

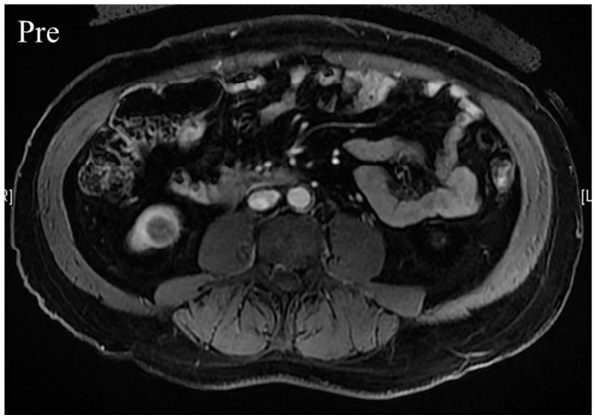

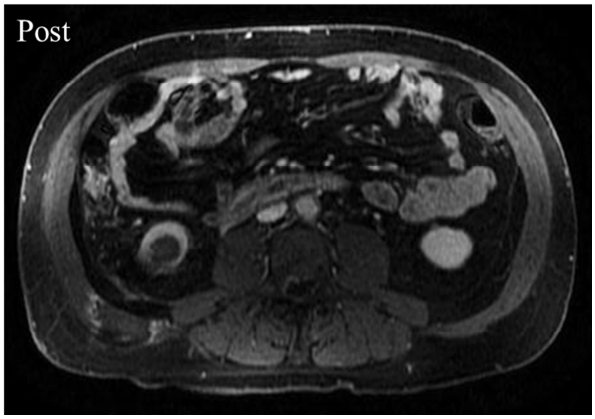

10.3.10 Patient 5.23

Patient	Age (years)	36	BMI (kg/m^2)	25
Tumour	Size (mm)	22	NS score	6
	Fat (trans, mm)	8	Fat (AP, mm)	3
	Side	Right	Location	Lower pole
HIFU	Anaesthetic time	228 mins	Treatment time	148 mins
	HIFU on-time	10 mins	B-mode score[1]	3-1-1
	Complications	Nil		
Follow-up[2]	Hb (g/dL)	14.5-14.9-14.2	WCC (*10^9/L)	6.0-10.0-8.6
	CRP (mmol/L)	2.0-1.2-0.5	Creatinine (mmol/L)	84-78-76
% ablation	MRI	1.12	Histology	60

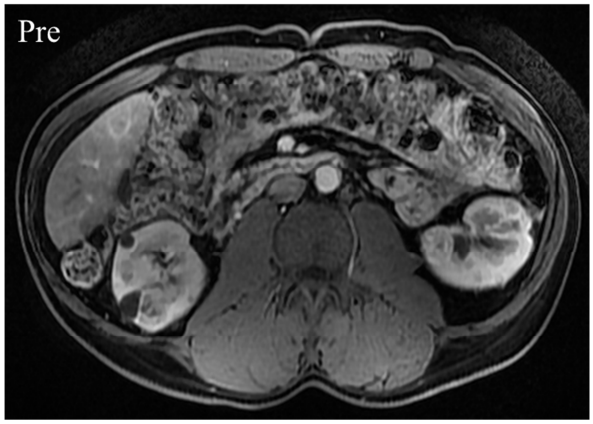

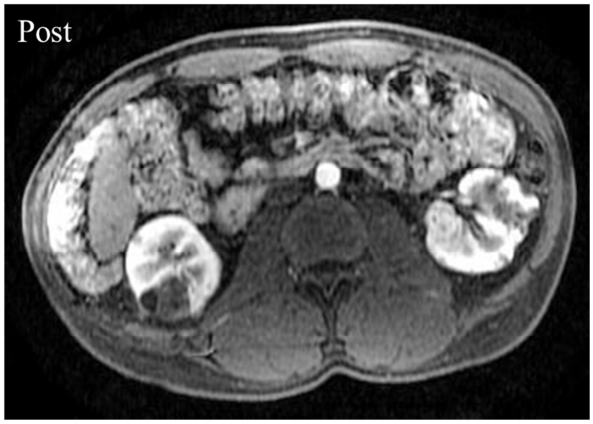

10.3.11 Patient 5.29

Patient	Age (years)	35	BMI (kg/m^2)	
Tumour	Size (mm)	30	NS score	10
	Fat (trans, mm)	14	Fat (AP, mm)	4
	Side	Left	Location	Upper
HIFU	Anaesthetic time	169 mins	Treatment time	51 mins

	HIFU on-time	3 mins	B-mode score[1]	2-1-1
	Complications	Nil		
Follow-up[2]	Hb (g/dL)		WCC (*10^9/L)	
	CRP (mmol/L)		Creatinine (mmol/L)	
% ablation	MRI	0	Histology	0

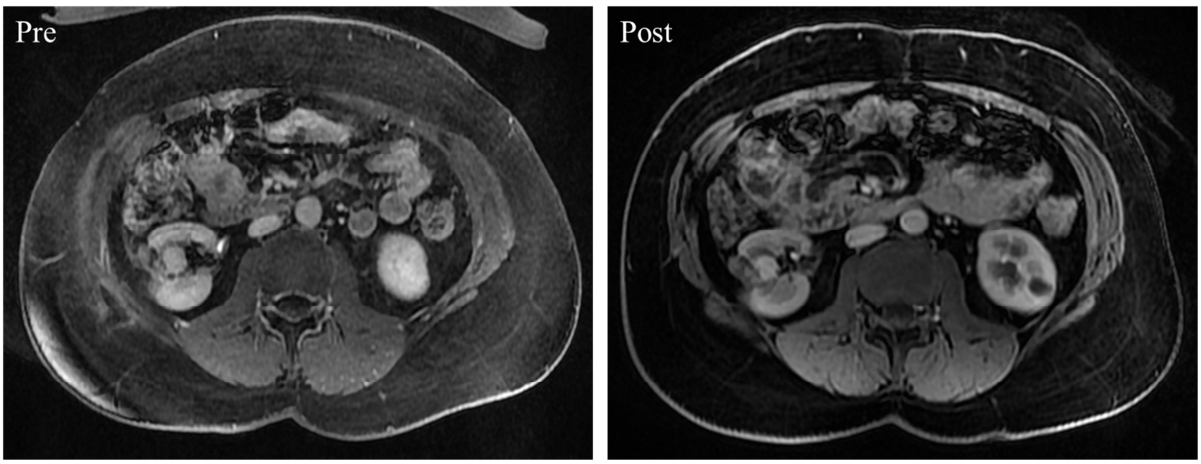

10.3.12 Patient 5.38

Patient	Age (years)	60	BMI (kg/m^2)	31.5
Tumour	Size (mm)	21	NS score	4
	Fat (trans, mm)	32	Fat (AP, mm)	17
	Side	Left	Location	Lower pole
HIFU	Anaesthetic time	130 mins	Treatment time	85 mins
	HIFU on-time	3 mins	B-mode score[1]	2-1-1
	Complications	Nil		
Follow-up[2]	Hb (g/dL)	16.4-15.4-16.3	WCC (*10^9/L)	9.2-13.6-8.2
	CRP (mmol/L)	11.6-14.7-20.4	Creatinine (mmol/L)	93-82-90
% ablation	MRI	1.40	Histology	60

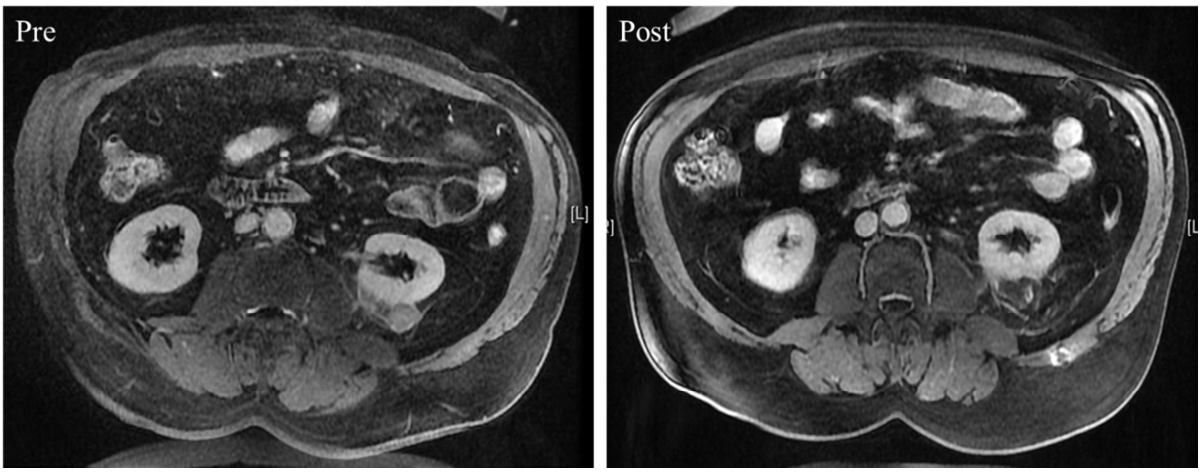

10.3.13 Patient 5.39

Patient	Age (years)	67	BMI (kg/m^2)	18
Tumour	Size (mm)	18	NS score	4
	Fat (trans, mm)	1	Fat (AP, mm)	1
	Side	Right	Location	Lower pole
HIFU	Anaesthetic time	115mins	Treatment time	80 mins
	HIFU on-time	9 mins	B-mode score[1]	5-4-4
	Complications	Nil		
Follow-up[2]	Hb (g/dL)	11.5-11.8-12.7	WCC (*10^9/L)	9.2-7.7-9.1
	CRP (mmol/L)	7.4-7.8-6.8	Creatinine (mmol/L)	58-55-60
% ablation	MRI	1.06	Histology	

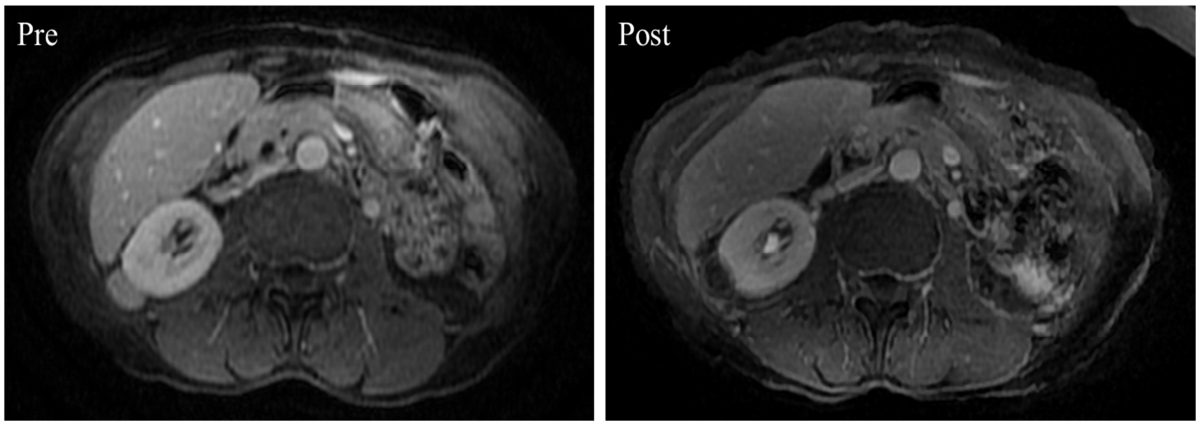

10.4 Transducer calibrations

10.5 Radiation force balance

The device manufacturers (HAIFU Technology Company Ltd, Chongqing, China) supplied a purpose-built RFB to measure the transducer output with the therapeutic head in-situ. The device allowed regular calibration of the transducer for quality assurance purpose as well as an assessment of the impact of the PCD array.

The RFB consists of a horizontally-aligned circular absorbing target which is attached to an electronic force balance directly above it. These two pieces of equipment are held in place by a cylindrical metal mount which is custom-fit to the clinical transducer being tested. Its

bottom edge fits precisely around the lip of the transducer so it is fixed firmly in place without affecting the HIFU drive signal, as shown in Figure 80. The force balance measures the ultrasound radiation force in grams and is accurate to ±0.1g.

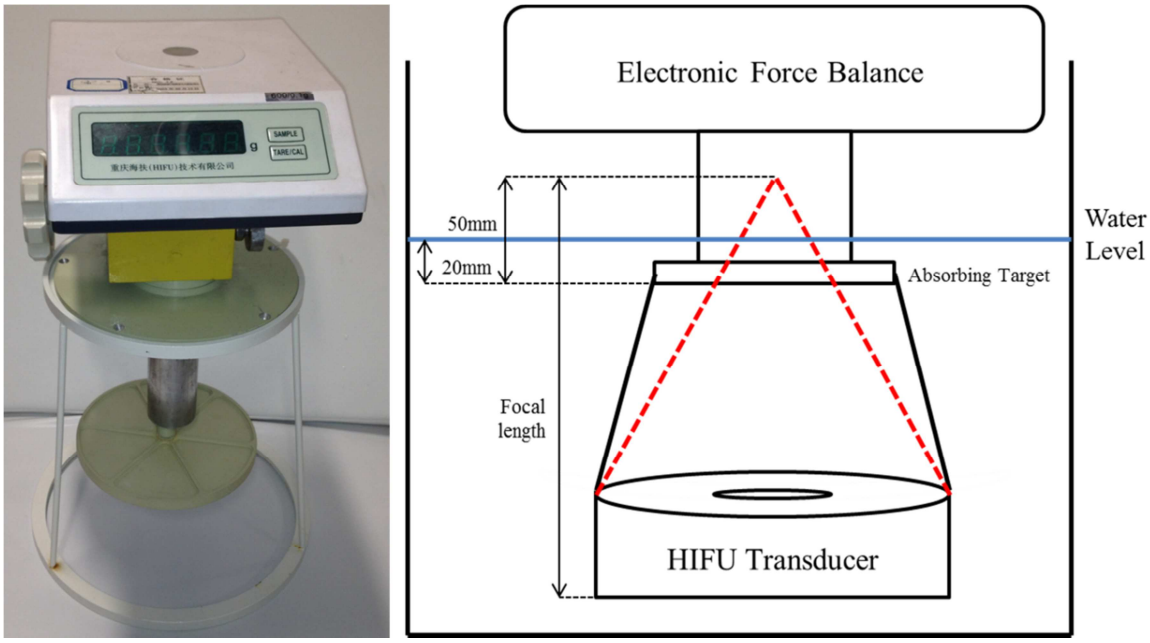

Figure 80 – Photograph of RFB (left) and schematic of setup (right) on Model JC & Model JC-200 HIFU device.

The mount also ensures that the absorbing target is aligned perpendicular to the beam axis. The mount is applied with the transducer at its highest position for convenience; the transducer is then moved to its lowest position and the reservoir filled with degassed water so that the entire absorbing target lies 20mm under the water level. Using the height adjustment the absorbing target is positioned so that the transducer focus lies 5cm beyond the target.

The power calibration was conducted by adjusting the HIFU input voltage from 100V to 240V in steps of 10V. Continuous wave HIFU was activated for 5 seconds and the radiation force recorded for each input voltage. Each voltage was recorded three times. The acoustic power (P) is then calculated as follows:

$$P = \xi . F_{rad}$$

where F is the acoustic radiation force (g) and ξ is a fixed coefficient for each transducer which is provide by the manufacturer.

10.6 Publications

10.6.1 Radiology 2012 Jan;262(1):252-61

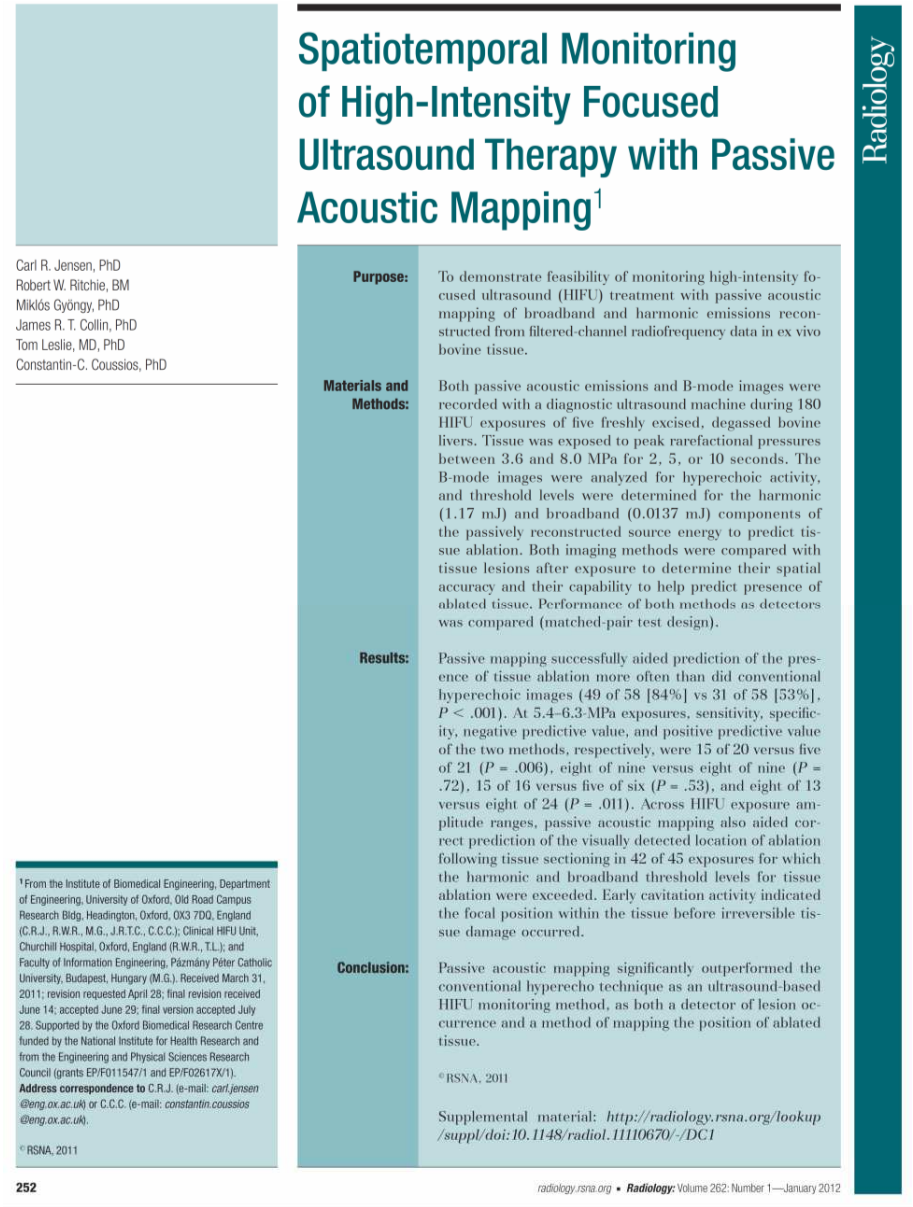

Radiology

Spatiotemporal Monitoring of High-Intensity Focused Ultrasound Therapy with Passive Acoustic Mapping[1]

Carl R. Jensen, PhD
Robert W. Ritchie, BM
Miklós Gyöngy, PhD
James R. T. Collin, PhD
Tom Leslie, MD, PhD
Constantin-C. Coussios, PhD

Purpose: To demonstrate feasibility of monitoring high-intensity focused ultrasound (HIFU) treatment with passive acoustic mapping of broadband and harmonic emissions reconstructed from filtered-channel radiofrequency data in ex vivo bovine tissue.

Materials and Methods: Both passive acoustic emissions and B-mode images were recorded with a diagnostic ultrasound machine during 180 HIFU exposures of five freshly excised, degassed bovine livers. Tissue was exposed to peak rarefactional pressures between 3.6 and 8.0 MPa for 2, 5, or 10 seconds. The B-mode images were analyzed for hyperechoic activity, and threshold levels were determined for the harmonic (1.17 mJ) and broadband (0.0137 mJ) components of the passively reconstructed source energy to predict tissue ablation. Both imaging methods were compared with tissue lesions after exposure to determine their spatial accuracy and their capability to help predict presence of ablated tissue. Performance of both methods as detectors was compared (matched-pair test design).

Results: Passive mapping successfully aided prediction of the presence of tissue ablation more often than did conventional hyperechoic images (49 of 58 [84%] vs 31 of 58 [53%], $P < .001$). At 5.4–6.3-MPa exposures, sensitivity, specificity, negative predictive value, and positive predictive value of the two methods, respectively, were 15 of 20 versus five of 21 ($P = .006$), eight of nine versus eight of nine ($P = .72$), 15 of 16 versus five of six ($P = .53$), and eight of 13 versus eight of 24 ($P = .011$). Across HIFU exposure amplitude ranges, passive acoustic mapping also aided correct prediction of the visually detected location of ablation following tissue sectioning in 42 of 45 exposures for which the harmonic and broadband threshold levels for tissue ablation were exceeded. Early cavitation activity indicated the focal position within the tissue before irreversible tissue damage occurred.

Conclusion: Passive acoustic mapping significantly outperformed the conventional hyperecho technique as an ultrasound-based HIFU monitoring method, as both a detector of lesion occurrence and a method of mapping the position of ablated tissue.

Supplemental material: *http://radiology.rsna.org/lookup/suppl/doi:10.1148/radiol.11110670/-/DC1*

[1] From the Institute of Biomedical Engineering, Department of Engineering, University of Oxford, Old Road Campus Research Bldg, Headington, Oxford, OX3 7DQ, England (C.R.J., R.W.R., M.G., J.R.T.C., C.C.C.); Clinical HIFU Unit, Churchill Hospital, Oxford, England (R.W.R., T.L.); and Faculty of Information Engineering, Pázmány Péter Catholic University, Budapest, Hungary (M.G.). Received March 31, 2011; revision requested April 28; final revision received June 14; accepted June 29; final version accepted July 28. Supported by the Oxford Biomedical Research Centre funded by the National Institute for Health Research and from the Engineering and Physical Sciences Research Council (grants EP/F011547/1 and EP/F02617X/1). **Address correspondence to** C.R.J. (e-mail: *carl.jensen@eng.ox.ac.uk*) or C.C.C. (e-mail: *constantin.coussios@eng.ox.ac.uk*).

10.6.2 BJU Int. 2011 Apr;107(8):1290-6

BJUI BJU INTERNATIONAL

Laparoscopic high-intensity focused ultrasound for renal tumours: a proof of concept study

Robert W. Ritchie*†, Tom A. Leslie*†, Gareth D.H. Turner†, Ian S.D. Roberts†, Leonardo D'Urso§, Devis Collura§, Andrea Demarchi§, Giovanni Muto§ and Mark E. Sullivan*†

**Department of Urology, Churchill Hospital, †Nurfield Department of Surgery, John Radcliffe Hospital, †Department of Cellular Pathology and Nurfield Department of Clinical Laboratory Sciences, John Radcliffe Hospital, Oxford, UK, and §Department of Urology, St Giovanni Bosco Hospital, Turin, Italy*

Accepted for publication 25 May 2010

Study Type – Therapy (case series)
Level of Evidence

OBJECTIVES

- To test and establish clinical proof of concept for a laparoscopic high-intensity focused ultrasound (HIFU) device that facilitates delivery of ultrasound by direct application of a probe to the tumour surface.

PATIENTS AND METHODS

- Twelve patients with renal tumours were treated with laparoscopic HIFU using a newly designed probe inserted via an 18-mm laparoscopic port.
- HIFU treatment was targeted at a pre-defined proportion of the tumour and immediate laparoscopic partial or radical nephrectomy was then performed.

RESULTS

- No tumour ablation was seen in the first five patients which made modifications in the treatment protocol necessary. After this, definite histological evidence of ablation was seen in the remaining seven patients.
- The ablated zones were within the targeted area in all patients and no intra-lesional skipping was seen.
- Subcapsular skipping was seen at the probe–tumour interface in two patients with viable tumour cells seen at microscopy.
- One patient did not undergo surgical extirpation; subsequent biopsy revealed no viable tumour cells.
- There were no intraoperative or postoperative complications directly related to HIFU therapy and patients have reached a mean (range) follow-up of 15 (8–24) months with no evidence of metastatic disease or late complications.

CONCLUSIONS

- Tumour ablation with laparoscopic HIFU is feasible.
- Homogenous ablation can be achieved with no vital tissue within the targeted zone.
- The technique is associated with low morbidity and may have a role in the definitive management of small tumours.

KEYWORDS

kidney neoplasms, high-intensity focused ultrasound, HIFU, nephrectomy, renal cancer, minimally invasive therapy

INTRODUCTION

The incidence of renal cancer is increasing; recent USA and UK statistics suggest an annual increase of 2–4% depending on sex and ethnic origin [1,2]. This increase is partly, but not entirely, attributable to the increased use of abdominal imaging [1,3]. There is evidence that both the stage and tumour dimensions at the time of diagnosis are decreasing [4,5] and more than 60% of these are discovered in the absence of symptoms attributable to the pathology [6]. These changes have resulted in a new entity – the small renal mass (SRM). The best management of these SRMs is uncertain and is made more challenging by the marked increase in incidence of SRMs in the elderly and co-morbid. Conventionally, the SRM has been considered to be slow growing. Indeed, a study of 287 tumour-bearing (up to 4 cm) kidneys found nearly 20% were benign and more than 85% of the malignant lesions were Fuhrman grade I or II [7]. In contrast, the same study also demonstrated that of the 3–4 cm tumours, 25% were of Fuhrman grade III or IV and more than 35% were stage 3a or greater; 8% of these tumours had metastasized at the time of diagnosis.

Currently the 'gold standard' management for radiologically suspicious SRMs (clinical stage T1a) is partial nephrectomy. Studies have shown similar oncological outcomes with less impact on renal function in comparison with radical nephrectomy [8–10]. However, complication rates associated with partial nephrectomy may approach 20%, whether performed openly or laparoscopically [11]. Of these complications, nearly half are medical (renal failure, myocardial infarction, pulmonary embolism), reflecting the co-morbidity within the population group.

As a result of high rates of benignity and high surgical complication rates, minimally invasive ablative technologies have developed over the last 20 years. Thermal damage can result in tumour destruction without the need for surgical incision into the highly vascular renal parenchyma [12]. This can be done using radiofrequency ablation (RFA), cryoablation (CA) or high-intensity focused ultrasound ablation (HIFU) [13–15]. Of these methods,

10.6.3 BJU Int. 2010 Oct;106(7):1004-9

BJUI BJU INTERNATIONAL

Extracorporeal high intensity focused ultrasound for renal tumours: a 3-year follow-up

Robert W. Ritchie*, Tom Leslie*, Rachel Phillips[¶], Feng Wu, Rowland Illing[†], Gail ter Haar[‡], Andrew Protheroe[§] and David Cranston

Nuffield Department of Surgery, University of Oxford, Departments of [¶]Radiology, [†]Urology and [§]Medical Oncology, Churchill Hospital, Oxford, and [‡]Joint Department of Physics, Institute of Cancer Research, Sutton, Surrey, UK

Accepted for publication 21 December 2009

*Robert W. Ritchie and Tom Leslie are joint first authors.

Study Type – Therapy (case series)
Level of Evidence 4

OBJECTIVE

To determine whether primary extracorporeal high-intensity focused ultrasound (HIFU) is safe, feasible and effective for managing small renal tumours.

PATIENTS AND METHODS

Although surgery currently remains the standard treatment for localized renal cell carcinoma (RCC), the increasing incidence of small renal cancers has led to a shift towards nephron-sparing surgery, with associated morbidity in 20–25% of cases, and minimally invasive ablative therapies present an alternative management. HIFU results in 'trackless' homogenous tissue ablation and when administered via an extracorporeal device, is entirely noninvasive. The study comprised 17 patients (mean tumour size 2.5 cm) with radiologically suspicious renal tumours who underwent extracorporeal HIFU using the Model-JC System (Chongqing HAIFU™, China), under general anaesthesia with one overnight hospital stay. Real-time diagnostic ultrasonography was used for targeting and monitoring. Patients were followed with a clinical review and gadolinium-enhanced magnetic resonance imaging at 12 days and every 6 months for a mean of 36 months. The outcomes measures were patient morbidity and oncological efficacy of HIFU treatment.

RESULTS

Of the 17 patients, 15 were treated according to protocol; two procedures were abandoned due to intervening bowel. There were no major complications related to HIFU. Radiological evidence of ablation was apparent at 12 days in seven of the 15 patients. Before the 6-month follow-up one patient had surgery due to persisting central enhancement. Fourteen patients were evaluated at the 6-month follow-up; eight tumours had involuted (mean 12% decrease in tumour area). Four patients had irregular enhancement on imaging and had alternative therapies. Ten patients remain on follow-up at a mean (range) of 36 (14–55) months after HIFU (mean 30% decrease in tumour area). There was central loss of enhancement in all.

CONCLUSIONS

Renal HIFU achieves stable lesions in two-thirds of patients, with minimal morbidity, and might be appropriate in selected cases. Further trials with accurate histological follow-up are essential to fully evaluate this novel technique.

KEYWORDS

high-intensity focused ultrasound, renal cell carcinoma, minimally invasive surgery, therapeutic hyperthermia

INTRODUCTION

The last 30 years have seen a dramatic shift in the epidemiology and clinical presentation of renal cancer. Improved abdominal imaging and a genuine increase in the occurrence of renal tumours has led to a significant overall increase in incidence and early detection [1–3]. Notably, the greatest increase in incidence has occurred in the older population, with the percentage of patients aged >65 years nearly doubling [3].

This change has led urologists to question how best to manage renal tumours, particularly incidental small renal masses (SRMs). Observations of renal cancer show that low-grade, low-stage masses grow slowly and are not an immediate threat to a patient's life [4,5]. Further studies also showed that synchronous metastatic disease was detected in just 5% of tumours of <3 cm and does not occur with tumours of <2.0 cm [6].

Active surveillance of the SRM is a reasonable strategy. However, the odds of synchronous metastatic disease increase by 22% with every 1 cm tumour growth and double with 3.5 cm of growth [6]. Radiographic imaging alone is unable to determine high-risk tumours and consequently current opinion is that active surveillance should be considered for selected groups only, when surgery is not an option [7].

Surgery remains the default position for renal tumours. It is accepted that partial nephrectomy should be undertaken for T1a tumours, given its favourable effect on renal function compared with radical surgery [8,9]. However, complications occur in 21% of laparoscopic and open partial nephrectomies, and half of these are medical [10]. Surgery in the elderly population is particularly risky, with a 15% perioperative mortality rate in octogenarians undergoing nephrectomy in two European institutions [11].

10.6.4 BJR 2012 February; in press, accepted for publication

The British Journal of Radiology

High Intensity Focused Ultrasound treatment of liver tumours: post-treatment MRI correlates well with intra-operative estimates of treatment volume.

--Manuscript Draft--

Manuscript Number:	BJR-D-11-00816R1
Full Title:	High Intensity Focused Ultrasound treatment of liver tumours: post-treatment MRI correlates well with intra-operative estimates of treatment volume.
Short Title:	Clinical and MRI outcomes in liver HIFU
Article Type:	Full Paper
Corresponding Author:	Robert Ritchie, BM MRCS Oxford University Hospitals Oxford, UNITED KINGDOM
Corresponding Author Secondary Information:	
Corresponding Author's Institution:	Oxford University Hospitals
Corresponding Author's Secondary Institution:	
First Author:	Tom Leslie, MB ChB PhD
First Author Secondary Information:	
Order of Authors:	Tom Leslie, MB ChB PhD
	Robert Ritchie, BM MRCS
	Rowland Illing, BM BCh FRCR
	Gail ter Haar, DSc
	Rachel Phillips, MB ChB FRCR
	Mark Middleton, BM BCh PhD
	Feng WU, MD PhD
	David Cranston, MB ChB PhD
Order of Authors Secondary Information:	
Abstract:	Objectives To assess the safety and feasibility of high intensity focused ultrasound (HIFU) ablation of liver tumours and to determine whether post-operative MRI correlates with intra-operative imaging. Methods Thirty-one patients were recruited into two ethically-approved clinical trials (median age 64; mean BMI 26 kgm-2). Patients with liver tumours (primary or metastatic) underwent a single HIFU treatment monitored using intra-operative B-mode ultrasound. Follow-up consisted of radiology and histology (surgical trial) or radiology alone (radiology trial). Radiological follow-up was digital subtraction contrast-enhanced MRI. Results Treatment according to protocol was possible in 30 of 31 patient. One treatment was abandoned due to equipment failure. Transient pain and superficial skin burns were seen in 81% (25/31) & 39% (12/39). One moderate skin burn occurred. One patient died prior to radiological follow-up. Radiological evidence of ablation was seen in 93% (27/29). Ablation accuracy was good in 89% (24/27). In three patients the zone of ablation lay 2mm or less outside the tumour. The median cross-sectional area (CSA) of the zone of ablation was 5.0cm2 & 5.1cm2 using intra-operative and post-operative imaging respectively. The mean MRI:Bmode CSA ratio was 1.57 (95% CI

10.7 Conference presentations

Size of tumour determines duration of surgery in laparoscopic radical nephrectomy EAU Annual Scientific Meeting, Milan Poster presentation & published abstract	March 2008
Laparoscopic HIFU in the treatment of small kidney tumours International Symposium for Therapeutic Ultrasound, Minne. Oral presentation & published abstract	Sep. 2008
Extracorporeal HIFU for small kidney tumours EAU Annual Scientific Meeting, Stockholm Oral presentation & published abstract	March 2009
HIFU Ablation of small renal tumours with an extracorporeal device AUA Annual Scientific Meeting, Chicago	April 2009

Poster presentation & published abstract	
Laparoscopic HIFU for small kidney tumours – Phase I trial results BAUS Annual Scientific Meeting, Glasgow Poster presentation & published abstract	June 2009
Monitoring of lesioning during HIFU with passive cavitation detection International Symposium for Therapeutic Ultrasound, France Oral presentation (Miklos Gyongy) & published abstract	Sep. 2009
Does HIFU for renal cancer upregulate anti-tumour immunity in vivo EAU Annual Scientific Meeting, Barcelona Poster presentation & published abstract	March 2010
Does HIFU for cancer upregulate anti-tumour immunity? AUA Annual Scientific Meeting, San Francisco Podium presentation & published abstract	June 2010
Development of anti-tumour immunity following extracorporeal HIFU for renal cancer International Symposium for Therapeutic Ultrasound, Tokyo Poster presentation & published abstract	June 2010
Passive cavitation mapping for real-time monitoring of HIFU ablation and ultrasound-enhanced drug delivery International Symposium for Therapeutic Ultrasound, Tokyo Podium presentation (Constantin Coussios) & published abstract	June 2010
Immune upregulation in-vivo following for HIFU for renal cancer BAUS Annual Scientific Meeting, Manchester Poster presentation & published abstract	June 2010
The impact of peri-nephric fat attenuation on HIFU ablation for renal cancer International Symposium for Therapeutic Ultrasound, New York Poster presentation & published abstract	June 2011
Significant skins burns may occur with the use of a water balloon in HIFU treatment International Symposium for Therapeutic Ultrasound, New York Poster presentation & published abstract	June 2011

11 References

[1] Carstensen EL, Law WK, McKay ND, Muir TG. Demonstration of nonlinear acoustical effects at biomedical frequencies and intensities. Ultrasound Med Biol. 1980: **6**:359-68
[2] Duck FA. Nonlinear acoustics in diagnostic ultrasound. Ultrasound Med Biol. 2002 Jan: **28**:1-18
[3] Duck F. Tissue non-linearity. Proc Inst Mech Eng H. 2010: **224**:155-70
[4] Humphrey VF. Nonlinear propagation in ultrasonic fields: measurements, modelling and harmonic imaging. Ultrasonics. 2000 Mar: **38**:267-72
[5] Muir TG, Carstensen EL. Prediction of nonlinear acoustic effects at biomedical frequencies and intensities. Ultrasound Med Biol. 1980: **6**:345-57
[6] Sehgal CM, Greenleaf JF. Scattering of ultrasound by tissues. Ultrason Imaging. 1984 Jan: **6**:60-80
[7] del Grosso VA, Mader CW. Speed of sound in pure water. J Acoust Soc Am. 1972: **52**:1442-6
[8] Wells P. Ultrasonic imaging of the human body. Rep Prof Phys. 1999: **62**:671-721
[9] Bacon DR, Carstensen EL. Increased heating by diagnostic ultrasound due to nonlinear propagation. J Acoust Soc Am. 1990 Jul: **88**:26-34
[10] Miller MW, Ziskin MC. Biological consequences of hyperthermia. Ultrasound Med Biol. 1989: **15**:707-22
[11] Rabkin JM, Hunt TK. Local heat increases blood flow and oxygen tension in wounds. Arch Surg. 1987 Feb: **122**:221-5
[12] Hadjiargyrou M, McLeod K, Ryaby JP, Rubin C. Enhancement of fracture healing by low intensity ultrasound. Clin Orthop Relat Res. 1998 Oct:S216-29
[13] Nussbaum E. The influence of ultrasound on healing tissues. J Hand Ther. 1998 Apr-Jun: **11**:140-7
[14] Dewey WC, Diederich CJ, Dewhirst MW. Hyperthermia classic commentary: 'Arrhenius relationships from the molecule and cell to the clinic' by William Dewey, Int. J. Hyperthermia, 10:457-483, 1994. Int J Hyperthermia. 2009 Feb: **25**:21-4
[15] Sapareto SA, Dewey WC. Thermal dose determination in cancer therapy. Int J Radiat Oncol Biol Phys. 1984 Jun: **10**:787-800
[16] Kennedy JE. High-intensity focused ultrasound in the treatment of solid tumours. Nat Rev Cancer. 2005 Apr: **5**:321-7
[17] Nandlall SD, Schiffter HA, Vonhoff S, Bazan-Peregrino M, Arora M, Coussios CC. Real-time optical measurement of biologically relevant thermal damage in tissue-mimicking hydrogels containing bovine serum albumin. Int J Hyperthermia. 2010: **26**:456-64

[18] Wu F, Chen WZ, Bai J, et al. Pathological changes in human malignant carcinoma treated with high-intensity focused ultrasound. Ultrasound Med Biol. 2001 Aug: **27**:1099-106
[19] Chen L, Rivens I, ter Haar G, Riddler S, Hill C, Bensted J. Histological changes in rat liver tumours treated with high-intensity focused ultrasound. Ultrasound Med Biol. 1993: **19**:67-74
[20] Carstensen EL, Gates AH. The effects of pulsed ultrasound on the fetus. J Ultrasound Med. 1984 Apr: **3**:145-7
[21] Sikov MR. Effect of ultrasound on development. Part 2: Studies in mammalian species and overview. J Ultrasound Med. 1986 Nov: **5**:651-61
[22] Hill CR, ter Haar GR. Review article: high intensity focused ultrasound--potential for cancer treatment. Br J Radiol. 1995 Dec: **68**:1296-303
[23] Wood R, Loomis A. The physical and biological effects of high-frequency sound waves of great intensity. London, Edinburgh, Dublin Phil Mag J Sci. 1927: **4**:417-36
[24] Fry W, Mosberg W, Barnard J, Fry F. Production of focal destructive lesions in the central nervous system with ultrasound. J Neurosurg. 1954: **11**:471-8
[25] Fry WJ, Barnard JW, Fry EJ, Krumins RF, Brennan JF. Ultrasonic lesions in the mammalian central nervous system. Science. 1955 Sep 16: **122**:517-8
[26] Burov A. The production of high-intensity ultrasonic vibrations for action on animal and human malignant tumours. Doklady Akad Nauk SSSR. 1956: **106**:239-41
[27] Bamber JC, Hill CR. Ultrasonic attenuation and propagation speed in mammalian tissues as a function of temperature. Ultrasound in Medicine & Biology. 1979: **5**:149-57
[28] Bamber JC, Hill CR. Acoustic properties of normal and cancerous human liver--I. Dependence on pathological condition. Ultrasound in Medicine & Biology. 1981: **7**:121-33
[29] Frizzell LA. Threshold dosages for damage to mammalian liver by high intensity focused ultrasound. IEEE Trans Ultrason Ferroelectr Freq Control. 1988: **35**:578-81
[30] Goss SA, Frizzell LA, Dunn F. Ultrasonic absorption and attenuation in mammalian tissues. Ultrasound Med Biol. 1979: **5**:181-6
[31] Linke CA, Carstensen EL, Frizzell LA, Elbadawi A, Fridd CW. Localized tissue destruction by high-intensity focused ultrasound. Arch Surg. 1973 Dec: **107**:887-91
[32] Illing R, Kennedy J, Wu F, et al. The safety and feasibility of extracorporeal high-intensity focused ultrasound (HIFU) for the treatment of liver and kidney tumours in a Western population. Br J Cancer. 2005 Oct: **93**:890-5
[33] Wu F, Wang Z-B, Cao Y-D, et al. A randomised clinical trial of high-intensity focused ultrasound ablation for the treatment of patients with localised breast cancer. Br J Cancer. 2003 Dec: **89**:2227-33
[34] Wang X, Sun J. High-intensity focused ultrasound in patients with late-stage pancreatic carcinoma. Chin Med J (Engl). 2002 Sep: **115**:1332-5
[35] Poissonnier L, Chapelon JY, Rouviere O, et al. Control of prostate cancer by transrectal HIFU in 227 patients. Eur Urol. 2007 Feb: **51**:381-7
[36] Klingler H, Susani M, Seip R, Mauermann J, Sanghvi N, Marberger M. A novel approach to energy ablative therapy of small renal tumours: laparoscopic high-intensity focused ultrasound. Eur Urol. 2008 Apr: **53**:810-6; discussion 7-8
[37] Liberman B, Gianfelice D, Inbar Y, et al. Pain palliation in patients with bone metastases using MR-guided focused ultrasound surgery: a multicenter study. Ann Surg Oncol. 2009 Jan: **16**:140-6
[38] Okada A, Morita Y, Fukunishi H, Takeichi K, Murakami T. Non-invasive magnetic resonance-guided focused ultrasound treatment of uterine fibroids in a large Japanese population: impact of the learning curve on patient outcome. Ultrasound Obstet Gynecol. 2009 Nov: **34**:579-83

[39] Wu F, Wang ZB, Chen WZ, et al. Extracorporeal focused ultrasound surgery for treatment of human solid carcinomas: early Chinese clinical experience. Ultrasound Med Biol. 2004 Feb: **30**:245-60
[40] Church CC. Spontaneous homogeneous nucleation, inertial cavitation and the safety of diagnostic ultrasound. Ultrasound Med Biol. 2002 Oct: **28**:1349-64
[41] Miller DL. Acoustic cavitation series: part six. Gas body activation. Ultrasonics. 1984 Nov: **22**:261-9
[42] Apfel RE. Acoustic cavitation: a possible consequence of biomedical uses of ultrasound. Br J Cancer Suppl. 1982 Mar: **5**:140-6
[43] Neppiras EA. Acoustic Cavitation. Physics Reports. 1980: **61**:1590251
[44] Leighton T. The Acoustic Buble, London: Academic Press, 1994
[45] Hill C, JC; B, ter Haar G. Physical Principles of Medical Ultrasonics (2nd edition), Chichester: John Wiley & Sons Ltd, 2004
[46] Coussios C, Farny C, Haar G, Roy R. Role of acoustic cavitation in the delivery and monitoring of cancer treatment by high-intensity focused ultrasound (HIFU). Int J Hyperthermia. 2007 Mar: **23**:105-20
[47] Rassweiler JJ, Knoll T, Kohrmann KU, et al. Shock wave technology and application: an update. Eur Urol. 2011 May: **59**:784-96
[48] Khokhlova VA, Bailey MR, Reed JA, Cunitz BW, Kaczkowski PJ, Crum LA. Effects of nonlinear propagation, cavitation, and boiling in lesion formation by high intensity focused ultrasound in a gel phantom. J Acoust Soc Am. 2006 Mar: **119**:1834-48
[49] Miller DL. A review of the ultrasonic bioeffects of microsonation, gas-body activation, and related cavitation-like phenomena. Ultrasound Med Biol. 1987 Aug: **13**:443-70
[50] Miller DL. Update on safety of diagnostic ultrasonography. J Clin Ultrasound. 1991 Nov-Dec: **19**:531-40
[51] Miller MW, Nyborg WL, Dewey WC, Edwards MJ, Abramowicz JS, Brayman AA. Hyperthermic teratogenicity, thermal dose and diagnostic ultrasound during pregnancy: implications of new standards on tissue heating. Int J Hyperthermia. 2002 Sep-Oct: **18**:361-84
[52] Fowlkes JB, Holland CK. Mechanical bioeffects from diagnostic ultrasound: AIUM consensus statements. American Institute of Ultrasound in Medicine. J Ultrasound Med. 2000 Feb: **19**:69-72
[53] Dyson M. Non-thermal cellular effects of ultrasound. Br J Cancer Suppl. 1982 Mar: **5**:165-71
[54] Meaney PM, Cahill MD, ter Haar GR. The intensity dependence of lesion position shift during focused ultrasound surgery. Ultrasound Med Biol. 2000 Mar: **26**:441-50
[55] Frenkel V. Ultrasound mediated delivery of drugs and genes to solid tumors. Adv Drug Deliv Rev. 2008 Jun 30: **60**:1193-208
[56] Hancock HA, Smith LH, Cuesta J, et al. Investigations into pulsed high-intensity focused ultrasound-enhanced delivery: preliminary evidence for a novel mechanism. Ultrasound Med Biol. 2009 Oct: **35**:1722-36
[57] Miller DL, Dou C. The potential for enhancement of mouse melanoma metastasis by diagnostic and high-amplitude ultrasound. Ultrasound Med Biol. 2006 Jul: **32**:1097-101
[58] Oosterhof GO, Cornel EB, Smits GA, Debruyne FM, Schalken JA. The influence of high-energy shock waves on the development of metastases. Ultrasound Med Biol. 1996: **22**:339-44
[59] Oosterhof G, Cornel E, Smits G, Debruyne F, Schalken J. Influence of high-intensity focused ultrasound on the development of metastases. Eur Urol. 1997: **32**:91-5

[60] Wu F, Wang Z, Jin C, et al. Circulating tumor cells in patients with solid malignancy treated by high-intensity focused ultrasound. Ultrasound Med Biol. 2004 Apr: **30**:511-7
[61] Liu HL, Chen WS, Chen JS, Shih TC, Chen YY, Lin WL. Cavitation-enhanced ultrasound thermal therapy by combined low- and high-frequency ultrasound exposure. Ultrasound Med Biol. 2006 May: **32**:759-67
[62] Farny CH, Holt RG, Roy RA. The correlation between bubble-enhanced HIFU heating and cavitation power. IEEE Trans Biomed Eng. 2010 Jan: **57**:175-84
[63] Hu Z, Yang XY, Liu Y, et al. Investigation of HIFU-induced anti-tumor immunity in a murine tumor model. J Transl Med. 2007: **5**:34
[64] Xing Y, Lu X, Pua E, Zhong P. The effect of high intensity focused ultrasound treatment on metastases in a murine melanoma model. Biochem Biophys Res Commun. 2008 Oct: **375**:645-50
[65] Yang R, Reilly C, Rescorla F, et al. Effects of high-intensity focused ultrasound in the treatment of experimental neuroblastoma. J Pediatr Surg. 1992 Feb: **27**:246-50; discussion 50-1
[66] Hu Z, Yang X, Liu Y, et al. Release of endogenous danger signals from HIFU-treated tumor cells and their stimulatory effects on APCs. Biochem Biophys Res Commun. 2005 Sep: **335**:124-31
[67] Wu F, Wang Z-B, Lu P, et al. Activated anti-tumor immunity in cancer patients after high intensity focused ultrasound ablation. Ultrasound Med Biol. 2004 Sep: **30**:1217-22
[68] Xu Z-L, Zhu X-Q, Lu P, Zhou Q, Zhang J, Wu F. Activation of tumor-infiltrating antigen presenting cells by high intensity focused ultrasound ablation of human breast cancer. Ultrasound Med Biol. 2009 Jan: **35**:50-7
[69] Zhou Q, Zhu X-Q, Zhang J, Xu Z-L, Lu P, Wu F. Changes in circulating immunosuppressive cytokine levels of cancer patients after high intensity focused ultrasound treatment. Ultrasound Med Biol. 2008 Jan: **34**:81-7
[70] Chen S. MRI-guided focused ultrasound treatment of uterine fibroids. Issues Emerg Health Technol. 2005 Jul:1-4
[71] Fennessy FM, Tempany CM. MRI-guided focused ultrasound surgery of uterine leiomyomas. Acad Radiol. 2005 Sep: **12**:1158-66
[72] Gianfelice D, Khiat A, Amara M, Belblidia A, Boulanger Y. MR imaging-guided focused ultrasound surgery of breast cancer: correlation of dynamic contrast-enhanced MRI with histopathologic findings. Breast Cancer Res Treat. 2003 Nov: **82**:93-101
[73] Hokland SL, Pedersen M, Salomir R, Quesson B, Stodkilde-Jorgensen H, Moonen CT. MRI-guided focused ultrasound: methodology and applications. IEEE Trans Med Imaging. 2006 Jun: **25**:723-31
[74] Honeck P, Peters K, Wendt-Nordahl G, et al. Magnetic resonance imaging as a technique for assessing noninvasive tissue ablation using high-intensity ultrasound: an experimental study. J Endourol. 2009 Jan: **23**:161-8
[75] Hynynen K. MRI-guided focused ultrasound treatments. Ultrasonics. 2010 Feb: **50**:221-9
[76] Hynynen K, Darkazanli A, Unger E, Schenck JF. MRI-guided noninvasive ultrasound surgery. Med Phys. 1993 Jan-Feb: **20**:107-15
[77] Hynynen K, McDannold N. MRI guided and monitored focused ultrasound thermal ablation methods: a review of progress. Int J Hyperthermia. 2004 Nov: **20**:725-37
[78] Jolesz FA. MRI-guided focused ultrasound surgery. Annu Rev Med. 2009: **60**:417-30
[79] Quesson B, de Zwart JA, Moonen CT. Magnetic resonance temperature imaging for guidance of thermotherapy. J Magn Reson Imaging. 2000 Oct: **12**:525-33

[80] de Senneville BD, Mougenot C, Moonen CTW. Real-time adaptive methods for treatment of mobile organs by MRI-controlled high-intensity focused ultrasound. Magn Reson Med. 2007 Feb: **57**:319-30
[81] Wu T, Felmlee JP, Greenleaf JF, Riederer SJ, Ehman RL. Assessment of thermal tissue ablation with MR elastography. Magn Reson Med. 2001 Jan: **45**:80-7
[82] Muthupillai R, Ehman RL. Magnetic resonance elastography. Nat Med. 1996 May: **2**:601-3
[83] Damianou C, Pavlou M, Velev O, Kyriakou K, Trimikliniotis M. High intensity focused ultrasound ablation of kidney guided by MRI. Ultrasound Med Biol. 2004 Mar: **30**:397-404
[84] Bohris C, Jenne JW, Rastert R, et al. MR monitoring of focused ultrasound surgery in a breast tissue model in vivo. Magn Reson Imaging. 2001 Feb: **19**:167-75
[85] ter Haar G, Sinnett D, Rivens I. High intensity focused ultrasound--a surgical technique for the treatment of discrete liver tumours. Phys Med Biol. 1989 Nov: **34**:1743-50
[86] Vaezy S, Shi X, Martin R, et al. Real-time visualization of high-intensity focused ultrasound treatment using ultrasound imaging. Ultrasound Med Biol. 2001 Jan: **27**:33-42
[87] Rabkin BA, Zderic V, Crum LA, Vaezy S. Biological and physical mechanisms of HIFU-induced hyperecho in ultrasound images. Ultrasound Med Biol. 2006 Nov: **32**:1721-9
[88] Souchon R, Bouchoux G, Maciejko E, et al. Monitoring the formation of thermal lesions with heat-induced echo-strain imaging: a feasibility study. Ultrasound Med Biol. 2005 Feb: **31**:251-9
[89] Miller NR, Bamber JC, ter Haar GR. Imaging of temperature-induced echo strain: preliminary in vitro study to assess feasibility for guiding focused ultrasound surgery. Ultrasound Med Biol. 2004 Mar: **30**:345-56
[90] Nasoni RL, Bowen T, Connor WG, Sholes RR. In vivo temperature dependence of ultrasound speed in tissue and its application to noninvasive temperature monitoring. Ultrason Imaging. 1979 Jan: **1**:34-43
[91] Straube WL, Arthur RM. Theoretical estimation of the temperature dependence of backscattered ultrasonic power for noninvasive thermometry. Ultrasound Med Biol. 1994: **20**:915-22
[92] Khaled W, Reichling S, Bruhns OT, Ermert H. Ultrasonic strain imaging and reconstructive elastography for biological tissue. Ultrasonics. 2006 Dec 22: **44 Suppl 1**:e199-202
[93] Ophir J, Alam SK, Garra B, et al. Elastography: ultrasonic estimation and imaging of the elastic properties of tissues. Proc Inst Mech Eng H. 1999: **213**:203-33
[94] Curiel L, Souchon R, Rouviere O, Gelet A, Chapelon JY. Elastography for the follow-up of high-intensity focused ultrasound prostate cancer treatment: initial comparison with MRI. Ultrasound Med Biol. 2005 Nov: **31**:1461-8
[95] Mast TD, Salgaonkar VA, Karunakaran C, Besse JA, Datta S, Holland CK. Acoustic emissions during 3.1 MHz ultrasound bulk ablation in vitro. Ultrasound in Medicine and Biology. 2008: **34**:1434-48
[96] Roy RA, Madanshetty SI, Apfel RE. An acoustic backscattering technique for the detection of transient cavitation produced by microsecond pulses of ultrasound. J Acoust Soc Am. 1990 Jun: **87**:2451-8
[97] Madanshetty SI, Apfel RE. Acoustic microcavitation: enhancement and applications. J Acoust Soc Am. 1991 Sep: **90**:1508-14
[98] Madanshetty SI, Roy RA, Apfel RE. Acoustic microcavitation: its active and passive acoustic detection. J Acoust Soc Am. 1991 Sep: **90**:1515-26

[99] Holland CK, Deng CX, Apfel RE, Alderman JL, Fernandez LA, Taylor KJ. Direct evidence of cavitation in vivo from diagnostic ultrasound. Ultrasound Med Biol. 1996: **22**:917-25
[100] Collin J. Detection and Interpretation of Thermally Relevant Cavitation During HIFU Exposure [DPhil]. Oxford: University of Oxford, 2009. Available from:
[101] Farny CH, Holt RG, Roy RA. Temporal and spatial detection of HIFU-induced inertial and hot-vapor cavitation with a diagnostic ultrasound system. Ultrasound Med Biol. 2009 Apr: **35**:603-15
[102] Gyöngy M. Passive Cavitation Mapping for Monitoring Ultrasound Therapy. Oxford: University of Oxford, 2010. Available from: http://ora.ox.ac.uk/objects/uuid:af6f3c5a-bec5-4378-a617-c89d2b16d95d
[103] Gyöngy M, Coussios C-C. Passive spatial mapping of inertial cavitation during HIFU exposure. IEEE Trans Biomed Eng. 2010 Jan: **57**:48-56
[104] Norton S, Carr B, Witten A. Passive imaging of under-ground acoustic sources. The Journal of the Acoustical Society of America. 2006: **119**:2840-7
[105] Norton SJ, Won IJ. Time exposure acoustics. #IEEE_J_GRS#. 2000: **38**:1337-43
[106] Madersbacher S, Schatzl G, Djavan B, Stulnig T, Marberger M. Long-term outcome of transrectal high- intensity focused ultrasound therapy for benign prostatic hyperplasia. Eur Urol. 2000 Jun: **37**:687-94
[107] Schatzl G, Madersbacher S, Djavan B, Lang T, Marberger M. Two-year results of transurethral resection of the prostate versus four 'less invasive' treatment options. Eur Urol. 2000 Jun: **37**:695-701
[108] Chaussy C, Thuroff S. High-intensity focused ultrasound in prostate cancer: results after 3 years. Mol Urol. 2000 Fall: **4**:179-82
[109] Thuroff S, Chaussy C. High-intensity focused ultrasound: complications and adverse events. Mol Urol. 2000 Fall: **4**:183-7;discussion 9
[110] Aus G. Current status of HIFU and cryotherapy in prostate cancer--a review. Eur Urol. 2006 Nov: **50**:927-34; discussion 34
[111] Lukka H, Waldron T, Chin J, et al. High-intensity focused ultrasound for prostate cancer: a systematic review. Clin Oncol (R Coll Radiol). 2011 Mar: **23**:117-27
[112] Lecornet E, Ahmed HU, Moore CM, Emberton M. Conceptual basis for focal therapy in prostate cancer. J Endourol. 2010 May: **24**:811-8
[113] Ahmed HU, Freeman A, Kirkham A, et al. Focal therapy for localized prostate cancer: a phase I/II trial. J Urol. 2011 Apr: **185**:1246-54
[114] Ng KK, Poon RT, Chan SC, et al. High-intensity focused ultrasound for hepatocellular carcinoma: a single-center experience. Ann Surg. 2011 May: **253**:981-7
[115] Jin C, Zhu H, Wang Z, et al. High-intensity focused ultrasound combined with transarterial chemoembolization for unresectable hepatocellular carcinoma: long-term follow-up and clinical analysis. Eur J Radiol. 2011 Dec: **80**:662-9
[116] Wu F, Wang ZB, Chen WZ, et al. Advanced hepatocellular carcinoma: treatment with high-intensity focused ultrasound ablation combined with transcatheter arterial embolization. Radiology. 2005 May: **235**:659-67
[117] Wang K, Chen Z, Meng Z, et al. Analgesic effect of high intensity focused ultrasound therapy for unresectable pancreatic cancer. Int J Hyperthermia. 2011: **27**:101-7
[118] Wu F, Wang ZB, Zhu H, et al. Feasibility of US-guided high-intensity focused ultrasound treatment in patients with advanced pancreatic cancer: initial experience. Radiology. 2005 Sep: **236**:1034-40

[119] Zhang L, Chen WZ, Liu YJ, et al. Feasibility of magnetic resonance imaging-guided high intensity focused ultrasound therapy for ablating uterine fibroids in patients with bowel lies anterior to uterus. Eur J Radiol. 2010 Feb: **73**:396-403
[120] Li C, Wu P, Zhang L, Fan W, Huang J, Zhang F. Osteosarcoma: limb salvaging treatment by ultrasonographically guided high-intensity focused ultrasound. Cancer Biol Ther. 2009 Jun: **8**:1102-8
[121] Chen W, Zhu H, Zhang L, et al. Primary bone malignancy: effective treatment with high-intensity focused ultrasound ablation. Radiology. 2010 Jun: **255**:967-78
[122] Grond S, Zech D, Diefenbach C, Radbruch L, Lehmann KA. Assessment of cancer pain: a prospective evaluation in 2266 cancer patients referred to a pain service. Pain. 1996 Jan: **64**:107-14
[123] van den Beuken-van Everdingen MHJ, de Rijke JM, Kessels AG, Schouten HC, van Kleef M, Patijn J. Prevalence of pain in patients with cancer: a systematic review of the past 40 years. Ann Oncol. 2007 Sep: **18**:1437-49
[124] Pockett RD, Castellano D, McEwan P, Oglesby A, Barber BL, Chung K. The hospital burden of disease associated with bone metastases and skeletal-related events in patients with breast cancer, lung cancer, or prostate cancer in Spain. Eur J Cancer Care (Engl). 2009 Aug 26:
[125] Catane R, Beck A, Inbar Y, et al. MR-guided focused ultrasound surgery (MRgFUS) for the palliation of pain in patients with bone metastases--preliminary clinical experience. Ann Oncol. 2007 Jan: **18**:163-7
[126] Gianfelice D, Gupta C, Kucharczyk W, Bret P, Havill D, Clemons M. Palliative treatment of painful bone metastases with MR imaging--guided focused ultrasound. Radiology. 2008 Oct: **249**:355-63
[127] Marquet F, Pernot M, Aubry JF, et al. Non-invasive transcranial ultrasound therapy based on a 3D CT scan: protocol validation and in vitro results. Phys Med Biol. 2009 May 7: **54**:2597-613
[128] Larrat B, Pernot M, Aubry JF, et al. MR-guided transcranial brain HIFU in small animal models. Phys Med Biol. 2010 Jan 21: **55**:365-88
[129] Damianou C, Ioannides K, Hadjisavvas V, Mylonas N, Couppis A, Iosif D. In vitro and in vivo brain ablation created by high-intensity focused ultrasound and monitored by MRI. IEEE Trans Ultrason Ferroelectr Freq Control. 2009 Jun: **56**:1189-98
[130] Ritchie RW, Leslie TA, Turner GD, et al. Laparoscopic high-intensity focused ultrasound for renal tumours: a proof of concept study. BJU Int. 2011 Apr: **107**:1290-6
[131] Wu F, Wang Z, Chen W, Bai J, Zhu H, Qiao T. Preliminary experience using high intensity focused ultrasound for the treatment of patients with advanced stage renal malignancy. J Urol. 2003 Dec: **170**:2237-40
[132] Kennedy JE, Wu F, ter Haar GR, et al. High-intensity focused ultrasound for the treatment of liver tumours. Ultrasonics. 2004 Apr: **42**:931-5
[133] Wang W, Wang Y, Tang J. Safety and efficacy of high intensity focused ultrasound ablation therapy for adenomyosis. Acad Radiol. 2009 Nov: **16**:1416-23
[134] Goldberg SN, Grassi CJ, Cardella JF, et al. Image-guided tumor ablation: standardization of terminology and reporting criteria. J Vasc Interv Radiol. 2005 Jun: **16**:765-78
[135] Leon-Villapalos J, Kaniorou-Larai M, Dziewulski P. Full thickness abdominal burn following magnetic resonance guided focused ultrasound therapy. Burns. 2005 Dec: **31**:1054-5

[136] Gelet A, Chapelon JY, Poissonnier L, et al. Local recurrence of prostate cancer after external beam radiotherapy: early experience of salvage therapy using high-intensity focused ultrasonography. Urology. 2004 Apr: **63**:625-9
[137] Ripert T, Azemar MD, Menard J, et al. Transrectal high-intensity focused ultrasound (HIFU) treatment of localized prostate cancer: review of technical incidents and morbidity after 5 years of use. Prostate Cancer Prostatic Dis. 2010 Jun: **13**:132-7
[138] Crouzet S, Rebillard X, Chevallier D, et al. Multicentric Oncologic Outcomes of High-Intensity Focused Ultrasound for Localized Prostate Cancer in 803 Patients. Eur Urol. 2010 Jul 3:
[139] Cancer Research UK. UK Cancer Statistics. 2010 [cited; Available from: http://info.cancerresearchuk.org/cancerstats/types/kidney/index.htm?script=true
[140] Chow W, Devesa S, Warren J, Fraumeni JJ. Rising incidence of renal cell cancer in the United States. JAMA. 1999 May: **281**:1628-31
[141] Jayson M, Sanders H. Increased incidence of serendipitously discovered renal cell carcinoma. Urology. 1998 Feb: **51**:203-5
[142] Luciani LG, Cestari R, Tallarigo C. Incidental renal cell carcinoma-age and stage characterization and clinical implications: study of 1092 patients (1982-1997). Urology. 2000 Jul: **56**:58-62
[143] Birnbaum BA, Bosniak MA, Megibow AJ, Lubat E, Gordon RB. Observations on the growth of renal neoplasms. Radiology. 1990 Sep: **176**:695-701
[144] Bosniak M, Birnbaum B, Krinsky G, Waisman J. Small renal parenchymal neoplasms: further observations on growth. Radiology. 1995 Dec: **197**:589-97
[145] Kunkle DA, Crispen PL, Li T, Uzzo RG. Tumor size predicts synchronous metastatic renal cell carcinoma: implications for surveillance of small renal masses. J Urol. 2007 May: **177**:1692-6; discussion 7
[146] Van Poppel H, Joniau S. Is surveillance an option for the treatment of small renal masses? Eur Urol. 2007 Nov: **52**:1323-30
[147] Hemal A, Kumar A, Kumar R, Wadhwa P, Seth A, Gupta N. Laparoscopic versus open radical nephrectomy for large renal tumors: a long-term prospective comparison. J Urol. 2007 2007 Mar: **177**:862-6
[148] Makhoul B, De La Taille A, Vordos D, et al. Laparoscopic radical nephrectomy for T1 renal cancer: the gold standard? A comparison of laparoscopic vs open nephrectomy. BJU Int. 2004 Jan: **93**:67-70
[149] Shuford MD, McDougall EM, Chang SS, LaFleur BJ, Smith JA, Jr., Cookson MS. Complications of contemporary radical nephrectomy: comparison of open vs. laparoscopic approach. Urol Oncol. 2004 Mar-Apr: **22**:121-6
[150] Clark A, Breau R, Morash C, Fergusson D, Doucette S, Cagiannos I. Preservation of renal function following partial or radical nephrectomy using 24-hour creatinine clearance. Eur Urol. 2008 Jul: **54**:143-52
[151] Lucas S, Stern J, Adibi M, Zeltser I, Cadeddu J, Raj G. Renal function outcomes in patients treated for renal masses smaller than 4 cm by ablative and extirpative techniques. J Urol. 2008 Jan: **179**:75-9; discussion 9-80
[152] McKiernan J, Simmons R, Katz J, Russo P. Natural history of chronic renal insufficiency after partial and radical nephrectomy. Urology. 2002 Jun: **59**:816-20
[153] Lau WK, Blute ML, Weaver AL, Torres VE, Zincke H. Matched comparison of radical nephrectomy vs nephron-sparing surgery in patients with unilateral renal cell carcinoma and a normal contralateral kidney. Mayo Clinic proceedings Mayo Clinic. 2000 Dec: **75**:1236-42

[154] Patard J, Shvarts O, Lam J, et al. Safety and efficacy of partial nephrectomy for all T1 tumors based on an international multicenter experience. J Urol. 2004 Jun: **171**:2181-5, quiz 435
[155] Leibovich BC, Blute ML, Cheville JC, Lohse CM, Weaver AL, Zincke H. Nephron sparing surgery for appropriately selected renal cell carcinoma between 4 and 7 cm results in outcome similar to radical nephrectomy. J Urol. 2004 Mar: **171**:1066-70
[156] Fergany AF, Hafez KS, Novick AC. Long-term results of nephron sparing surgery for localized renal cell carcinoma: 10-year followup. J Urol. 2000 Feb: **163**:442-5
[157] Porpiglia F, Volpe A, Billia M, Scarpa RM. Laparoscopic versus open partial nephrectomy: analysis of the current literature. Eur Urol. 2008 Apr: **53**:732-42; discussion 42-3
[158] Thompson RH, Boorjian SA, Lohse CM, et al. Radical nephrectomy for pT1a renal masses may be associated with decreased overall survival compared with partial nephrectomy. J Urol. 2008 Feb: **179**:468-71; discussion 72-3
[159] Weight CJ, Larson BT, Gao T, et al. Elective partial nephrectomy in patients with clinical T1b renal tumors is associated with improved overall survival. Urology. 2010 Sep: **76**:631-7
[160] Weight CJ, Larson BT, Fergany AF, et al. Nephrectomy induced chronic renal insufficiency is associated with increased risk of cardiovascular death and death from any cause in patients with localized cT1b renal masses. J Urol. 2010 Apr: **183**:1317-23
[161] Huang WC, Elkin EB, Levey AS, Jang TL, Russo P. Partial nephrectomy versus radical nephrectomy in patients with small renal tumors--is there a difference in mortality and cardiovascular outcomes? J Urol. 2009 Jan: **181**:55-61; discussion -2
[162] Weight CJ, Lieser G, Larson BT, et al. Partial nephrectomy is associated with improved overall survival compared to radical nephrectomy in patients with unanticipated benign renal tumours. Eur Urol. 2010 Aug: **58**:293-8
[163] Van Poppel H, Da Pozzo L, Albrecht W, et al. A prospective, randomised EORTC intergroup phase 3 study comparing the oncologic outcome of elective nephron-sparing surgery and radical nephrectomy for low-stage renal cell carcinoma. Eur Urol. 2011 Apr: **59**:543-52
[164] Liguori G, Trombetta C, Pomara G, et al. Major invasive surgery for urologic cancer in octogenarians with comorbid medical conditions. Eur Urol. 2007 Jun: **51**:1600-4; discussion 5
[165] Kunkle DA, Uzzo RG. Cryoablation or radiofrequency ablation of the small renal mass : a meta-analysis. Cancer. 2008 Nov 15: **113**:2671-80
[166] Chapelon J, Margonari J, Theillère Y, et al. Effects of high-energy focused ultrasound on kidney tissue in the rat and the dog. Eur Urol. 1992: **22**:147-52
[167] Susani M, Madersbacher S, Kratzik C, Vingers L, Marberger M. Morphology of tissue destruction induced by focused ultrasound. Eur Urol. 1993: **23 Suppl 1**:34-8
[168] Adams JB, Moore RG, Anderson JH, Strandberg JD, Marshall FF, Davoussi LR. High-intensity focused ultrasound ablation of rabbit kidney tumors. J Endourol. 1996 Feb: **10**:71-5
[169] Köhrmann K, Michel M, Gaa J, Marlinghaus E, Alken P. High intensity focused ultrasound as noninvasive therapy for multilocal renal cell carcinoma: case study and review of the literature. J Urol. 2002 Jun: **167**:2397-403
[170] Paterson RF, Barret E, Siqueira TM, et al. Laparoscopic partial kidney ablation with high intensity focused ultrasound. J Urol. 2003 Jan: **169**:347-51

[171] Hacker A, Michel MS, Marlinghaus E, Kohrmann KU, Alken P. Extracorporeally induced ablation of renal tissue by high-intensity focused ultrasound. BJU Int. 2006 Apr: **97**:779-85
[172] Ritchie RW, Leslie T, Phillips R, et al. Extracorporeal high intensity focused ultrasound for renal tumours: a 3-year follow-up. BJU Int. 2010 Mar 4:
[173] Goldberg S, Charboneau J, Dodd Gr, et al. Image-guided tumor ablation: proposal for standardization of terms and reporting criteria. Radiology. 2003: **228**:335-45-
[174] Goldberg SN, Grassi CJ, Cardella JF, et al. Image-guided tumor ablation: standardization of terminology and reporting criteria. Radiology. 2005 Jun: **235**:728-39
[175] Wunder JS, Paulian G, Huvos AG, Heller G, Meyers PA, Healey JH. The histological response to chemotherapy as a predictor of the oncological outcome of operative treatment of Ewing sarcoma. The Journal of bone and joint surgery American volume. 1998 Jul: **80**:1020-33
[176] Bensalah K, Pantuck AJ, Rioux-Leclercq N, et al. Positive surgical margin appears to have negligible impact on survival of renal cell carcinomas treated by nephron-sparing surgery. Eur Urol. 2010 Mar: **57**:466-71
[177] Permpongkosol S, Colombo JR, Jr., Gill IS, Kavoussi LR. Positive surgical parenchymal margin after laparoscopic partial nephrectomy for renal cell carcinoma: oncological outcomes. J Urol. 2006 Dec: **176**:2401-4
[178] Yossepowitch O, Thompson RH, Leibovich BC, et al. Positive surgical margins at partial nephrectomy: predictors and oncological outcomes. J Urol. 2008 Jun: **179**:2158-63
[179] Rabkin BA, Zderic V, Vaezy S. Hyperecho in ultrasound images of HIFU therapy: involvement of cavitation. Ultrasound Med Biol. 2005 Jul: **31**:947-56
[180] Wu F, Wang Z, Cao Y, et al. "Wide local ablation" of localized breast cancer using high intensity focused ultrasound. J Surg Oncol. 2007 Aug: **96**:130-6
[181] Wu F, Wang Z-B, Chen W-Z, et al. Extracorporeal high intensity focused ultrasound ablation in the treatment of 1038 patients with solid carcinomas in China: an overview. Ultrason Sonochem. 2004 May: **11**:149-54
[182] Yu T, Xu C. Hyperecho as the indicator of tissue necrosis during microbubble-assisted high intensity focused ultrasound: sensitivity, specificity and predictive value. Ultrasound Med Biol. 2008 Aug: **34**:1343-7
[183] Leslie TA, Kennedy JE, Illing RO, et al. High-intensity focused ultrasound ablation of liver tumours: can radiological assessment predict the histological response? Br J Radiol. 2008 Jul: **81**:564-71
[184] Goss SA, Johnston RL, Dunn F. Comprehensive compilation of empirical ultrasonic properties of mammalian tissues. The Journal of the Acoustical Society of America. 1978: **64**:423-57
[185] Chivers RC, Parry RJ. Ultrasonic velocity and attenuation in mammalian tissues. J Acoust Soc Am. 1978 Mar: **63**:940-53
[186] Damianou C. In vitro and in vivo ablation of porcine renal tissues using high-intensity focused ultrasound. Ultrasound Med Biol. 2003 Sep: **29**:1321-30
[187] Froelich B. A simple apparatus for automatic pulse echo tracking. J Phys E Scient Inst. 1977: **10**:210-1
[188] Kremkau FW, Barnes RW, McGraw CP. Ultrasonic attenuation and propagation speed in normal human brain. J Acoust Soc Am. 1981: **70**:29-38
[189] Amirlak B. Skin Anatomy. 2011 [cited 2011 23/11]; Available from: http://emedicine.medscape.com/article/1294744-overview

[190] Al-Refaie WB, Parsons HM, Henderson WG, et al. Body mass index and major cancer surgery outcomes: lack of association or need for alternative measurements of obesity? Ann Surg Oncol. 2010 Sep: **17**:2264-73
[191] Orvieto MA, Zorn KC, Lyon MB, et al. High intensity focused ultrasound renal tissue ablation: a laparoscopic porcine model. J Urol. 2009 Feb: **181**:861-6
[192] Petros F, Sukumar S, Haber GP, et al. Multi-institutional Analysis of Robotic Partial Nephrectomy for Renal Tumors > 4cm vs. </= 4cm in 445 Consecutive Patients. J Endourol. 2011 Nov 3:
[193] Patard JJ, Pantuck AJ, Crepel M, et al. Morbidity and clinical outcome of nephron-sparing surgery in relation to tumour size and indication. Eur Urol. 2007 Jul: **52**:148-54
[194] Lifshitz DA, Shikanov S, Jeldres C, et al. Laparoscopic partial nephrectomy: predictors of prolonged warm ischemia. J Urol. 2009 Sep: **182**:860-5
[195] Venkatesh R, Weld K, Ames CD, et al. Laparoscopic partial nephrectomy for renal masses: effect of tumor location. Urology. 2006 Jun: **67**:1169-74; discussion 74
[196] Fox Chase Cancer Center. R.E.N.A.L. Nephrometry Scoring System. 2011 [cited 2011 23/11]; Available from: http://www.nephrometry.com/
[197] Kutikov A, Uzzo RG. The R.E.N.A.L. nephrometry score: a comprehensive standardized system for quantitating renal tumor size, location and depth. J Urol. 2009 Sep: **182**:844-53
[198] Bruner B, Breau RH, Lohse CM, Leibovich BC, Blute ML. Renal nephrometry score is associated with urine leak after partial nephrectomy. BJU Int. 2011 Jul: **108**:67-72
[199] Hayn MH, Schwaab T, Underwood W, Kim HL. RENAL nephrometry score predicts surgical outcomes of laparoscopic partial nephrectomy. BJU Int. 2011 Sep: **108**:876-81
[200] Rosevear HM, Gellhaus PT, Lightfoot AJ, Kresowik TP, Joudi FN, Tracy CR. Utility of the RENAL nephrometry scoring system in the real world: predicting surgeon operative preference and complication risk. BJU Int. 2011 Jul 20:
[201] Simhan J, Smaldone MC, Tsai KJ, et al. Objective measures of renal mass anatomic complexity predict rates of major complications following partial nephrectomy. Eur Urol. 2011 Oct: **60**:724-30
[202] Canter D, Kutikov A, Manley B, et al. Utility of the R.E.N.A.L. Nephrometry Scoring System in Objectifying Treatment Decision-making of the Enhancing Renal Mass. Urology. 2011 Nov: **78**:1089-94
[203] Jamis-Dow CA, Choyke PL, Jennings SB, Linehan WM, Thakore KN, Walther MM. Small (< or = 3-cm) renal masses: detection with CT versus US and pathologic correlation. Radiology. 1996 Mar: **198**:785-8
[204] Helenon O, Correas J, Ballyguier C, Ghouadni M, Cornud F. Ultrasound of renal tumours. European Radiology. 2001: **11**:1890-901
[205] Park BK, Kim CK, Choi HY, et al. Limitation for performing ultrasound-guided radiofrequency ablation of small renal masses. Eur J Radiol. 2010 Aug: **75**:248-52
[206] Bailey MR, Couret LN, Sapozhnikov OA, et al. Use of overpressure to assess the role of bubbles in focused ultrasound lesion shape in vitro. Ultrasound Med Biol. 2001 May: **27**:695-708
[207] Gyöngy M, Arora M, Noble A, Coussios CC. A passive array technique for cavitation mapping during HIFU treatment. J Acoust Soc Am. 2008: **123**:3223
[208] Gyongy M, Coussios CC. Passive cavitation mapping for localization and tracking of bubble dynamics. J Acoust Soc Am. 2010 Oct: **128**:EL175-80
[209] Clarke RL, ter Haar GR. Temperature rise recorded during lesion formation by high-intensity focused ultrasound. Ultrasound Med Biol. 1997: **23**:299-306

[210] Malcolm AL, ter Haar GR. Ablation of tissue volumes using high intensity focused ultrasound. Ultrasound Med Biol. 1996: **22**:659-69
[211] Parker KJ. Ultrasonic attenuation and absorption in liver tissue. Ultrasound Med Biol. 1983: **9**:363-9
[212] Maleke C, Konofagou EE. Harmonic motion imaging for focused ultrasound (HMIFU): a fully integrated technique for sonication and monitoring of thermal ablation in tissues. Phys Med Biol. 2008 Mar 21: **53**:1773-93
[213] Canney MS, Khokhlova VA, Bessonova OV, Bailey MR, Crum LA. Shock-induced heating and millisecond boiling in gels and tissue due to high intensity focused ultrasound. Ultrasound Med Biol. 2010 Feb: **36**:250-67
[214] Chen L, ter Haar G, Robertson D, Bensted JP, Hill CR. Histological study of normal and tumor-bearing liver treated with focused ultrasound. Ultrasound Med Biol. 1999 Jun: **25**:847-56
[215] McLaughlan J, Rivens I, Leighton T, Ter Haar G. A study of bubble activity generated in ex vivo tissue by high intensity focused ultrasound. Ultrasound Med Biol. 2010 Aug: **36**:1327-44
[216] Motulsky H. Intuitive Biostatistics: Oxford University Press, 1995
[217] Leisenring W, Alonzo T, Pepe MS. Comparisons of predictive values of binary medical diagnostic tests for paired designs. Biometrics. 2000 Jun: **56**:345-51
[218] Hockham N, Coussios CC, Arora M. A real-time controller for sustaining thermally relevant acoustic cavitation during ultrasound therapy. IEEE Trans Ultrason Ferroelectr Freq Control. 2010 Dec: **57**:2685-94
[219] Simone G, Papalia R, Guaglianone S, Gallucci M. 'Zero ischaemia', sutureless laparoscopic partial nephrectomy for renal tumours with a low nephrometry score. BJU Int. 2011 Dec 16:
[220] Luo JH, Zhou FJ, Xie D, et al. Analysis of long-term survival in patients with localized renal cell carcinoma: laparoscopic versus open radical nephrectomy. World J Urol. 2010 Jun: **28**:289-93
[221] Crispen P, Boorjian S, Lohse C, et al. Outcomes following partial nephrectomy by tumor size. J Urol. 2008 Nov: **180**:1912-7
[222] Heuer R, Gill IS, Guazzoni G, et al. A critical analysis of the actual role of minimally invasive surgery and active surveillance for kidney cancer. Eur Urol. 2010 Feb: **57**:223-32
[223] Permpongkosol S, Link R, Su L, et al. Complications of 2,775 urological laparoscopic procedures: 1993 to 2005. J Urol. 2007 Feb: **177**:580-5
[224] Ramani AP, Desai MM, Steinberg AP, et al. Complications of laparoscopic partial nephrectomy in 200 cases. J Urol. 2005 Jan: **173**:42-7
[225] Frank I, Blute ML, Cheville JC, Lohse CM, Weaver AL, Zincke H. Solid renal tumors: an analysis of pathological features related to tumor size. J Urol. 2003 Dec: **170**:2217-20
[226] Chawla SN, Crispen PL, Hanlon AL, Greenberg RE, Chen DY, Uzzo RG. The natural history of observed enhancing renal masses: meta-analysis and review of the world literature. J Urol. 2006 Feb: **175**:425-31
[227] Remzi M, Ozsoy M, Klingler H, et al. Are small renal tumors harmless? Analysis of histopathological features according to tumors 4 cm or less in diameter. J Urol. 2006 Sep: **176**:896-9
[228] Guethmundsson E, Hellborg H, Lundstam S, Erikson S, Ljungberg B. Metastatic Potential in Renal Cell Carcinomas </=7cm: Swedish Kidney Cancer Quality Register Data. Eur Urol. 2011 Nov: **60**:975-82

[229] Gill IS, Novick AC, Meraney AM, et al. Laparoscopic renal cryoablation in 32 patients. Urology. 2000 Nov: **56**:748-53
[230] Cestari A, Guazzoni G, dell'Acqua V, et al. Laparoscopic cryoablation of solid renal masses: intermediate term followup. J Urol. 2004 Oct: **172**:1267-70
[231] Gill IS, Remer EM, Hasan WA, et al. Renal cryoablation: outcome at 3 years. J Urol. 2005 Jun: **173**:1903-7
[232] Hegarty NJ, Gill IS, Desai MM, Remer EM, O'Malley CM, Kaouk JH. Probe-ablative nephron-sparing surgery: cryoablation versus radiofrequency ablation. Urology. 2006 Jul: **68**:7-13
[233] Davol PE, Fulmer BR, Rukstalis DB. Long-term results of cryoablation for renal cancer and complex renal masses. Urology. 2006 Jul: **68**:2-6
[234] Schwartz BF, Rewcastle JC, Powell T, Whelan C, Manny T, Jr., Vestal JC. Cryoablation of small peripheral renal masses: a retrospective analysis. Urology. 2006 Jul: **68**:14-8
[235] Permpongkosol S, Link RE, Kavoussi LR, Solomon SB. Percutaneous computerized tomography guided cryoablation for localized renal cell carcinoma: factors influencing success. J Urol. 2006 Nov: **176**:1963-8; discussion 8
[236] Aron M, Kamoi K, Remer E, Berger A, Desai M, Gill I. Laparoscopic renal cryoablation: 8-year, single surgeon outcomes. J Urol. 2010 Mar: **183**:889-95
[237] Guazzoni G, Cestari A, Buffi N, et al. Oncologic results of laparoscopic renal cryoablation for clinical T1a tumors: 8 years of experience in a single institution. Urology. 2010 Sep: **76**:624-9
[238] Sidana A, Aggarwal P, Feng Z, Georgiades CS, Trock BJ, Rodriguez R. Complications of renal cryoablation: a single center experience. J Urol. 2010 Jul: **184**:42-7
[239] Gervais DA, McGovern FJ, Arellano RS, McDougal WS, Mueller PR. Radiofrequency ablation of renal cell carcinoma: part 1, Indications, results, and role in patient management over a 6-year period and ablation of 100 tumors. AJR Am J Roentgenol. 2005 Jul: **185**:64-71
[240] Park S, Anderson JK, Matsumoto ED, Lotan Y, Josephs S, Cadeddu JA. Radiofrequency ablation of renal tumors: intermediate-term results. J Endourol. 2006 Aug: **20**:569-73
[241] Zagoria RJ, Traver MA, Werle DM, Perini M, Hayasaka S, Clark PE. Oncologic efficacy of CT-guided percutaneous radiofrequency ablation of renal cell carcinomas. AJR Am J Roentgenol. 2007 Aug: **189**:429-36
[242] Breen DJ, Rutherford EE, Stedman B, et al. Management of renal tumors by image-guided radiofrequency ablation: experience in 105 tumors. Cardiovasc Intervent Radiol. 2007 Sep-Oct: **30**:936-42
[243] Veltri A, Garetto I, Pagano E, Tosetti I, Sacchetto P, Fava C. Percutaneous RF thermal ablation of renal tumors: is US guidance really less favorable than other imaging guidance techniques? Cardiovasc Intervent Radiol. 2009 Jan: **32**:76-85
[244] Lu X, Suo S, Liu H, Zhang S. Three-dimensional multimodal image non-rigid registration and fusion in a High Intensity Focused Ultrasound system. Computer aided surgery : official journal of the International Society for Computer Aided Surgery. 2012: **17**:1-12
[245] Quesson B, Laurent C, Maclair G, et al. Real-time volumetric MRI thermometry of focused ultrasound ablation in vivo: a feasibility study in pig liver and kidney. NMR Biomed. 2011 Feb: **24**:145-53

[246] Cornelis F, Grenier N, Moonen CT, Quesson B. In vivo characterization of tissue thermal properties of the kidney during local hyperthermia induced by MR-guided high-intensity focused ultrasound. NMR Biomed. 2011 Aug: **24**:799-806
[247] Pernot M, Tanter M, Fink M. 3-D real-time motion correction in high-intensity focused ultrasound therapy. Ultrasound Med Biol. 2004 Sep: **30**:1239-49
[248] Ries M, de Senneville BD, Roujol S, Berber Y, Quesson B, Moonen C. Real-time 3D target tracking in MRI guided focused ultrasound ablations in moving tissues. Magn Reson Med. 2010 Dec: **64**:1704-12
[249] Ritchie R, Collin J, Wu F, Coussios C, Leslie T, Cranston D. Significant skin burns may occur with the use of a water balloon in HIFU treatment. Proceedings of the International Society for Therapeutic Ultrasound. 2011: **11th Symposium**
[250] Cirillo S, Petracchini M, D'Urso L, et al. Endorectal magnetic resonance imaging and magnetic resonance spectroscopy to monitor the prostate for residual disease or local cancer recurrence after transrectal high-intensity focused ultrasound. BJU Int. 2008 Aug: **102**:452-8
[251] De Visschere PJ, De Meerleer GO, Futterer JJ, Villeirs GM. Role of MRI in follow-up after focal therapy for prostate carcinoma. AJR Am J Roentgenol. 2010 Jun: **194**:1427-33
[252] Kim YS, Lim HK, Kim JH, et al. Dynamic contrast-enhanced magnetic resonance imaging predicts immediate therapeutic response of magnetic resonance-guided high-intensity focused ultrasound ablation of symptomatic uterine fibroids. Invest Radiol. 2011 Oct: **46**:639-47
[253] Kim SH, Jung SE, Kim HL, Hahn ST, Park GS, Park WC. The potential role of dynamic MRI in assessing the effectiveness of high-intensity focused ultrasound ablation of breast cancer. Int J Hyperthermia. 2010: **26**:594-603
[254] Kirkham AP, Emberton M, Hoh IM, Illing RO, Freeman AA, Allen C. MR imaging of prostate after treatment with high-intensity focused ultrasound. Radiology. 2008 Mar: **246**:833-44
[255] Mahnken A, Rohde D, Brkovic D, Günther R, Tacke J. Percutaneous radiofrequency ablation of renal cell carcinoma: preliminary results. Acta Radiol. 2005 Apr: **46**:208-14
[256] Joniau S, Tailly T, Goeman L, Blyweert W, Gontero P, Joyce A. Kidney radiofrequency ablation for small renal tumors: oncologic efficacy. J Endourol. 2010 May: **24**:721-8
[257] Aron M, Kamoi K, Remer E, Berger A, Desai M, Gill I. Laparoscopic renal cryoablation: 8-year, single surgeon outcomes. J Urol. 2010 Mar: **183**:889-95
[258] Schirmang TC, Mayo-Smith WW, Dupuy DE, Beland MD, Grand DJ. Kidney neoplasms: renal halo sign after percutaneous radiofrequency ablation--incidence and clinical importance in 101 consecutive patients. Radiology. 2009 Oct: **253**:263-9
[259] Ljungberg B, Cowan NC, Hanbury DC, et al. EAU guidelines on renal cell carcinoma: the 2010 update. Eur Urol. 2010 Sep: **58**:398-406